STUDIES OF NATURAL PRODUCTS THAT REVEAL NOVEL

STRATEGIES FOR EFFICIENT MODIFICATION OF DNA

A Dissertation

Presented to

The Faculty of the Graduate School

University of Missouri-Columbia

In Partial Fulfillment

Of the Requirements for the Degree

Doctor of Philosophy

---

by

JOSEPH SZEKELY

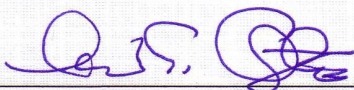Prof. Kent S. Gates, Dissertation Supervisor

May, 2006

APPROVAL PAGE

The undersigned, appointed by the Dean of the Graduate School, have examined the dissertation entitled:

STUDIES OF NATURAL PRODUCTS THAT REVEAL NOVEL

STRATEGIES FOR EFFICIENT MODIFICATION OF DNA

Presented by Joseph Szekely

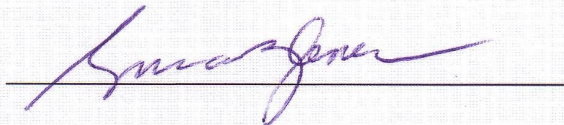a candidate for the degree of Doctor of Philosophy

and hereby certify that in their opinion it is worthy of acceptance
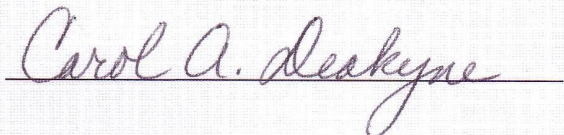
_____

Chair

_____

_____

_____

_____

Carol A. Deakyne

"Legyenek kedvedre valók szájam mondásai, és az én szívem gondolatai előtted legyenek, oh Uram, kősziklám és megváltóm."

Zsoltárok 19:15

ACKNOWLEDGEMENTS

ABSTRACT

DNA is the central molecule in cells. The correct function of cells depends on the structure of DNA. DNA damaging natural products often show cytotoxic or mutagenic properties, which many times land them medicinal value as antibacterial or anticancer therapeutics. Efficient DNA modifications by these agents usually endow them with outstanding biological efficiency. In the present dissertation, we investigated novel DNA damaging natural products with novel DNA modification strategies.

We showed that weak noncovalent binding of the natural product leinamycin to DNA accelerates its DNA-alkylation reaction (Chapter 1). We demonstrated that leinamycin intercalates DNA with an unprecedented DNA-intercalating functional group. Likewise, we uncovered novel molecular recognition features of the natural product azinomycin using similar tools (Chapter 4). We characterized novel, reversible chemical reactions of leinamycin (Chapter 3). Amongst these were reversible DNA-alkylation and reversible adduct formation with biologically relevant nucleophiles. We showed that thiols and chloride ion can add to the leinamycin episulfonium ion reveribly to protect it from unproductive hydrolysis and to help its transport to DNA. We synthesized precursors for the biosynthesis of leinamycin (Chapter 5) to prove the principle that synthetic molecules can be incorporated into the biosynthetic machinery of natural products.

We worked with the labile and mutagenic fatty acid metabolite: fecapentaene-12, and clarified its mechanism of oxidative DNA damage. We also showed that this poly-unsaturated hydrocarbon compound binds the DNA duplex noncovalently (Chapter 6)

TABLE OF CONTENTS

CHAPTER 2. LEINAMYCIN: A STRUCTURALLY NOVEL DNA INTERCALATOR...55

CHAPTER 3. REVERSIBLE DNA ALKYLATION BY LEINAMYCIN AND RELATED DNA-ALKYLATORS

LIST OF TABLES

CHAPTER 4

CHAPTER 6

LIST OF FIGURES

CHAPTER 2

CHAPTER 4

TABLE OF SCHEMES

CHAPTER 4

CHAPTER 5

CHAPTER 6

_____

Chapter 1. DNA Alkylation by Leinamycin: Measurement of the Rate Acceleration Provided By Noncovalent Binding In The Major Groove of the Double Helix

1.1. Discovery and Biological Activity of Leinamycin

Leinamycin (**1**), initially named DC107, was found in Japanese soils, during screening for antibiotics. It was isolated in 1985 from a species of *Streptomyces* [1,2] by the Kyowa Hakko Kogyo (KHK) Pharmaceutical Company. Soon, **1** showed antibacterial activity against *Bacillus subtilis* (IC_{50} = 80 ng/mL; 160 nM) and mouse sarcoma (1 mg/kg). Additionally, **1** displays antitumor activity (IC_{50} of 11 nM against HeLa S3 tumor cells). Leinamycin increases the life span of mice with murine leukemia P388 by ~60% at a dosage of 0.38 mg/kg.[3] Leinamycin and its derivatives continue to be investigated as potential anticancer agents. [4-7]

The structure of **1** was elucidated by spectroscopic means.[2,3,8] Leinamycin possesses an unusual 1,2-dithiolan-3-one 1-oxide moiety that is connected by a spiro-linkage to an 18-membered macrocycle that contains a novel *Z,E*-5-(thiazol-4-yl)-penta-2,4-dienone assembly. The 1,2-dithiolan-3-one 1-oxide moiety (Figure 1) is crucial for the antitumor activity of the drug, shown by the fact that the S-deoxy analog **2** (Figure 1) showed much less efficient antitumor properties.[2]

DNA is an important biological target of the natural product. [2,9] The natural product activates Ckh2 kinase enzymes in human pancreatic carcinoma cells, indicating that the apoptotic cell death is the result of extensive fragmentation of genomic DNA by

the drug. This further suggests that leinamycin mostly expresses its biological activity via oxidative DNA damage.[9]
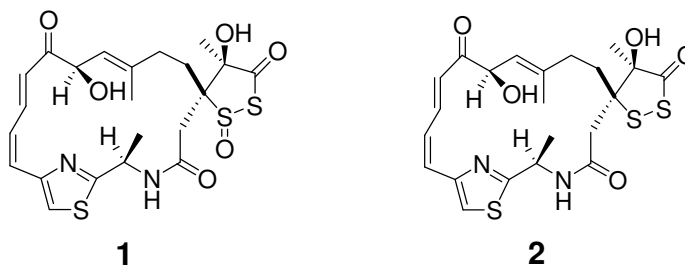
Figure 1. The chemical structure of leinamycin (**1**) and its S-deoxy analog (**2**).

1.2. DNA Binding and the Mechanism of DNA Damage by 1

Because DNA is an important target for antitumor agents,[10] detailed studies of the DNA damaging properties of **1** were undertaken in 1990. [2] In this study, leinamycin was seen to cleave pBR322 DNA at micromolar concentrations. Only nicked (form II) DNA was found to be the product, meaning that **1** does not cause double-strand breaks. DNA cleavage by **1** is thiol dependent, but the identity of the thiol does not affect the efficiency of DNA-damage.

1.2.1. Thiol-Triggered Oxidative DNA Damage by Leinamycin[11]

Leinamycin is a thiol-triggered DNA damaging agent (Scheme 2). The DNA-cleaving properties of small synthetic analogs of the leinamycin (Scheme 1, **3-5**) were studied in our laboratory. [12] The strand cleavage caused by these molecules exclusively involves the conversion of molecular oxygen to DNA damaging hydroxyl radical (OH$^{\bullet}$) as shown at the bottom of Scheme 2. Mechanistic studies in our laboratory earlier showed the production of reactive oxygen species and thiol-mediated DNA-cleavage by

_____

leinamycin.[13] In this process initial attack of the thiol at the S2-sulfur of the dithiolanone-1-oxide ring results in the formation of a sulfenic acid (**6**) intermediate. The oxygen of this sulfenic acid will form the 5-membered 1,2-oxathiolan-5-one ring (**9**) and yields the labile hydrodisulfide (**7**). The unstable hydrodisulfide intermediate (RSSH, **7**) will reduce molecular oxygen to superoxide-radical species and the DNA-damaging hydroxyl radical via Fenton chemistry. This, in turn, initiates oxidative DNA damage. The details of this chemistry are shown in Scheme 3.

3   **4**   **5**
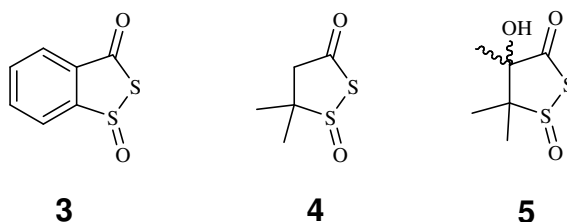
Scheme 1. Small synthetic analogs of leinamycin (**1**)

1.2.2. Thiol-Triggered DNA Alkylation by Leinamycin[11]

In addition to the oxidative DNA damage described above, leinamycin damages DNA by another mechanism, which involves the alkylation of duplex DNA. [8] After thiol-triggered formation of the 1,2-oxathiolan-5-one (**9**) ring, this species undergoes intramolecular reaction with the C6-C7 alkene of the natural product and forms an episulfonium-ion alkylating agent (**10**). The episulfonium-ion efficiently alkylates double-stranded DNA with a covalent attachment at the N7 atom of deoxyguanosine residues (Scheme 2). DNA alkylation competes with hydrolysis of the episulfonium ion,[8] however, DNA alkylation takes place efficiently (75%) in the presence of 400 μM

leinamycin and 600 μM thiol at physiological DNA concentrations (7.6 mM)[14,15]. Interestingly, **10** does not alkylate single stranded DNA or 2'-deoxyguanosine, [8,16] which suggests a role for noncovalent binding of **10** to duplex DNA in the efficient N7G-alkylation.

The leinamycin derived episulfonium-ion (**10**) exists in equilibrium with its constitutional isomer, the leinamyin-epoxide (**11**). The episulfonium ring of **10** is opened by the nucleophilic attack of the C8-OH group to form the epoxide **11** in an equilibrium reaction. [17] One might ask if this epoxide can be a DNA-alkylating species. There are known epoxide DNA alkylating agents, [18] however, in case of leinamycin, DNA alkylation clearly occurs via the episulfonium intermediate **10**, as was proved by NMR studies.[8] The leinamycin-DNA adduct is an unusually labile lesion, prone to rapid depurination ($t_{1/2}$ ~ 3 h at 37 °C). The typical half-life of this reaction is 100 h amongst all known N7G adducts.[19]

_____
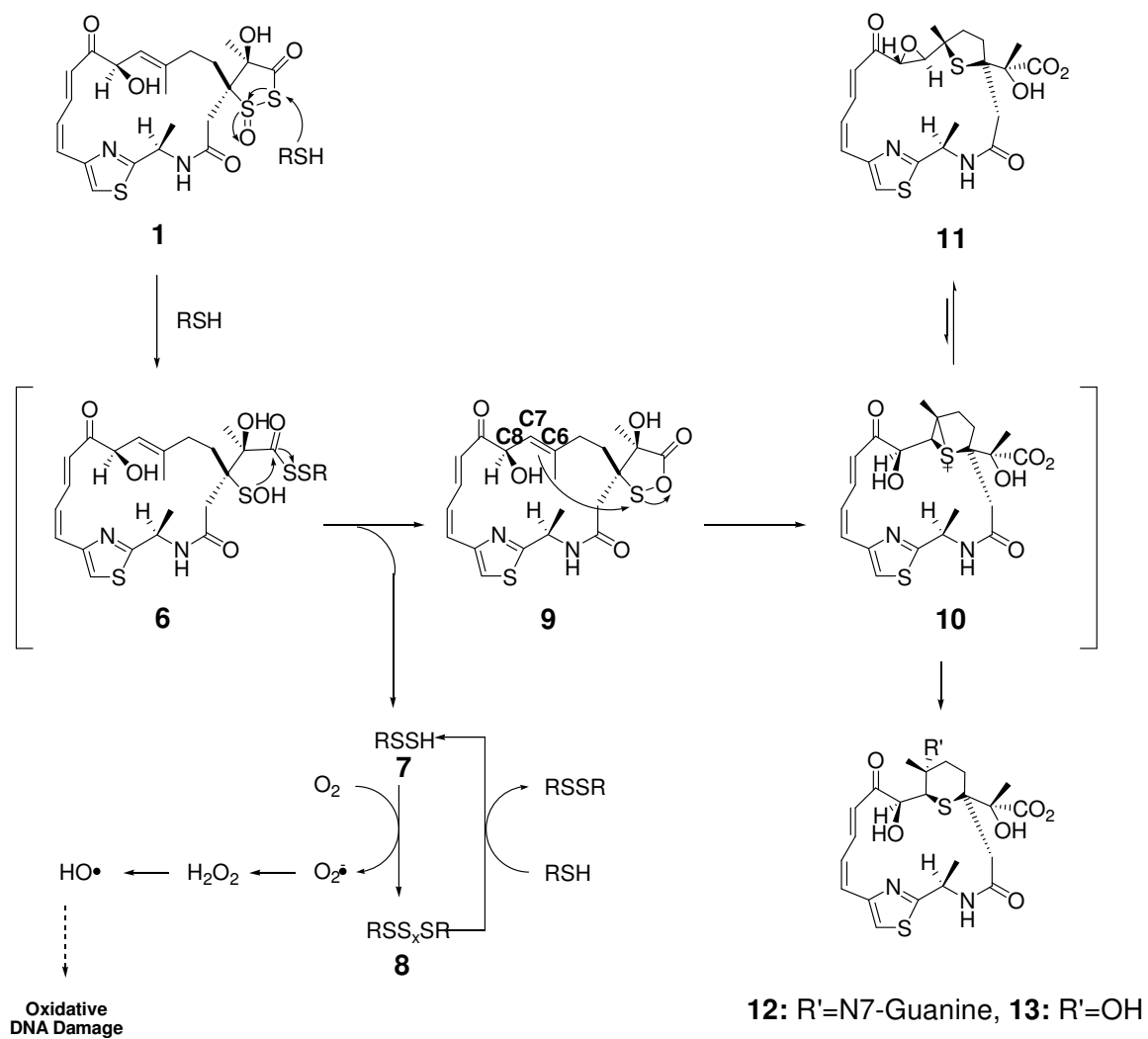
Scheme 2. Thiol triggered DNA damage by the natural product leinamycin

_____

RSH
RSSR + H$_2$S ⟹ Anaerobic Decomposition

RSSSR + RSH ⟶ RSSH + RSSR

RSH, Fe^{3+}

O$_2^{-•}$ O$_2$

Dismutation ↓

Fenton Rxn
H$_2$O$_2$ ⟶ •OH ⟹ Oxidative DNA Damage

Fe^{2+} Fe^{3+}

•RSS   RSSH
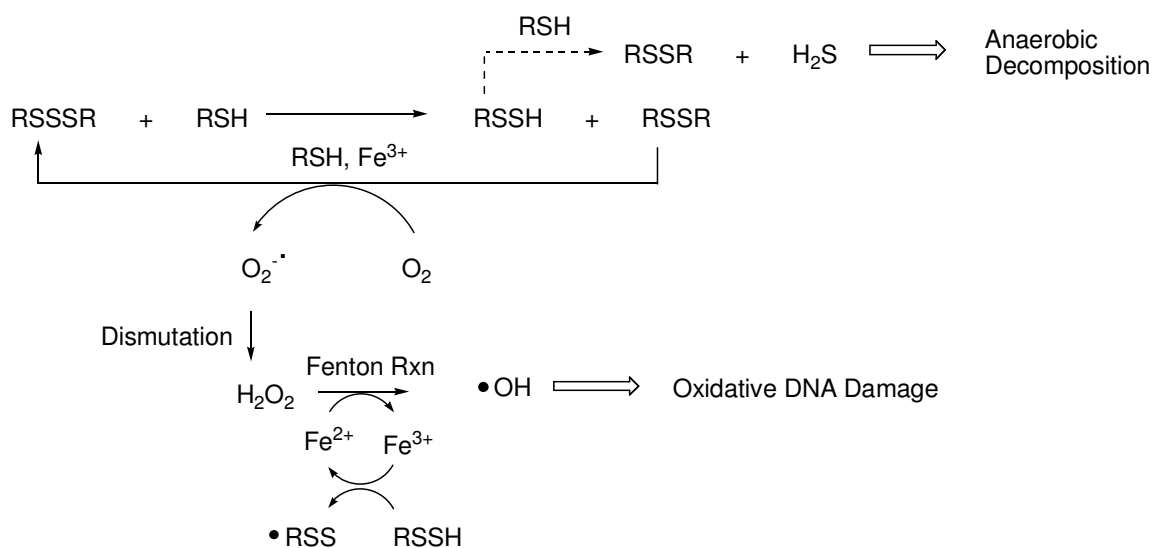
Scheme 3. Fate of polysuflides in the presence of thiol

1.2.3. DNA Alkylation May Be Driven by Noncovalent Association of the Natural Product With the Double Helix

Several lines of evidence indicate that leinamycin associates noncovalently with DNA. [8,16] For example, it was noticed that **1** did not react with the guanosine nucleotide monomer or single-stranded DNA in aqueous buffer under conditions where DNA alkylation is efficient.[8,16] This suggests a role for the duplex DNA structure in the alkylation. Later, we discovered[16] that **1** alkylates duplex DNA in a sequence specific manner with the following order of efficiency:

5'-**G**G>**G**T>**G**C>**G**A

This data implies that noncovalent interaction between the natural product and the DNA-base on the 3'-side of the alkylation site is important. This interaction will be further investigated in Chapter 2.

The facts that leinamycin alkylated only duplex DNA and in a sequence specific manner were intriguing, because leinamycin does not contain any classical DNA-binding functional groups,[20] like a positively charged functional group as seen in spermine, a polyamide-type groove binder as seen in distamycin, or a polycyclic aromatic intercalators as seen in ethidium bromide (Figure 2).

Spermine　　　　　　　　**Distamycin**　　　　　　　**Ethidium bromide**
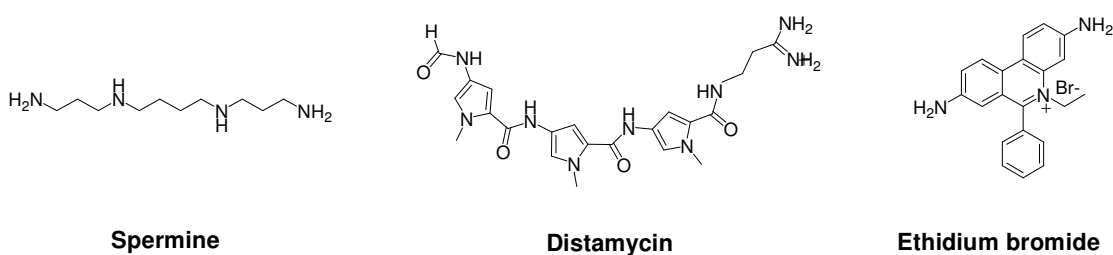
Figure 2. Typical DNA-binders that can associate DNA noncovalently. *Spermine:* electrostatic DNA binders; *distamycin:* minor-groove binding agent, *ethidium-bromide:* DNA-intercalator.

We suspected that the thiazole-dienone moiety of the leinamycin macrocycle might be the noncovalent DNA-binding domain of the natural product,[21] as it represents a large hydrophobic surface in the molecule, which might drive noncovalent association of the molecule in the hydrophobic DNA grooves. This was confirmed by studying the binding constants of truncated leinamycin analogs (**14-17**, Figure 3) in our group. [22] Additionally, an affinity cleaving approach [23-25] was used to compare the DNA alkylation ability of an epoxide analog (**18**) with the small epoxide molecule glycidol. The epoxide in the molecular framework of leinamycin (**18**) alkylates DNA more efficiently than the small epoxide glycidol. The noncovalent binding of **1** and its hydrolysis product (**13**) to DNA was also measured by dialysis methods, and a binding constant ~ 1000 M^{-1} was obtained (Figure 1).

_____

14
$K_B = 1000$ M^{-1}

15
$K_B < 100$ M^{-1}

16
$K_B < 100$ M^{-1}

17
$K_B = 900$ M^{-1}

1
$K_B \sim 1000$ M^{-1}

13
$K_B \sim 1500$ M^{-1}

18

glycidol
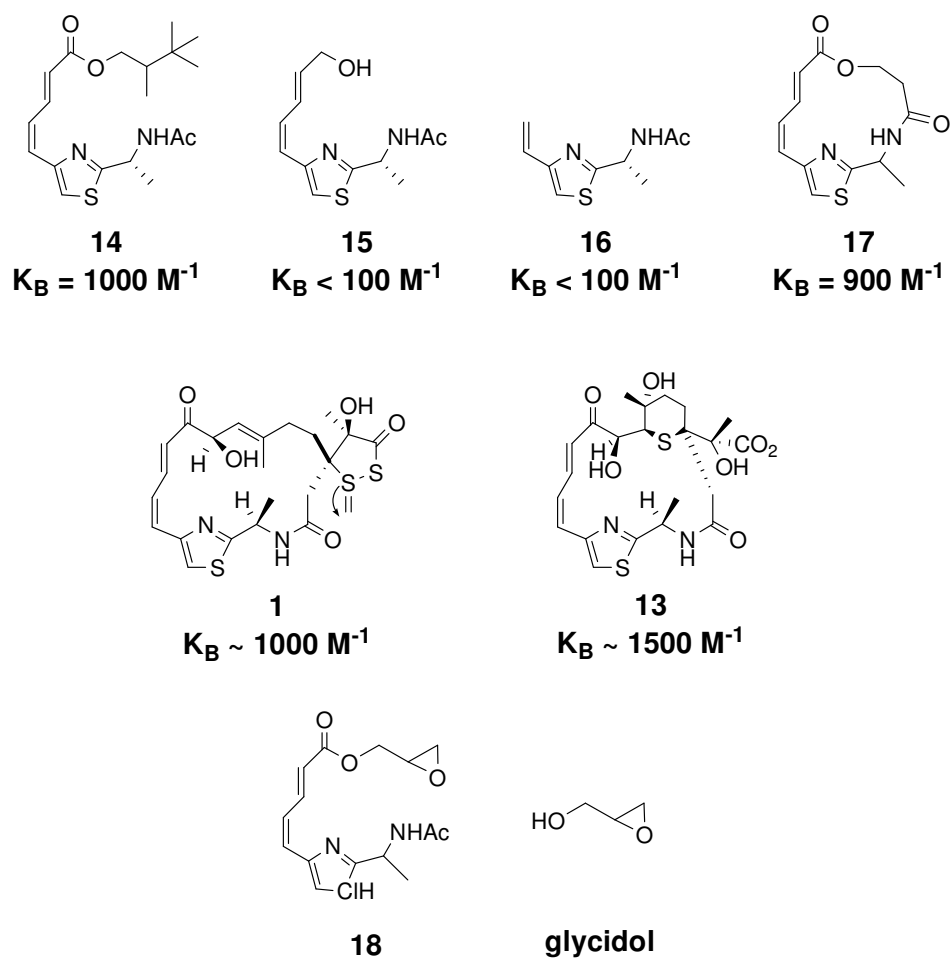
Figure 3. Small synthetic analogs of leinamycin.

1.3. Noncovalent Binding by Natural Products Can Enhance their DNA Alkylation

There are known DNA damaging agents that bind DNA noncovalently, which enhances their DNA alkylation (Figure 4).[26-32]

The idea that DNA binding can enhance the rate of DNA-damage has been demonstrated chemically by attaching small electrophilic organic molecules to noncovalent DNA binders. For example, the alkylation rate of the small N7G-DNA-

_____

alkylator α-bromo-acetamide was studied and compared to that of α-bromo-acetamide attached to an oligonucleotide capable of triple-helix formation. Attachment of α-bromo-acetamide to a triple helix forming oligonucleotide yields an effective molarity of 0.8 M α-bromo acetamide in the major groove of DNA.[33] The attachment of an electrostatic DNA-binding polyamine to chlorambucil (**20**) increased its DNA-damaging potency. [34] These and other examples showed that noncovalent DNA binding can enhance the efficiency of DNA-damaging agents compared to small molecules with a similar DNA-alkylating electrophilic functional group. [24,32,35-38]
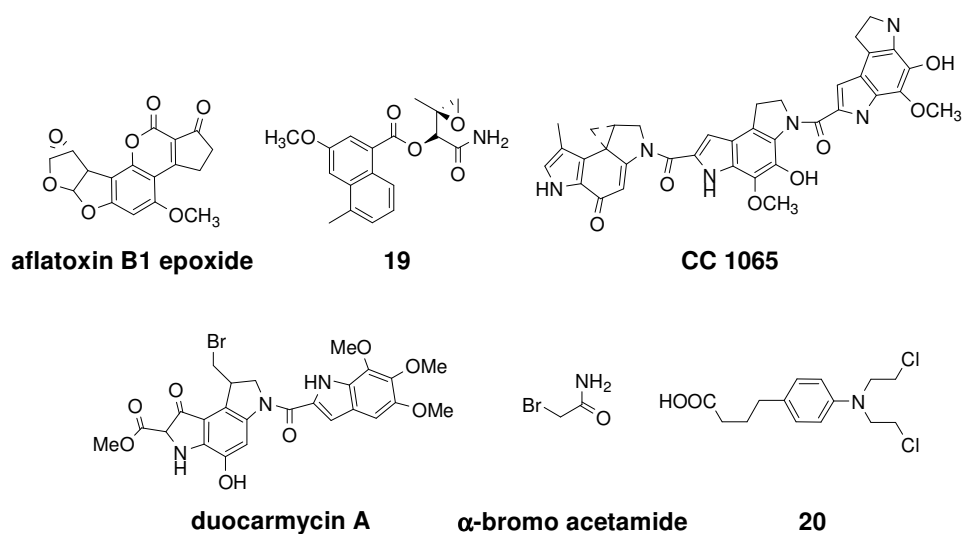
Figure 4. DNA damaging agents that bind DNA noncovalently.

1.4. The Goals of Our Work

Surprisingly, only a few studies have qualitatively examined how noncovalent association facilitates DNA modification by drugs, toxins and mutagens.[27,28,33] With the evidence showing the noncovalent association of **1** to DNA, we hypothesized[39] that noncovalent binding plays an important role in its efficiency of DNA alkylation.[8] We set out to measure the rate acceleration/equivalent molarity that **1** achieves upon DNA binding in the major-groove of DNA in its N7G alkylation in comparison to 2'-dG. Additionally, we wanted to establish the binding constant of the active (episulfonium ion) form of leinamycin (**10**) using enzyme-kinetic analysis.

1.5. DNA Alkylation by Activated Leinamycin (10) Under Physiological Conditions Follows Michaelis-Menten Kinetics

1.5.1. Initial Rates of DNA Alkylation by 10 Followed by UV Absorbance Measurements

Initially, we measured the initial rates of DNA alkylation by **10** using a UV-absorbance based kinetic assay. DNA alkylation by **10** is accompanied by an increase in UV-absorbance at 380 nm. At this wavelength, the contribution of the competitive hydrolysis reaction of **10** is negligible. Initial rates of DNA alkylation were derived from the first derivative of the A_{380nm} vs. time curve, and plotted as a function of applied DNA concentration (Figure 5). This plot, along with the Eadie-Hoofstee, Hanes-Woolf, Lineweaver-Burk and Kitz-Wilson plots were analyzed in terms of Michaelis-Menten kinetics (Equation 1 and Equation 2, Section 1.5.2.) for the calculation of the maximum rate constant of DNA alkylation, $k_2 = 1.68 \pm 0.05 \times 10^{-3}$ s^{-1}, (t$_{1/2}$ = 7 min), the Michaelis-

_____

constant ($K_M = 4.2 \pm 0.1 \times 10^{-4}$ M) and the binding constant of **10** to the DNA duplex (K_B

$= 2\ 065 \pm 60$ M^{-1}). These values represent the average of those originated from each of

these plots (Table 1).
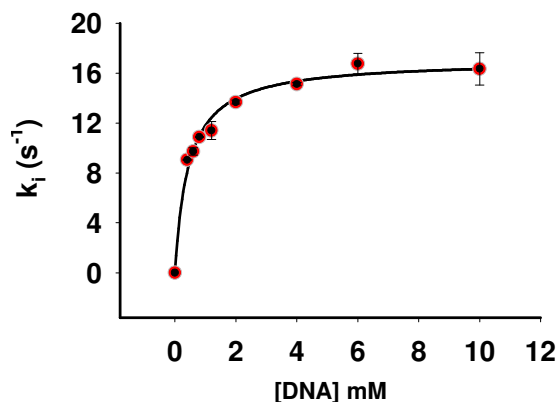
Figure 5. Initial rate constants of DNA alkylation by **10** using an UV based kinetic assay. 200 μM 1 was incubated with 1 mM β-mercaptoethanol in 50 mM MOPS buffer (pH 7.4) at 8 °C. UV-absorbance readings were taken every 5 s at 380 nm for 20 min. Errors were calculated using 67% confidence (n=2).
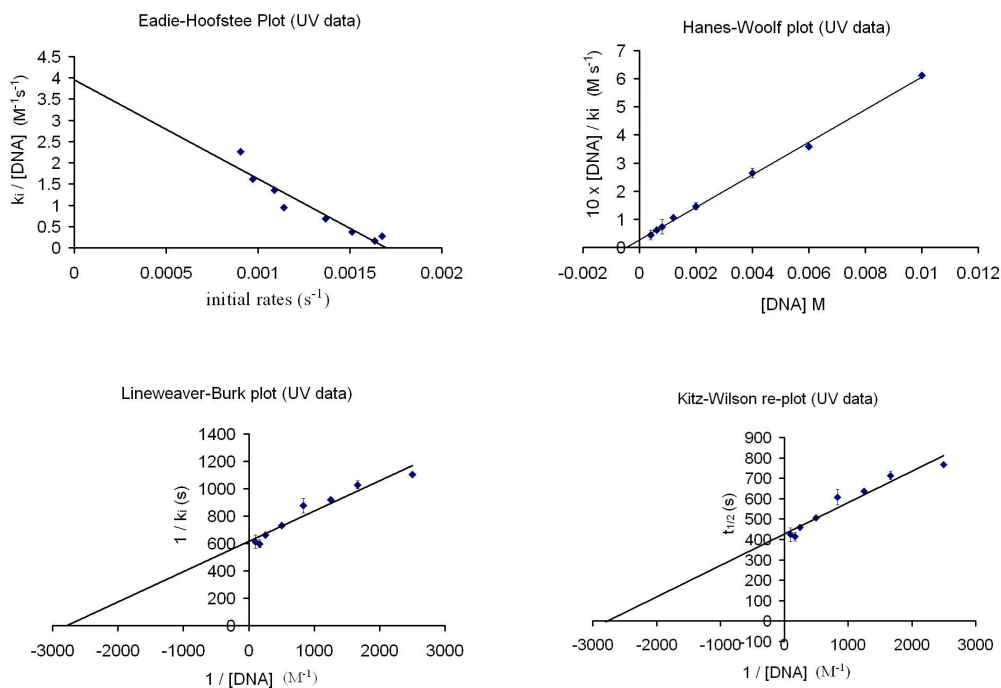
Figure 6. of the Eadie-Hoofstee, Hanes-Woolf, Lineweaver-Burk and Kitz-Wilson plots of the initial rate constants of DNA alkylation by **10**. 200 μM 1 was incubated with 1 mM β-mercaptoethanol in 50 mM MOPS buffer (pH 7.4) at 8 °C. UV-absorbance readings were taken every 5 s at 380 nm for 20 min. Errors were calculated using 67% confidence (n=2).

_____

	k_2 (s^{-1})	K_M (M)	K_B (M^{-1})
Eadie-Hofstee plot	$1.73 \pm 0.05 \times 10^{-3}$	$4.3 \pm 0.1 \times 10^{-4}$	$2\,327 \pm 49$
Hanes-Woolf plot	$1.76 \pm 0.06 \times 10^{-3}$	$4.8 \pm 0.1 \times 10^{-4}$	$2\,100 \pm 44$
Lineweaver-Burk plot	$1.6 \pm 0.03 \times 10^{-3}$	$3.6 \pm 0.1 \times 10^{-4}$	$2\,775 \pm 58$
Kitz-Wilson plot	$1.6 \pm 0.03 \times 10^{-3}$	$3.7 \pm 0.1 \times 10^{-4}$	$2\,774 \pm 58$
Pseudo-Michaelis-Menten plot	$1.71 \pm 0.06 \times 10^{-3}$	$4.5 \pm 0.1 \times 10^{-4}$	$2\,240 \pm 50$

Table 1. Maximum rate of DNA alkylation, K_M and K_B calculated from different graphical representation of the initial rates. Errors were calculated using 67% confidence (n=2).

1.5.2. Rates of DNA Alkylation by 10 Using Competition Kinetic Analysis

Alternatively, we measured the partitioning of activated leinamycin (**10**) between formation of the guanine adduct (**12**) and the hydrolysis product (**13**) as a function of DNA concentration. The products were quantitatively measured using HPLC.

The thiol-activation of **1** to generate the DNA-alkylation episulfonium (**10**) is a fast process $k_{act} = 1.6 \pm 0.3 \times 10^{-3}$ s^{-1}, ($t_{1/2} = 7.5 \pm 1.5$ min, Section 1.9.6.), thereby it does not limit the rate of noncovalent complex and covalent adduct formation. The products of this reaction are solely the guanine adduct (**12**) and the hydrolysis product (**13**) (Figure 13). The identity of the peaks in this HPLC were previously confirmed by LC-MS methods.

As expected, the yield of the guanine adduct increases with increasing DNA concentration (Figure 7). More interestingly, the alkylation rate reaches a plateau at high DNA concentrations when virtually all of the activated leinamycin in the reaction mixture becomes complexed with the duplex. This is consistent with a process involving a

reversible noncovalent binding step prior to DNA alkylation. This type of DNA-alkylation reaction can be analyzed in terms of Michaelis-Menten-type kinetics (Equation 1 and Equation 2), as has been recognized for other DNA-damaging agents. [27,40,41]

$$\text{LM*} + \text{DNA} \underset{k_{-1}}{\overset{k_1}{\rightleftharpoons}} \text{LM*} \bullet \text{DNA} \overset{k_2}{\longrightarrow} \text{LM-DNA} \qquad \textbf{Equation 1}$$
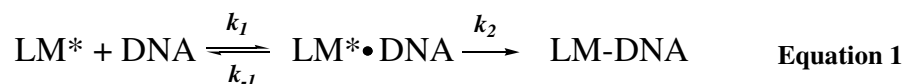
$$k_{obs} = \frac{k_2[DNA]}{K_M + [DNA]} \qquad \textbf{Equation 2}$$
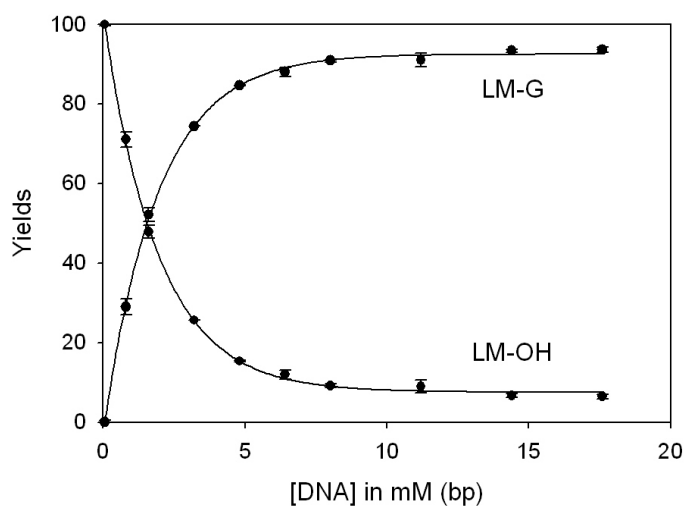
Figure 7. Yields of the DNA adduct (**12**, LM-G) and hydrolysis product (**13**, LM-OH) as a function of DNA concentration. Leinamycin (**1**, 400 μM) and β-mercaptoethanol (1.5 equiv, 600 μM) were incubated in the presence of varying concentrations of herring DNA in 50 mM MOPS buffer (pH 7.0) at 4 °C for 2 h. Products were analyzed by RP-HPLC and their amounts measured using the HPLC data. The applied DNA concentrations were as follows: 0 mM, 0.8 mM, 1.6 mM, 3.2 mM, 4.8 mM, 6.4 mM, 8 mM, 11.2 mM, 14.4 mM, 17.6 mM. The maximum error in these data was 1.95 %, calculated by statistical analysis.

Competition kinetic analysis employing the data in Figure 7 along with the rate constant measured independently for the hydrolysis of leinamycin (k_{H2O} = 4.3 ± 0.1 x 10^{-5} s^{-1}, $t_{1/2}$ = 5 ± 0.3 h, Section 1.9.6.) in the absence of DNA (Eqn 3-4) allows us to calculate the average velocity of the alkylation reaction at each DNA concentration examined. This is different from the initial rate measurements by UV (Section 1.5.1) in that there the fastest initial rate is calculated at each DNA concentration within the first 5 s of DNA alkylation. Here, we obtain DNA alkylation rates that is the average DNA alkylation rate over the full course of the reaction (full consumption of **10** ~ 40 min).

$$[LMOH] = k_{H20}[LM *_{total}]$$

Equation 3

$$\frac{[LM - G]}{[LMOH]} = \frac{k_2[DNA]}{\dfrac{(\dfrac{k_{-1}}{k_1} + [DNA])}{k_{OH}}} .... = \frac{k_{app}}{k_{OH}}$$

Equation 4

At saturating DNA concentrations the ratio of products **12** and **13** provide us with the maximum observed rate constant k_2 = 9.0 ± 0.5 x 10^{-4} s^{-1}, (t ½ = 13 ± 0.6 min) of DNA alkylation according to Equation 4. The apparent rate of DNA alkylation can be determined using this equation, by measuring the ratio of [**12**]/[**13**] (Equation 9 in Experimental). The calculated apparent rates of DNA alkylation were plotted vs. [DNA] (Figure 8) and are shown in Table 2.

_____
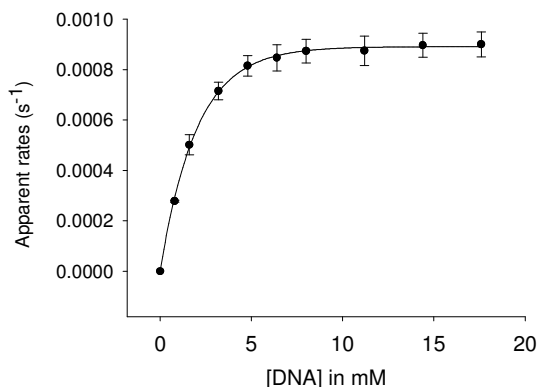
Figure 8. **The apparent rates of DNA alkylation by** 10 **as a function of DNA concentration. Errors were calculated using 67%**
confidence (n=2).

[DNA] (mM)	v_{app} (s^{-1}) x 10^4
0	0
0.8	2.78 ± 0.04
1.6	5.02 ± 0.40
3.2	7.15 ± 0.35
4.8	8.15 ± 0.41
6.4	8.47 ± 0.52
8	8.73 ± 0.47
11.2	8.75 ± 0.58
14.4	8.97 ± 0.48
17.6	9.00 ± 0.49

Table 2. **The apparent rates of DNA-alkylation by leinamycin. Errors were calculated using 67% confidence (n=2).**

A Hanes-Woolf plot [42] of these apparent velocities (Figure 9) yields the K_M (k_{-1}/k_1) = 1.05 ± 0.01 x 10^{-3} M, and confirmation of our rate constant k_2 = 9.0 ± 0.6 x 10^{-4} s^{-1}. Alternatively (and perhaps more appropriately), a Kitz-Wilson plot (Figure 9), [42,43] typically used for the analysis of covalent enzyme modification by mechanism-based inactivators and affinity-labeling agents, can be employed to obtain a K_I of 1.13 ± 0.01 x 10^{-3} M, k_{inact} = 9.7 ± 0.6 x 10^{-4} s^{-1}. These plots are all functionally equivalent in this context. The apparent association constants for activated leinamycin (**10**) obtained using this kinetic approach are comparable to those measured previously for the parent

compound (**1**) and its synthetic analogs under thermodynamic conditions described in Section 1.2.3. The calculated binding constant of **10** to duplex DNA, $K_B \sim 1/K_M = 935 \pm 26\ M^{-1}$ represents a weak noncovalent binding.

A

from y-intercept
$k_2 = 9.00 \pm 0.60 \times 10^{-4}\ s^{-1}$

from x-intercept
$K_m = 1.05 \pm 0.01 \times 10^{-3}\ M$

$1/v_{DNA}$

1/[DNA]

B

from y-intercept
$k_{inact} = 9.70 \pm 0.60 \times 10^{-4}\ s^{-1}$

from x-intercept
$K_I = 1.13 \pm 0.01 \times 10^{-3}\ M$

$t_{1/2}$ (min)

1/[DNA]
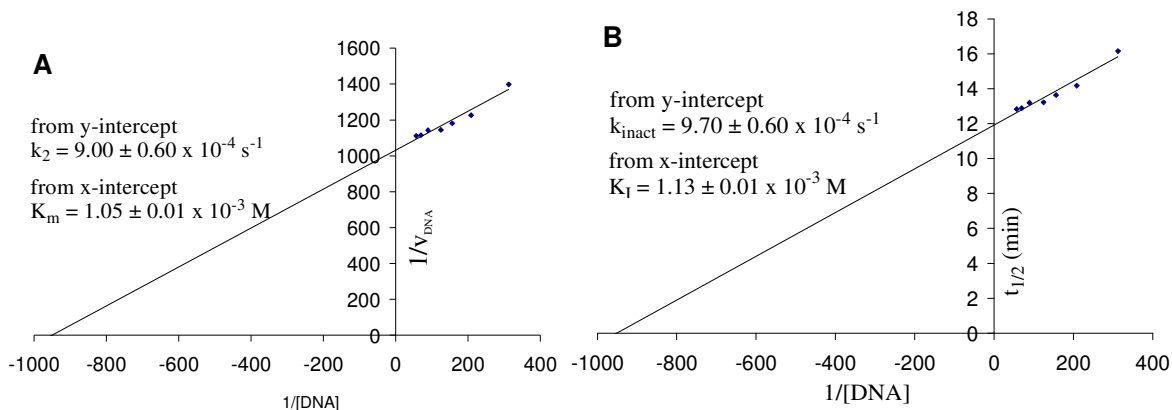
Figure 9. Hanes-Woolf plot (**A**) of the apparent rates of DNA alkylation and the Kitz-Wilson replot (**B**) of $t_{1/2}$ of DNA alkylation by leinamycin. Leinamycin (**1**, 400 μM) and β-mercaptoethanol (1.5 equiv, 600 μM) were incubated in the presence of varying concentrations of herring DNA in 50 mM MOPS buffer (pH 7.0) at 4 °C for 2 h. Products were analyzed by RP-HPLC and their amounts measured using the HPLC data. The applied DNA concentrations were as follows: 0 mM, 0.8 mM, 1.6 mM, 3.2 mM, 4.8 mM, 6.4 mM 8 mM, 11.2 mM, 14.4 mM, 17.6 mM. Errors were calculated using 67% confidence (n=2).

1.5.3. Comparison of the Kinetic and Thermodynamic Parameters Obtained by

The Initial Rate (UV) and Competition Kinetic (HPLC) Methods.

For a comparison, we tabulated the second order rate of DNA alkylation (k_2/K_M), K_M and K_B obtained by the two different methods: initial rates (UV), and competition kinetics in (Table 3). In addition the rate of activation of leinamycin and that of its hydrolysis is tabulated in the same table.

_____

	Initial Rates method (UV)	*Competition Method (HPLC)*
Second order DNA alk. k_2/K_M (*$M^{-1}s^{-1}$*)	4.32 ± 0.13	0.86 ± 0.03
Effective Molarity k_2/k_{dG} (*M*)	6.0 ± 0.4	3.4 ± 0.2
Rate acceleration versus hydrolysis $k_2/K_M / k_{H2O}/[H_2O]$	5.5×10^6 times	1.1×10^6 times
Rate of activation k_{act}	$1.6 \pm 0.3 \times 10^{-3}$ s^{-1} $t_{1/2}=7.5 \pm 1.5$ min	
Rate of hydrolysis $k_{OH \, of}$ *10*	$4.3 \pm 0.5 \times 10^{-5} s^{-1}$ $t_{1/2}=5.0 \pm 0.3$ h	

Table 3. Second order rate of DNA alkylation, Effective Molarity, Rate Acceleration and rate of activation and hydrolysis in the initial rate method (UV) and the competition kinetic method (HPLC). Reactions were carried out at the following temperatures: Initial rates method: 7 °C, Competition method: 4 °C. Errors were calculated using 67% confidence (n=2).

1.6. Measuring the Rate of the "Uncatalyzed" Reaction: Alkylation of 2'-Deoxyguanosine in TFE:Water Buffer

1.6.1. Alkylation of 2'-Deoxyguaosine by 10 in TFE:MOPS Buffer

The apparent association constants measured here for the interaction of activated leinamycin with duplex DNA are rather modest, $K_B = 935 \pm 26$ M^{-1} (for comparison, the binding constant for ethidium bromide is 9.5×10^6 M^{-1} and that for distamycin A is 2.5×10^7 M^{-1}.) [38,44] It is interesting to consider the extent to which this level of noncovalent binding can accelerate reaction of the alkylating agent with guanine residues in the double helix. To address this issue it is necessary to measure the rate of the "background or uncatalyzed reaction" of activated leinamycin with a 2'-deoxyguanosine residue that does not reside within the context of double-helical DNA.

Accordingly, we analyzed the reaction of activated leinamycin with the free nucleoside 2'-dG in a 1:1 (v/v) mixture of 2,2,2,-trifluoroethanol:MOPS buffer (50 mM, pH 7.0). This solvent system offers two distinct advantages for our studies:

(1) it provides a dielectric constant of about $\varepsilon \sim 55$, [45] comparable to that of the major groove of DNA (Figure 12), [46] where alkylation by leinamycin takes place.

(2) it suppresses the hydrolysis of activated leinamycin that would normally overwhelm an attempt to observe alkylation of the free 2'-deoxyguanosine nucleoside in aqueous solution. [8,47]

The 2'-deoxyguanosine adduct (**21**, Figure 10), its depurination product (**12**, Scheme 2) and hydrolyzed leinamycin (**13**, Scheme 2) are the only major products generated under these conditions (sample HPLCs in Figure 20). Competition kinetic analysis involving the independent measurement of the rate of hydrolysis under these conditions $k_{H2O,\varepsilon=55}$ = 6.6 x 10^{-6} s^{-1}, (t$_{1/2}$ = 29 ± 0.7 h) and measurement of the relative yields of LM-2'dG (**21**) and LM-OH (**13**) at several concentration yielded pseudo-first order rate constants at each applied 2'-dG concentrations (1 mM, 2 mM, 4 mM, 6 mM). These rate constants (Table 4) were plotted versus the concentration of 2'-deoxyguanosine (Figure 11), and the slope of this curve provided us with the second-order rate constant: 2.7 ± 0.2 x 10^{-4} M^{-1}s^{-1}
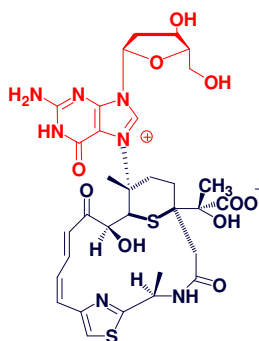
21

Figure 10. The 2'-deoxyguanosine adduct of leinamycin.

[2'-dG] (M)	$K\psi$ x 10^7 (s^{-1})
0.001	1.82 ± 0.05
0.002	3.74 ± 0.18
0.004	7.82 ± 0.12
0.006	12.72 ± 0.63

Table 4. The *pseudo*-first-order rate constants of alkylation of 2'-dG by activated leinamycin **10**.
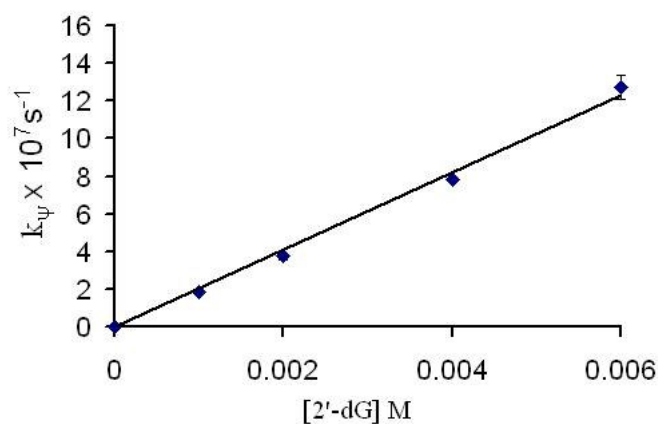
Figure 11. The *pseudo*-first-order rates of 2'-dG alkylation by **10** plotted vs. [2'-dG]. Conditions are described above. Concentrations of 2'-deoxyguanosine: 1 mM, 2 mM, 4 mM, 6 mM. The slope gives the second-order rate of 2'-dG alkylation: $k_{dG, 2nd}$ = 2.7 ± 0.2 x 10^{-4} $M^{-1}s^{-1}$. Errors were calculated using 67% confidence (n=2).

Major groove
$\varepsilon = 55$
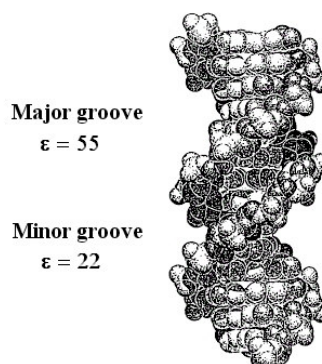
Minor groove
$\varepsilon = 22$

Figure 12. The grooves of the DNA duplex, showing their effective dielectric constants.

1.7. Rate Acceleration and Equivalent Molarity in the Major Groove of DNA for The N7-G Alkylation Reaction

There are only a few examples where rate acceleration by noncovalent binding of DNA-alkylating agent was measured. [28,33] Most of these examples involved agents with strong binding constants (CC-1065: $K_B \sim 10^6$ M^{-1}) [40], although an example involving a natural product with weaker binding (aflatoxin B1 epoxide: $K_B \sim 10^3$ M^{-1}) has been reported.[27] It is interesting to calculate how much the modest noncovalent binding of **1** can accelerate its DNA-damaging reaction.

Our measurements reported in this chapter allow us to calculate the rate acceleration provided by noncovalent binding of leinamycin in the major groove of DNA. Comparison of the apparent second-order rate constant for the reaction of leinamycin with duplex DNA ($k_2/K_M = 0.86$ M^{-1}s^{-1}) with the second-order rate constant for the alkylation of 2'deoxyguanosine (2.7 ± 0.2 x 10^{-4} M^{-1}s^{-1}) reveals a 3200 ± 100 fold rate enhancement. This represents a conservative estimate because the inherent reactivity of

guanine is *decreased* in the duplex as compared to monomeric nucleosides (measured in the yield of their reactions with simple alkylating agents like dimethylsulfate). Alternatively, we can think of rate acceleration in terms of effective molarity. [48,49] Our results indicate that the effective concentration (k_2/k_{dG}) of leinamycin in the major groove of DNA is 3.4 ± 0.1 M.

Two previous studies have considered how noncovalent binding favors the reaction of alkylating agents with DNA over that with water. [27,28] Such measurements are of great value, because hydrolysis is likely to be the primary reaction that competes with DNA alkylation. The apparent second-order rate constant for the reaction of the CC 1065 analogue (Figure 4) with duplex DNA is approximately 10^{10} times larger than the rate constant for the reaction of this compound with water. [28] The apparent second-order rate constant for the reaction of aflatoxin B_1 epoxide (Figure 4) with DNA is 2.3×10^6 times larger than the rate constant for hydrolysis. [27] Finally, the apparent second-order rate constant for the reaction of activated leinamycin with DNA is 1.1×10^6 times larger than the rate for its reaction with water. Large differences are seen in the magnitude of the kinetic advantage afforded by noncovalent DNA association for the various alkylating agents discussed here. This reflects an interplay of binding affinity, rigidity of the alkylating agent, and proper alignment of the reaction partners in the noncovalent complex.

1.8.Chapter Discussion and Conclusions

Noncovalent binding of natural products to DNA enhance their alkylation rate. [26,27] Noncovalent binding of **1** has been suggested and provided the foundation of our kinetic studies. We studied the alkylation of DNA by **1** using *pseudo*-Michaelis-Menten kinetics, using two different methods:

(1) Measurement of initial rates of DNA alkylation by **10** using a UV assay.

(2) Competition kinetics between the hydrolysis and DNA alkylation by **10** using HPLC based assay.

The active form of leinamycin (**10**) binds non-covalently to DNA prior to alkylation with a modest binding strength $K_B = 2\,065 \pm 60$ M^{-1} (initial rate method), $K_B = 935 \pm 26$ M^{-1} (competition kinetics method). During these reactions the activation of leinamycin was not a rate limiting factor, $t\,\frac{1}{2} < 8$ min compared to its hydrolysis, $t_{1/2,\,H2O} = 5.0 \pm 0.3$ h and DNA-alkylation reaction, $t_{1/2,\,[DNA]sat} = 0.1 \pm 0.01$ h (initial rates), $t_{1/2,\,[DNA]sat} = 0.3 \pm 0.02$ h (competition kinetics). We measured the rate of alkylation of 2'-deoxyguanosine in a mixture of TFE:MOPS buffer (50:50 v/v%, 2.7 ± 0.2 x 10^{-4} M^{-1} s^{-1}), which represented the background N7G alkylation reaction. The dielectric constant of this reaction mixture was parallel to that of the major-groove of DNA. The rate of thiol-activation of **1** was fast under these conditions ($t_{1/2} = 9.3 \pm 0.3$ min). The alkylation of N7G in ds-DNA is ~ 5650 times (initial rates) or ~ 3200 times (competition kinetics) faster than alkylation of N7 in 2'-dG. The effective molarity of leinamycin in the major groove of DNA was found to be ~ 6.0 M (initial rates) or ~ 3.4 M (competition kinetics). This exceeds the value of 0.8 M observed by Taylor and Dervan for guanine alkylation by an α-bromoketone tethered via a seven-atom linker to a triple helix-forming oligonucleotide bound in the major groove

of DNA. [33] The effective molarity of leinamycin is superior to that achieved by many synthetic systems that catalyze bimolecular reactions [48] but is modest compared to the effective molarity seen for many unimolecular and enzyme-catalyzed reactions. [49-51] Finally, the DNA alkylation by activated leinamycin is 5.5 million times (initial rates) or 1.1 million times (competition kinetics) faster than its hydrolysis under physiological conditions.

Noncovalent association of activated leinamycin with DNA is not remarkably strong, but has profound functional consequences. Noncovalent binding yields a nearly 5650-fold (initial rates) or 3200-fold (competition kinetics) rate enhancement for the alkylation of guanine residues in duplex DNA versus the free 2'-deoxyguanosine nucleoside. The apparent second-order rate constant for the reaction of activated leinamycin with DNA is 5.5 million times (initial rates) or 1.1 million times (competition kinetics) larger than the rate for its reaction with water. Thereby, noncovalent association of leinamycin with the duplex drives the natural product predominantly toward the formation of the guanine adduct rather than hydrolysis under physiologically-relevant conditions.

Finally, we devised a mathematical description of epoxide-episulfonium equilibrium on and off DNA, and its kinetic consequences using the "Rapid Equilibrium Assumption Method" [52] (Section 1.9.12.) and the method of "King & Altman" [53] (Section 1.9.13.).

Noncovalent binding can concentrate reactive intermediates near the double helix, favoring reactions with DNA over those with water or other biomolecules. There are known biologically-active agents that gain their efficient DNA-alkylating properties via

_____

noncovalent binding to DNA,[26,27] for example aflatoxin B_1 epoxide (Figure 4, $K_B \sim 1400$ M^{-1}) and the "left-half" of azinomycin B (Figure 4, **19**, $K_B \sim 1000$ M^{-1}, Chapter 5). Both compounds are epoxides, and their DNA alkylation takes place faster than that of a small molecular epoxide, glycidol. In addition, the competitive and fast hydrolysis of these agents does not result in appreciable yields of the hydrolysis products. The antitumor antibiotic CC1065 [28] and duocarmycin A[29-31,32] possess additional DNA-alkylating functional groups, and also show enhanced DNA alkylation via noncovalent DNA binding (Figure 4).

1.9. Experimental

1.9.1. Materials and Methods.

Leinamycin (**1**) was a gift from researchers at Kyowa Hakko Kogyo Ltd. Additional reagents were purchased from the following suppliers and were of the highest purity available: MOPS buffer, sodium acetate and sodium phosphate buffers, trifluoroethanol, triethylamine, Aldrich Chemical Co. (Milwaukee, WI); HPLC grade solvents (water, acetonitrile, ethanol), Fisher (Pittsburgh, PA); herring sperm DNA, Roche Molecular Biochemicals (Indianapolis, IN); HPLC vials, National Scientific Corporation; analytical HPLC columns, Varian Inc. (Palo Alto, CA). HPLC: Varian Prostar Dynamax, vs. 5.1. LC-MS: ThermoFinnigan TSQ7000 triple-quadrupole with API2 source.

1.9.2. DNA Alkylation by Leinamycin in Aqueous Buffer Followed by UV Spectroscopy

The following DNA concentrations were applied: 0.4 mM, 0.6 mM, 0.8 mM, 1.2 mM, 2 mM, 4 mM, 6 mM and 10 mM. For simplicity, we describe the reaction with 2 mM DNA, here. In a 400 μL short-path UV cuvette (0.2 mM) the following components were mixed: 284 μL water, 16 μL leinamycin (5 mM in acetonitrile), 40 μL buffer (500 mM MOPS, pH 7.4 in water), 40 μL β-mercaptoethanol (10 mM in water) at 7 °C. The components were thoroughly mixed with the help of a long plastic pipette tip and the cuvette was placed into a thermostated UV cuvette holder for the activation of leinamycin (10 min). Finally, 20 μL DNA (40 mM in water) was mixed well into the cuvette (45 sec mixing time) and UV scans were carried out over the next 20 min every 5 s.

1.9.3. DNA Alkylation by Leinamycin Using Competition Kinetics

In a typical reaction the following components were mixed in microcentrifuge tubes (500 μL) in a cold-room at 4 °C: MOPS buffer (10 μL of a 500 mM stock solution), β-mercaptoethanol (10 μL of 6 mM fresh stock in water), DNA (0-59 μL of a 30 mM solution in water), water (72-23 μL). Mixtures were vortexed gently, and the reaction was initiated with the addition of leinamycin (8 μL of a 5 mM solution in acetonitrile). The final solution was vortexed gently (10 s). The resulting mixtures were incubated at 4°C for 6 h. The final concentrations of DNA were: 0 mM, 0.8 mM, 1.6 mM, 3.2 mM, 4.8 mM, 6.4 mM, 8 mM, 11.2 mM, 14.4 mM and 17.6 mM. After 6 h the mixtures were extracted at 4°C with 100 μL butanol (twice) to isolate the hydrolysis product **13** and to remove additional small organic molecules (β-mercaptoethanol, **1** and activated leinamycin, **10**). The butanol extracts were collected, frozen on dry ice and dried in a speed-vac instrument. Dried samples were further stored at –20 °C for HPLC analysis. The remaining aqueous phase containing our adducted DNA was treated with 200 μL DNA precipitating solution (0.3 M sodium acetate in 70% ethanol, pH 5.0). Mixtures were vortexed and placed on dry ice for freezing for 10-20 min. The frozen samples were centrifuged at 4°C in an Eppendorf 5415 C centrifuge at 10.000 r.p.m. for 30 min to assure complete precipitation of the adducted DNA. The supernatant of the centrifuged samples was carefully discarded and the remaining white pellets were washed with 100 μL 80% ethanol in water (twice). Pellets might be invisibly small-sized. The ethanol-wash was discarded and the samples were dried under a stream of nitrogen gas. Samples can be stored at -20 °C before the heat-induced depurination reactions. For the depurination reactions, the dried DNA-adduct samples were dissolved in 50 mM MOPS

solution at room temperature (150 μL, pH 7.0) and incubated on a heat-block at 70°C for 1 h to assure complete depurination. After 1 h the mixtures were cooled back to room temperature. The guanine adduct (**12**) was extracted with butanol 150 μL (twice). The organic extracts were collected, frozen on dry ice and dried in a speed vacuum instrument until complete dryness (~ 2 h). Samples can be stored at -20 °C before HPLC analysis.

1.9.4. HPLC Analysis of the Yields of The Guanine Adduct (12) and The Hydrolysis Product (13).

Dried samples were removed from the freezer (-20 °C) prior to HPLC-injection and dissolved into 150 μL of the HPLC-injection mixture (90% A and 10% B, where A, 0.2% trifluoroacetic acid, pH 2.0; B, acetonitrile). 25 μL of this mixture was injected onto a reversed-phase, narrow-bore analytical HPLC column: 0.2 mm x 250 mm x 5 μm x 120 Å, C-18, SUPELCO. HPLC separations were done by a gradient elution program shown in Table 5. The eluents were: A, 0.2% trifluoroacetic acid, pH 2.0 and B, acetonitrile. HPLC was carried out by a VARIAN ProStar 210 HPLC instrument with Star Chromatography Workstation vs. 5.1.1. The wavelength of detection was 324 nm. Sample HPLC-s are shown in Figure 13.

_____

Time (min)	%A:	%B:	Flow rate (ml/min)
0	90	10	0.2
46	64	36	0.2
52	35	65	0.2
56	35	65	0.2
62	90	10	0.2
72	90	10	0.2

Table 5. HPLC gradient elution solvent system used for the analysis of our reactions. Eluents: A, 0.2% trifluoroethanol, pH 2.0; B, acetonitrile.
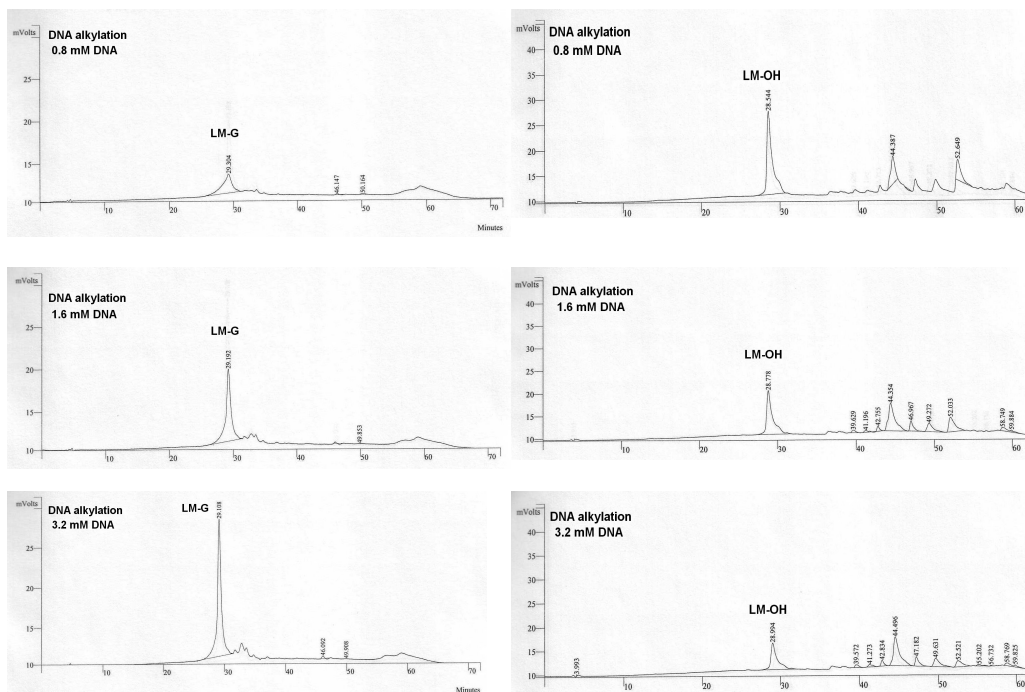
Figure 13. HPLC chromatogram of the products of the DNA and of the 2'-deoxyguaosine alkylation reactions by leinamycin. Retention times: leinamycin-guanine adduct (**12**) 26.5 min; leinamycin-2'-deoxyguanosine adduct, 27.0 min; leinamycin-hydroxide (**13**), 29.5 min; leinamycin (**1**) 45.5 min; activated leinamycin (**10**) (thiol conjugate), 53 min. The concentration of DNA shown: 0.8 mM, 1.6 mM, 3.2 mM. DNA was incubated in the presence of **10** at 4°C for 2 h, extracted with butanol to isolate **13**. Ethanol precipitation, heat induced depurination followed by butanol extraction was used to extract **12**.

28

1.9.5. Calculation of the Relative Yields of Guanine Adduct (12) and Hydrolysis Product From HPLC Peak Area (13).

We assumed that their extinction coefficients at our detection wavelength (324 nm) are determined solely by the *Z*, *E*-5-(thiazol-4-yl)-penta-2,4-dienone portion of the molecules and that their extinction coefficient at 324 nm are the same. Accordingly, the peak sizes (P_{12}, P_{13}) were measured at each applied DNA concentration (Figure 13), since only these two products are formed in the reactions. The relative percentage yields were calculated by calculating the percentage each peak area (P_{12} or P_{13}) would add to the total peak area ($P_{12} + P_{13}$) of these two products (Equation 5 and Equation 6). The relative yields were then plotted against the concentration of DNA (Figure 7, in Section 1.5.2).

$$rel\%13 = \frac{100\,P_{13}}{(P_{13} + P_{12})}$$

Equation 5

$$rel\%12 = \frac{100\,P_{12}}{(P_{13} + P_{12})}$$

Equation 6

1.9.6. Measurement of the Rate of Hydrolysis (k_{H2o}) of *Activated* Leinamycin (10) in the Absence of DNA.

All reactions were carried out at 4 °C in a cold-room. For every reaction in our present studies the following stock solutions were placed in the cold-room for cooling prior to reaction: MOPS buffer (500 mM, pH 7.0), β-mercaptoethanol in water (6 mM), leinamycin in acetonitrile (5 mM) and a stop mixture (90% A and 10% B where A: 0.2% trifluoroacetic acid pH 2.0; B: acetonitrile), TFE, water (HPLC grade). After 30 minutes reactions were set up in 500 μL microcentrifuge tubes as follows: MOPS (20 μL, 500

mM, pH 7.0), β-mercaptoethanol (20 μL, 6 mM in water), and water (144 μL). This solution was gently vortexed (10 s). Reactions were initiated with the addition of **1** (16 μL of a 5 mM solution in acetonitrile), and after gentle vortexing (10 s), sample collection began. At different times (0 min, 1 min, 2 min, 4 min, 8 min, 12 min, 18 min, 30 min, 50 min, 5 h, 8 h, 24 h) 15 μL aliquots were taken from the mixture and immediately mixed with the stop mixture (115 μL), vortexed for 20 s and placed on top of dry ice for freezing. Frozen samples were stored in a freezer at -20 °C. Before HPLC injection the samples were quickly melted at room temperature, vortexed (5 s) and 25 μL of this mixture was immediately injected into the HPLC and analyzed by our method shown in Table 5. Alternatively, to confirm our analysis, we also carried out sample analyses as was described by Asai et al.[17] The appearance of **10** was followed (Figure 14) for the calculation of the rate constant of the activation of the natural product (**1**). The activation reaction was fast, a non-rate-limiting reaction: $k_{act} = 1.6 \pm 0.3 \times 10^{-3}$ s^{-1}, ($t_{1/2} = 7.5 \pm 0.5$ min) (Figure 15; Equation 7). The degradation of the activated leinamycin (**10**) was followed from our HPLCs (Figure 14), and plotted as a semi-logarithmic function (Equation 8) vs. time (Figure 16). The slope yields the rate constant of hydrolysis of **10** in aqueous buffer $k_{H2O} = 4.3 \pm 0.1 \times 10^{-5}$ s^{-1}, ($t_{1/2} = 5 \pm 0.3$ h). The measurements were carried out twice, independently and the errors were calculated by means of statistical analysis using confidence values at the 67% confidence level.
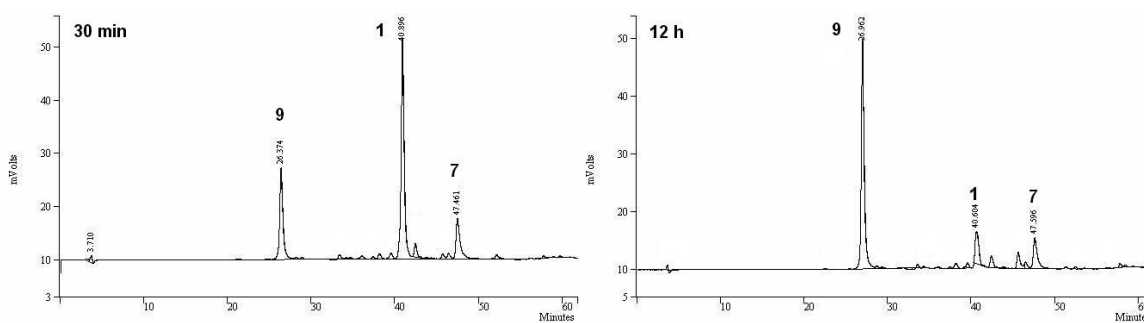
Figure 14. Sample HPLCs showing the appearance of activated leinamycin (**10**) in the reactions between **1** and β-mercaptoethanol. Conditions are given in experimental. HPLCs are shown for sample collections at 30 min, 12 h.

$$\ln \frac{[LM^*]}{[LM^*]_{init}} = k_{act}t + C \qquad \textbf{Equation 7}$$
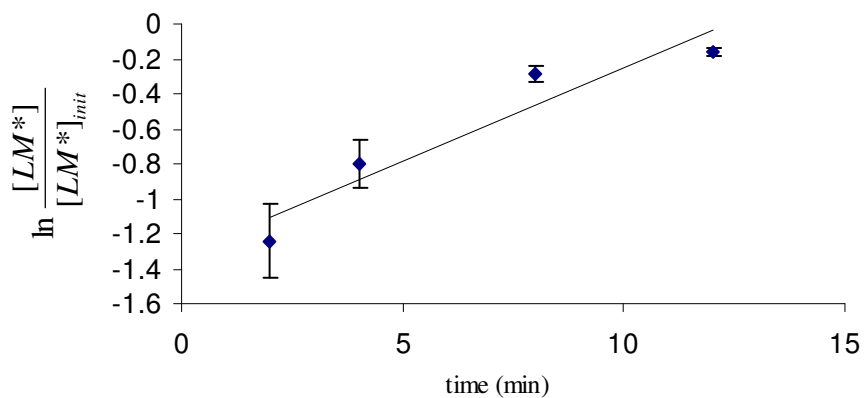
Figure 15. **The semi-logarithmic plot for the calculations of the first order rate constant of activation of leinamycin in aqueous buffer (*left, k_{act} = 1.6 ± 0.3 x 10^{-3} s^{-1}, t$_{1/2}$ = 7.5 ± 1.5 min). Errors were calculated using 67% confidence (n=2).**

$$\ln \frac{[LM^*]}{[LM^*]_0} = -k_{H2O}*t + C \qquad \textbf{Equation 8}$$
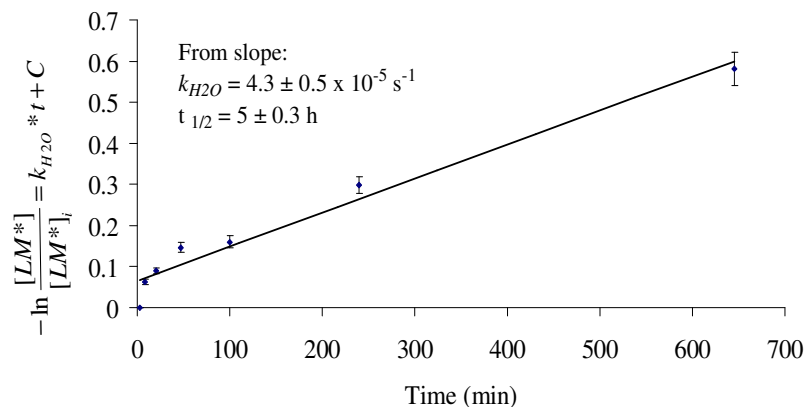
Figure 16. The semi-logarithmic plot to calculate the first-order rate constant of the hydrolysis of **10**. The calculated first-order rate of hydrolysis of **10**: $k_{H2O} = 4.3 \pm 0.05 \times 10^{-5}$ s^{-1}, $t_{1/2} = 5 \pm 0.3$ h. Errors were calculated using 67% confidence (n=2).

1.9.7. Calculation of the Apparent Rates of DNA Alkylation at Each DNA Concentration, K_2, K_M.

To calculate the apparent rate of DNA alkylation at each DNA concentration, we applied a blend of competition kinetic analysis with Michaelis-Menten enzyme kinetics employing the data in (Figure 7), using Equation 1-Equation 1. We measured the rate-constant for the hydrolysis of **10** (k_{H2O}) in the absence of DNA. The maximum rate constant for DNA-alkylation (DNA-alkylation at saturating DNA concentration, k_2) was calculated using the ratio of the peak sizes: (P_{12} / P_{13} = k_2 / k_{H2O}). The apparent rates of DNA alkylation at each DNA concentration were calculated similarly using the ratio of the guanine-adduct and hydrolysis products formed as shown in Equation 9.

$$\frac{v_{app}}{k_{H2O}} = \frac{P_{12[DNA]}}{P_{13[DNA]}} \qquad \textbf{Equation 9}$$

The calculated apparent rate constants were plotted vs. the concentration of DNA (Figure 8), and summarized in Table 2.

1.9.8. Measurement of the Rate of Hydrolysis of 10 (k_{H2o}) in TFE:Buffer.

Reactions were carried out at 4 °C in a cold-room. After thermal equilibration of the stock solutions the reaction components were mixed in 500 μL microcentrifuge tubes as follows: MOPS (20 μL of 500 mM, pH 7.0), β-mercaptoethanol (20 μL, 50 mM) **1** (400 μM), water (44 μL), TFE (100 μL to a final 50% v/v). Reactions were initiated with the addition of leinamycin (16 μL of a 5 mM solution in acetonitrile). The mixture was gently vortexed (5 s). *Note:* [H$_2$O] in this mixture: 27.8 M. Sample collection and quenching began as follows: at different times (0 min, 1 min, 2 min, 4 min, 8 min, 12 min, 18 min, 30 min, 50 min, 5 h, 8 h, 24 h, 48 h, 96 h, 168 h) 15 μL aliquots were taken from the mixture and immediately mixed with the stop mixture (115 μL of a 0.2 % v/v TFA solution in water, pH = 2.0), vortexed for 20 s and placed on top of dry ice for freezing. Frozen samples were stored in a freezer at -20 °C. Before HPLC injection the samples were quickly melted at room temperature, vortexed and 25 μL was injected into the HPLC. The appearance of *activated leinamycin* (**10**) was followed for the calculation of the rate constant of activation $k_{act.}$ We plotted ln([LM*]/[LM*]$_i$) versus time (Figure 17). The activation reaction was a fast, non-rate-limiting reaction: $k_{act} = 1.8 \pm 0.1 \times 10^{-3}$ s^{-1}, ($t_{1/2} = 9.3 \pm 0.5$ min). The degradation of the activated leinamycin (**10**) was followed from our HPLC (Figure 18), and plotted as a semi-logarithmic function (Equation 11) vs. time (Figure 19). The slope of this plot yields the rate constant of hydrolysis of **10** in the TFE:buffer mixture $k_{H2O,TFE} = 6.6 \pm 0.2 \times 10^{-6}$ s^{-1}, ($t_{1/2} = 29 \pm 0.7$ h). The measurements were carried out twice, independently and the errors were calculated by means of statistical analysis using confidence values at the 67% confidence level. *Note:*HPLC analyses of these reactions were confirmed by the method as reported by Asai et.al. [17]

_____

$$\ln \frac{[LM^*]}{[LM^*]_i} = k_{act,TFE} + C$$

Equation 10
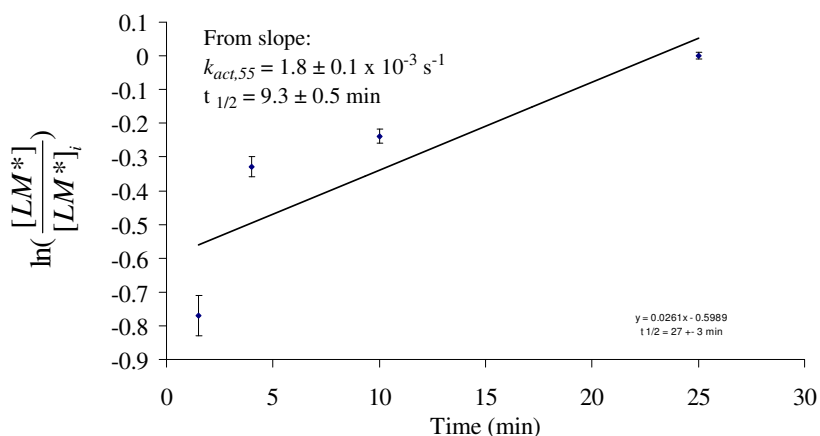
Figure 17. Plot of appearance of activated leinamycin (**10**) vs. time for the calculation of the rate of activation of leinamycin in TFE:MOPS buffer. Conditions are described in the experimental. Sample collection times: 2 min, 5 min, 10 min, 30 min. Errors were calculated using 67% confidence (n=2).
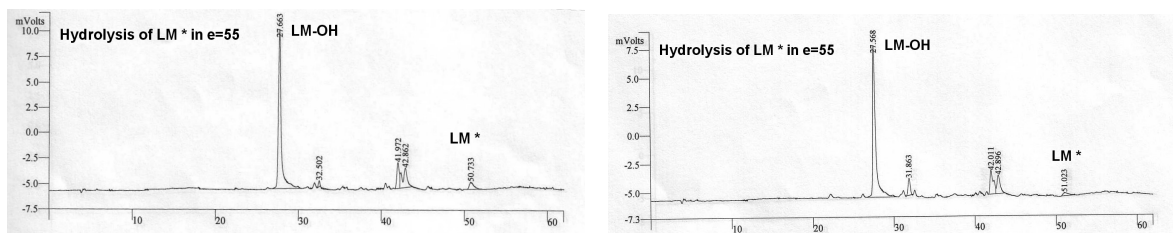
Figure 18. HPLC traces of the hydrolysis reaction of **1** in TFE:buffer mixture. The times of sample collection are given in the text above. HPLCs are shown for times: 24 h, 48 h. The disappearance of the episulfonium peak at 51 min (**10**) was followed.

$$-\ln \frac{[LM^*]}{[LM^*]_{initial}} = k_{H2O,TFE} + C$$

Equation 11

_____
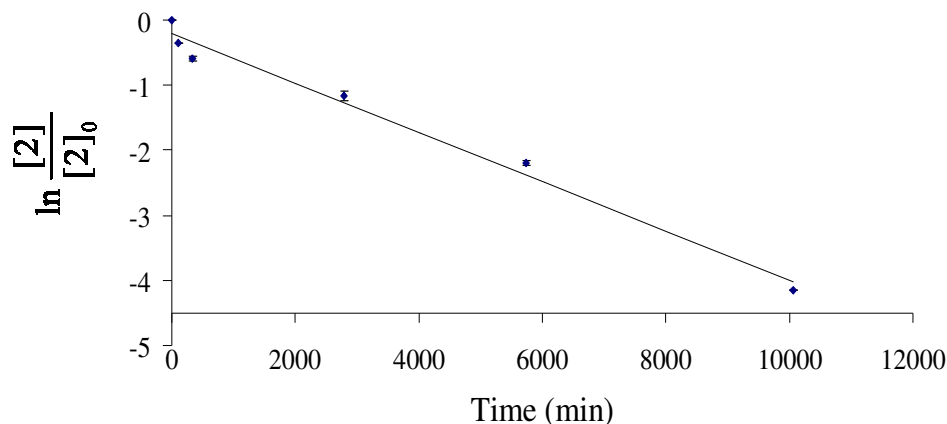
Figure 19. Plot of disappearance of **10** vs. time in the hydrolysis of leinamycin in TFE:MOPS buffer. Conditions are given in experimental. The slope of the curve yields the rate of hydrolysis: $k_{TFE} = 5.3 \pm 0.3$ x 10^{-6} s^{-1}, $t_{1/2} = 38.5 \pm 3.5$ h. Errors were calculated using 67% confidence (n=2).

1.9.9. Reaction of *Activated* (10) Leinamycin with 2'-Deoxyguanosine in TFE:Buffer;

the Formation of 21.

Reactions were carried out at 4 °C in a cold-room. After stock solutions reached thermal equilibrium, reactions mixtures were made up in 500 µL microcentrifuge tubes accordingly: MOPS buffer (20 µL of a 500 mM solution, pH 7.0), 2'-deoxyguanosine (0-100 µL 12 mM solution in TFE), β-mercaptoethanol (20 µL of a 50 mM solution in water), water (44 µL), TFE (100-0 µL). The mixture was vortexed gently (5 s), then the reactions were started with the addition of **1** (16 µL in acetonitrile). The final concentrations of 2'-dG were as follows: 1 mM, 2 mM, 4 mM, 6 mM. The final TFE content was 50 % v/v. At different times (2 h, 4 h, 8 h, 24 h, 48 h, 96 h, 168 h) small aliquots (15 µL) were immediately injected into the stop mixture at 4 °C (135 µL of a 0.2% v/v TFA solution in water, pH 2.0) vortexed for 10 s and frozen on dry ice. Frozen samples were further stored at -20 °C.

_____
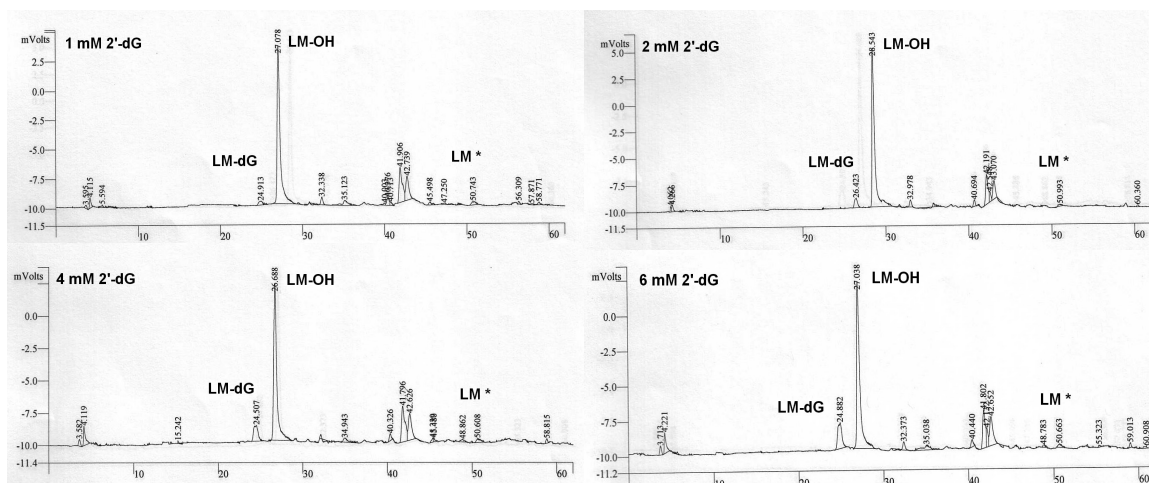
Figure 20. Sample HPLCs showing the separation of products in the reaction of leinamycin with 2'-deoxyguanosine. Peaks: 4 min: buffer, RSH; 24 min: LM-dG (**21**) + LM-G (**12**), 27 min, 44 min: leinamycin; 52 min: activated leinamycin. Conditions are described in Experimental. HPLCs are shown for 8 h reaction time at the following 2'-deoxyguanosine concentrations: 1 mM, 2 mM, 4 mM, 6 mM.

1.9.10. HPLC Analysis of The 2'-Deoxyguanosine Reactions.

Samples were melted prior to HPLC injection, vortexed, and 25 μL was injected to the HPLC, onto an RP-C18, narrow-bore analytical HPLC-column, as described in Section 1.9.10. Sample HPLC-s are shown in Figure 20. The ratios of the peak integrals for the peak of the guanine-adduct (**21**, 27 min) and the hydrolysis product (**13**, 29 min) were calculated from our HPLC-s (Figure 20, Section 1.9.7.), and used for the calculation of the pseudo-first-order rate constants and the second order rate of 2'-deoxyguanosine alkylation in the TFE:buffer mixture (Section 1.9.11.).

1.9.11. Calculation of the First- and Second-Order Rates of 2'-deoxyguanosine Alkylation by 10.

First, the rate of hydrolysis of **10** had been determined in TFE:buffer mixture independently (Section 1.9.8.). Then, we calculated the ratios of the guanine vs. hydrolysis product peak integrals (P_{21} / P_{13}) from our HPLC plots in the 2'-dG alkylation reactions (Figure 20). The pseudo first order rates of the 2'-dG reactions were calculated from this ratio, using Equation 12. To calculate the second order rate of alkylation, the pseudo-first order rates were plotted vs. the corresponding concentrations of 2'-deoxyguanosine (Figure 11) and the slope of this plot gave us the second order rate of alkylation ($k_G = 2.7 \pm 0.2 \times 10^{-4}\,\mathrm{M^{-1}s^{-1}}$). The alkylation reactions were carried out twice, independently, and errors were calculated using 67% confidence. The first and second order rates are collected in table 2.

$$\frac{[LM-G]}{[LM-OH]} = \frac{k_{dG,1st}}{k_{TFE}} \qquad\qquad \textbf{Equation 12}$$

1.9.12. Kinetic Description of the Precovalent DNA-Binding and DNA Alkylation by Leinamycin Episulfonium in Equilibrium with its Epoxide Form Using The Rapid Equilibrium Assumption Method [52]

In Section 1.5.2., Equation 1 shows the Michaelis-Menten kinetic scheme for DNA alkylation by leinamycin. We showed that DNA alkylation by leinamycin takes place from a pre-equilibrium complex between the DNA and the episulfonium ion. It was shown by NMR that the N7-nitrogen of guanine in DNA is attached directly to the C6-

carbon of the episulfonium ion (**10** in Scheme 2). [8] The episulfonium ion exists in equilibrium with the epoxide form (**11**, Scheme 2). [17] With their structural similarities we assume that epoxide also binds non-covalently to DNA, and the epoxide-episulfonium equilibrium can interconvert these structures to one-another both on DNA and off DNA as shown in Scheme 4. In this Section we show the derivation of a kinetic equation for the Michaelis-Menten interpretation of this complex equilibrium using the Rapid Equilibrium Assumption method.

$$[\text{Epi}] \; + \; [\text{DNA}] \quad \xrightleftharpoons{K_B} \quad [\text{Epi*DNA}] \quad \xrightarrow{k_2} \quad \text{LM-DNA (LMG)}$$

$$K_2 \Updownarrow \qquad\qquad\qquad K_4 \Updownarrow$$

$$[\text{Epo}] \; + \; [\text{DNA}] \quad \underset{K_3}{\longrightarrow} \quad [\text{Epo*DNA}]$$
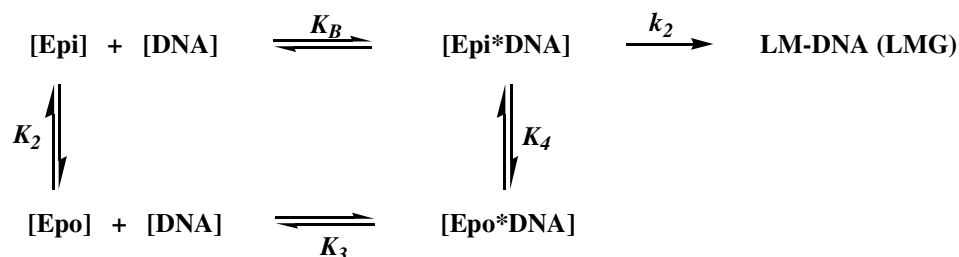
Scheme 4. The equilibrium between the epoxide (**11**) and episufonium (**10**) of leinamycin, their noncovalent DNA binding and interconversion on DNA.

In the rapid equilibrium assumption method, we assume that k_2 is much smaller than any of the preceding rates. The formation of the DNA adduct kinetically can be described by Equation 13.

$$v_0 = k_2[Epi * DNA]$$

Equation 13

The total concentration of activated leinamycin in this system is expressed in Equation 14.

$$[LM*] = [Epi] + [Epi * DNA] + [Epo] + [Epo * DNA]$$

Equation 14

_____

Their ratio (Equation 13/Equation 14) is expressed in Equation 15.

$$\frac{v_0}{[LM*]} = \frac{k_2[Epi*DNA]}{[Epi]+[Epi*DNA]+[Epo]+[Epo*DNA]}$$
Equation 15

Multiplying by [LM*] will give a more handy form in Equation 16.

$$v_o = \frac{k_2[LM*][Epi*DNA]}{[Epi]+[Epi*DNA]+[Epo]+[Epo*DNA]}$$
Equation 16

We may introduce *Vmax* into this equation by a relationship from enzyme kinetics (Equation 17) to yield Equation 18.

$$k_2[LM*] = V_{max}$$
Equation 17

$$v_o = \frac{V_{max}[Epi*DNA]}{[Epi]+[Epi*DNA]+[Epo]+[Epo*DNA]}$$
Equation 18

Now, we will divide each term in Equation 18 by *[Epi]*, so that we will be able to use the equilibrium constants (K_B, K_2, K_3, K_4).

$$v_o = \frac{V_{max}\dfrac{[Epi*DNA]}{[Epi]}}{1+\dfrac{[Epi*DNA]}{[Epi]}+\dfrac{[Epo]}{[Epi]}+\dfrac{[Epo*DNA]}{[Epi]}}$$
Equation 19

Equation 19 can be written into Equation 20, which only has the following terms: *[DNA]* and K_i.

$$v_o = \frac{K_B[DNA]V_{max}}{1+K_B[DNA]+K_BK_4[DNA]+\dfrac{1}{K_2}}$$
Equation 20

To further shape this similar to a Michaelis-Menten equation, we divide both the numerator and the denominator by K_B. In addition besides, I returned V_{max} to $k_2[LM*]$.

_____

$$v_0 = \frac{k_2[DNA][LM*]}{\dfrac{1}{K_B} + [DNA] + K_4[DNA] + \dfrac{1}{K_B K_2}} = \frac{k_2[DNA][LM*]}{\dfrac{K_2+1}{K_B K_2} + [DNA](1+K_4)}$$

Equation 21

In the general Michaelis-Menten equation the [DNA] term does not have a multiplying

factor. We can cancel it by dividing both the numerator and the denominator terms with

(1+K_4) to yield Equation 22.

$$v_0 = \frac{\dfrac{k_2[DNA][LM*]}{(1+K_4)}}{\dfrac{K_2+1}{K_B K_2(K_4+1)} + [DNA]}$$

Equation 22

The laws of thermodynamics dictate the following relationship:

$$K_4 = \frac{1}{K_B K_2 K_3}$$

Equation 23

From the above equation we can express (1+K_4) shown in   Equation 24.

$$1 + K_4 = \frac{K_B K_2 K_3 + 1}{K_B K_2 K_3}$$

Equation 24

Equation 23 and Equation 24 will allow us to rearrange Equation 22 to a format that will

allow us to apply our final rate equation to the "open-loop" version of Scheme 4 (shown

as Scheme 5). The "open-loop" equilibrium is analogous to the one in Scheme 4. "*Adding*

or removing a pathway from an equilibrium system in a way that does not change the

number of equilibrating species will not change or affect the equilibrium." [52] The open

loop scheme has the following parameters: k_2, K_B, K_2, K_3.

_____

$$[\text{Epi}] + [\text{DNA}] \xrightleftharpoons{K_B} [\text{Epi*DNA}] \xrightarrow{k_2} \text{LM-DNA (LMG)}$$

$$K_2 \updownarrow$$

$$[\text{Epo}] + [\text{DNA}] \xrightleftharpoons[K_3]{} [\text{Epo*DNA}]$$
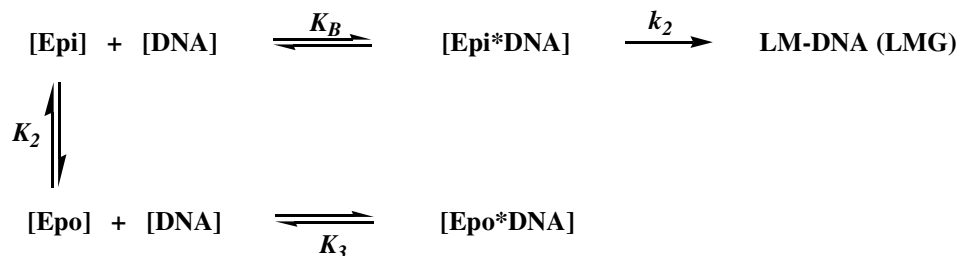
Scheme 5. The "open-loop" form of the complex equilibrium between the leinamycin-epoxide and the leinamycin episulfonium ion. This is analogous thermodynamically and kinetically to the closed equilibrium circle.

$$v_0 = \frac{\dfrac{\dfrac{k_2[DNA][LM*]}{K_B K_2 K_3 + 1}}{K_B K_2 K_3}}{\dfrac{K_2 + 1}{K_B K_2 (\dfrac{K_B K_2 K_3 + 1}{K_B K_2 K_3}) + [DNA]}} = \frac{\dfrac{k_2 K_B K_2 K_3 [DNA][LM*]}{K_B K_2 K_3 + 1}}{\dfrac{K_3(K_2 + 1)}{K_B K_2 K_3 + 1} + [DNA]} = \frac{k_{cat}}{K_M + [DNA]}$$

Equation 25

Equation 25 is a clear Michaelis-Menten equation, which can be used to express k_{cat} (Equation 26), K_M (Equation 27) and the specificity constant: k_{cat}/K_M (Equation 1).

$$k_{cat} = \frac{k_2 K_B K_2 K_3}{K_B K_2 K_3 + 1}$$

Equation 26

$$K_M = \frac{K_3(K_2 + 1)}{K_B K_2 K_3 + 1}$$

Equation 27

$$\frac{k_{cat}}{K_M} = \frac{k_2 K_B K_2}{(K_2 + 1)}$$

Equation 28

_____

1.9.13. Kinetic Description of Precovalent DNA-Binding and DNA Alkylation by Leinamycin Episulfonium in Equilibrium With its Epoxide Form Using the Method Of King and Altman [53]

In Scheme 4 we show that both the epoxide and episulfonium ion of leinamycin can bind to DNA noncovalently, and their conversion may happen on and off DNA. Here, we show the derivation of the Michaelis-Menten parameters using the method of King and Altman. For our discussion here, we used the "open-loop" form of the equilibrium (Scheme 5).

In this method, N is the number of enzyme species in equilibrium (N = 4 in our case). Each enzyme species will be described with N-1 number of rate equations: E1 → E2 for example has two enzyme species but only one rate equation connects them.

(1) We generate a "master-plan", which is an equilateral polygon with N sides Figure 21.

Figure 21. The master-plan for the King and Altman discussion of our open-loop mechanism with four-"enzyme" species.

(2) We assign each corner of our polygon with the name of the enzyme (leinamycin) species in the equilibrium-loop (Figure 22).

_____

[Epi] + [DNA]   [Epi:DNA]

[Epo] + [DNA]   [Epo:DNA]
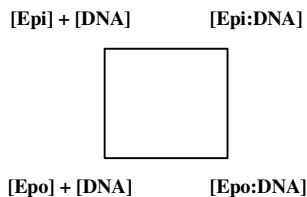
Figure 22. The master-plan showing the leinamycin ("enzyme") containing species on the appropriate corners.

(3) Next, let us assign each side of the master-plan polygon with the appropriate rate-constants. Here, the method of King and Altman connects the enzyme species that precedes the product formation ([Epi:DNA]) to the first one ([Epo:DNA]) with the rate constant of the product formation (k_p). This may look misleading in chemical sense, but mathematically it is appropriate (Figure 23).

[Epi] + [DNA]   **[Epi:DNA]**

k_1

k_{-1}

k_2 k_{-2} k_p

k_{-3}

[Epo] + [DNA] k_3 **[Epo:DNA]**
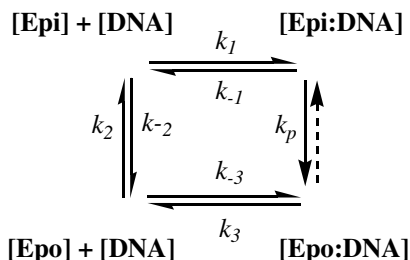
Figure 23. The master-plan with its sides assigned to the microscopic rate-constants and the rate of DNA-adduct formation (k_p).

(4) We can generate open-loops in four different ways (Figure 24).

(1)   (2)   (3)   (4)
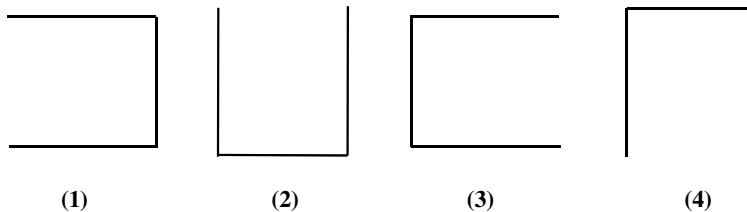
Figure 24. The four possible loop equilibrium.

(5) We need to generate an N x N matrix (4 x 4 here).

    i. Repeat the row in Figure 24 four times (Figure 25)

    ii. For each pattern in a row assign one of the corners as the final product (shown with a ball in Figure 25).

    iii. Make the sides of the open loops into single-direction arrows, and label them with first order rate constants. All products with [DNA] component will be formed with the first order rate constant multiplied by [DNA].

    iv. "Formulate" the assigned product in four different ways, so that the corresponding rate constants will be positive.

    v. Discard the matrix members that have a k_{rev} factor.

Steps (5.1. – 5.5.) are shown in Figure 25.

_____
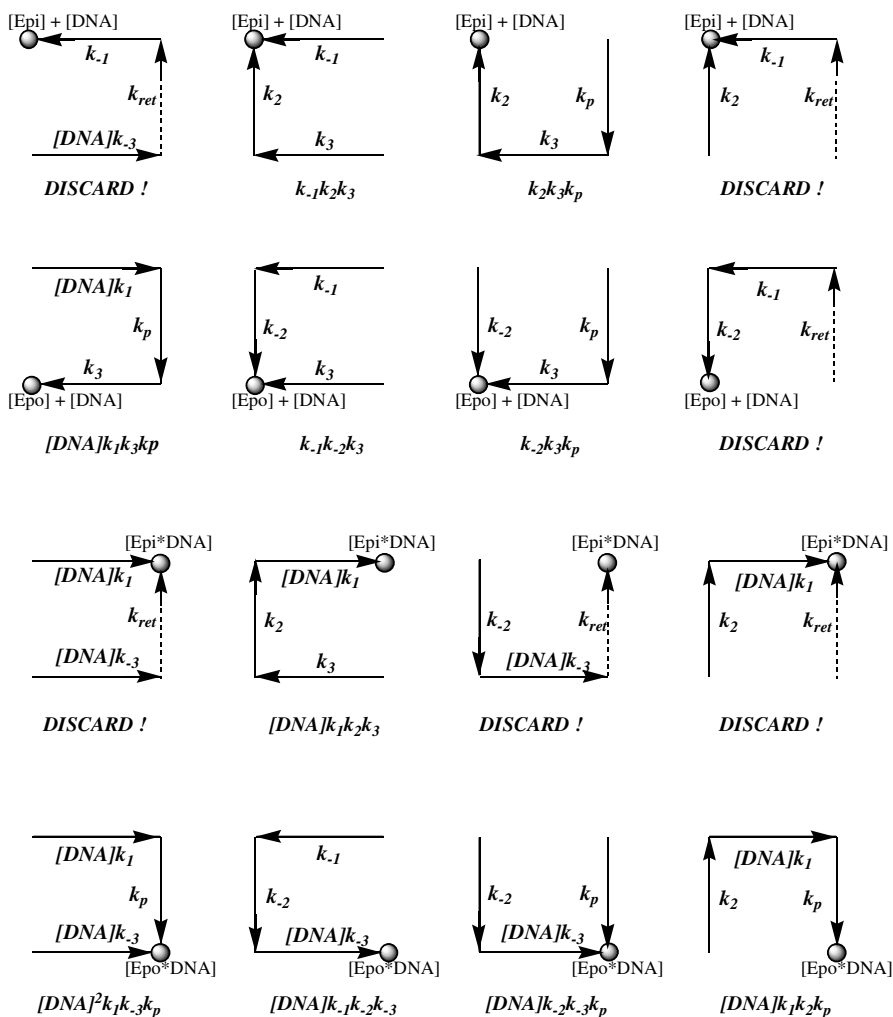
Figure 25. The 4 x 4 matrix of "open-loops" for the construction of the rate equation of the epoxide/episulfonium equilibria off/on DNA.

(6) We can start the construction of the rate equation algebraically now. At intermediate stages this equation will look complicated, however it will simplify with simple mathematical operations. First, we need to realize that the "sum" of all terms in the matrix is the total concentration of activated leinamycin [LM*] containing species in

_____

the equilibrium. This will be 10 total terms, since there are 6 DISCARD terms containing the rate factor: $k_{rev.}$ In addition to the six discard terms, we will discard all those having a rate factor: k_p, since the magnitude of these will be smaller than the rest of the terms, k_p being the slowest step in the total system. Thereby:

$$sum = k_{-1}k_2k_3 + k_{-1}k_{-2}k_3 + [DNA](k_1k_2k_3 + k_{-1}k_{-2}k_{-3})$$

Equation 29

The ratio of the DNA-bound episulfonium to the total activated leinamycin is:

$$\frac{[epi*DNA]}{[LM*]} = \frac{[DNA]k_1k_2k_3}{sum}$$

Equation 30

From the third row it is evident that the product forms:

$$v_0 = k_p[epi*DNA]$$

Equation 31

A combination of Equation 30 and Equation 31 will form Equation 32:

Equation 32

$$v_o = \frac{k_p[DNA][LM*]k_1k_2k_3}{k_{-1}k_2k_3 + k_{-1}k_{-2}k_3 + [DNA](k_1k_2k_3 + k_{-1}k_{-2}k_{-3})}$$

The Michaelis-Menten equation has a [DNA] term factored by one. We divide both numerator and denominator by $(k_1k_2k_3+k_{-1}k_{-2}k_{-3})$:

$$v_0 = \frac{\dfrac{k_p[DNA][LM*]k_1k_2k_3}{k_1k_2k_3 + k_{-1}k_{-2}k_{-3}}}{\dfrac{k_{-1}k_2k_3 + k_{-1}k_{-2}k_3}{k_1k_2k_3 + k_{-1}k_{-2}k_{-3}} + [DNA]}$$

Equation 33

_____

From Equation 33 we can read out the Michaelis parameters:

$$k_{cat} = \frac{k_p k_1 k_2 k_3}{k_1 k_2 k_3 + k_{-1} k_{-2} k_{-3}}$$

Equation 34

$$K_M = \frac{k_{-1} k_2 k_3 + k_{-1} k_{-2} k_3}{k_1 k_2 k_3 + k_{-1} k_{-2} k_{-3}}$$

Equation 35

Simplification of the k_{cat} and the K_M expression is simple by dividing both the numerator and denominator by $k_1 k_2 k_3$:

$$k_{cat} = \frac{k_p}{1 + \dfrac{1}{K_1 K_2 K_3}} = \frac{k_p K_1 K_2 K_3}{K_1 K_2 K_3 + 1}$$

Equation 36

$$K_M = \frac{k_{-1} k_2 k_3 + k_{-1} k_{-2} k_3}{k_1 k_2 k_3 + k_{-1} k_{-2} k_{-3}} = \frac{\dfrac{k_{-1} k_2 k_3}{k_1 k_2 k_3} + \dfrac{k_{-1} k_{-2} k_3}{k_1 k_2 k_3}}{\dfrac{k_1 k_2 k_3}{k_1 k_2 k_3} + \dfrac{k_{-1} k_{-2} k_{-3}}{k_1 k_2 k_3}} = \frac{\dfrac{1}{K_1} + \dfrac{1}{K_1 K_2}}{1 + \dfrac{1}{K_1 K_2 K_3}} = \frac{\dfrac{K_2 + 1}{K_1 K_2}}{\dfrac{K_1 K_2 K_3 + 1}{K_1 K_2 K_3}} =$$

$$= \frac{K_1 K_2 K_3 (K_2 + 1)}{K_1 K_2 (K_1 K_2 K_3 + 1)} = \frac{K_3 (K_2 + 1)}{K_1 K_2 K_3 + 1}$$

Equation 37

This is exactly the same equation that we obtained by the Rapid Equilibrium Assumption Method (Equation 26 and Equation 27).

References

1.   Hara, M.; Asano, K.; Kawamoto, I.; Takiguchi, T.; Katsumata, S.; Takahashi, K.; Nakano, H., Leinamycin, a new antitumor antibiotic from Streptomyces; producing organism, fermentation and isolation. *Journal of Antibiotics* **1989,** 42, 1768-1774.

2.   Hara, M.; Saitoh, Y.; Nakano, H., DNA strand scission by the novel antitumor antibiotic leinamycin. *Biochemistry* **1990,** 29, 5676-5681.

3.   Hara, M.; Takahashi, I.; Yoshida, M.; Asano, K.; Kawamoto, I.; Morimoto, M.; Nakano, H., DC 107, a novel antitumor antibiotic produced by a Streptomyces sp. *Journal of Antibiotics* **1989,** 42, 333-335.

4.   Kanda, Y.; Ashizawa, T.; Saitoh, Y.; Saito, H.; Gomi, K.; Okabe, M., Synthesis and antitumor activity of leinamycin derivatives: Modifications of C-8 hydroxy and C-9 keto groups. *Bioorg. Med. Chem. Lett.* **1998,** 8, 909-912.

5.   Ashizawa, T.; Kawashima, K.; Kanda, Y.; Gomi, K.; Okabe, M.; Ueda, K.; Tamaoki, T., Antitumor activity of KF22678, a novel thioester derivative of leinamycin. *Anti-Cancer Drugs* **1999,** 10, 829-836.

6.   Kanda, Y.; Ashizawa, T.; Kakita, S.; Takahashi, Y.; Kono, M.; Yoshida, M.; Saitoh, Y.; Okabe, M., Synthesis and Antitumor Activity of Novel Thioester Derivatives of Leinamycin. *J. Med. Chem.* **1999,** 42, 1330-1332.

7.   Kanda, Y.; Ashizawa, T.; Kawashima, K.; Ikeda, S.-i.; Tamaoki, T., Synthesis and antitumor activity of novel C-8 ester derivatives of leinamycin. *Bioorg. Med. Chem. Lett.* **2003,** 13, 455-458.

_____

8.   Asai, A.; Hara, M.; Kakita, S.; Kanda, Y.; Yoshida, M.; Saito, H.; Saitoh, Y., Thiol-Mediated DNA Alkylation by the Novel Antitumor Antibiotic Leinamycin. *J. Am. Chem. Soc.* **1996,** 118, 6802-6803.

9.   Bassett, S.; Urrabaz, R.; Sun, D., Cellular response and molecular mechanism of antitumor activity by leinamycin in MiaPaCa human pancreatic cancer cells. *Anti-Cancer Drugs* **2004,** 15, 689-696.

10.   Foye, W. O.; Lemke, T. L.; Williams, D. A.; Editors, *Principles of Medicinal Chemistry*. 1995; p 995 pp.

11.   Gates, K. S., Mechanisms of DNA Damage by Leinamycin. *Chem. Res. Toxicol.* **2000,** 13, 953-956.

12.   Behroozi, S. J.; Kim, W.; Dannaldson, J.; Gates, K. S., 1,2-Dithiolan-3-one 1-Oxides: A Class of Thiol-Activated DNA-Cleaving Agents That Are Structurally Related to the Natural Product Leinamycin. *Biochemistry* **1996,** 35, 1768-1774.

13.   Mitra, K.; Kim, W.; Daniels, J. S.; Gates, K. S., Oxidative DNA cleavage by the antitumor antibiotic leinamycin and simple 1,2-dithiolan-3-one 1-oxides: Evidence for thiol-dependent conversion of molecular oxygen to DNA-cleaving oxygen radicals mediated by polysulfides. *J. Am. Chem. Soc.* **1997,** 119, 11691-11692.

14.   Manuelidis, L.; Chen, T. L., A unified model of eukaryotic chromosomes. *Cytometry* **1990,** 11, 8-25.

15.   Daban, J.-R., Physical constraints in the condensation of eukaryotic chromosomes. Local concentration of DNA versus linear packing ratio in higher order chromatin structures. *Biochemistry* **2000,** 39, 3861-3866.

16. Gates, K. S.; Zang, H., Sequence Specificity of DNA Alkylation by the Antitumor Natural Product Leinamycin. *Chem. Res. Toxicol.* **2003,** 16, 1539-1546.

17. Asai, A.; Saito, H.; Saitoh, Y., Thiol-independent DNA cleavage by a leinamycin degradation product. *Bioorg. Med. Chem.* **1997,** 5, 723-729.

18. Hansen, M. R.; Hurley, L. H., Pluramycins. Old Drugs Having Modern Friends in Structural Biology. *Accounts Chem. Res.* **1996,** 29, 249-58.

19. Gates, K. S.; Nooner, T.; Dutta, S., Biologically Relevant Chemical Reactions of N7-Alkylguanine Residues in DNA. *Chem. Res. Toxicol.* **2004,** 17, 840.

20. Suh, D.; Chaires, J. B., Criteria for the mode of binding of DNA binding agents. *Bioorg. Med. Chem.* **1995,** 3, 723-8.

21. Breydo, L.; Barnes, C. L.; Gates, K. S., Two (E,E)- and (Z,E)-thiazol-5-ylpenta-2,4-dienones. *Acta Crystallogr. C* **2002,** C58, o447-o449.

22. Breydo, L.; Zang, H.; Gates, K. S., Synthesis and noncovalent DNA-binding properties of thiazole derivatives related to leinamycin. *Tetrahedron Lett.* **2004,** 45, 5711-5716.

23. Dervan, P. B., Design of sequence-specific DNA-binding molecules. *Science* **1986,** 232, 464-71.

24. Baker, B. F.; Dervan, P. B., Sequence-specific cleavage of DNA by N-bromoacetyldistamycin. Product and kinetic analyses. *J. Am. Chem. Soc.* **1989,** 111, 2700-12.

25. Povsic, T. J.; Dervan, P. B., Sequence-specific alkylation of double-helical DNA by oligonucleotide-directed triple-helix formation. *J. Am. Chem. Soc.* **1990,** 112, 9428-30.

26.   Zang, H.; Gates, K. S., DNA Binding and Alkylation by the \"Left Half\" of Azinomycin B. *Biochemistry* **2000,** 39, 14968-14975.

27.   Johnson, W. W.; Guengerich, F. P., Reaction of aflatoxin B1 exo-8,9-epoxide with DNA: kinetic analysis of covalent binding and DNA-induced hydrolysis. *Proc. Natl. Acad. Sci. Unit. States. Am.* **1997,** 94, 6121-6125.

28.   Warpehoski, M. A.; Harper, D. E., Enzyme-like Rate Acceleration in the DNA Minor Groove. Cyclopropylpyrroloindoles as Mechanism-Based Inactivators of DNA. *J. Am. Chem. Soc.* **1995,** 117, 2951-2952.

29.   Asai, A.; Nagamura, S.; Saito'J, H., A Novel Property of Duocarmycin and Its Analogues for Covalent Reaction with DNA. *J. Am. Chem. Soc.* **1994,** 116, 4171-4177.

30.   Boger, D. L.; Garbaccio, R. M., Catalysis of the CC-1065 and duocarmycin DNA alkylation reaction: DNA binding induced conformational change in the agent results in activation. *Bioorg. Med. Chem.* **1997,** 5, 263-276.

31.   Boger, D. L.; Hertzog, D. L.; Bollinger, B.; Johnson, D. S.; Cai, H.; Goldberg, J.; Turnbull, P., Duocarmycin SA shortened, simplified, and extended agents: a systematic examination of the role of the DNA binding subunit. *J. Am. Chem. Soc.* **1997,** 119, 4977-4986.

32.   McClean, S.; Costelloe, C.; Denny, W. A.; Searcey, M.; Wakelin, L. P. G., Sequence selectivity, cross-linking efficiency and cytotoxicity of DNA-targeted 4-anilinoquinoline aniline mustards. *Anti Canc. Drug Des.* **1999,** 14, 187-204.

33.   Taylor, M. J.; Dervan, P. B., Kinetic Analysis of Sequence-Specific Alkylation of DNA by Pyrimidine Oligodeoxyribonucleotide-Directed Triple Helix Formation. *Bioconjugate Chem.* **1997,** 8, 354-364.

_____

34.   Cullis, P. M.; Merson-Davies, L.; Weaver, R., DNA alkylation sites of nitrogen mustards conjugated to polyamines and their implications for polyamine-DNA interactions. *Chem. Comm. (Cambridge)* **1998,** 16, 1699-1700.

35.   Zhang, Y.; Chen, F. X.; Mehta, P.; Gold, B., Groove- and sequence-selective alkylation of DNA by sulfonate esters tethered to lexitropsins. *Biochemistry* **1993,** 32, 7954-65.

36.   Cullis, P. M.; Merson-Davies, L.; Weaver, R., Conjugation of a Polyamine to the Bifunctional Alkylating Agent Chlorambucil Does Not Alter the Preferred Crosslinking Site in Duplex DNA. *J. Am. Chem. Soc.* **1995,** 117, 8033-4.

37.   Mehta, P.; Church, K.; Williams, J.; Chen, F.-X.; Encell, L.; Shuker, D. E. G.; Gold, B., The Design of Agents To Control DNA Methylation Adducts. Enhanced Major Groove Methylation of DNA by an N-Methyl-N-nitrosourea Functionalized Phenyl Neutral Red Intercalator. *Chem. Res. Toxicol.* **1996,** 9, 939-948.

38.   Baliga, R.; Crothers, D. M., The Kinetic Basis for Sequence Discrimination by Distamycin A. *J. Am. Chem. Soc.* **2000,** 122, 11751-11752.

39.   Semmelhack, M. F.; Gallagher, J. J., The Effect on DNA Cleavage Potency of Tethering a Simple Cyclic Enediyne to a Netropsin Analog. *J. Org. Chem.* **1994,** 59, 4357-4359.

40.   Warpehoski, M. A.; Harper, D. E., Enzyme-like Rate Acceleration in the DNA Minor Groove. Cyclopropylpyrroloindoles as Mechanism-Based Inactivators of DNA. *J. Am. Chem. Soc.* **1995,** 117, 2951.

41.   Geacintov, N. E., Is intercalation a critical factor in the covalent binding of mutagenic and tumorigenic polycyclic aromatic diol epoxides to DNA? *Carcinogenesis* **1986,** 7, 759-766.

42.   Silverman, R. B., *The Organic Chemistry of Enzyme Catalyzed Reactions.* Academic Press: San Diego, 2000.

43.   Kitz, R.; Wilson, I. B., Esters of methanesulfonic acid as irreversible inhibitors of acetylcholinesterase. *J. Biol. Chem.* **1962,** 237, 3245-49.

44.   Baguley, B. C.; Denny, W. A.; Atwell, G. J.; Cain, B. F., Potential antitumor agents. 34. Quantitative relationships between DNA binding and molecular structure for 9-anilinoacridines substituted in the anilino ring. *J. Med. Chem.* **1981,** 24, 170-177.

45.   Sierra, P. S.; Tejuca, C. C.; Garcia-Blanco, F.; Oliva, C. D.; Sierra, J. C.; Gorostidi, G. E., Properties of 2,2,2-trifluoroethanol/water mixtures: acidity, basicity, and dipolarity. *Helv. Chim. Acta* **2005,** 88, 312-324.

46.   Jadhav, V. R.; Barawkar, D. A.; Ganesh, K. N., Polarity Sensing by Fluorescent Oligonucleotides: First Demonstration of Sequence-Dependent Microenvironmental Changes in the DNA Major Groove. *J. Phys. Chem. B* **1999,** 103, 7383-7385.

47.   Nooner, T.; Dutta, S.; Gates, K. S., Chemical Properties of the Leinamycin-Guanine Adduct in DNA. *Chem. Res. Toxicol.* **2004,** 17, 942-949.

48.   Cacciapaglia, R.; Di Stefano, S.; Mandolini, L., Effective Molarities in Supramolecular Catalysis of Two-Substrate Reactions. *Accounts Chem. Res.* **2004,** 37, 113-122.

_____

49.   Page, M. I.; Jencks, W. P., Entropic contributions to rate accelerations in enzymic and intramolecular reactions and the chelate effect. . *Proc. Natl. Acad. Sci. Unit. States. Am.* **1971,** 68, 1678-1683.

50.   Bruice, T. C.; Pandit, U. K., Intramolecular models depicting the kinetic importance of fit in enzymic catalysis. *Proc. Natl. Acad. Sci. Unit. States. Am.* **1960,** 46, 402-4.

51.   Wolfenden, R.; Snider, M. J., The depth of chemical time and the power of enzymes as catalysts. *Accounts Chem. Res.* **2001,** 34, 938-945.

52.   Leskovac, V.; Editor, *Comprehensive Enzyme Kinetics*. 2003; p 442 pp.

53.   King, E. L.; Altman, C., A schematic method of deriving the rate laws for enzyme-catalyzed   reactions.   *J.   Phys.   Chem.*   **1956,**   60,   1375-8

_____

Chapter 2. Leinamycin: A Structurally Novel DNA Intercalator

2.1. DNA-Intercalators

It is well known that the preferred reversible, noncovalent DNA binding mode of planar polyaromatic ligands (dimethyl acridine, ethidium bromide, Figure 27) is intercalation.[1] In the process of intercalation, the planar, polyconjugated chromophore of the small organic molecule is sandwiched between the DNA base pairs with their π-electrons taking part in a stacking interaction (Figure 26). This process will change the structure of DNA by increasing the distances and decreasing the winding angle between the DNA-bases flanking the intercalators. Numerous results have suggested that a minimum of two fused-rings (as in naphthalene, Figure 27) are necessary for intercalative binding, [2,3] and intercalating drugs with two fused-rings have been classified as "minimal intercalators" (Figure 28, Section 2.2.).[4] Intercalation can be a strong interaction (K_B ~ $10^4 – 10^6 \text{ M}^{-1}$).
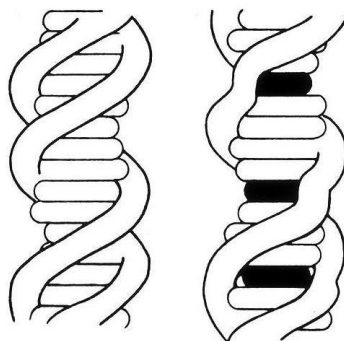
Figure 26. Physical changes in the structure of duplex-DNA upon intercalation. With intercalators stacked in between the DNA base-pairs, the DNA molecule elongates along its long axis. At the same time, the winding angle between the "sandwiching" base-pairs will decrease causing the unwinding of the DNA duplex. Furthermore, these structural alterations will change the physical and spectroscopic properties of its solutions.

_____
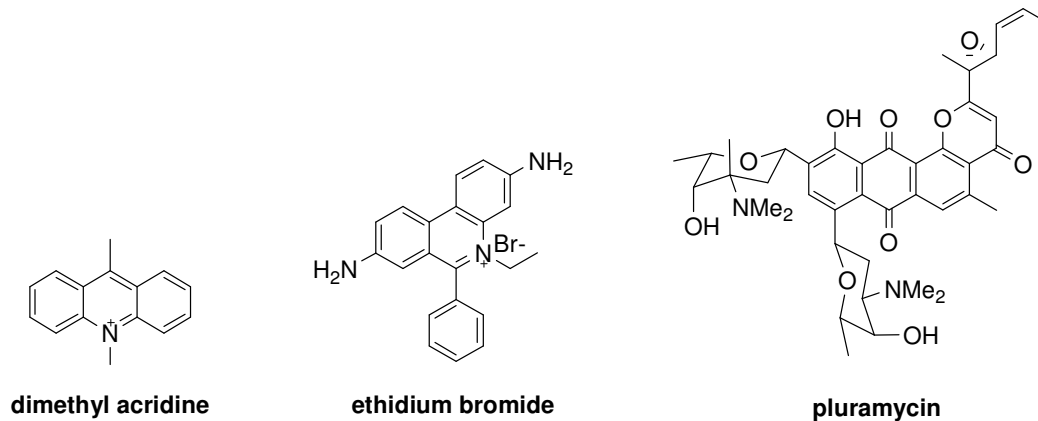
Figure 27. Classical DNA intercalators (dimethyl acridine, ethidium bromide). Finally, the structure of pluramycin, an anti-tumor antibiotic is presented.

2.2. Non-Classical DNA-Intercalators

There are small organic molecules with only one aromatic ring or non-fused ring-structures that have been recognized to intercalate DNA (Figure 28). Such is the anticancer drug esperamicin A1 (Figure 28). This molecule binds the major groove of DNA with its methoxyanthranilate ring intercalated.[5] Amiloride is an interesting non-classical intercalator.[6] The non-fused bi-thiazole component of the complex antitumor antibiotic bleomycin is an intercalating agent.[7] Finally, the newly discovered antibiotic, nitrofurantoin, used in the treatment of urinary tract inflammations, has two isolated five-membered rings that have shown DNA-intercalation. [8]

_____
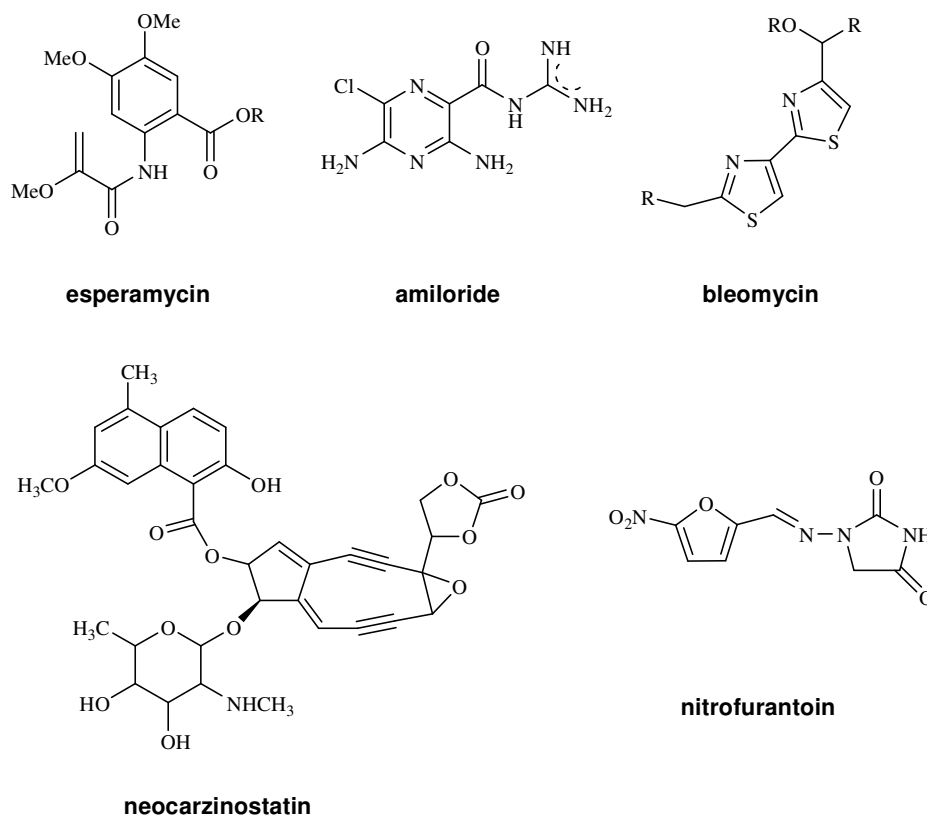
Figure 28. Nonclassical DNA intercalators structures. Esperamycin, amiloride, bleomycin, nitrofurantoin and neocarzinostatin.

2.3. Biological Consequences of DNA-Intercalation

There are biological consequences of DNA-intercalation.[9-11] Intercalators can cause inhibition of cell-growth, induction of cell death and cell transformation, changes in the chromatin structure, and inhibition of virtually any DNA or RNA dependent enzymes (polymerases, nucleases, helicases).[12,13] Several intercalating molecules can induce single strand breaks in the DNA of mammalian cells.[14,15] This usually happens via topoisomerase poisoning.[16] Topoisomerases are responsible for the separation of DNA strands in replication and transcription. Photochemical induction of DNA nicks in the

presence of ethidium bromide (a widely used laboratory reagent!) has been noted. [17,18]

DNA intercalation can also have medicinally useful properties. For example, there are

known antitumor agents that are DNA-intercalators, like pluramycin (Figure 27)[19] or the

anticancer aza-anthrapyrazoles.[20]

2.4. Changes in DNA Structure and the Detection of Intercalation

Intercalation causes changes in the structure of duplex DNA as discussed above.[21]

This binding causes changes in the physical and spectral properties of DNA solutions,

which can be followed to identify the intercalative binding mode of organic molecules.

2.4.1. Biophysical Tools for Detecting Intercalation

Viscosity:

The lengthening and stiffening of DNA caused by intercalation (Figure 26) causes

a characteristic increase in the viscosity of DNA-containing solutions. [1,22] Hydrodynamic

methods such as viscosity or sedimentation measurements thus can provide evidence of

intercalation.[23] To date there have not been published reports that show that other DNA-

binding modes could give a positive response in these assays. Changes in viscosity can be

measured in an Oswald-type flow viscometer by measuring changes in flow-time of the

solution through the viscometer. Normally, the relative viscosities are calculated as $\eta = (t/t_o)$, where t is the flow time of DNA containing solution with the intercalators, and t_o is

the flow time of DNA solution without the intercalators. From this measurement, the

DNA fragment length (L/L_o) is usually calculated as $(\eta/\eta_o)^{1/3}$ and plotted versus r, where

η_o represents the viscosity of DNA solution alone, r represents the ratio of ligand to DNA

base pairs. In our current work (Chapter 2 and 4), we used this assay to monitor changes

_____

in viscosity as a consequence of DNA-alkylation. Alkylation of DNA by small organic molecules incapable of DNA intercalation does not show increases in viscosity. [24]

DNA-unwinding:

Intercalation unwinds supercoiled plasmid DNA (Figure 26).[25,26] Most groove binders do not cause DNA unwinding, [23] although a few do,[27] so this phenomenon is generally used an evidence of intercalation. The unwinding of the DNA-helix can be studied by various experimental tools like sedimentation,[28] viscometry,[29] electron microscopy,[30] and electrophoretic methods.[31] We used DNA agarose-gel electrophoresis of plasmid DNA to monitor leinamycin-induced DNA winding effects (Section 2.7.). For noncovalent DNA intercalators, where the DNA topoisomers cannot be separated by electrophoresis due to their equilibrium exchange, unwinding usually is studied on linearized plasmid DNA, which is ligated into a supercoiled form after the addition of the suspected intercalator. [32] Depending on the degree of original unwinding, the supercoiled form will have different number of supercoils. The resulting different topoisomers can be separated and visualized on agarose gel. It is important to note here that the electrophoretic mobility of these topoisomers decreases with fewer numbers of supercoils, reaching the lowest mobility for the open-circular form of DNA (see gel image in Figure 33). Once rewinding takes place in the opposite direction (Figure 29), the electrophoretic mobility increases again. Since the agarose-gel is a chiral medium, the mirror-image topoisomers (topoisomers with opposite direction of superhelical structures but the same number of supercoils) will show different electrophoretic mobility. Overall, an agarose gel separation of these results is a tilted Gaussian distribution of topoisomers

_____

(Figure 29 and Figure 33) along the direction of electric current versus a linear increase

in the concentration of the intercalator.
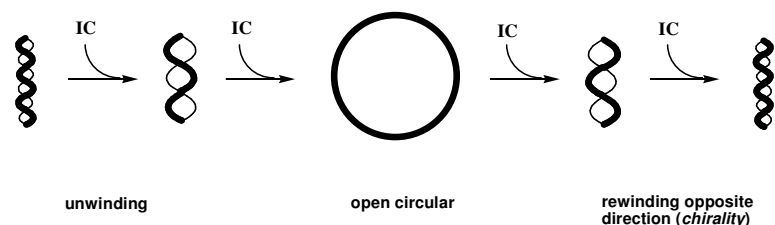
Figure 29. Plasmid DNA unwinding by increasing concentration of the intercalators. **IC**: intercalators.

Changes in the Melting Point of DNA:

Finally, it is worth mentioning that an increase in thermal stability of the DNA-

duplex accompanies intercalation. This is evidenced in the increase in the melting

temperature (T_m) of the DNA. [33] Note that this effect is by no means unique to

intercalation and is seen for any DNA-binding ligand.

2.4.2. Spectroscopic Analysis of Intercalation

Drug-DNA intercalation changes the diffraction (X-ray)[34], optical (fluorescence [35]

and UV-vis[23]) and magnetic (NMR)[34] properties of DNA and that of the intercalator.

Accordingly, Fluorescence Contact Energy Transfer (FCET) and NMR experiments have

been utilized in our research. These methods are introduced below.

Fluorescence Contact Energy Transfer experiment:

The FCET phenomenon involves transfer of energy from the donor (DNA) to the

acceptor (intercalators) as pictured in Figure 30. [23,36] DNA is photoexcited in the range of

200-300 nm. In the absence of intercalators, DNA will relax this excess energy in

_____

molecular motions, which ultimately means that DNA shows no observable fluorescence under normal conditions. However, when an intercalator is stacked in between the base-pairs of DNA, this excitation energy can be quenched by energy transfer to the intercalators (Figure 30). Finally, the energy obtained from DNA can be emitted from the intercalator molecule as light at a wavelength of its normal emission peak. This energy transfer is highly sensitive to the proximity and orientation of the donor and acceptor; thereby, this technique can differentiate between binding modes reliably. [35] If we excite the system at a variety of wavelengths in the range of 220-280 nm, in the presence of intercalators with detection at the emission wavelength of the intercalators, we expect to obtain an emission intensity spectrum that resembles the UV-spectrum of DNA (Chapter 4, Section 4.9.)
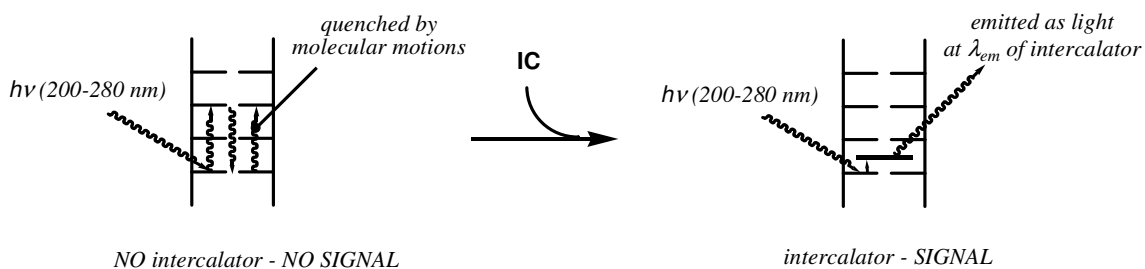
Figure 30. The theory of the FCET experiment. UV excitation of DNA will not result in fluorescence (*left side*), since molecular motions will quench the excitation energy. An intercalator, however, can pick up some of the excitation energy and emit it as its own resonance energy (*right side*) yielding fluorescence. **IC**: DNA-intercalator.

_____

NMR Experiments:

i., The protons that are stacked in DNA suffer an upfield chemical-shift perturbation as a result of magneticity from ring currents induced in the DNA bases by the NMR magnetic field.[34,37] Protons that do not take part in the intercalation will not suffer similar changes in their chemical shifts.

ii., Upon intercalation, the NOE interactions between the neighboring base pairs at the intercalation sites will be disrupted. This can be visualized as a breaking of the sequential NOE-NOE connectivities in 2D-NOESY experiments.

iii., Finally, the protons of the intercalators are expected to interact with the protons of the sandwiching base-pairs magnetically, resulting in ligand-DNA NOE signals.

2.5. Leinamycin Does not Have any Structural Motifs Suggesting DNA-Intercalation

Typical noncovalent DNA-binding structural motifs (Figure 31) are absent from the molecular framework of leinamycin (**1**) and the leinamycin episulfonium ion (**10**). For example, these agents do not have an overall positive charge that would make it bind DNA electrostatically, as seen in polyamines, spermidine for example. In addition **1** and **10** do not have an extended concave curved "backbone" which would suggest that it may act as a groove-binder similar to distamycin (Figure 31). Finally, an aromatic ring structure capable of intercalation (Sections 2.1. and 2.2.) is not evident in leinamycin.

_____
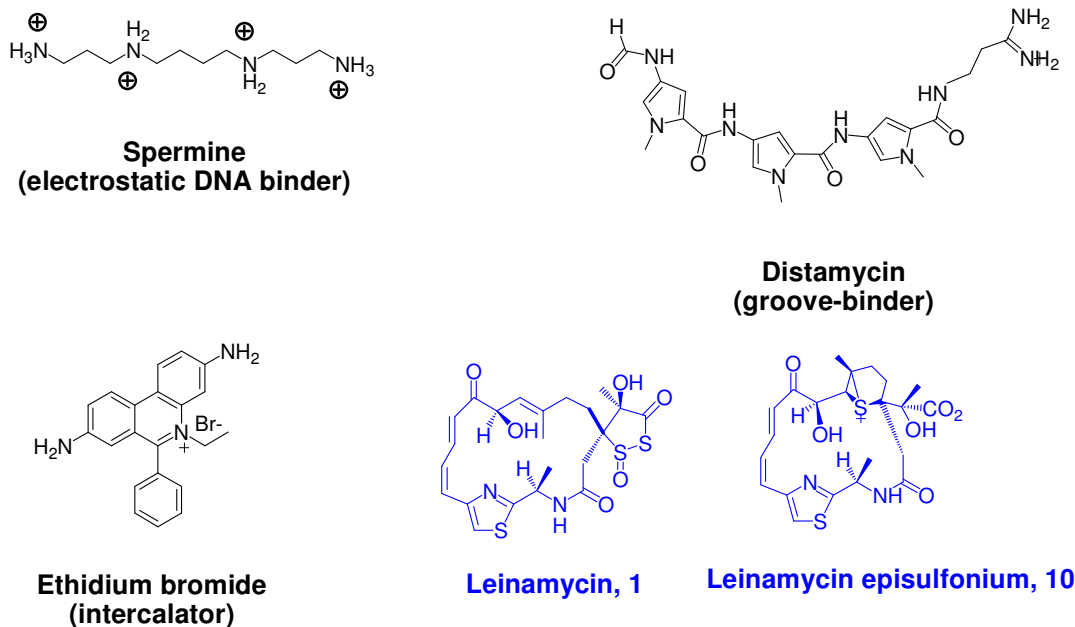
Figure 31. Typical noncovalent DNA-binders. Spermine: electrostatic-binder; Distamycin: groove-binder; ethidium bromide: DNA-intercalator and leinamycin (**1**), leinamycin episulfonium ion (**10**). Elements of regular DNA-binding structural motifs (overall positive charge, curved molecule, polyaromatic intercalator) are absent from the structure of leinamycin.

2.6. Hypothesis: Leinamycin is a Novel, Nonclassical DNA-Intercalator

Leinamycin does not possess any structurally classical DNA binding elements (electrostatic binding groups, groove binding or intercalating moieties), and still it has been shown to bind DNA noncovalently, which is absolutely critical to efficient DNA alkylation.

An initial molecular model of the N7G-leinamycin-oligonucleotide adduct revealed very interesting information about the DNA-adduct of leinamycin. The model showed that the natural product perfectly fits between the base pairs in duplex DNA. Additionally, the DNA-alkylating episulfonium electrophile is placed in a restricted trajectory in front of the N7-nitrogen of the guanine base. The natural product can only

_____

approach the N7 of guanine with a limited number of trajectories (Section 2.10, Figure

43) supporting the eventual intercalation of the *Z,E*-5-(thiazol-4-yl)-penta-2,4-dienone

macrocycle in between the DNA base-pairs on top of the 3'-side of the alkylated guanine

residue (Figure 32).

The observed asymmetry of our model is supported by our earlier sequencing

studies [38] showing the effect of the 3'-base neighbor on the efficiency of N7G-alkylation

by leinamycin. Consequently, intercalation of **1** is structurally possible, and this initial

model even shows that sufficient surface area of the natural product is available for DNA

intercalation (Figure 32) This highlights the idea of studying DNA-intercalation by our

natural product. Finally, it is important to realize that there are valuable cancer treating

drugs amongst intercalators. [39,40]
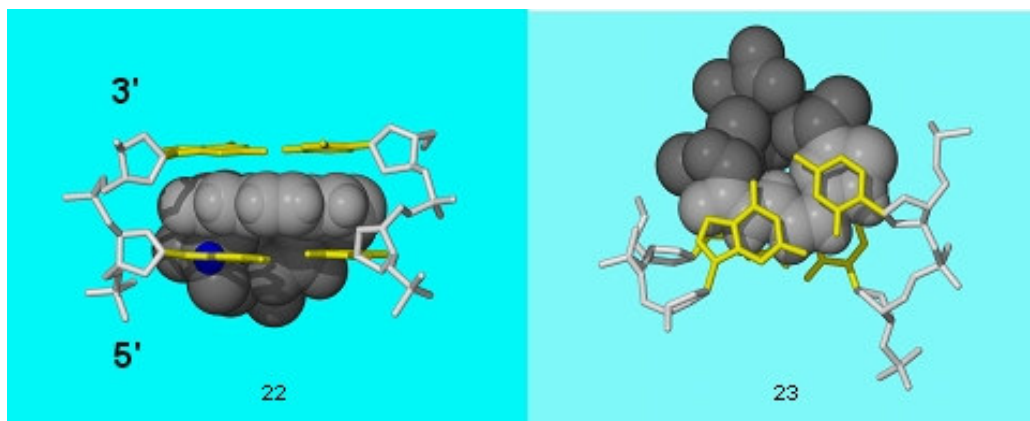
Figure 32. Model building showing the positioning of leinamycin in duplex DNA attached to N7G in the DNA-adduct, frontal view (**22**), top view (**23**). Limited trajectories are available for leinamycin to approach N7G, all suggesting the eventual intercalation of *Z,E*-5-(thiazol-4-yl)-penta-2,4-dienone portion on the 3'side of the alkylated guanine residue. *Modeling procedures:* the episulfonium.pdb file was constructed by ChemDraw 3D vs. 9.0. This model was energy minimized using the MM2 package of the software. The model was docked with into a DNA-duplex.pdb model with distance restraints between episulfonium and N7G. The validity of the computer model was confirmed by manual model building using plastic model building kit.

_____

2.7. Covalent Association of Leinamycin Unwinds Plasmid DNA

We examined whether adduct formation unwinds DNA (see introduction in Section 2.4.1.). We alkylated plasmid DNA (PGL2BASIC) under conditions to minimize the depurination of the LM-DNA adduct (4 °C, 50 min). In the presence of constant DNA concentration (35 μM bp), an increasing concentration of leinamycin (0-1 mM) was applied. Samples were then mixed with stain and loaded to 0.9% agarose at 4 °C. After visualization of the gel, we observed that increasing equivalents of leinamycin adduct on DNA unwound DNA as described Section 2.4.1. (Figure 29 and Figure 33). Plasmid DNA alkylation by small N7G alkylators that are incapable of DNA-intercalation do not result in unwinding of DNA. We demonstrated this in the alkylation and electrophoresis of plasmid DNA by glycidol under identical conditions (Figure 34).

This result is consistent with our intercalation model, though in rare cases it remains possible that groove binding could yield unwinding.
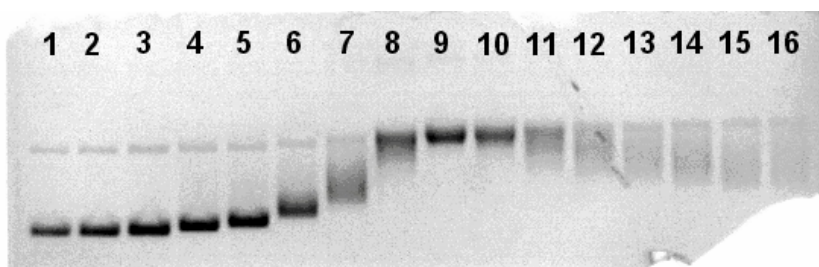
Figure 33. The unwinding of plasmid DNA (PGL2BASIC) by increasing concentrations of **10**. The following concentrations of **10** were used: lane 1: 0 mM, 2: 0.02 mM, 3: 0.04 mM, 4: 0.08 mM, 5: 0.1 mM, 6: 0.15 mM, 7: 0.2 mM, 8: 0.3 mM, 9: 0.4 mM, 10: 0.5 mM, 11: 0.6 mM, 12: 0.7 mM, 13: 0.8 mM, 14: 0.9 mM, 15: 1.0 mM, 16: 1.1 mM.

_____
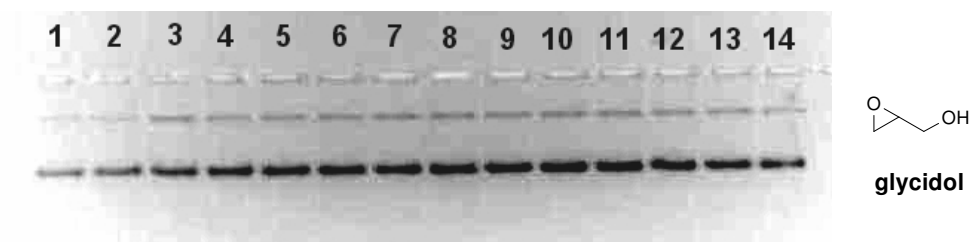
Figure 34. The unwinding of plasmid DNA (PGL2BASIC) by increasing concentrations of **glycidol**. The following concentrations were used: lane 1: 0 mM, 2: 0.02 mM, 3: 0.04 mM, 4: 0.08 mM, 5: 0.1 mM, 6: 0.15 mM, 7: 0.2 mM, 8: 0.3 mM, 9: 0.4 mM, 10: 0.5 mM, 11: 0.6 mM, 12: 0.7 mM, 13: 0.8 mM, 14: 0.9 mM. Reaction conditions and incubation times were identical to that of the unwinding experiment by leinamycin.

2.8. A Transitory Fluorescence Contact Energy Transfer (FCET) Supports Intercalated Leinamycin

We alkylated CT DNA (0.8 mM) with leinamycin (200 μM) in the presence of β-mercaptoethanol (240 μM) in 10 mM sodium-phosphate buffer at 4 °C for 2 h to synthesize the DNA-adduct of leinamycin (**44**). The adduct was diluted to 1 μM concentration into a quartz fluorescence cuvette and fluorescence readings were taken. FCET signal was calculated as described in Section 2.4.2. and in Chapter 4 for the left-half of azinomycin. A transitory existing FCET signal was observed (Figure 35), which is difficult to reproduce. We think that at this low concentration, the DNA-adduct of leinamycin degrades quickly due to reversion (Chapter 3) to the hydrolysis product (**13**) and depurination (**43**, Chapter 3).
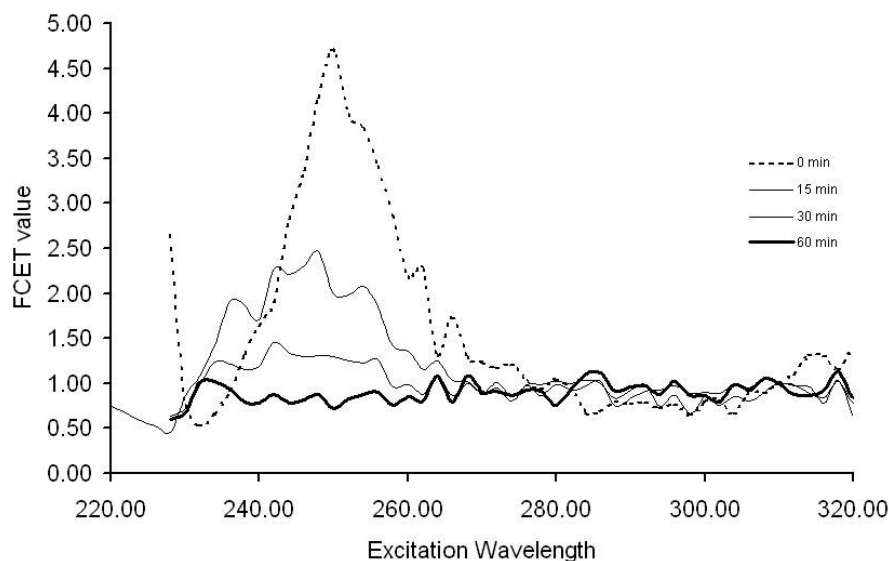
Figure 35. Transitory FCET signal of a 1 uM leinamycin-DNA adduct (**44**).

2.9. Viscometric Monitoring of the DNA-alkylation Reaction Demonstrates that the Leinamycin-DNA Adduct is Intercalated [40]

As was described above, it is possible to detect DNA intercalation by the accompanying change in the viscosity of DNA solutions. Based upon the adduct model structure (Figure 32) we suggested that the adduct should be intercalated. Thereby, we designed a viscometric monitoring system to follow adduct formation by viscosity changes in time. Similarly, time-dependent changes *in vivo* and *in vitro* have been studied by viscometric methods in the past. Classically, for example, the cellular degradation of DNA can be followed by viscosity measurements,[41,42] and other cellular events, like the unpacking of chromosomes, have also been analyzed by kinetic viscometry.[43]

Incubation of calf-thymus DNA (1 mM) with activated leinamycin (**10**) resulted in a time-dependent change in viscosity. The viscosity increased in an exponential fashion,

_____

consistent with the idea that changes in viscosity parallel the chemical modification of DNA (Figure 36). Increasing the equivalents of leinamycin linearly increases the final relative viscosity, which further substantiates this idea. The half-lives were calculated by a non-linear regression, using an exponential rising curve fit to our experimental data. We found that the half-life of the increase in viscosity matched that of the DNA alkylation calculated from the rate of DNA alkylation (k_2) earlier (Chapter 1). This data conclusively shows that the leinamycin-DNA adduct is intercalated into the double helix.

On the basis of our hypothesis that the increased viscosity is the result of an intercalated adduct, the degradation of the adduct via depurination should reduce the gained viscosity. This was observed by bringing the solution to room temperature, where depurination is pronounced, and studying the changes of solution viscosity. A gradual decrease in viscosity was observed (Figure 37), eventually going below the viscosity of intact DNA solution. The changes in the viscosity of the DNA solution are exclusively characteristic of DNA-intercalation. Groove binders (distamycin in our control experiment) do not increase the viscosity of DNA-containing solution.[23] We demonstrated this by titrating 1 mM CT DNA with distamycin (Figure 31). No changes in viscosity were observed (Figure 38).

It is interesting to investigate if activated leinamycin itself (**10**) is intercalated in DNA before the alkylation is accomplished. We tested this by pre-activating the natural product outside the DNA reaction, and transferring it to the CT DNA followed by viscometry. Since similar half-lives were observed for the changes in the relative viscosity, we concluded that activated leinamycin itself did not intercalate to a measurable extent, but associates with the DNA-helix by some other noncovalent binding-mode. With the

_____

known binding constant of activated leinamycin to duplex DNA ($K_B \sim 2500$ M^{-1}, Chapter 1), under these conditions, a minimum of 75% of activated leinamycin (**10**) is associated to DNA noncovalently.

Finally, we tested if covalent bond formation by non-intercalating N7G-DNA-alkylators produce increased viscosity of DNA solutions. We incubated C.T.DNA in the presence of dimethyl sulfate under identical conditions, and followed changes in its viscosity. There was no increase in viscosity. Rather a slight reduction in viscosity was observed (Figure 38), probably as a result of depurination and strand cleavage.[44]

Our viscosity experiments demonstrated that the natural product is intercalated in the DNA-adduct (Figure 32).
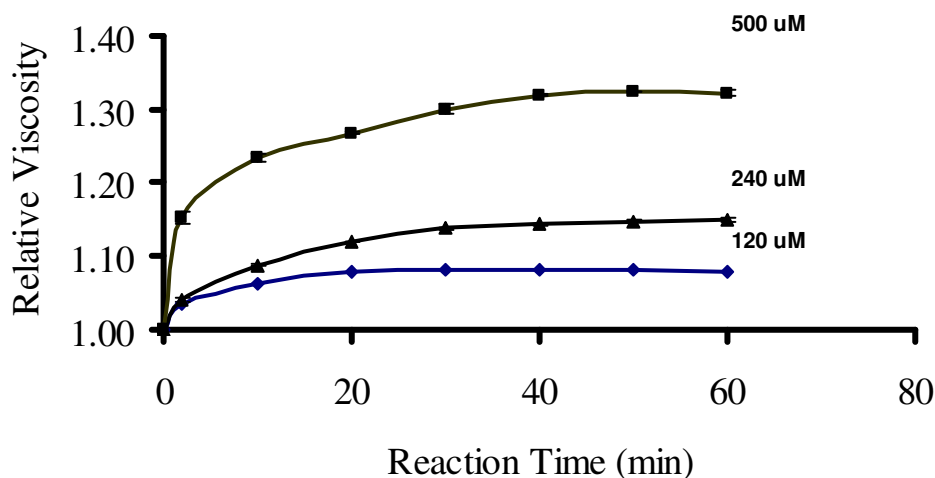
Figure 36. Time dependent changes in the relative viscosity of 1 mM C.T.DNA solution in the presence of **10**. Higher equivalents of the natural products produces linearly larger changes in viscosities.

_____
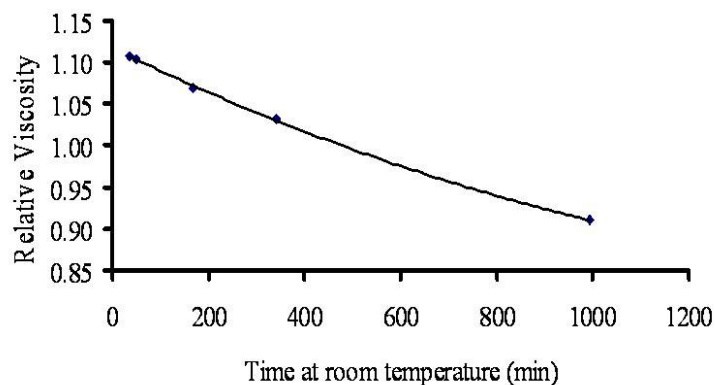
Figure 37. Changes in the viscosity of alkylated C.T.DNA solution after it had been warmed up to room temperature. The decreased viscosity is the result of the depurination of the leinamycin-DNA adduct and the fragmentation of the DNA chains.
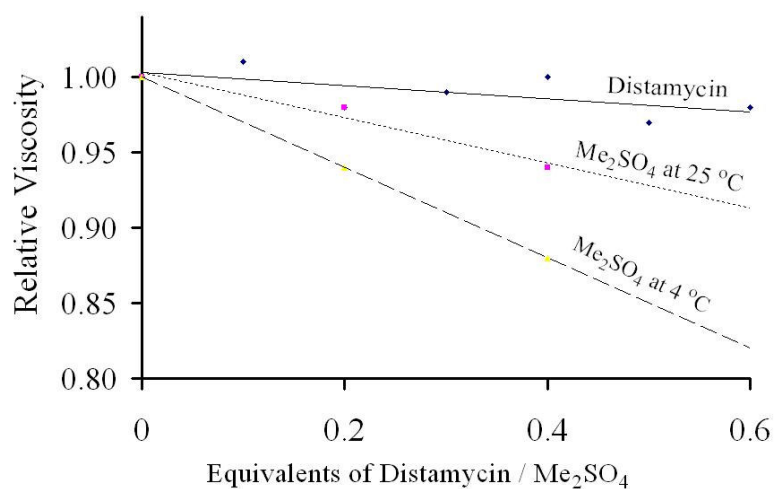
Figure 38. Effect of added groove-binder distamycin (Figure 31) and small DNA-alkylator: Me_2SO_4 on the viscosity of 1 mM C.T. DNA solution. Groove binding and DNA alkylation by small molecular DNA-alkylators do not generate extra viscosity to the DNA-solution.

_____

2.10. Where Does Leinamycin Contact the Duplex During the Alkylation Reaction? The Harris-Stone Experiment [37,45]

We have reported that the efficiency of alkylation of a guanine base in duplex DNA depends on the 3'-neigboring base, which was reflected in our molecular model of the leinamycin-DNA adduct (Figure 32). As we have seen above, the only way that the intercalated leinamycin-DNA adduct can be formed from the noncovalently bound episulfonium (**10**) is to arrange its polyene moiety on the 3'-top of the alkylated guanine. We wished to examine where leinamycin makes any contact with the duplex during the alkylation reaction. We believed that this information would reveal some of the structural features of the transition state of the alkylation reaction.

2.10.1. Quantitative Alkylation of Self Complementary Oligonucleotides can Reveal Which Surface of Guanine is Contacted by the Natural Product

We alkylated self complementary sequences of DNA (**24** and **25**, Figure 39) with one guanine residue on each strand. Six-mer sequences were used, and the guanine residues were nearest neighbors in the middle of the strands so that either their 3'-surfaces (**24**, **25**) or their 5'-surfaces (**26**, **27**) faced one another. If alkylation requires a contact between leinamycin and the 3'- guanine, then the duplex with guanines facing each other with their 3'-surfaces (**24**, **25**) will get alkylated only once, because one alkylation event will block the accessibility of the 3'-surface of the guanine on the opposite strand. On the other hand, the alkylation of the duplex with guanines facing with their 5'-faces will allow both the strands to be alkylated, because after one alkylation event the 3'-surface of the remaining guanine is still accessible by leinamycin. Based on our model (Figure 32)

_____

and sequencing data, [38] we predicted that leinamycin should contact the 3'-surface of the

alkylated guanine base in the process of alkylation. Note that complete alkylation

(essentially a 100% yield in alkylation) is required for this experiment.
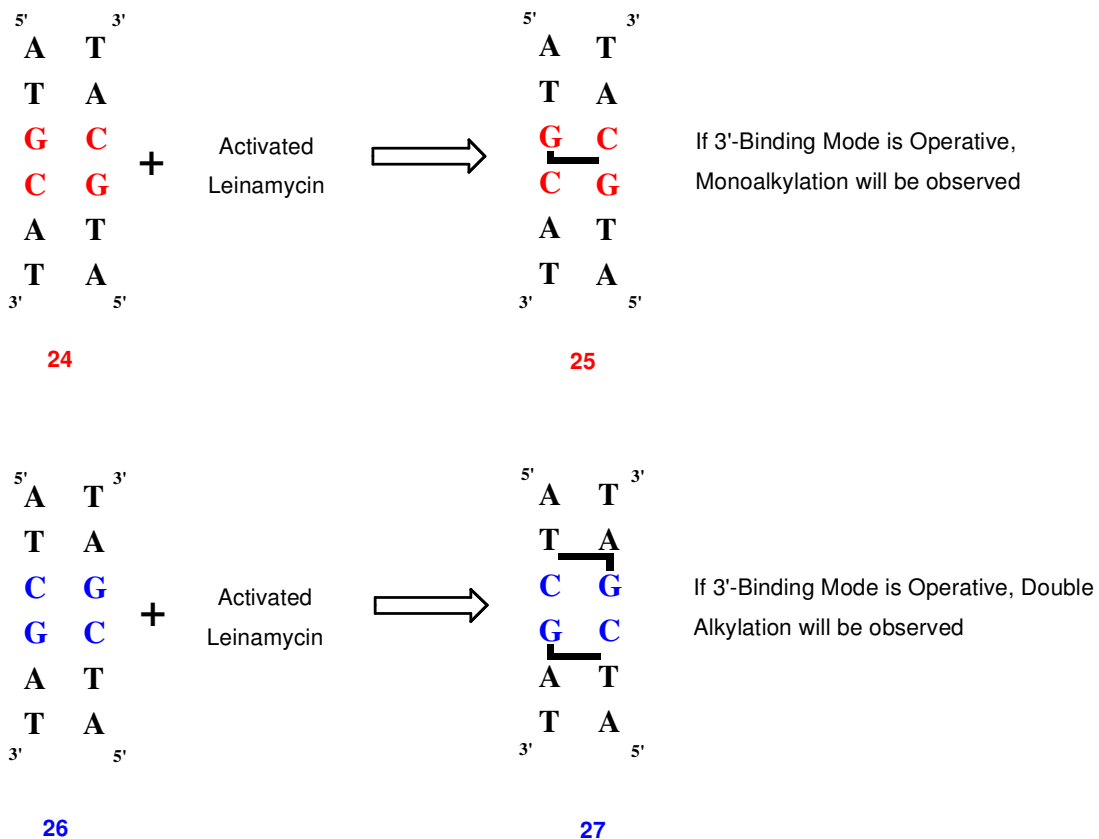
Figure 39. The self complementary oligonucleotides used in the leinamycin-G contact experiments. 6-mer self complementary sequences with one G base in each strand were designed. The guanines are nearest neighbors, so either their 3'-surface or 5'-surface will face one another.

_____

2.10.2. Alkylation of Self Complementary Oligonucleotides and their HPLC Analysis

Our initial attempts to alkylate our oligonucleotides in aqueous buffers failed to provide us with quantitative yield (67% per strand after multiple re-alkylation attempts and requiring high excess of the natural product). Since in this assay we analyze the yields of alkylated vs. non-alkylated strands, quantitative alkylation is essential. Eventually, we used a biphasic alkylation system to sequester the thiol-activated natural product against hydrolysis in a methylene chloride layer. On top of this we layered a mixture of our oligonucleotide in a buffered solution. Reactions were done at 4 °C to suppress depurination and the reversion of the DNA adduct. After routine purification the adducted oligonucleotides were studied by HPLC separation of the adducted and intact chain.
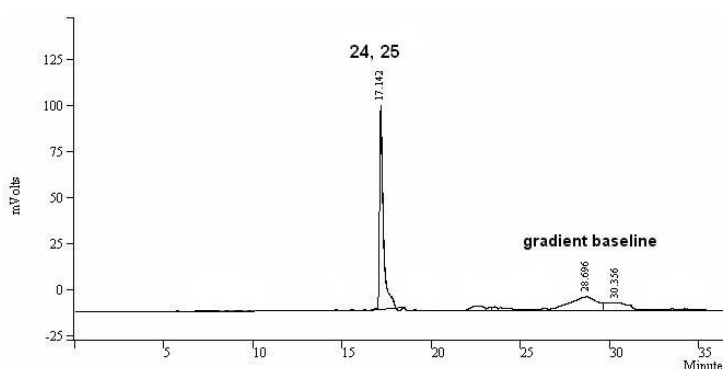
Figure 40. The HPLC of the oligonucleotides used in the Harris-Stone experiment. The humps in the HPLCs in the region of 27-32 min is a fluctuation of the baseline due to a quick-change in the elution gradient. Solvents used: A: 50 mM ammonium formate, pH 7.0, B: acetonitrile, gradient elution at 45 °C.

_____

HPLC analysis reveals (Figure 41) that alkylation of the oligonucleotide 5'…GC…3' (**24**) results in 50% yield in strand alkylation, suggesting that the first alkylation event blocks the second guanine from alkylation. In contrast, duplex with sequence 5'…CG…3' (**26**) undergoes double alkylation as expected. This appears as complete alkylation of the oligonucleotide.
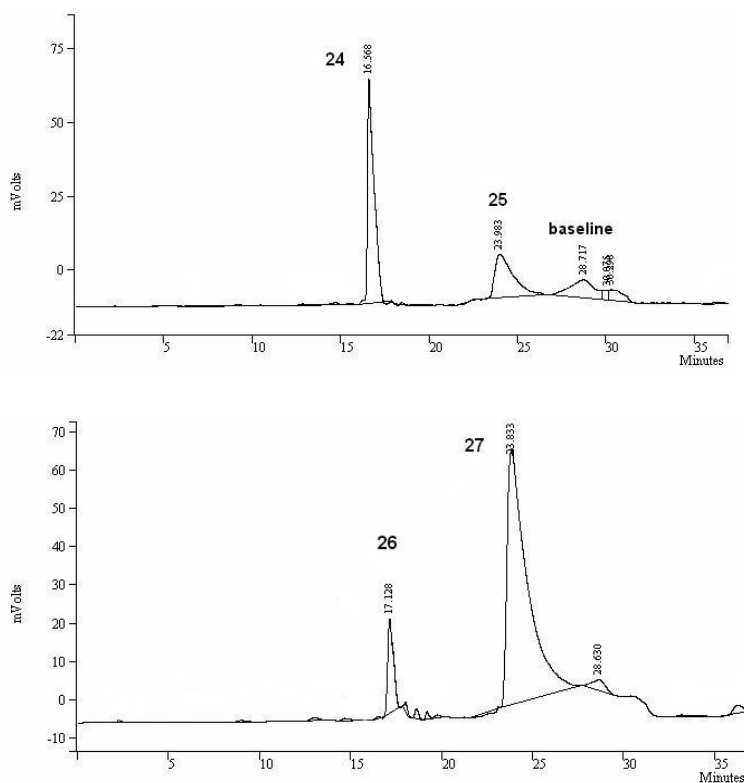
Figure 41. HPLCs of the alkylated oligonucleotides in the Harris-Stone reactions.

For identification of the adducts, we treated the oligonucleotide adducts (**25** and **27**) with 1M piperidine at 80 °C for 1 h and analyzed their degradation products by HPLC (Figure 42). As expected, the HPLC peaks for the putative adducted oligonucleotide disappear to yield two peaks with shorter retention times (12 min 13 min), characteristic of the cleaved degradation products of this workup.

_____
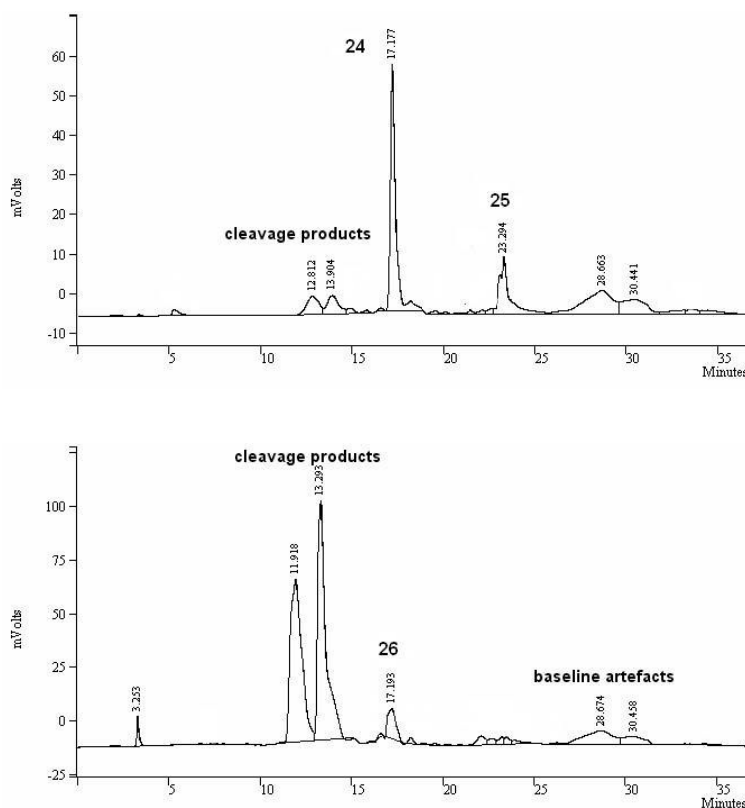
Figure 42. HPLCs of the adducted oligonucleotides after their treatment with piperidine 1M, 80 °C, 1 h).

In conclusion, the results show that leinamycin must make contacts on the 3'-side of the targeted guanine in order for alkylation to occur. Based upon our additional data, we suspect that this contact is most probably intercalation, though the Harris-Stone experiment does not speak to binding mode. The results presented in this Section are in perfect agreement with our earlier observation that the sequence specificity of DNA-alkylation by leinamycin is determined only by the nearest 3'-neighbor base to the alkylation point.[38]
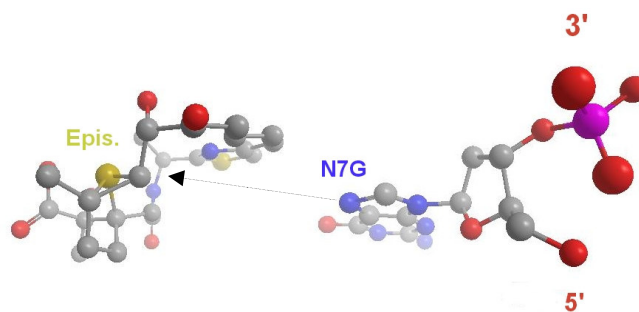
Figure 43. The position of the episulfonium ion over the 3'-surface of the guanine base in the approach of the N7G nitrogen. The approach from the 5'-side of guanine would place the episulfonium and the N7G in distant locations in the context of duplex DNA.

2.11. Effect of DNA Bulges in the DNA-alkylation by Leinamycin

2.11.1. Occurrence of DNA-Bulges In Vivo and their Structure

Bulged DNA structures[46-53] typically cause a bend in the DNA-backbone and contain a base either flipped away (out) from the DNA axis[51] or stacked between the DNA bases[50] (Figure 44) . Such structures present in nucleic acids are biologically interesting and can be targets for therapeutics. [48] Studies show that bulged DNA sequences are preferential alkylation sites for numerous DNA intercalating DNA-damaging natural products, for example neocarzinostatin (Figure 45), bleomycin, 9-aminoacridine and Altromycin B (structures of intercalators: Figure 28).[48,49,53,54] Bulged structures are also mutational hot-spots for frameshift mutations (insertion or deletion),[55] and their lifetime is stabilized with intercalators.[54]

_____
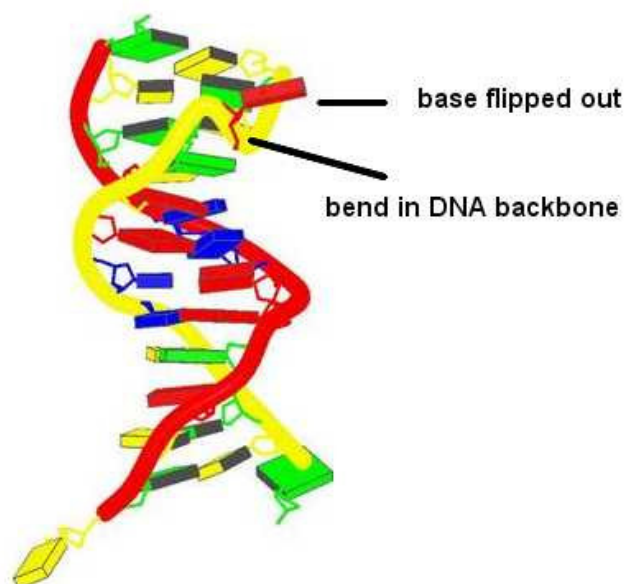
Figure 44. Image of a DNA bulge. [46]

Figure 45. Binding of neocarzinostatin in the DNA-bulge [56]

_____

2.11.2. Alkylation of Oligonucleotides with Bulges near the Targeted Guanine

Bulged DNA structures can be used in the identification of DNA-intercalation.[49] We investigated the effect of DNA bulges on the efficiency of alkylation at nearby guanines by **10** (Figure 46). We studied the effect of one-base bulges positioned 3' or 5' to the alkylation spot on the efficiency of DNA-alkylation by leinamycin. Using ^{32}P-labelled oligonucleotides (**28**,-**32**,Figure 46) we found that if a bulge is present 3' from the alkylation site the efficiency of alkylation increases no matter if the bulge is on the strand of the alkylation site (**30**) or the opposite strand (**32**). However, a bulge at the 5' side of alkylation (viewed along the strand of alkylation) does not affect the efficiency of alkylation. The efficiency of alkylation is considerable enhanced when the bulge is on the 3'-side of the alkylation spot (average 3.1 times), independent of whether it is on the strand of alkylation or the opposite strand. A smaller increase in the alkylation efficiency is seen when the alkylated G is in the bulge (average 1.9 times). A very slight increase is seen when the alkylation spot is 5'-to the bulge (average 1.4 times). The increase in the efficiency of alkylation of bulged sequences follow the order: *bulge 3' > bulge at alkylation spot > bulge 5'*. In conclusion, a bulge in the DNA-structure "pre-opens" an intercalation site. The yields of these alkylations at the bulge Gs are tabulated in Table 6.

The preferential binding of leinamycin to bulged-DNA sequences in a sequence specific manner supports the idea of its intercalation, because a bulge opens a space in the core of the DNA-duplex. Additional binding modes may no be affected by this opening.

_____

Sequence	k$_{bulge}$/k$_{TGT}$	*POSITION*	k$_{bulge}$/k$_{TGT}$
28	1.9	*bulge 3' to G*	*3.1*
29	2.8	*G in bulge*	*1.9*
30	1.4	*bulge 5' to G*	*1.4*
31	1.3		
32	3.4		

Table 6. The increases in G-alkylation in bulged DNA sequences.
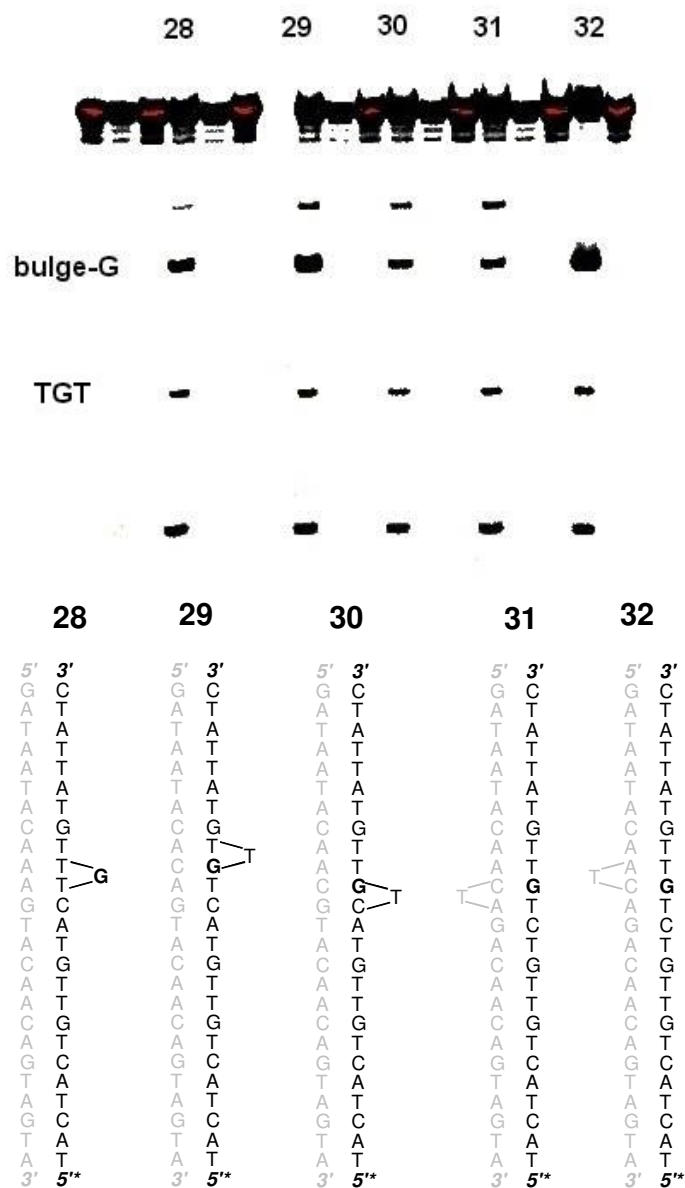
Figure 46. The sequencing gel of oligonucleotide bulged-oligonucleotides alkylated by 10 and the sequences.

_____

2.12. Chapter Conclusions

We demonstrated that the leinamycin-DNA adduct is intercalated. Initial molecular modeling (Section 2.6., Figure 32) showed that intercalation is possible and in fact is the only way to place the natural product in the DNA-adduct. The features of this model were also supported by earlier sequencing data. [38]

The intercalation of leinamycin in the DNA adduct was supported by DNA unwinding (Section 2.7). A short-lived FCET signal also supports an intercalated DNA-adduct (Section 2.8). Our viscosity studies (Section 2.9.) conclusively showed that the natural product is intercalated in the DNA-duplex. Alkylation of self complementary oligonucleotides (Section 2.10.) showed that leinamycin requires a contact with the 3'-side of the target guanine during the DNA alkylation reaction. Finally, increased yields of guanine alkylations in bulged DNA-sequences, preferentially 3'-to the target guanine suggested that a "pre-opened" intercalation site 3' from the target guanine increases the efficiency of alkylation at that site (Section 2.11.).

Leinamycin is a structurally novel minimal DNA intercalating agent.
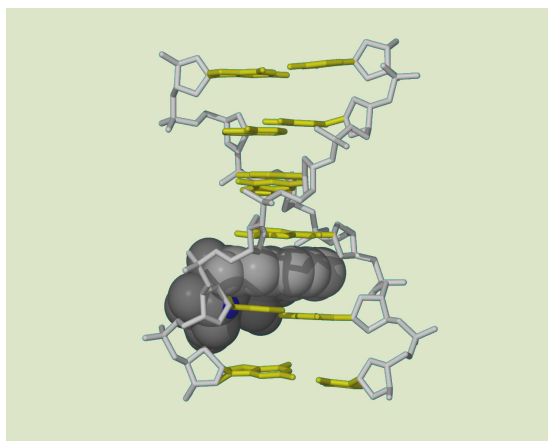
Figure 47. The position of leinamycin in duplex DNA.

_____

2.13. Experimental

2.13.1. Materials and Methods.

Leinamycin (**1**) was a gift from researchers at Kyowa Hakko Kogyo Ltd. Additional reagents were purchased from the following suppliers and were of the highest purity available: MOPS buffer, sodium acetate and sodium phosphate buffers, trifluoroethanol, triethylamine, Aldrich Chemical Co. (Milwaukee, WI); HPLC grade solvents (water, acetonitrile, ethanol), Fisher (Pittsburgh, PA); herring sperm DNA, Roche Molecular Biochemicals (Indianapolis, IN); HPLC vials, National Scientific Corporation; analytical HPLC columns, Varian Inc. (Palo Alto, CA). HPLC: Varian Prostar Dynamax, vs. 5.1. LC-MS: ThermoFinnigan TSQ7000 triple-quadrupole with API2 source.

2.13.2. Plasmid DNA Unwinding by 10

In 500 μL microcentrifuge tubes the following components were added together at 4 °C: 2.5 μL of sodium-phosphate buffer (500 mM, pH 7.0) 3 μL of PGL2BASIC plasmid-DNA (1 μg/mL solution), 2.5 μL β-mercaptoethanol (20 mM in HPLC water), then 11 μL HPLC water, followed by the following leinamycin stock solutions together with acetonitrile to make the total acetonitrile content of the reactions 6 μL: 1 μL or 2 μL (500 μM leinamycin in acetonitrile), 2 μL or 2.5 μL (1 mM leinamycin in acetonitrile), 0.74 μL or 1 μL or 1.5 μL or 2 μL or 2.5 μL (5 mM leinamycin in acetonitrile), 1.5 μL or 1.75 μL or 2 μL or 2.25 μL or 2.5 μL (10 mM leinamycin in acetonitrile). Samples were gently vortexed and incubated for 50 min at 4 °C in a cold room. After incubation samples were treated with 6 μL of glycerol loading buffer (7 μL) containing 0.25% bromophenol blue and 40% sucrose, and the mixtures were vortexed gently (5 s). Samples were loaded on a

_____

2% (m/m%) agarose-gel and electrophoresed vs. 40 V for approximately 16 h in a 4 °C-cold-room.

2.13.3. Viscometric Monitoring of DNA-alkylation by 10 And the Spontaneous Depurination Reaction

These studies were carried out in a custom-made flow viscometer (ACE Glass) with a 1 mL-volume sample size with a 100 s flow-time for distilled water at room-temperature. The reactions and viscosity studies were done at 4 °C in a cold-room. Samples were composed of 100 mL sodium phosphate buffer (100 mM, pH 6.5), 285 µL calf thymus DNA solution (3.5 mM in water), 415 µL water, 100 µL β-mercaptoethanol (7.2 mM in water), followed by 24 µL or 48 µL or 100 µL leinamycin stock solution (5 mM in acetonitrile) respectively, and 76 µL or 52 µL or no acetonitrile respectively. Samples were placed in the flow-viscometer with the help of a glass Pasteur pipette and bubbled. The flow times were recorded and the relative viscosity of the solution at a given time-point was calculated as: $(t-t_0)/t_0$ where t is the flow time of the actual data point, t_0 is the flow time of the solution without leinamycin. The calculated relative viscosities were plotted vs. time (Figure 36).

2.13.4. Viscometric Monitoring of DNA-Titration by Distamycin.

For this experiment the same flow-viscometer (1 mL sample size, 100 s flow time for water at room temperature) was used. Titration was done at 4 °C. The initial DNA solution was made as follows: 100 µL sodium phosphate buffer (100 mM, pH 7.0), 100 µL β-mercaptoethanol (7.2 mM), 285 µL calf thymus DNA solution (3.5 mM in water),

415 μL water. The flow time of this DNA solution was recorded and taken as t_0. Aliquots of concentrated acetonitrile solution of distamycin (4 μL of a 25 mM solution in acetonitrile) were added. The resulting mixture was bubbled intensively for mixing (10-20 s), and the flow-time was recorded. The relative viscosity was calculated and plotted vs. the added equivalents of distamycin (Figure 38).

2.13.5. Viscometric Monitoring of the DNA-alkylation by Small-Molecular DNA Alkylator Dimethyl Sulfate.

In a custom-made flow-viscometer (1 mL sample, 100 s for water at room temperature) the following DNA solutions was made: 100 μL sodium phosphate buffer (100 mM, pH 7.0), 100 μL β-mercaptoethanol (7.2 mM), 285 μL calf thymus DNA solution (3.5 mM in water), 415 μL water. The flow time of this DNA solution was recorded and taken as t_0. Then, a fresh stock solution of dimethyl-sulfate was prepared (100 mM in water) and 25 μL of this solution was added to the flow-viscometer with the DNA solution. The mixture was bubbled for 10 s and the flow time was recorded periodically. The relative viscosity was calculated and plotted vs. reaction time (Figure 38).

2.13.6. Alkylation of Self Complementary Oligonucleotides 24 and 26 by 10 and their Purification.

Oligonucleotides **24, 26** were custom made by Integrated DNA Technologies. To approximately 700 nmol (for strands) oligonucleotide was added 120 μL sodium chloride solution (500 mM NaCl) and 90 μL sodium phosphate buffer (100 mM, pH 7.0) and 90 μL of HPLC water. This provides a solution of ~ 2.3 mM oligonucleotide (single-strand

concentration, 1.15 mM for duplex concentration), 200 mM sodium chloride, 30 mM sodium phosphate. The mixture was vortexed well (1-2 min) to solubilize the oligonucleotide and placed on an 80°C-heat-block for 10 minutes. The heat-block was placed together with the samples in a pyrofoam box into a 4°C-cold-rooom for slow-cooling to anneal the oligo strands over the next 12-16 h. The exact concentration was determined after the annealing by U.V. absorbance reading of the diluted oligonucleotide solution in HPLC water (A_{260nm} = 1 of a 75 μM b.p. DNA solution which is 50 μg/mL). DNA alkylation was carried out in a biphasic system as reported by Stone and Harris. [37,57] Accordingly, the 40 μL of the aqueous oligonucleotide solution (~1.15 mM for duplex that can be higher, 200 mM NaCl, 30 mM NaPi) was treated with 4 μL β-mercaptoethanol solution (130 mM) in a 500 μL eppendorf tube. 100 μL leinamycin (5 mM in acetonitrile) was evaporated to dryness under a stream of nitrogen gas, and redissolved into 50 μL of methylene chloride (yields a 10 mM solution of leinamycin). This organic solution was placed in a 4-degree cold-room for thermal equilibration. The cold oligonucleotide solution was placed on top of the methylene-chloride solution and intensive vortexing begun in a centrifuge-tube vortex mixer over the next 4 h. After the DNA-alkylation reaction vortexing stopped and the sample was centrifuged in a bench top centrifuge (1000 r.p.m., 20 s) to separate the organic and aqueous layers. The bottom phase was carefully removed and discarded with the help of a pipette tip. To the remaining aqueous DNA-adduct mixture 60 μL water (HPLC) and 100 μL cold butanol were added. The mixture was intensively vortexed and the top layer (butanol) was removed and discarded. Another portion of butanol (100 μL) was layered on the aqueous phase, vortexed and the butanol layer was discarded again. The aqueous layer can now be

_____

analyzed by HPLC or furthered purified by DNA precipitation. For DNA precipitation 200 µL of a precipitating stock solution (0.3 M for sodium acetate and 70% ethanol) was mixed with the solution and the mixture vortexed and placed on dry ice for precipitation for 30 min. Then, the frozen samples were centrifuged in a bench-top centrifuge 10.000 r.p.m. fro 30 min. The DNA-pellets were washed with 50 µL of 80% ethanol twice, and then stored at minus 20 °C before the HPLC analysis.

2.13.7. HPLC Separation and Analysis of the Oligonucleotides 24, 25, 26 and 27.

For the HPLC separation of oligonucleotides and alkylated oligonucleotides we used 50 mM ammonium formate pH 7.0 (solvent A) and acetonitrile (solvent B) in a gradient elution method (Table 7) with a flow rate of 1.5 mL/min and a RP-HPLC C18 4.6 x 250 column heated to 45 °C in a thermostated-water bath.

Time (min)	B (%)
0	1
20	9
26	56
29	56
30	80
32	80
37	1
39	1

Table 7. HPLC method used for the elution of our oligonucleotides **24-27**. Column: RP-HPLC C18 4.6 x 250. Temperature: 45 °C.

_____

2.13.8. Polyacrylamide Gel Electrophoresis of Bulged-DNA-Sequences (28-32) after Alkylation with 10.

Oligonucleotides shown in Figure 46 (Section 2.11.) were labeled using T4 polynucleotide kinase and γ-^{32}P ATP. The radiolabelled oligonucleotides (**28-32**) were annealed with the complementary strand by heating to 90 °C for 5 min, and slow cooling. The duplexes were reacted with 20 μM leinamycin in the presence of 200 μM β-mercaptoethanol and 50 mM MOPS pH 7.0 buffer and 200 μM Herring Sperm DNA and 100 mM sodium chloride for 2 h. Samples were extracted with equivolume butanol (twice). DNA was further purified by precipitation using 0.3 M sodium acetate in 70% ethanol. The precipitated DNA was placed on top of dry ice (30 min) and was centrifuged at 10.000 r.p.m. for 30 min. The supernatant was discarded, and the DNA pellets were further washed with 80% chilled ethanol. The DNA pellets were redissolved into 200 mM piperidine solution and were kept at 95 °C for 30 min. After cooling samples were loaded onto a polyacrylamide-gel (16%) and were electrophoresed for 3h at 1200 V in TAE buffer. Radioactivity was visualized by phosphoimager. The Maxam-Gilbert G/A+G were performed following standard protocols. [58]

2.13.9. Fluorescence Contact Energy Transfer Experiments

The DNA adduct of leinamycin (**44**) was synthesized accordingly: In a 500 μL microcentrifuge tube the following solutions were mixed at 4 °C: 10 μL sodium phosphate buffer (100 mM, pH 7.0), 10 μL CT DNA solution (8 mM in water), 10 μL β-mercaptoethanol (2.4 mM in water) and 62 μL water. The alkylation reaction was initiated by the addition of 8 μL leinamycin (5 mM in acetonitrile). After 2 h 15 μL of

_____

this mixture was diluted by 10 mM sodium phosphate buffer (pH 7.0) to 3 mL and placed

into a quartz fluorescence cuvette. Fluorescence readings were taken with the following

instrumental settings: lamp power: 75 Watts, detector: 1000 V, slots: 8 nm, integration:

0.1 s.

_____

References

1. Lerman, L. S., Structural considerations in the interaction of deoxyribonucleic acid and acridines. *J. Mol. Biol.* **1961,** 3, 18-30.

2. Atwell, G. J.; Bos, C. D.; Baguley, B. C.; Denny, W. A., Potential antitumor agents. 56. Minimal DNA-intercalating ligands as antitumor drugs: phenylquinoline-8-carboxamides. *J. Med. Chem.* **1988,** 31, 1048-52.

3. Sartorius, J.; Schneider, H.-J., Intercalation mechanisms with ds-DNA: binding modes and energy contributions with benzene, naphthalene, quinoline and indole derivatives including some antimalarials. *Journal of the Chemical Society, Perkin Transactions 2: Physical Organic Chemistry* **1997**, 2319-2328.

4. Denny, W. A., *Acridine-4-carboxamides and the concept of minimal DNA intercalators.* 2003; Vol. 2, p 482-502.

5. Kumar, R. A.; Ikemoto, N.; Patel, D. J., Solution structure of the esperamicin A1-DNA complex. *J. Mol. Biol.* **1997,** 265, 173-186.

6. Bailly, C.; Cuthbert, A. W.; Gentle, D.; Knowles, M. R.; Waring, M. J., Sequence-selective binding of amiloride to DNA. . *Biochemistry* **1993,** 32, 2514-2524.

7. Shields, H.; McGlumphy, C., The orientation of the ligands in iron(III)-bleomycin intercalated with DNA. *Biochim. Biophys. Acta* **1984,** 800, 277-81.

8. Chadfield, M. S.; Hinton, M. H., In vitro activity of nitrofuran derivatives on growth and morphology of Salmonella enterica serotype Enteritidis. *J. Appl. Microbiol.* **2004,** 96, 1002-1012.

_____

9.   Gale, E. F.; Cundliffe, E.; Waring, M. J.; Reynolds, P. E.; Richmond, M. H., *The Molecular Basis of Antibiotic Action*. 1972; p 474 pp.

10.   Neidle, S., The molecular basis for the action of some DNA-binding drugs. *Progr. Med. Chem.* **1979,** 16, 151-221.

11.   Schwartz, H. S., Biochemical action and selectivity of intercalating drugs. *Advances in Cancer Chemotherapy* **1979,** 1, 1-60.

12.   Boehner, R.; Hagen, U., Action of intercalating agents on the activity of DNA polymerase I. *Biochim. Biophys. Acta Nucleic Acids Protein. Synth.* **1977,** 479, 300-10.

13.   Sarris, A. H.; Niles, E. G.; Canellakis, E. S., The mechanism of inhibition of bacteriophage T7 RNA synthesis by acridines, diacridines and actinomycin D. *Biochim. Biophys. Acta Nucleic Acids Protein. Synth.* **1977,** 474, 268-78.

14.   Kanter, P. M.; Schwartz, H. S., Quantitative models for growth inhibition of human leukemia cells by antitumor anthracycline derivatives. *Canc. Res.* **1979,** 39, 3661-72.

15.   Ross, W. E.; Glaubiger, D.; Kohn, K. W., Protein-associated DNA breaks in cells treated with adriamycin or ellipticine. *Biochim. Biophys. Acta Nucleic Acids Protein. Synth.* **1978,** 519, 23-30.

16.   D'Arpa, P.; Liu, L. F., Topoisomerase-targeting antitumor drugs. *Biochimica et Biophysica Acta, Reviews on Cancer* **1989,** 989, 163-77.

17.   Deniss, I. S.; Morgan, A. R., Studies on the mechanism of DNA cleavage by ethidium. *Nucleic Acids. Res.* **1976,** 3, 315-24.

18.   Martens, P. A.; Clayton, D. A., Strand breakage in solutions of DNA and ethidium bromide exposed to visible light. *Nucleic Acids. Res.* **1977,** 4, 1393-407.

19.   Sun, D.; Hansen, M.; Clement, J. J.; Hurley, L. H., Structure of the altromycin B (N7-guanine)-DNA adduct. A proposed prototypic DNA adduct structure for the pluramycin antitumor antibiotics. *Biochemistry* **1993,** 32, 8068-8074.

20.   Sissi, C.; Moro, S.; Richter, S.; Gatto, B.; Menta, E.; Spinelli, S.; Krapcho, A. P.; Zunino, F.; Palumbo, M., DNA-interactive anticancer Aza-anthrapyrazoles: biophysical and biochemical studies relevant to the mechanism of action. *Mol. Pharmacol.* **2001,** 59, 96-103.

21.   Cairns, J., Application of autoradiography to the study of DNA [deoxyribonucleic acid] viruses. *Cold Spring Harbor Symposia on Quantitative Biology* **1962,** 27, 311-18.

22.   Waring, M. J., Variation of the supercoils in closed circular DNA by binding of antibiotics and drugs. Evidence for molecular models involving intercalation. *J. Mol. Biol.* **1970,** 54, 247-79.

23.   Suh, D.; Chaires, J. B., Criteria for the mode of binding of DNA binding agents. *Bioorg. Med. Chem.* **1995,** 3, 723-728.

24.   Uhlenhopp, E. L.; Krasna, A. I., Alterations in the structure of deoxyribonucleic acid on chemical methylation. *Biochemistry* **1971,** 10, 3290-5.

25.   Povirk, L. F.; Dattagupta, N.; Warf, B. C.; Goldberg, I. H., Neocarzinostatin chromophore binds to deoxyribonucleic acid by intercalation. *Biochemistry* **1981,** 20, 4007-4014.

26.   Long, E. C.; Barton, J. K., On demonstrating DNA intercalation. *Accounts. Chem. Res.* **1990,** 23, 271-273.

_____

27.   Sun, D.; Hurley, L. H.; Harshey, R. M., Structural distortions induced by IHF at the H' site of phage l probed by (+)-CC-1065, pluramycin, and KMnO4 and by DNA cyclization studies. *Biochemistry* **1996,** 35, 10815-10827.

28.   Bauer, W.; Vinograd, J., Interaction of closed circular DNA with intercalative dyes. I. Superhelix density of SV40 DNA in the presence and absence of dye. *J. Mol. Biol.* **1968,** 33, 141-71.

29.   Watson, R.; Bauer, W. R., The viscometric behavior of native and relaxed closed circular PM2 DNAs at intermediate and high ethidium bromide concentrations. *Biopolymers* **1977,** 16, 1343-56.

30.   Liu, L. F.; Wang, J. C., On the degree of unwinding of the DNA helix by ethidium. II. Studies by electron microscopy. *Biochim. Biophys. Acta* **1975,** 395, 401-12.

31.   Keller, W., Determination of the number of superhelical turns in simian virus 40 DNA by gel electrophoresis. *Proc. Natl. Acad. Sci. Unit. States Am.* **1975,** 72, 4876-80.

32.   Zeman, S. M.; Depew, K. M.; Danishefsky, S. J.; Crothers, D. M., Simultaneous determination of helical unwinding angles and intrinsic association constants in ligand-DNA complexes: the interaction between DNA and calichearubicin B. *Proc. Natl. Acad. Sci. Unit. States Am.* **1998,** 95, 4327-4332.

33.   Waring, M. J., Stabilization of two-stranded ribohomopolymer helices and destabilization of a three-stranded helix by ethidium bromide. *Biochem. J.* **1974,** 143, 483-6.

34.   Cruthers, D. M., Nucleic Acids: Structures, Properties and Functions. *University Science Books, California* **2000**.

35.   Suh, D.; Oh, Y.-K.; Chaires, J. B., Determining the binding mode of DNA sequence specific compounds. *Process Biochem.* **2002,** 37, 521-525.

36.   Le-Pecq, J. B.; Paoletti, C., A fluorescent complex between ethidium bromide and nucleic acids. *J. Mol. Biol.* **1967,** 27, 87-106.

37.   Gopalakrishnan, S.; Harris, T. M.; Stone, M. P., Intercalation of aflatoxin B1 in two oligodeoxynucleotide adducts: comparative proton NMR analysis of d(ATCAFBGAT)×d(ATCGAT) and d(ATAFBGCAT)2. *Biochemistry* **1990,** 29, 10438-10448.

38.   Zang, H.; Gates, K. S., Sequence Specificity of DNA Alkylation by the Antitumor Natural Product Leinamycin. *Chem. Res. Toxicol.* **2003,** 16, 1539-1546.

39.   Brana, M. F.; Cacho, M.; Gradillas, A.; De Pascual-Teresa, B.; Ramos, A., Intercalators as anticancer drugs. *Curr. Pharmaceut. Des.* **2001,** 7, 1745-1780.

40.   Hahn, F. E.; O'Brien, R. L.; Ciak, J.; Allison, J. L.; Olenick, J. G., Modes of action of chloroquine, quinacrine, and quinine and on chloroquine resistance. *Mil. Med., Suppl.* **1966,** 131, 1071-1089.

41.   Balbi, C.; Bordone, R.; Gelardi, A.; Marchesini, F.; Piccardo, M.; Sarma, D. S. R.; Taningher, M.; Parodi, S., Lack of DNA alterations induced by orotic acid in rat liver as evaluated with two DNA unwinding methods. *Canc. Biochem. Biophys.* **1990,** 11, 135-144.

42.   Balbi, C. A., Maria Luisa; Roner, R.; Giaretti, W.; Parodi, S.; Santi, L., Detection of DNA damage induced in vivo by a cross-linking agent with a circular channel crucible oscillating viscometer. *Chem. Biol. Interact.* **1985,** 55, 261-273.

43.   Nicolini, C.; Carlo, P.; Martelli, A.; Finollo, R.; Bignone, F. A.; Patrone, E.; Trefiletti, V.; Brambilla, G., Viscoelastic properties of native DNA from intact nuclei of mammalian cells. Higher-order DNA packing and cell function. *J. Mol. Biol.* **1982,** 161, 155-175.

44.   Zang, H.; Gates, K. S., DNA Binding and Alkylation by the \"Left Half\" of Azinomycin B. *Biochemistry* **2000,** 39, 14968-14975.

45.   Gopalakrishnan, S.; Byrd, S.; Stone, M. P.; Harris, T. M., Carcinogen-nucleic acid interactions: equilibrium binding studies of aflatoxin B1 with the oligodeoxynucleotide d(ATGCAT)2 and with plasmid pBR322 support intercalative association with the B-DNA helix. *Biochemistry* **1989,** 28, 726-734.

46.   Joshua-Tor, L.; Frolow, F.; Appella, E.; Hope, H.; Rabinovich, D.; Sussman, J. L., Three-dimensional structures of bulge-containing DNA fragments. *J. Mol. Biol.* **1992,** 225, 397-431.

47.   Nakatani, K.; Okamoto, A.; Saito, I., Specific alkylation of guanine opposite to a single nucleotide bulge: a chemical probe for the bulged structure of DNA. *Angew. Chem. Int. Ed.* **1999,** 38, 3378-3381.

48.   Gu, F.; Xi, Z.; Goldberg, I. H., DNA damage by thiol-activated neocarzinostatin chromophore at bulged sites. *Biochemistry* **2000,** 39, 4881-91.

49.   Williams, L. D.; Goldberg, I. H., Selective strand scission by intercalating drugs at DNA bulges. *Biochemistry* **1988,** 27, 3004-11.

50.   Kalnik, M. W.; Norman, D. G.; Swann, P. F.; Patel, D. J., Conformation of adenosine bulge-containing deoxytridecanucleotide duplexes in solution. Extra adenosine

stacks into duplex independent of flanking sequence and temperature. *Journal of Biological Chemistry* **1989,** 264, 3702-12.

51.   Gollmick, F. A.; Lorenz, M.; Dornberger, U.; Von Langen, J.; Diekmann, S.; Fritzsche, H., Solution structure of dAATAA and dAAUAA DNA bulges. *Nucleic Acids. Res.* **2002,** 30, 2669-2677.

52.   Morden, K. M.; Gunn, B. M.; Maskos, K., NMR studies of a deoxyribodecanucleotide containing an extrahelical thymidine surrounded by an oligo(dA).oligo(dT) tract. *Biochemistry* **1990,** 29, 8835-45.

53.   Nakatani, K.; Okamoto, A.; Saito, I., Specific alkylation of guanine opposite to a single nucleotide bulge: a chemical probe for the bulged structure of DNA. *Angew. Chem. Int. Ed.* **1999,** 38, 3378-3381.

54.   Woodson, S. A.; Crothers, D. M., Binding of 9-aminoacridine to bulged-base DNA oligomers from a frame-shift hot spot. *Biochemistry* **1988,** 27, 8904-14.

55.   Streisinger, G.; Owen, J., Mechanisms of spontaneous and induced frameshift mutation in bacteriophage T4. *Genetics* **1985,** 109, 633-59.

56.   Gao, X.; Stassinopoulos, A.; Ji, J.; Kwon, Y.; Bare, S.; Goldberg Irving, H., Induced formation of a DNA bulge structure by a molecular wedge ligand-postactivated neocarzinostatin chromophore. *Biochemistry* **2002,** 41, 5131-43.

57.   Gopalakrishnan, S.; Stone, M. P.; Harris, T. M., Preparation and characterization of an aflatoxin B1 adduct with the oligodeoxynucleotide d(ATCGAT)2. *J. Am. Chem. Soc.* **1989,** 111, 7232-7239.

58.   Sambrook, J.; Fritisch, E. F.; Maniatis, T., *Molecular Cloning: A Lab Manual.* Cold   Spring   Harbor   Press,   Cold   Spring   Harbor,   NY.:   1989.

_____

Chapter 3. Reversible DNA Alkylation by Leinamycin and Related DNA-Alkylators

3.1. Introduction to Reversible DNA Alkylators and their Importance

3.1.1. Reversible DNA Intercalators

DNA alkylation has been most commonly thought of as an irreversible covalent reaction between a DNA-alkylator and DNA. In only a few recent reports has it been shown that DNA adducts of natural products or small organic molecules can reverse with the release of intact DNA and either the original DNA-alkylator (CC1065,[1,2] duocarmycin A and SA,[3,4] ecteinascidin 743,[5] quinone methides, [6] leinamycin, [7,8], Scheme 6) or their modified forms (Cyclopropyl Quinone Methides,[9] base propenals,[10,11] metabolites of tobacco carcinogens: NNK or NNNAL [12,13], Scheme 7).

3.1.2. Chemical and Experimental Considerations of Reversible DNA Alkylations

In the chemistry presented in Scheme 6 and Scheme 7, DNA acts a leaving group. For N9-substituted purines (guanine, adenine) alkylated at the N7 position, the leaving group ability of DNA under physiological conditions can be estimated by the pKa of the corresponding protonated forms of the base-nitrogens (pKa $_{N7H+}$: 2.1; pKa $_{N1H+}$: 9.2).[14] In addition to the leaving group ability of DNA, the ease with which the alkylating agent is regenerated also determines reversion. In the structure of CC-1065 and duocarmycin, for example, the closure of the cyclopropyl ring takes place unusually easily.[2] The leaving group ability of the DNA-bases (G, A, C) attached to the C3-carbon of base-propenals correlates well with the ease of reversion.[11]
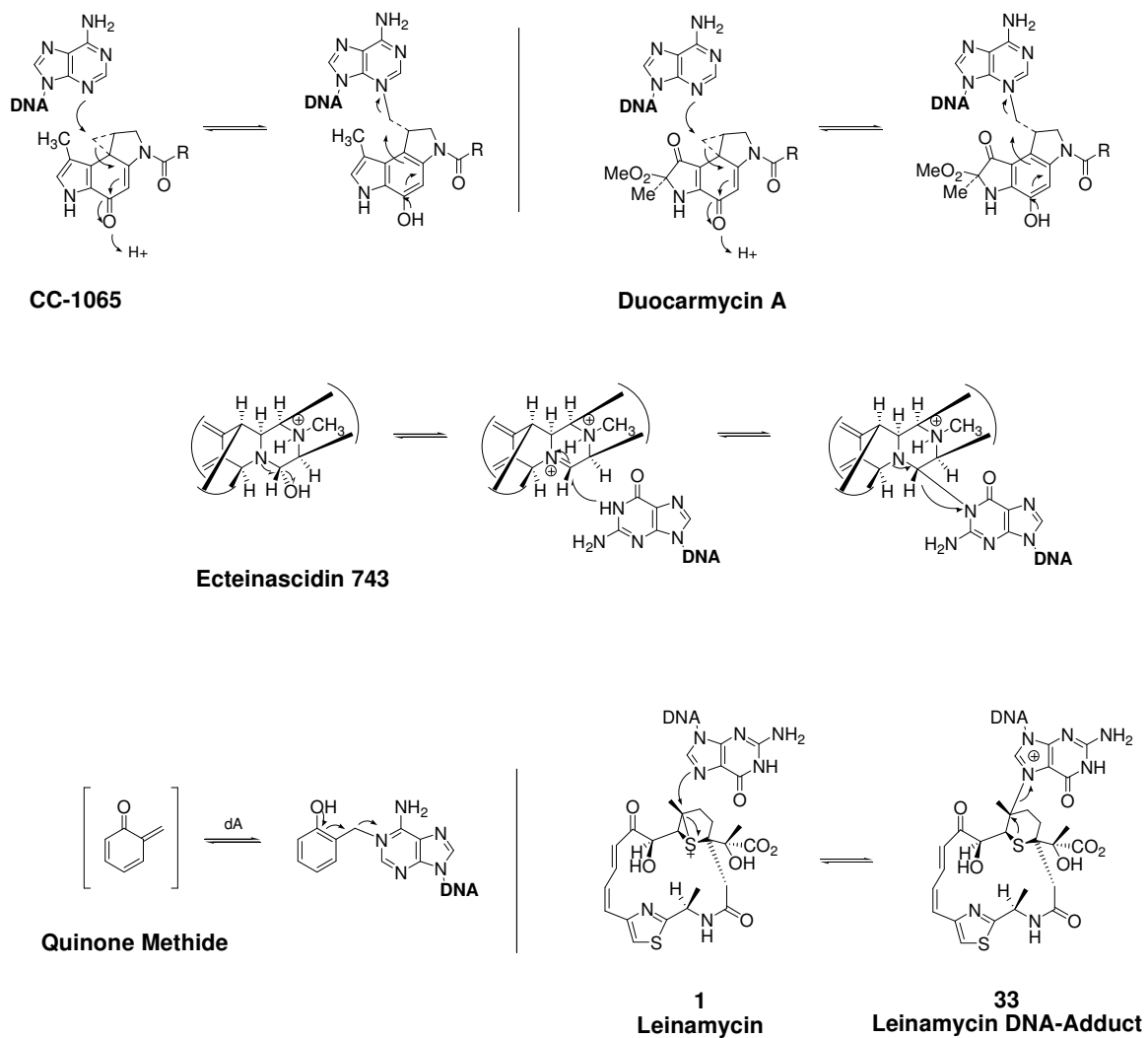
Scheme 6. Reversible DNA alkylators that are regenerated in their intact form from their DNA adducts during reversion.

cyclopropyl Quinone Methide

base propenal   **M₁G**

NNK metabolite

NNNAL metabolite
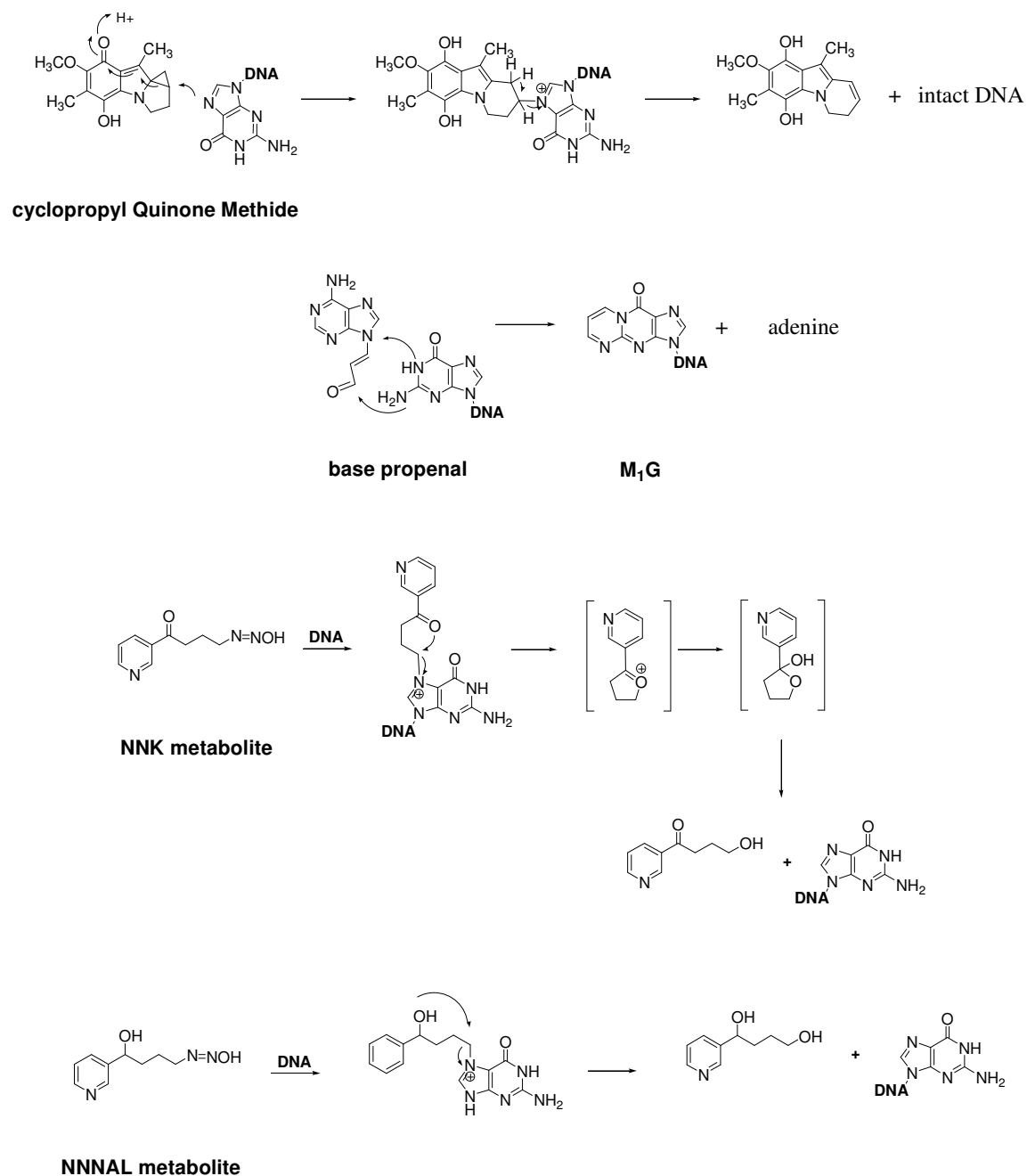
Scheme 7. Reversible DNA alkylators that are regenerated from the DNA adduct in their modified form during reversion.

_____

In cases where reversible DNA alkylation generates a small molecular species different from the original DNA alkylator (Scheme 7) DNA can be thought of as a catalyst for the transformation of the DNA-alkylating agent, [9-13] although one that acts at a very poor rate and yields.

The mechanism of reversion deserves some consideration. In cases where DNA is attached via a tertiary carbon to the DNA-alkylator, a direct displacement of DNA in an S_N2 attack at the carbon attached to the base by an external nucleophile is highly improbable for steric reasons. [15] In these situations, usually *intramolecular neighboring group participation* must promote the reversion step. This can take place in a direct displacement (ecteinascidin 743, leinamycin, NNK metabolite) or with the help of a β-elimination reaction (cyclopropyl quinone methides). Another mechanism is observed in a deprotonation induced quinone-formation reaction (CC-1065, duocarmycin A). In a few cases *intramolecular displacement* by water was observed (NNNAL metabolite). This latter process only takes place when DNA is attached to a primary or secondary carbon as S_N2 reactions do not take place readily on tertiary carbons. [15]

Reversion of DNA-adducts elongates the life time of the DNA-damaging agent in the proximity of DNA. Reversible DNA alkylation may allow "shuffling" of the kinetic alkylation products to thermodynamically more favorable sites. For example, quinone methides are known to alkylate the most nucleophilic (N^1) nitrogen in adenine, and then is transferred to the thermodynamically more favorable (N^6) nitrogen. [6] Migration along the DNA-chain is possible this way. For example, the rates of reversion of the Ecteinascidin 743 adduct show sequence dependence, occurring faster from 5'-AGT than

5'-AGC.[5] This also means that the kinetic product of DNA alkylation might not necessarily reveal the ultimate target sequence in DNA.[1] This would be revealed by a change in the sequence specificity of DNA-alkylation with time.

The conformation of DNA varies in cells, which can have an impact on the reversibility of adduct formation. The reversion of the duocarmycin adduct, for example, is facile from duplex DNA, whereas in single-stranded DNA it is slow.[4] On the other hand, as discussed below, leinamycin is released from single-stranded DNA at a higher rate than from the DNA-duplex.

Rates and yields of reversion steps for some reversible DNA-alkylators have been reported. Some, relevant to physiological conditions, will be reiterated here. The DNA adduct of CC-1065 (adenine N^3) was incubated in a mixture of butanol and 25 mM sodium phosphate buffer at 37°C at pH 7.4 for 5 days. This resulted in 20% extraction of the alkylator into the butanol phase.[1] In this report, an essentially quantitative reversion of the DNA-adduct was reported at pH 8.4 under otherwise similar conditions. Reversion of duocarmycin-DNA adduct (adenine N^3) above 50% was observed during a 4 day incubation at 37 °C in a butanol / 270 mM sodium phosphate buffer mixture at pH 8.0. This yield increased to 80% during a 6 day incubation time.[4] The reversal of the ecteinascidin 743-DNA adduct (guanine N^2) was studied [5] from 22-mer oligonucleotides with a single modification site. The rates of the reverse reaction from 5'-AGC, k_{r-1}: 2.8 x 10^{-4} s^{-1} (t$_{1/2}$ = 41 min, 0.7 h) and from 5'-AGT, k_{r-2}: 1.2 x 10^{-3}s^{-1} (t$_{1/2}$ = 9 min, 0.15 h) are clearly sequence dependent. Finally, the kinetic adduct of a quinone methide (adenine N^1) was studied.[6] This derivative hydrolyzed to 95% extent within 4 h. This work showed

that the released quinone methide can be transferred to additional nucleophilic alkylation sites in DNA (adenine N^6, guanine N^2, cytosine N^3), which are the major adducts formed with this alkylating agent.

3.1.3. Biological and Medicinal Consequences of Reversible DNA Alkylations

Reversal of a bioactive natural product from its DNA adduct can elongate its life-time as a DNA-damaging agent and may increase its mutagenic potential. The lipid peroxidation product malondialdehyde (MDA), for example, forms a mutagenic DNA-adduct (M_1G, shown in Scheme 7).[10,16] A similar DNA-adduct formed formed under oxidative stress in cells with adenine can "carry" malondialdehyde to guanines to form M_1G. This way, the life-time of MDA is increased in cells, and it is also spread further along the DNA strand. Additionally, it was also observed that the adenine-MDA adduct is more mutagenic than MDA itself.[10]

Since DNA adducts are generally cytotoxic and mutagenic lesions[17-21] the relative rates of reversion of intact DNA and that of depurination or repair of the DNA-adduct can determine the magnitude of their toxicity and mutagenicity.[9] Along these lines it has been expressed that if higher reversibility was achieved in normal cells than in tumor cells, these alkylating agents would be selectively cytotoxic to tumor cells. [4]

Successful DNA repair might depend upon the reversibility of a DNA adduct. DNA-repair induced cell toxicity was reported for ecteinascidin 743.[22] The ease of reversal of this drug depends on the sequence context of DNA. It was shown that this adduct induces nucleotide excision repair (NER). The repair protein assembly associates

the DNA adduct irreversibly, and leads to mutations and apoptosis. Using mammalian cell lines it was shown that ET 743-DNA adducts at different sequences with different inherent adduct stabilities are repaired at different efficiencies. The more stable ET 743-lesions are repaired to lesser extent.

Our understanding of reversible DNA alkylation by natural products is at an early stage. This fact itself speaks to exploring a novel reversible DNA alkylator, leinamycin.

3.2. Initial Discovery of Reversibility in the DNA-alkylation by Leinamycin [8,23]

Our research group observed the release of the hydrolysis product of leinamycin (**1**) from highly purified DNA-adduct. This reversion probably takes place in an S_N1 (first-order) reaction with the neighboring group effect of the ring sulfur in the DNA adduct. With the information that S_N2 reactions do not take place readily on tertiary centers,[15] we hypothesize that the highly reactive episulfonium-ion (**10**) is regenerated first and then undergoes hydrolysis to **13**.
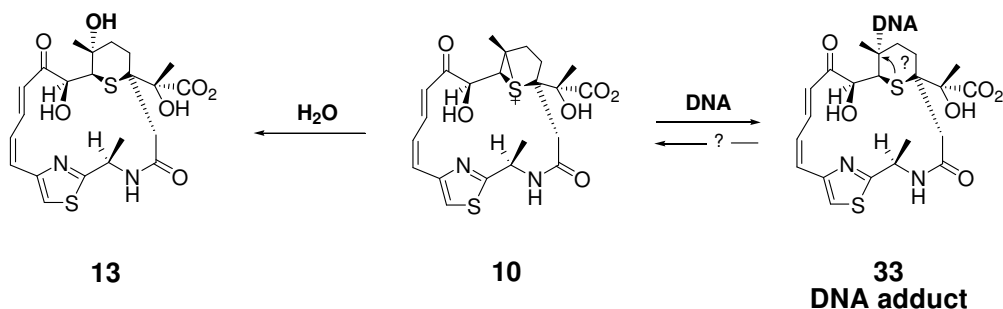
Scheme 8. The release of the hydrolysis product of activated leinamycin (**10**) from its purified DNA adduct (**33**). In the mechanism above, we hypothesize that the displacement of DNA happens with the help of the ring sulfur.

_____

Suggestively, we demonstrated that leinamycin-modified DNA could "carry" active alkylating agent to an unmodified DNA duplex. Similarly a 2'-deoxyguanosine adduct of leinamycin can alkylate plasmid DNA.[7] We suspected this involved the release of a free episulfonium ion (**10**) from these adducts.

3.3. Goals of this Work

The natural product leinamycin (**1**) has revealed novel chemistry in its DNA damaging reactions, [23] and it employs unique DNA binding strategies (Chapter 1, Chapter 2) to facilitate this chemistry. With the possibility that this natural product is also a reversible DNA-alkylating agent, additional unexpected chemical activities are expected to be found in leinamycin. Additionally, leinamycin would be the first reversible DNA-alkylating natural products that targets the N7 nitrogen in guanine.

- We set out to measure the rates of reversion from the DNA-duplex and from single-stranded DNA under physiological conditions. With this information we can calculate the relative yields of reversion/depurination, which would be important in evaluating what determines the cellular fate of the natural product. We will also learn here if the DNA-duplex promotes or inhibits the reversion. [4]

- We investigated whether the small N7G alkylator antitumor agent chlorambucil (**34,** Scheme 9) and a sulfur-mustard (CEES, **37,** Scheme 9) [24] similarly alkylate DNA reversibly. These compounds are important as drugs and war gases. Our work stands to reveal an important, unrecognized property of these drugs and toxins. These molecules alkylate DNA via aziridinium or episulfonium intermediates,

_____

respectively, and at a fundamental level, their adducts are structurally analogous to

leinamycin's.
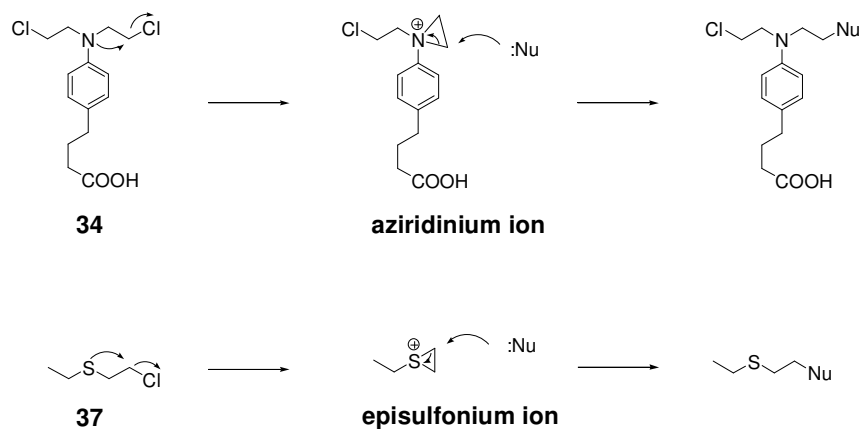
Scheme 9. The structures and DNA-alkylating forms of the nitrogen-sulfur: chlorambucil (**34**) and CEES (**37**).

- Finally, we examined whether thiols of different leaving-group ability (β-mercaptoethanol: $pK_a = 9.5$; glutathione: $pK_a = 8.5$ and thiophenol: $pK_a = 6$) and the biologically abundant chloride ion (Cl⁻: $pKa = -4$) would reversibly add to activated leinamycin. Reversible addition of these or related thiol molecules to activated leinamycin could effectively extend the cellular life-time of this DNA-alkylating agent, and help "carry" the natural product to its target in the cell nucleus.

_____

3.4. Proposing a Tentative Mechanism for the Reversion of 10 from the DNA Adduct (33)

A kinetic mechanism for reversible DNA alkylation by LM can be proposed (Scheme 10). [23]

Scheme 10. Release of activated leinamycin (**10**) from the DNA adduct (**33**) and its further hydrolysis to yield the leinamycin-hydroxide (**13**) with simultaneous depurination to **43**. The structures of **13** and **33** and **43** are shown. In the mechanism above we used results from earlier studies [23] that showed disproportionation of **10** between hydrolysis and depurination to yield **13** and **43**, respectively.

A simple inspection of this mechanism suggests that the relative yields of LM-OH and LM-G should depend on the concentration of DNA in the reaction. Low DNA concentration disfavors the formation of the noncovalent complex: [**10** • DNA], thus disfavoring alkylation versus hydrolysis to **13**. We derived a kinetic equation for this mechanism (Section 3.5.). We examined the yields of **13** and **43** (Section 3.6.). We measured the rate of decomposition of the leinamycin-DNA-adduct and calculated k_{rev} under different conditions (Sections 3.8. and 3.9.).

_____

3.5. Steady State Analysis to Derive a Rate Equation for our Hypothesized Mechanism

We derived a rate equation from our proposed mechanism (Scheme 10 and Scheme 11 below). The concentration of the DNA adduct gradually will decrease in time by the two terminal reactions in a competitive fashion (Equation 39). These reactions are the depurination of the leinamycin-DNA adduct (k_G) and the hydrolysis of the released episulfonium ion (**10**).

$$H_2O$$

$$\text{''}K_e\text{''}$$

$$13 \xleftarrow{k_{oh}} 10 + DNA \underset{}{\overset{K_b}{\rightleftharpoons}} [10] \bullet [DNA] \underset{k_{rev}}{\overset{k_{cat}}{\rightleftharpoons}} 33 \xrightarrow{k_g} 43$$

hydrolysis product　　　　　　　　　　　　　　　　　　　　　　**DNA-adduct**　　**depurination product**

$$k_{cat} / k_{rev} = K_e$$
$$K_B \times K_e = K_x$$
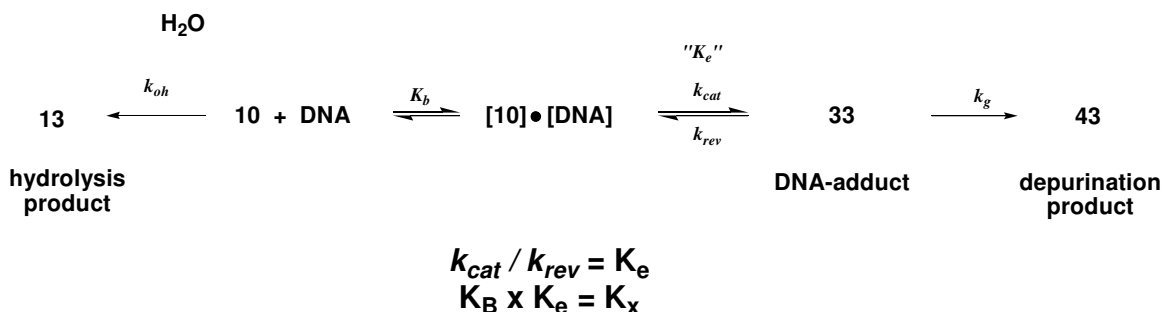
Scheme 11. Mechanism of reversion of the leinamycin episulfonium ion (**10**) from the leinamycin-DNA adduct (**33**), with the equilibrium constant **Kx**.

The newly introduced "equilibrium constant":

$$K_x = \frac{[33]}{[10][DNA]}$$

Equation 38

The degradation of the adduct in time:

Equation 39

$$\frac{d[33]}{dt} = -k_g[33] - k_{OH}[10]$$

To eliminate the factor: [**10**] from the equation we expressed it using the equilibrium constant (Equation 38):

_____

$$[10] = \frac{[33]}{K_x[DNA]}$$

Equation 40

…this rewrites Equation 39 to Equation 41 below:

$$\frac{d[33]}{dt} = -k_g[33] - \frac{k_{OH}[33]}{K_x[DNA]} = -[33]\left[k_g + \frac{k_{OH}}{K_X[DNA]}\right]$$

Equation 41

Rearranging Equation 41 to express the time dependence of its concentration change will give us Equation 42.

$$-\frac{d[33]}{[33]} = \left[k_g + \frac{k_{OH}}{K_X[DNA]}\right]dt = k*dt$$

Equation 42

Integration of Equation 42 will result in Equation 43:

$$[33] = [33]_0 \exp^{-\left[k_g + \frac{k_{OH}}{K_X[DNA]}\right]*t}$$

Equation 43

This equation above describes the actual concentration of the leinamycin-DNA adduct [**33**] at any given time point in the incubation reactions.

From Equation 42 and Equation 43 the rate of the degradation of the leinamycin-DNA adduct (**33**) can be expressed, Equation 44.

$$k_{LM-DNA} = k_g + \frac{k_{OH}}{K_X[DNA]}$$

Equation 44

Since DNA was fully converted to the adduct, the following is true: [**DNA**] ≈ [**33**], thereby:

$$k_{LM-DNA} = k_g + \frac{k_{OH}}{K_X[33]} = k_g + \frac{k_{rev}k_{OH}}{K_B k_{alk}[33]}$$

Equation 45

Equation 45 shows that the degradation of the leinamycin-DNA is the result of two reactions, the apparent rate of depurination (k_g, :rate of appearance of the depurination product in the incubation of the DNA-adduct) and apparent hydrolysis (Equation 46: rate of appearance of the hydrolysis product in the incubation of the DNA-adduct).

$$k_{(OH)app} = \frac{k_{OH}}{K_X[33]} = \frac{k_{rev}k_{OH}}{K_B k_{alk}[33]}$$

<div align="right">**Equation 46**</div>

Please, note that the apparent rate constant of hydrolysis here ($k_{(OH)app}$, the rate at which the appearance of the LM-OH product is observed in the incubation of pure DNA-adduct) is different from the rate of the pure hydrolysis of leinamycin (k_{OH}). Also, note that the apparent rate of depurination (k_g) is the observed rate of appearance of the depurination product in the incubation of the leinamycin-DNA adduct. As shown by Equation 46 and later confirmed by our results, $k_{(OH)app}$ and the final yield of **13** (Figure 49) will depend on the concentration of the adduct in the incubation. At the same time, k_g is independent of the concentration of the DNA-adduct incubated at a given temperature. However, the yield of the depurination product will change with the concentration of the DNA-adduct, since the $k_{(OH)app}$ is changing with the concentration of the adduct [**33**].

Measuring the rate of the disappearance of the leinamycin-DNA adduct (k_{LM-DNA}) and measuring the apparent rate of depurination (k_g) and the rate of the appearance of the hydrolysis product ($k_{(OH)app}$) in the same experiment, allows us to calculate the rate of the reversal step (k_{rev}). Note that a measurement of the noncovalent association constant (K_B), the maximum rate of DNA alkylation (k_{alk}) and the "inherent" rate of hydrolysis of the leinamycin episulfonium ion (k_{OH}) needs to be done in independent experiments.

_____

The yield of the hydrolysis product in the incubation of pure leinamycin-DNA adduct (from reversal Chemistry) can be expressed as the ratio of the rates of the terminal reactions: $100 \times k_{(OH)app} / k_g$. This ratio is expressed in Equation 47.

Equation 47

$$\%13 = \frac{100 * k_{(OH)app}}{k_g + k_{(OH)app}} = \frac{\dfrac{100 * k_{OH}}{K_X[33]}}{k_g + \dfrac{k_{OH}}{K_X[33]}} = \frac{\dfrac{100 * k_{OH}}{K_X[33]}}{\dfrac{k_g K_X[33] + k_{OH}}{K_X[33]}} =$$

$$= \frac{100 * k_{OH}}{k_g Kx[33] + k_{OH}}$$

Accordingly, the yield of the hydrolysis product will decrease in a hyperbolic fashion with increasing adduct concentration. Accordingly, the yield of the depurination product should increase.

Our data for the yields of LM-G and LM-OH at various DNA adduct concentrations perfectly fits this equation. At higher concentrations of the DNA-adduct, we see a decrease in the yield of the hydrolysis product (**13**).

_____

An alternative mechanism for the formation of the hydrolysis product (**13**) would be the

direct displacement of the LM-OH from duplex DNA by water as shown in Scheme 12.

$$
\begin{array}{c}
\textbf{33} \xrightarrow{ k_{OH} } \textbf{13} \\
\searrow^{k_G} \\
\textbf{43}
\end{array}
$$
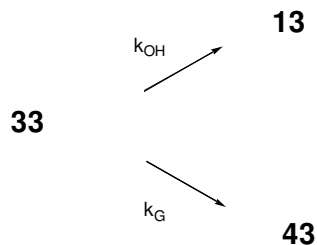
Scheme 12. Mechanism of reversion via direct displacement of hydrolysis product (**13**) by water from the DNA adduct (**33**) with the competitive depurination to the leinamycin-guanine molecule (**43**).

An analysis by Steady-State theory and derivation shows that the yield of the hydrolyzes

product (**13**) would not depend on the concentration of the incubated DNA-adduct, **33**

(Equation 48)

$$(\%13)_{direct.dipl.} = \frac{100k_{OH}}{k_{OH} + k_G} \qquad\qquad \textbf{Equation 48}$$

_____

3.6. The Yields of 13 and 43 Confirm our Reversion Mechanism

We incubated LM-DNA at 37 °C in 50 mM sodium phosphate buffer at pH 7.0 for 48 h at different adduct concentrations, and followed the production of **13** and **43** in time (Figure 48). Upon accomplishment of the degradation of the DNA-adduct, the yield of **13** (Figure 50) and the yield of **43** (Figure 49) were calculated at each adduct concentration. Our observed yields followed that proposed by our kinetic mechanism (Section 3.5.). Dilution of the DNA-adduct dilutes each reaction component, which will eventually help the disintegration of the DNA-adduct, and result in increased yields of reversion (the hydrolysis product, **13**). This has been predicted by the kinetic description of our mechanism (Section 3.5., Scheme 10, Equation 47).
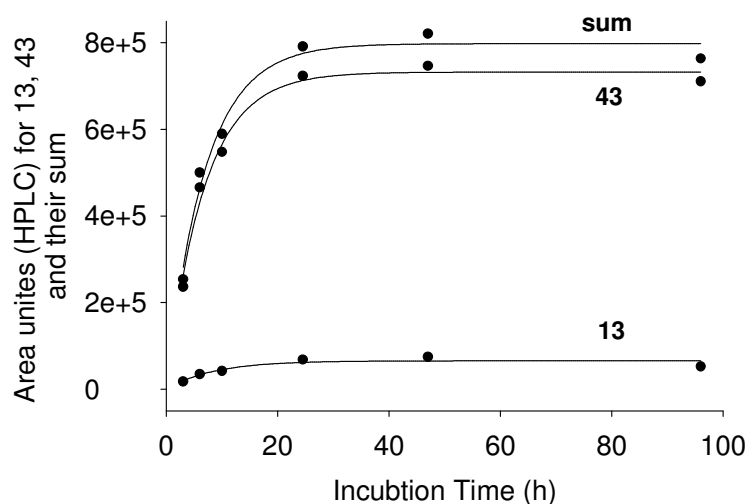
Figure 48. The appearance of the hydrolysis product (**13**) and the depurination product (**43**) from the DNA-adduct (**33**) of leinamycin (**1**) versus time.

_____
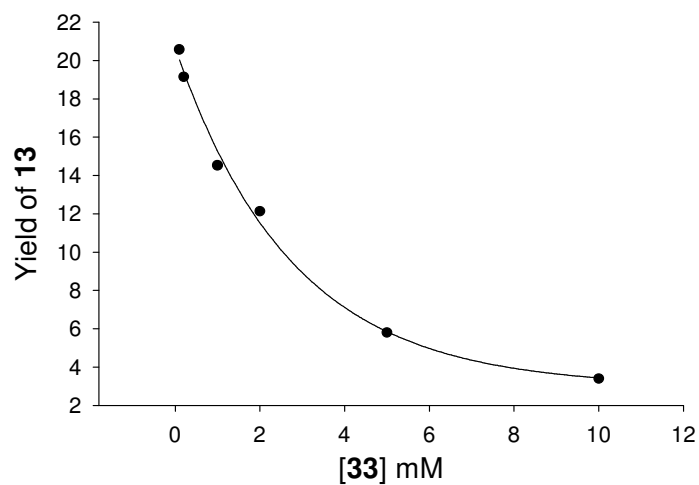
Figure 49. The yield of the hydrolysis product (**13**) from the DNA-adduct (**33**) via reversion. Conditions: Incubation at 37 °C in 50 mM sodium phosphate buffer (pH 7.0) for 48 h. Concentrations of the purified DNA adduct (**33**): 0.1 mM, 0.2 mM, 1 mM, 2 mM, 5 mM, 10 mM.
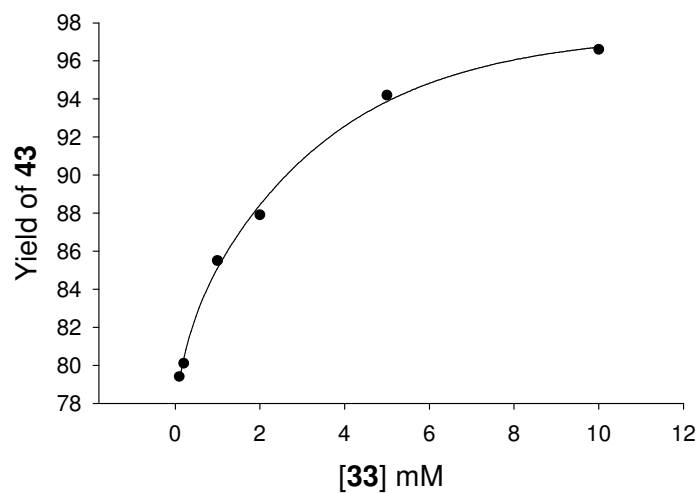
Figure 50. The yields of the depurination product (**43**) in the reversion chemistry.

_____

3.7. How do we Exclude "Carry Over"?

In the case of carry over, the hydrolysis of the released episulfonium ion (k_{OH}) and the depurination of the DNA-adduct (k_G) would be independent of each other. Assuming an initial n% carry over and 100-n% adducted leinamycin, upon the accomplishment of hydrolysis and depurination, the n% episulfonium would be converted to n% hydrolysis product and the 100-n% adduct would be converted to 100-n% depurination product, and would be independent of the concentration of the DNA in the degradation studies.
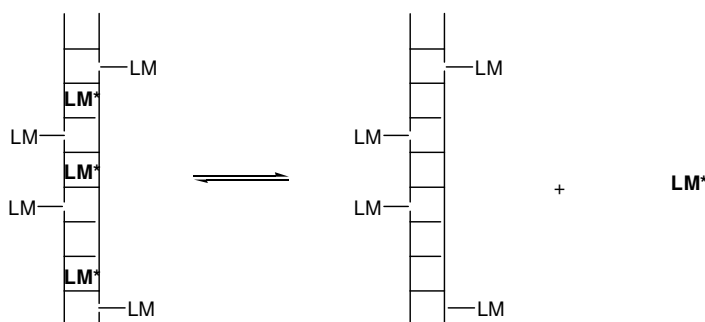
Scheme 13. Mechanism of the generation of the hydrolysis product of leinamycin (**13**) via noncovalently bound "carry over" episulfonium.

Such is not the case for reversal. As we have shown in our kinetic description (Section 3.5.), the release of the hydrolysis product should follow a hyperbolic dependence on the DNA-adduct concentration (Equation 47). This will consequently force a concentration dependence of the final yield of the depurination product in the reversal Chemistry.

_____

3.8. Calculation of the Rate of Reversion (k_{rev})

We incubated our DNA-adduct at 2 mM concentration in 50 mM sodium phosphate buffer (pH 7.0) at 37 °C, and followed the time appearance of the hydrolysis product (**13**) and the depurination product versus time (**43**). Non-linear regression of the products versus time curve (Figure 48) to a rising exponential allowed us the calculation of the rate of degradation of the adduct ($k_{LM\text{-}DNA}$). Using Equation 45 (repeated below), with an independent measurement of k_{OH}, (4.3 ± 0.5 x 10^{-5} s^{-1}, $t_{1/2}$ = 4.5 h), $K_{B,}$ (1000 M^{-1}) and k_{alk} (9.1 x 10^{-4} s^{-1}, $t_{1/2}$= 13 min) (Chapter 1), we were able to calculate **k_{rev} = 1.5 x 10^{-4} s^{-1}**, **$t_{1/2}$ = 1.3 h**. Please note that in Equation 45, the rate of depurination (k_g = 4.0 x 10^{-5} s^{-1}, $t_{1/2}$ = 4.8 h) is the apparent/observed rate of appearance of the depurination product from the adduct in our incubation calculated from Figure 48, using non-linear regression.

$$k_{LM-DNA} = k_g + \frac{k_{OH}}{K_X[33]} = k_g + \frac{k_{rev}k_{OH}}{K_B k_{alk}[33]}$$

Equation 45

From the data above we can conclude that the DNA adduct is more prone to reversion than to depurination (k_{rev}/k_g = 3.7). This simply means that reversion is favored kinetically over depurination.

The yields of **13** and **43** (Section 3.6) show us that eventually the winner of these reactions will be the depurination reaction. This is the consequence of the binding forces (K_B ~ 1000 M^{-1} and K_e = 6, K_B x K_e ~ 6000 M^{-1}, K_e = k_{alk}/k_{rev}) that holds the reversed natural product in the major-groove of DNA until the adduct bleeds out to depurination. Please, notice that the equilibrium between the non-covalently bound episulfonium (**10 • DNA**) and the covalent DNA-adduct (**33**) is in the direction of the adduct formation: K_e =

_____

"k_{alk}/k_{rev} = 6" ($\Delta G°$ ~ 1 kcal/mol). This equilibrium constant shows that leinamycin is more stable in the form of the covalent DNA-adduct than in the noncovalent complex [**10 • DNA**].

3.9. The DNA Duplex Stabilizes the Leinamycin DNA-Adduct (33)

To compare the rates of reversal from duplex DNA to that of single-stranded DNA, we incubated the ss-DNA adduct of leinamycin (5'-TATAT<u>G</u>CATATA-3') at 2 mM adduct concentration at 37 °C, in 50 mM sodium phosphate buffer. We followed the appearance of the products in time by HPLC. Nonlinear-regression allowed us to measure the rate of degradation of the single-stranded DNA-adduct (k_{TOTss}). We calculated the rate of reversion similarly to the situation for the duplex-DNA-adduct (Section 3.7). This, however, required us to use the same binding constant (K_B) and rate of DNA alkylation (k_{alk}) originally found for the alkylation of duplex-DNA. Finally, the rate of reversion for this system is: $k_{rev,\ ss\text{-}DNA}$ = **3.2 x 10^{-4} s^{-1}** (*t ½* = 0.6 h). Please, note that leinamycin would bind to single-stranded DNA less efficiently than to duplex DNA ($K_{Bss} < K_{Bds}$) and would alkylate single-stranded DNA at a lower rate ($k_{alk\text{-}ss} < k_{alk\text{-}ds}$). With our measured k_{TOT}, using a lower K_B and lower k_{alk} in Equation 45, the "real" k_{rev} for the reversal Chemistry of the single-stranded DNA-adduct would be somewhat different. Nevertheless, the measurement of reversion from single-stranded DNA should give us the true k_{rev}. The real rate of reversal ($k_{rev\text{-}ssREAL}$) would be smaller.

_____

Physically, the faster reversion from the single-stranded DNA in comparison to the duplex-DNA-adduct is the consequence of decreased adduct stabilization in the single stranded DNA. Interestingly, even the measured rate of depurination was faster from the single-stranded DNA-adduct ($k_{gss} > k_{gds}$), suggesting that the leinamycin-DNA-adduct enjoys stabilization in the context of duplex-DNA. Note: The depurination of the single-stranded DNA adduct of leinamycin (k_{gss}) was directly measured in these experiments.

We compared the rates of reversion (Figure 52) and the rates of depurination (Figure 52) and the yields of the final products (Figure 53) in bar graphs, below. A closer inspection of these bar-graphs helped us understand that the DNA-adduct of leinamycin is stabilized by duplex-DNA (Figure 51). The ratio: k_{alk} / k_{rev} is greater than 1 in both cases, which shows that the equilibrium between the noncovalently associated adduct of activated leinamycin (**10•DNA**) and the covalently bound LM-DNA adduct (**33**) favors the covalent adduct (**33**), shown in Figure 51.
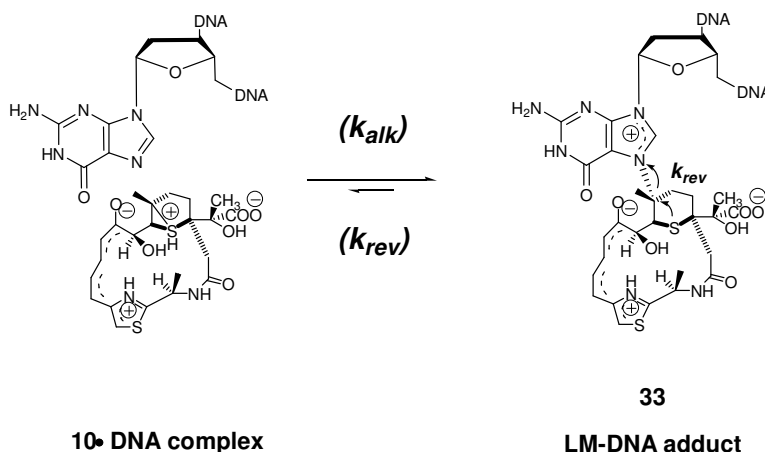
Figure 51. The Equilibrium between the **10•**DNA complex and its covalent adduct (**33**) favors the covalent DNA-adduct (**33**) of leinamycin in both single-stranded and duplex-DNA.

_____
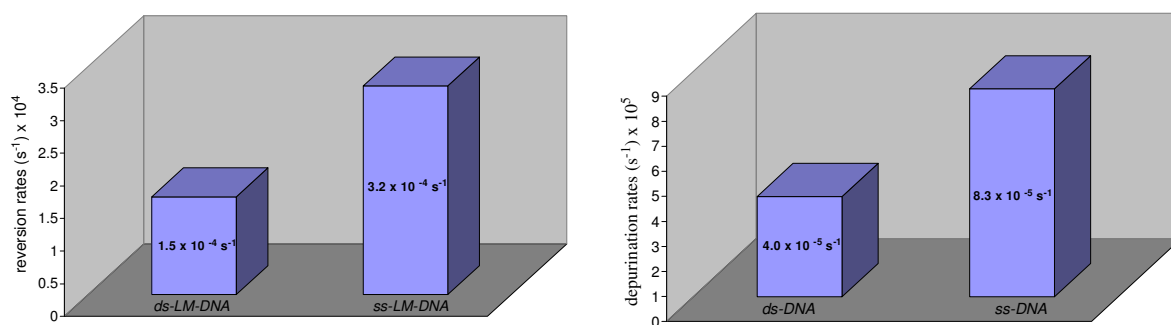
Figure 52. Comparison of the rate constants of reversion (*left*), rate constants of depurination (*right*) in the degradation of the DNA-adduct (**33**) in single-stranded and in duplex-DNA.
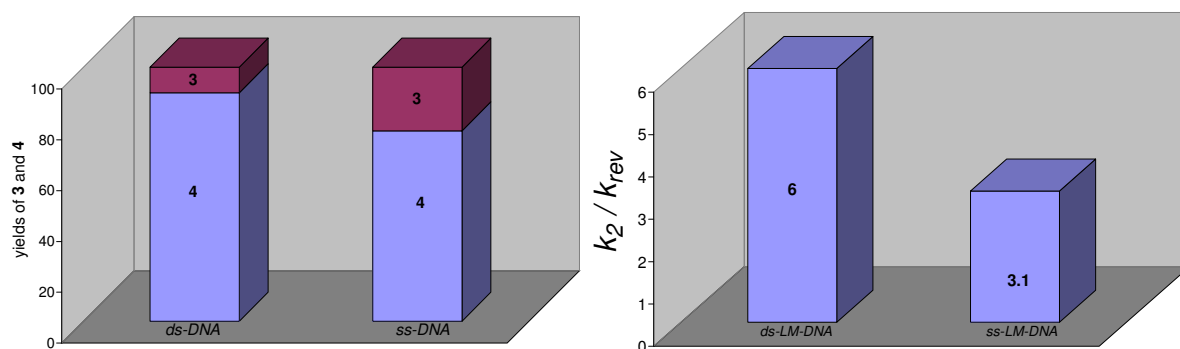
Figure 53. The yields of end products **13** and **43** = LM-G (*left*) and the ratio: k_{cat}/k_{rev} in the degradation of the DNA-adduct (**33**) in single-stranded and in duplex-DNA.

_____

3.10. Reversible Guanosine Alkylation by Structural Analogs of the Leinamycin-DNA Adduct

We set out to examine if the regeneration of the intact guanine base is possible from the N7-guanosine adduct of the anti-tumor agent chlorambucil (**34**) and that of CEES (**37**) under physiological conditions. Such reaction would involve the neighboring group attack of the heteroatom (N or S, respectively) on the carbon bound to the N7-nitrogen with a transient formation of an aziridinium or episulfonium ion (Scheme 14). We looked for the appearance of the hydrolysis products and the regeneration of intact guanosine.
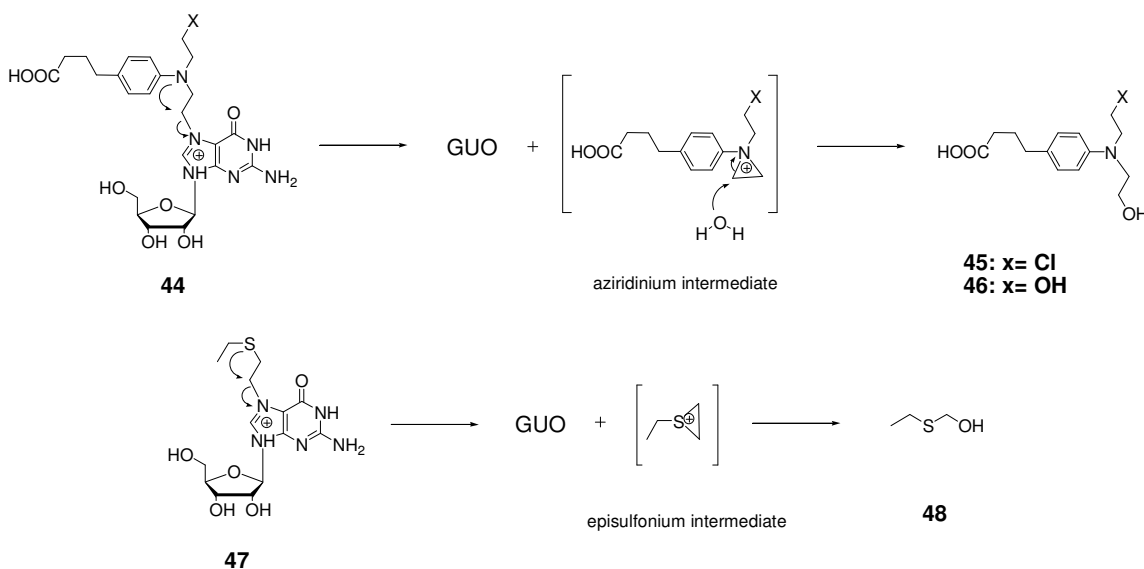
Scheme 14. Proposed mechanism of reversion of guanosine from the N7-guanosine adduct of chlorambucil (**44**) and that of CEES (**47**)

_____

3.10.1. Synthesis of The N7-Guanosine-Chlorambucil (44) and N7-Guanosine CEES (47) Adducts

First, we developed a synthesis of the N7 adducts (**44, 47**). Our attempt in using flash-chromatographic or preparative-TLC purification of the products failed. The starting materials, the expected products and the impurities turned out to be inseparable using either silica or reversed-phase-based separation methods. Our attempts for their recrystallizations failed, too. We anticipated that the HPLC purification of the adducts would be tedious, requiring high loads of HPLC solvents and desalting at the end, so eventually, we decided to synthesize **44** and **47** in stochiometrically controlled fashion in 2,2,2-trifluoroethanol solvent. DMF, DMSO, and THF solvents did not give us acceptable yields. Reactions were run at room temperature until the total disappearance of the starting materials and were followed using RP-HPLC (Figure 55 and Figure 58). Since CEES is undetectable by HPLC, the synthesis of the N7-GUO-CEES adduct was finished by evaporating the excess CEES from the mixture under high vacuum. LC-MS (Figure 56 and Figure 60) and NMR characterization revealed the regiochemistry of the adducts and concluded that they formed on the N7 nitrogen of guanosine in both **44** and **47**. The regiochemistry (N7 vs. N2 or O6 adducts) is confirmed by the chemical shift of the C8-H, [25] the presence of the N2 chemical shifts and the effect of added deuterium-oxide (D_2O) on the exchangeable protons of guanosine in the adduct. [8]

_____

3.10.2. Reversal of Sulfur Mustard and Nitrogen Mustard Guanosine-N7 Adducts of Chlorambucil and CEES

Guanosine adducts (**44**, **47**) were incubated in buffered solutions at 4°C and 37 °C for 3 days, and analyzed by HPLC. In the case of **44**, the reappearance of the hydrolysis product of chlorambucil (18 min peak in Figure 54 and Figure 57) and in the case of **47** the reappearance of intact guanosine (13 min peak in Figure 58, and Figure 59) were taken as signs of reversion. The percentage reversion was calculated from these product peaks. The adducts were found fairly stable, with 85% remaining intact. In both cases a minor reversion (total yield x < 2.9%) was observed (Table 8). Corrected for the remaining starting material this change is more significant: (~15%). The percentage reversion found for **44** and **47** was less than that of leinamycin (up to 20%). We explain this by the pre-organized nature of the natural product leinamycin for the intramolecular displacement reaction compared to the rather flexible adducts in **44** and **47** (Table 8).

Adduct	4 °C (3 days)	37 °C (3 days)
33	~ 12%	N.A.
44	0.3%	2.3%
47	2.3%	2.9%
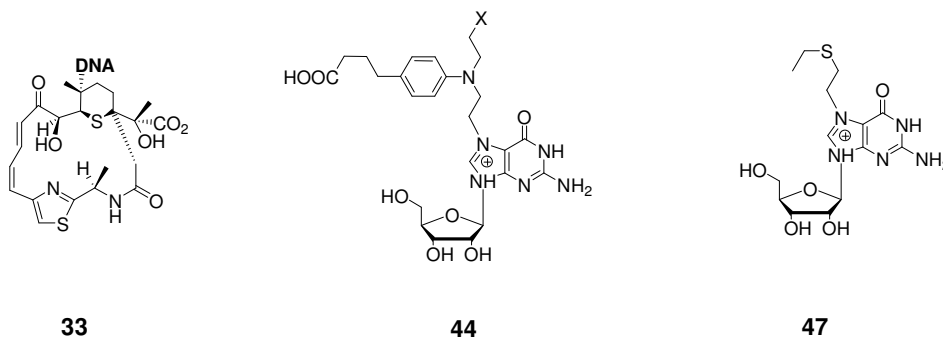
Table 8. Percentage reversible decomposition of **33, 44** and **47** and their structures.

_____
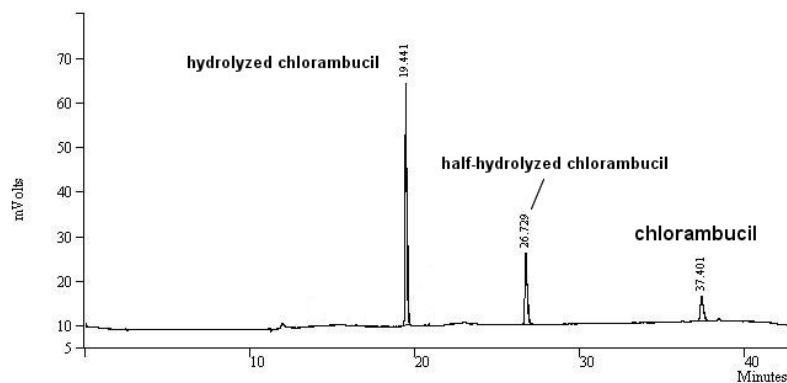
Figure 54. HPLC-trace of the hydrolysis products of chlorambucil (**34**)
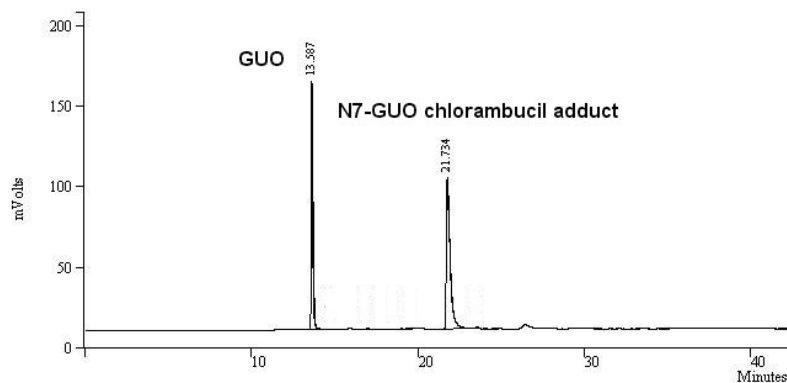
Figure 55. HPLC-trace of the N7-guanosine adduct of chlorambucil (**44**)

_____
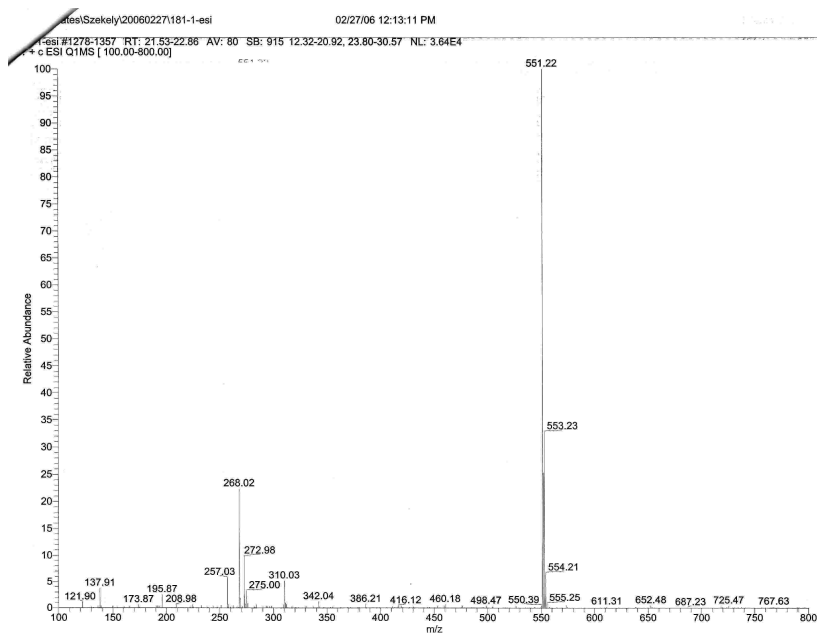
Figure 56. Mass Spectrum of the N7-guanosine adduct of chlorambucil (**44**)
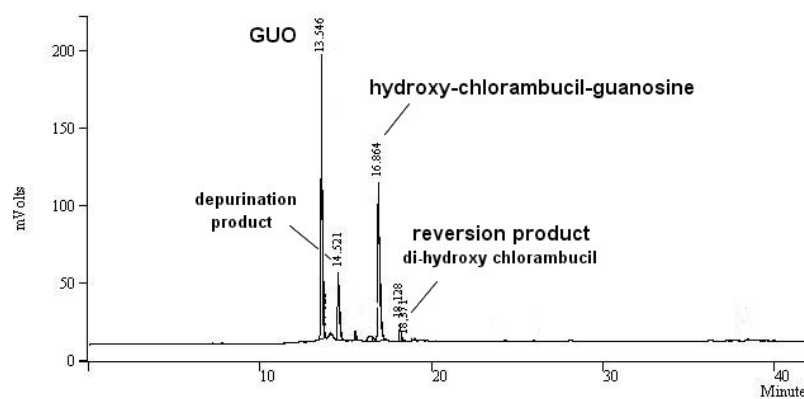
Figure 57. The HPLC-trace of N7-guanosine adduct of chlorambucil (**44**) after exposure to aqueous buffer (50 mM MOPS, pH 7.4, 3 days).

_____
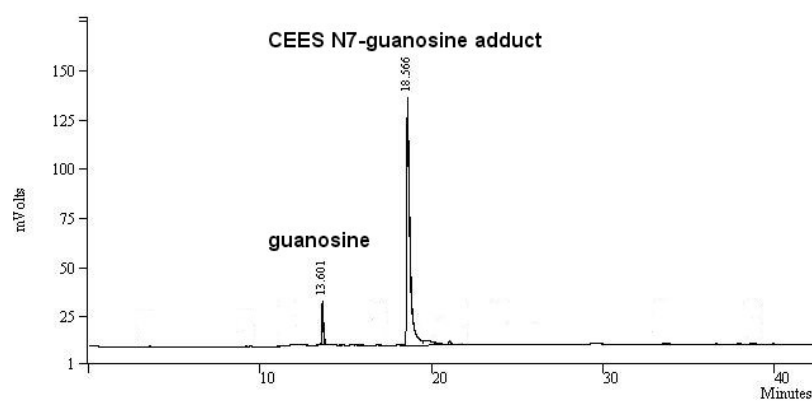
Figure 58. HPLC trace of the N7-guanosine-CEES adduct (**47**)
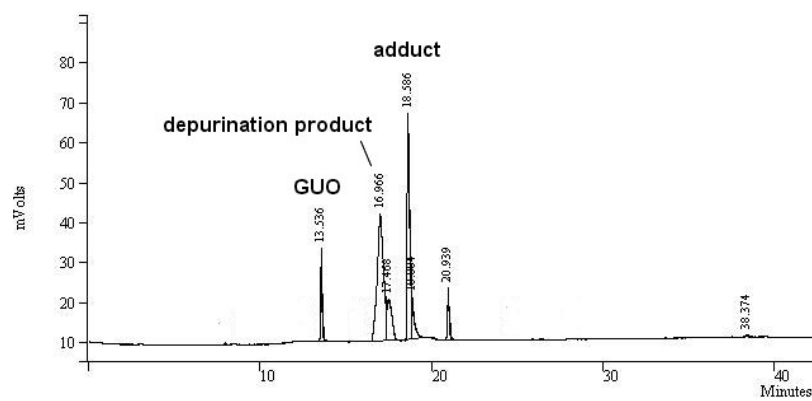
Figure 59. HPLC-trace of the N7-guanosine-CEES adduct (**47**) after exposure to aqueous buffer (50 mM MOPS, pH 7.4, 7 days)

122
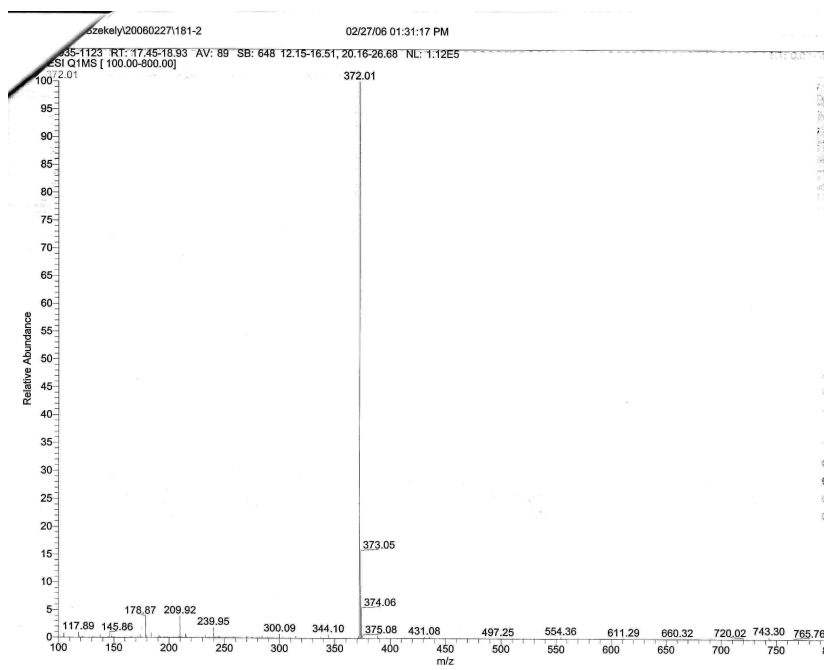
Figure 60. Mass spectrum of the N7-guanosine-CEES adduct (**47**)

3.11. Reversible Addition of Chloride Ion and Thiols to Activated Leinamycin and its Potential Role in Stabilizing and Carrying the Leinamycin Episulfonium Ion.

We set out to study if nucleophiles, other than the N7-nitrogen of guanine can add to the episulfonium ion in a reversible fashion. Such studies are interesting, because cells contain thiols and negatively charged species at considerable concentrations (thiols: 0-10 mM,[26] chloride ion ~ 200 mM[27]). The leaving group abilities of these nucleophiles cover a wide range from glutathione (pK_a = 8.5), protein thiols (5 < pK_a < 9), chloride (pK_a = -4).

We hypothesized that reversible thiol or chloride adduct may be able to "carry" the leinamycin episulfonium ion in cells and protect it from nonproductive hydrolytic decomposition (Scheme 15). It is known that hydrolytic instability can limit the DNA-alkylating efficiency (and the biological activity) of other agents such as nitrogen mustards.[28]

We expect that soft thiols (β-mercaptoethanol, pKa = 9.0; glutathione, pKa = 8.5) would add in a Michael-Fashion to the conjugated thiazole-dienone portion (the "left-half") of leinamycin (**42**). Consequently, harder thiols, like thiophenol (pKa = 6.5) would rather favor adduct formation with the harder electrophile, the three-membered-ring of the episulfonium (**41**). Similarly, we expect chloride ion to add directly to the episulfonium-ring (**40**, Scheme 15).
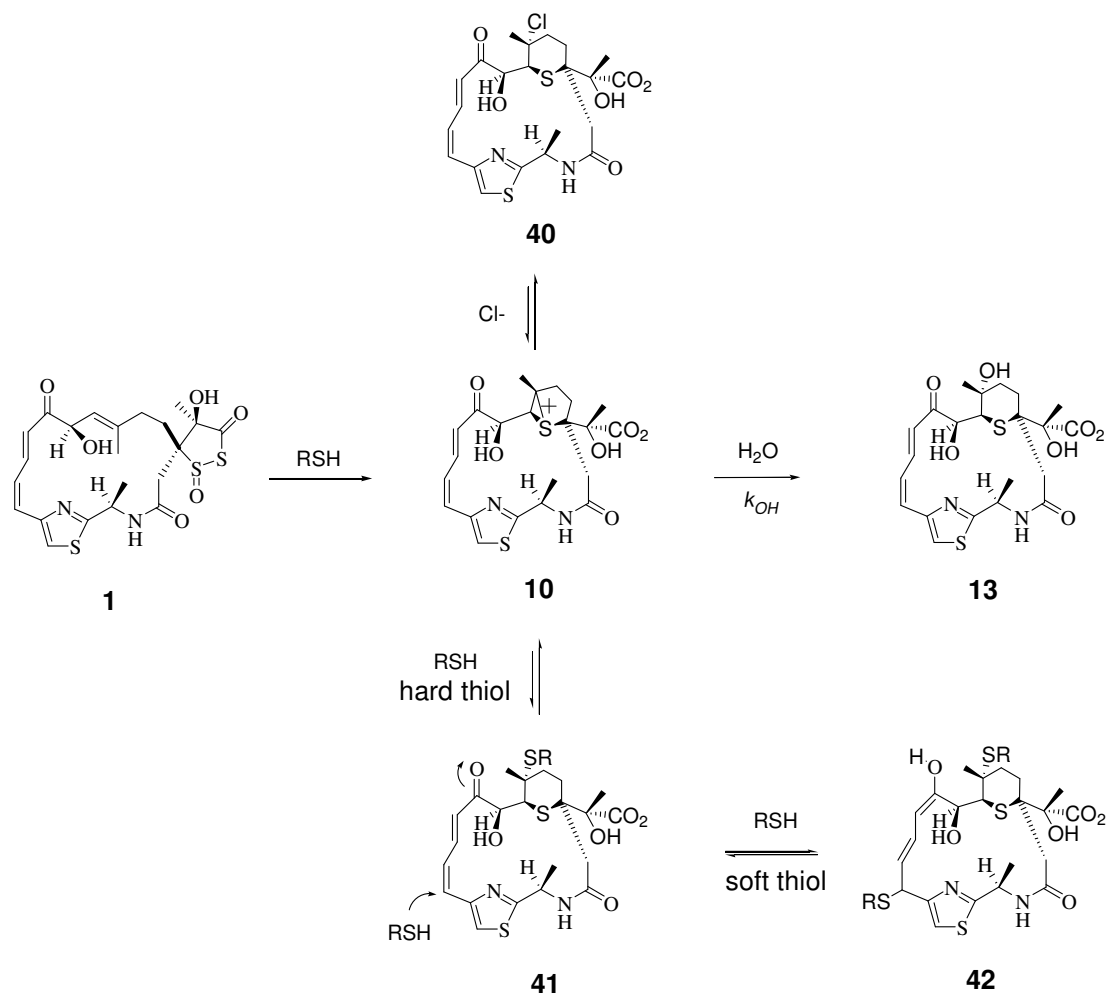
Scheme 15. Hypothesized thiol/chloride adducts of the alkylating form of leinamycin (**10**). Such adduct may "carry" and "protect" the episulfonium ion in cells.

_____

3.11.1. Soft Thiols: β-Mercaptoethanol (pK_a = 9.5) and Glutathione (pK_a = 8.5) May Carry Leinamycin in the Form of Michael-Adducts on The Thiazole-Dienone Moiety of Leinamycin (42)

We hypothesized that activated leinamycin (**10**) will reversibly react with thiols as shown in Scheme 15. Accordingly, in the presence of increasing concentrations of thiols, the apparent concentration of the free episulfonium ion will decrease, and so will its rate of hydrolysis to **13**. We aimed to study the rate of hydrolysis of 400 µM leinamycin in the presence of increasing concentration of thiols (1-6 mM), in 50 mM MOPS buffer at room temperature, using HPLC. We followed the disappearance of activated leinamycin (**10**) and the appearance of the hydrolysis product (**13**) at 324 nm (Figure 61).
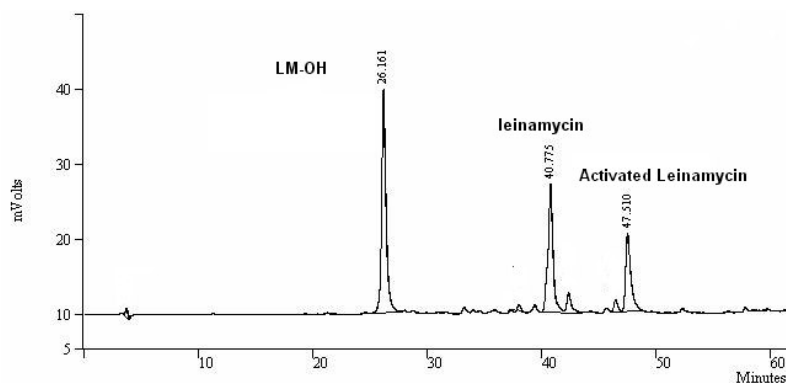
Figure 61. General HPLC trace of the hydrolysis products and activated leinamycin (**10**) after exposure to different thiols or the sodium chloride. Note: the shown retention times are 15 minutes less from the actual, as the trace above was recorded with 15 minutes delay in acquisition.

_____

We noticed that the rate of degradation of the activated leinamycin (**10**) increases with increasing thiol concentrations (Figure 62), consistent with our hypothesized mechanism (Scheme 15).
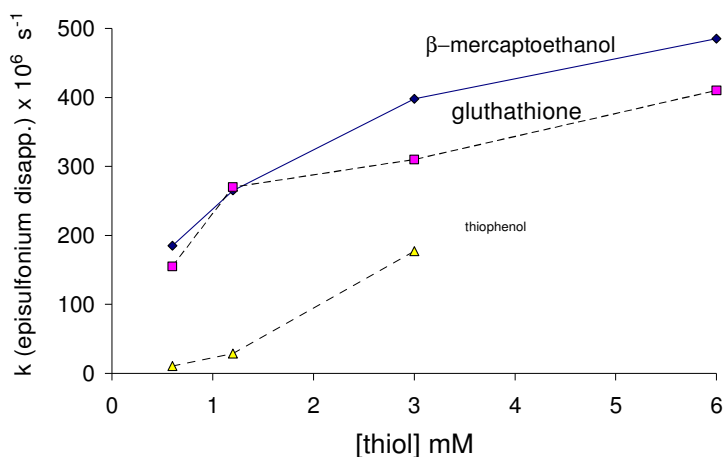
Figure 62. The rate of consumption of the leinamycin episulfonium ion (**10**) versus the applied thiol concentrations.

We followed the hydrolysis of leinamycin (200 μM) in 50 M MOPS buffer (pH 7.4) in the presence of two different concentrations of β-mercaptoethanol (1 mM, Figure 63 and 8 mM, Figure 64) at 37 °C. At lower β-mercaptoethanol concentration (1 mM) activated leinamycin was quantitatively converted to its hydrolysis product (**13**). According to our UV-data, the hydrolysis of **10** to **13** in the presence of 1 mM β-mercaptoethanol takes place with the direct conversion of **10** to **13** (*isosbestic point,* Figure 63) and without much final loss of absorbance at 350 nm. At 8 mM β-mercaptoethanol concentration, however, the yield of the hydrolysis product (**13**) was found to decrease gradually with time. These reactions were also followed by UV, and

the "loss" of leinamycin in the presence of 8 mM β-mercaptoethanol was accounted for by the loss of the conjugated chromophore in the leinamycin-macrocyle. This takes place, probably in a Michael-Addition reaction of the thiol to the conjugated dienone functionality of the episulfonium ion (**10)** (**42**, Scheme 15), and also to the molecule of the hydrolysis product, **13** (Scheme 16). This is supported by the absence of *isosbestic points* in the UV of the hydrolysis reaction at 8 mM β-mercaptoethanol (Figure 64).
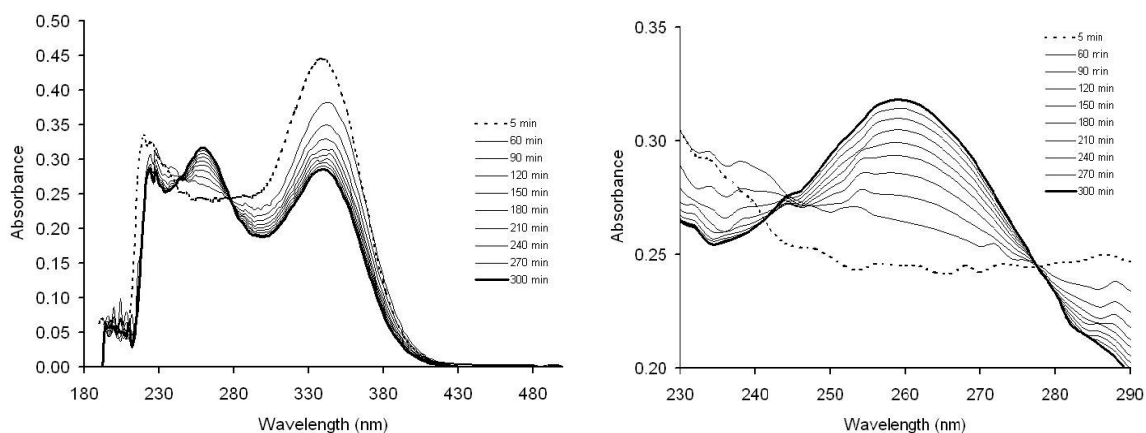
Figure 63. Changes in the UV of 200 μM activated leinamycin (**10**) in 50 mM MOPS buffer (pH 7.4) at 37 °C in the presence of 1 mM β-mercaptoethanol.
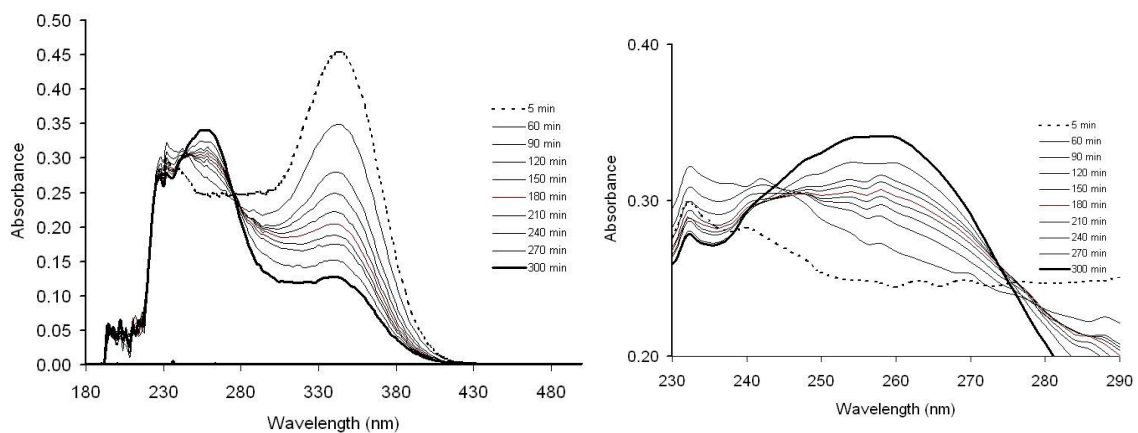
Figure 64. Changes in the UV of 200 uM activated leinamycin (**10**) in 50 mM MOPS buffer (pH 7.4) at 37 °C in the presence of 8 mM β-mercaptoethanol.

_____

(42)
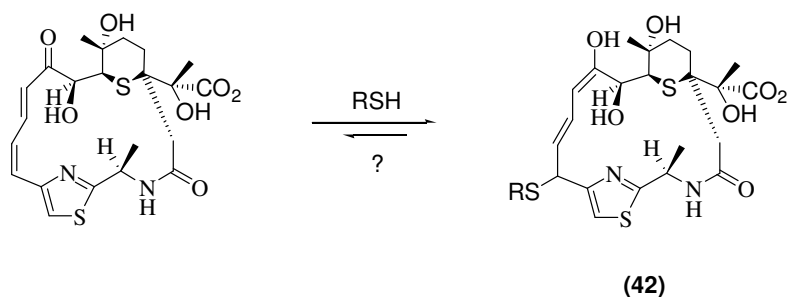
Scheme 16. Hypothesized Michael-Addition of soft-thiols to the leinamycin chromophore in the molecule of the hydrolysis product (**13**).

Further investigations are required to find the thiol-adducts in HPLC and identify their composition by LC-MS methods. It would also be interesting to study the fate of the purified hydrolysis product of leinamycin (**10**) in the presence of 8 mM β-mercaptoethanol or glutathione. These studies are in progress now.

3.11.2. Hard thiol: Thiophenol (pK$_a$ = 6.0) Carries Leinamycin in an Adducted Episulfonium-Ion (41)

The fate of activated leinamycin (**10**) was markedly different in the presence of the "low-pK$_a$-thiol", thiophenol (pK$_a$ = 6.0). We studied the hydrolysis of 400 μM activated leinamycin (**10**) in 50 mM MOPS buffer (pH 7.4) in the presence of increasing concentrations of thiophenol (1-3 mM). Due to the low solubility of thiophenol the system contained 30% acetonitrile. Here, the chromophore of leinamycin responsible for the 350 nm UV-absorbance was retained during the course of the reaction. We found the

appearance of four new peaks was found in our HPLC-s (A_1-A_4, Figure 65). These new peaks interconverted into each other, and eventually were converted to the HPLC-peak of the hydrolysis product (**13**).

The slow conversion of the new adduct peaks (A_1-A_4) to that of **13** allowed us to calculate a rate constant for the alkylation reaction, using non-linear regression. The rates of hydrolysis of leinamycin were plotted vs. the concentration of thiophenol (Figure 66), and found to decrease with increasing concentration of thiophenol.

_____
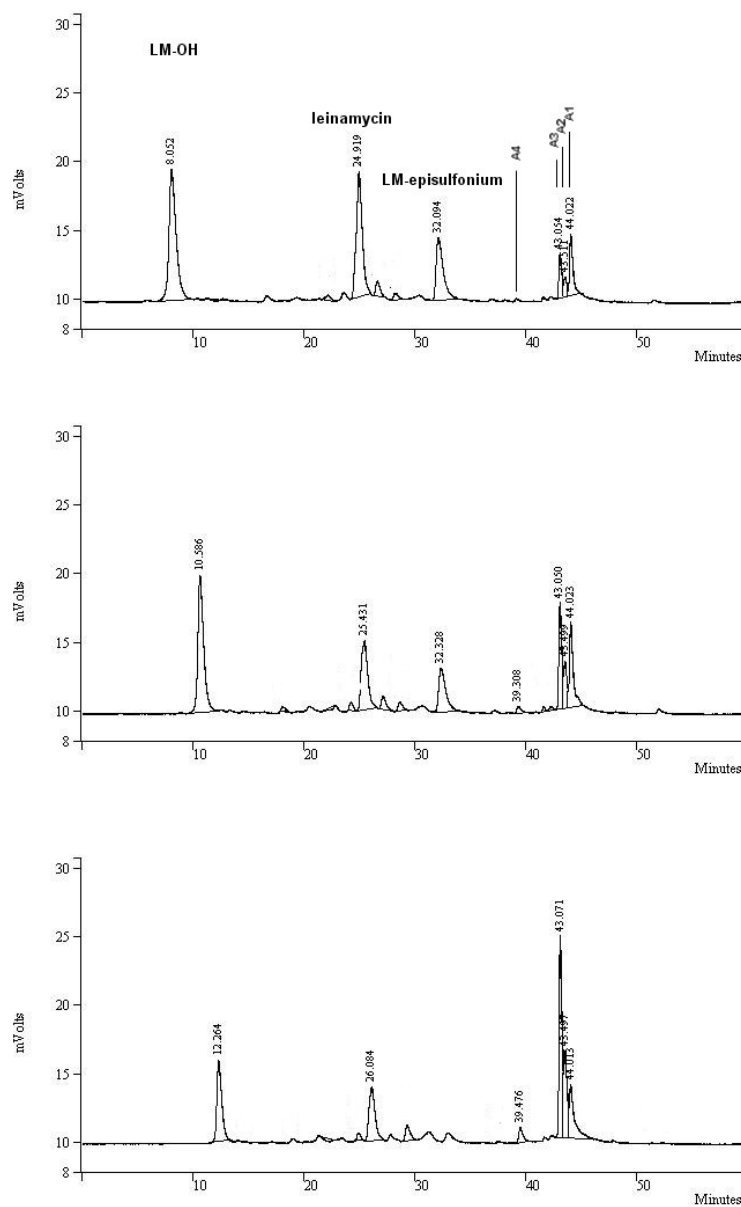
Figure 65. HPLC traces of the hydrolysis reaction of activated leinamycin (**10**) in the presence of thiophenol at room temperature, in 50 mM MOPS, pH 7.0 buffer after 1h incubation. The retention times shown here are 15 min less than the actual retention times due to delayed data acquisition. [thiophenol]: *top*, 400 µM; *middle*, 800 µM; *bottom*, 2 mM

_____
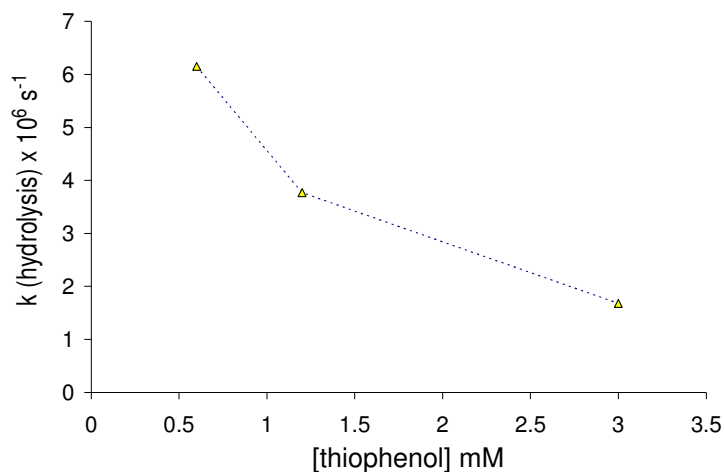
Figure 66. The rates of hydrolysis of activated leinamycin (**10**) versus the concentration of thiophenol. Leinamycin (200 μM) was hydrolyzed in 50 mM MOPS buffer (pH 7.4) in the presence of thiophenol (1-3 mM).

The pattern of peaks in our HPLC (Figure 65) and the retained absorptivity of the species suggests that the peaks (**A$_1$-A$_4$**) belong to thiophenol adducts on the episulfonuim-ring (Figure 67). These isomers come from two regioisomers, each in a pair of diastereomers.
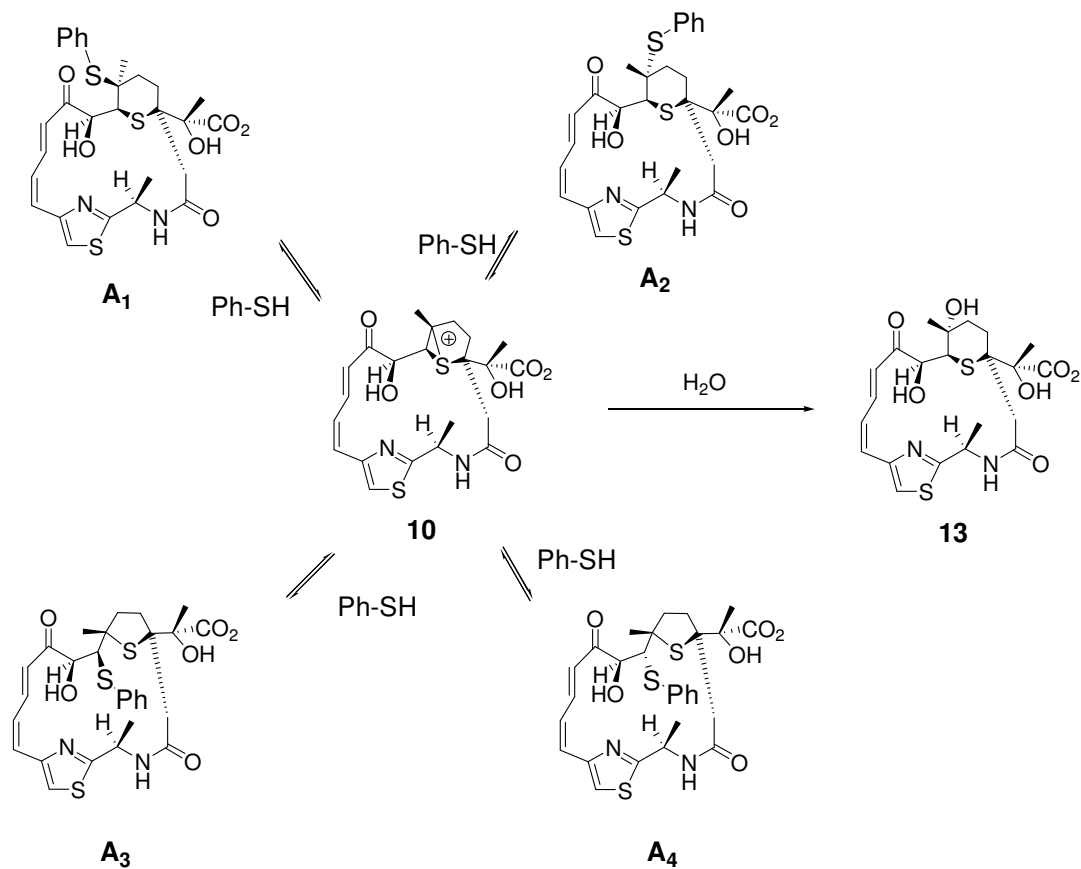
Figure 67. The hypothesized thiophenol adducts of the leinamycin episulfonium ion (**10**)

_____

3.11.3. Chloride Ion is a Carrier of Leinamycin (40)

Finally, we initiated studies to examine whether the physiologically profuse chloride ion[27] is able to "carry" the leinamycin episulfonium and protect it against hydrolysis (Scheme 17). We incubated 400 μM leinamycin in 50 mM MOPS buffer (pH 7.4) at room temperature, and followed the appearance of the leinamycin hydrolysis product (**13**) by HPLC. Rates of hydrolysis were calculated by non-linear regression analysis of the appearance of **13**, and plotted versus time (Figure 68). Very interestingly, the rate of hydrolysis of **10** dramatically decreases (~ 10 times) in the presence of the physiological concentration (200 mM) of sodium chloride. For a comparison, 500 mM sodium chloride was shown to increase the half-life of chlorambucil 3.5 fold.[29] This data is in line with our proposed mechanism (Scheme 17).
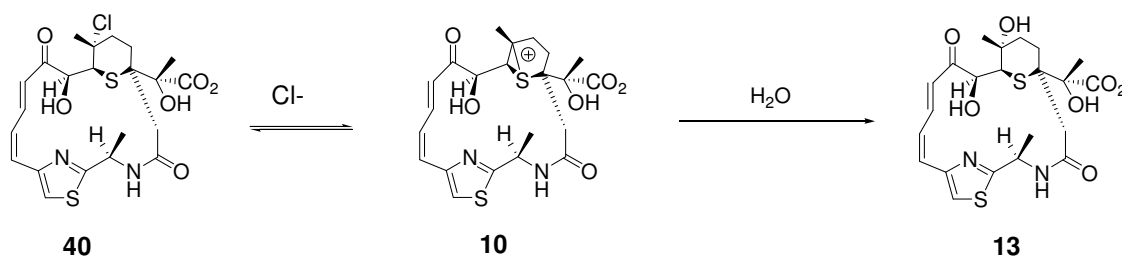
Scheme 17. The hypothetical chloride-adduct of the leinamycin episufonium ion (**10**).

_____
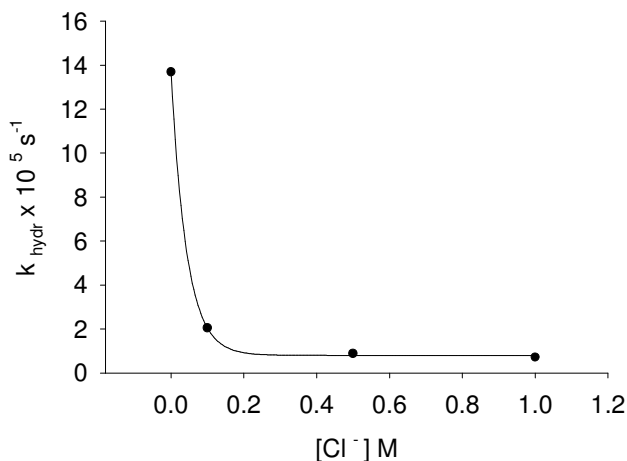
Figure 68. The rates of the disappearance of the episulfonium ion (here also the rate of hydrolysis) in the presence of various concentrations of sodium chloride.

Since we did not find an "adduct-peak" characteristic for the chloride adduct in our HPLC, probably doe to the quick disintegration of the adduct in HPLC eluent, this experiment was confirmed by following the hydrolysis of 200 μM **10** in the presence of 200 mM sodium chloride by UV absorbance measurements (Figure 69).

The features of the UV spectra (Figure 69) in the hydrolysis of **10** when chloride ion is present (200 mM) support the idea that an equilibrium exists between the chloride ion and the episulfonium ion, which bleeds out to the hydrolysis product of leinamycin (**13**), as shown in Scheme 17. It is interesting to compare the UV spectra in the hydrolysis of **10** without chloride ion (Figure 63) and in the presence of 200 mM chloride ion (Figure 69). The direct hydrolysis of **10** to **13** is revealed by *isosbestic points* in the UV spectra recorded during the reaction (Figure 63). On the other hand, the UV spectra recorded during the hydrolysis of **10** in the presence of **13** does not show the clear formation of isosbestic points (Figure 69). This is consistent with a reaction that contains

_____

the conversion between more than two species, supporting our mechanism for the episulfonium-chloride adduct (Scheme 17). The retained chromopore at 350 nm suggests that chloride adds to the episulfonium ring (**40**).
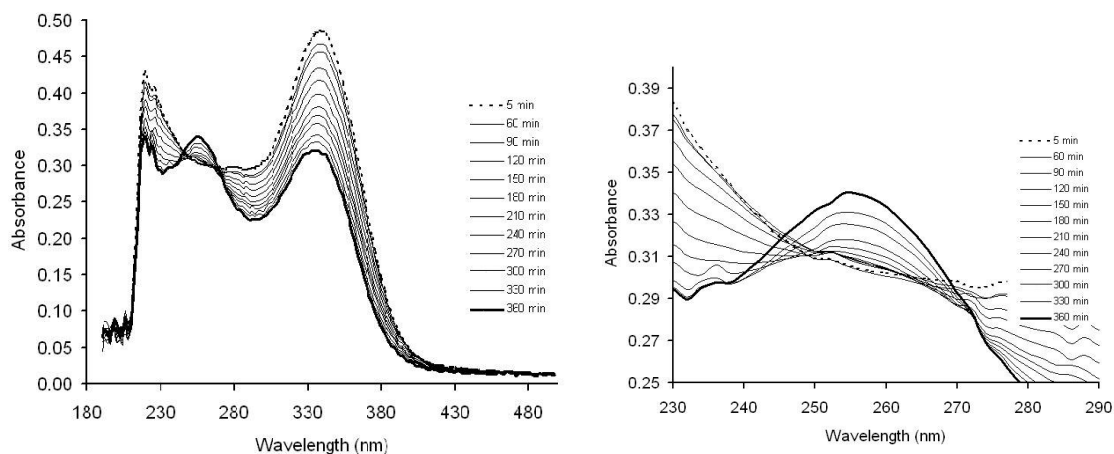
Figure 69. UV spectra recorded in the hydrolysis of 200 μM **10** in 50 mM MOPS buffer (pH 7.4) in the presence of 200 mM sodium chloride.

3.12. Discussion

3.12.1. Reversal of Leinamycin From DNA

We investigated the reversibility of DNA alkylation by the leinamycin episulfonium ion (**10**). In this process, the regeneration of intact DNA and the episulfonium ion (**10**) is expected. Our data is consistent with a unimolecular regeneration of activated leinamycin (**10**). We also showed that if the product of this reversion Chemistry arose by a direct attack of water on the DNA-adduct, the relative yields of **13** and **43** would not be dependent on the DNA concentration (Section 3.5.). We also explained that the appearance of **13** from the DNA adduct cannot be "carry over" (Section 3.7), because, in this case, the final yields of **10** and **43** had been already determined in the relative amounts of the leinamycin-DNA adduct and the activated leinamycin "impurity" on DNA, before the degradation reaction. Noticeably, the yields of the hydrolysis product (**10**) are very high (x > 22 %) at lower physiological DNA concentrations. This parallels those found for CC-1065 [1,3] and for duocarmycin,[4] though smaller than in case of the readily reversible DNA-adduct of ectenaiscidin.[5] This helps us appreciate that reversal of activated leinamycin may occur to an important extent in cells. The yield of the reversion product becomes invisible at higher DNA concentration. Higher DNA concentrations favor the formation of the noncovalent complex: [**10** • **DNA**]. Under such conditions, **10** simply "back-reacts" with DNA and will ultimately be found in the depurination product, rather than the hydrolysis product. Indeed, in single-stranded DNA, where noncovalent binding of **10** to a duplex structure obviously cannot occur, we observe that loss of adduct and conversion to **13** is fast (Section 3.9). Kinetic analysis of the reaction at 2 mM adduct

_____

concentration indicated a rate of reversion from duplex DNA: $k_{rev} = 1.5 \times 10^{-4}$ s^{-1}, (t$_{1/2}$ = **1.3 h**), and rate of reversion from single-stranded DNA: $k_{rev, \, ss\text{-}DNA} = 3.2 \times 10^{-4}$ s^{-1} (t ½ **= 0.6 h**). Interestingly, these measured rates of reversion are very close to those found for the readily reversible DNA-adduct of ecteinascidin.[5] The rate of reversion from single-stranded DNA should provide a clean measure of the k_{rev} step. Gratifyingly, we observed that this rate is similar to that calculated for the duplex DNA-adduct.

Overall, our data indicates that reversal of the leinamycin-DNA adduct in duplex DNA is facile and may allow the migration between kinetic and thermodynamic alkylation sites in DNA.[6] A further study would be interesting to find out whether the sequence preference of DNA alkylation by leinamycin changes in time. At this point, it is interesting to note that DNA-damaging agents preferentially alkylate the more accessible inter-nucleosome linker DNA regions of the chromosomes (Figure 70).[30] Reversal of the natural product would help the spreading of the DNA-damaging agent to other, less accessible surfaces of the genomic DNA (Figure 70) for a more extensive DNA damage.
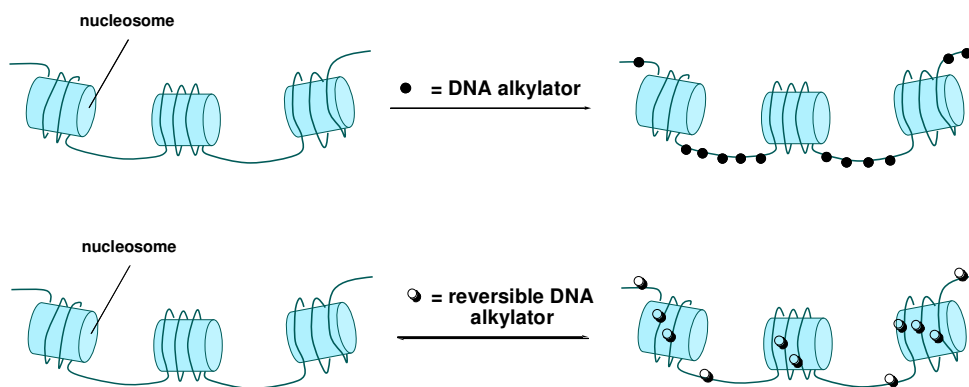
Figure 70. Alkylation of DNA in the chromosome structure takes place preferentially in inter-nucleosome Sections of DNA. Reversible DNA alkylators have the capacity to spread to other parts of the genome with time.

_____

3.12.2. Reversal of Sulfur Mustard and Nitrogen Mustard DNA Adducts

It is intriguing to see the product of reversion of the guanine adducts of nitrogen mustards and sulfur mustards (Section 3.10.2.). It remains unclear now, if the reversal appears as the result of direct hydrolysis or reversal of the adduct. A kinetic analysis could be employed to find out the mechanism. For example, if reversal is responsible for the observed products, then trapping of the adduct with thiocyanate would be independent of the concentration of thiocyanate: [SCN⁻]. We could also examine whether mustard-nucleoside adduct could act as a transporter to carry alkylating agent to unmodified DNA fragment. We expect to observe the characteristic aziridinium ion or episulfonium ion sequence specificity if reversal occurs.

3.12.3. Reversible Addition of Chloride and Thiols to Activated Leinamycin

We have shown that thiols (β-mercaptoethanol, glutathione and thiophenol) can add to activated leinamycin. Using a combination of HPLC and UV analyses (Section 3.11.1., Figure 63 and Figure 64), we can propose that softer-thiols (β-mercaptoethanol, $pK_a = 9$; glutathione, $pK_a = 8.5$) presumably add to the conjugated thiazole-dienone moiety of activated leinamycin (**10**) or the leinamycin hydrolysis product (**13**), presumably in a Michael-Addition reaction (**42**, Scheme 16). Further studies are needed to find and identify these adducts in HPLC, LC-MS experiments. Using a similar experimental setting, we suggest that the hard-thiol: thiophenol ($pK_a = 6.0$) adds to the small 3-membered episulfonium ring in the activated leinamycin molecule (**41**, Section 3.11.2., Figure 67).

_____

We also showed that the presence of chloride ion slows the hydrolysis of **10** dramatically (Section 3.11.3). We suggested that this might happen via an adduct formation between the chloride ion and activated leinamycin. This adduct formation probably takes place in the 3-membered ring of the episulfonium ion (**40**, Scheme 17), which is concluded from our UV experiments (Figure 69). It is very intriguing to realize that the chloride-concentration should be much decreased in the hydrophobic DNA-grooves, where DNA-damage takes place. Thereby, in proximity to DNA, the salt adduct is disintegrated and activated leinamycin is released.

It is interesting to note here that the leinamycin producing species of *Streptomyces* does not contain glutathione in its cells. These species bio-synthesize a small gluco-thiol: mycothiol (Figure 71). It is interesting to think about the role of mycothiol as a "carrier" of leinamycin, to protect *Streptomyces* from suicide by its own drug.
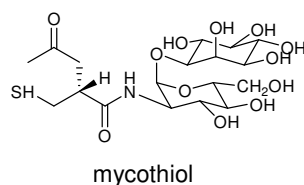
mycothiol

Figure 71. The structure of mycothiol, found in the leinamycin-producing *Streptomyces* species.

3.13. Conclusions

3.13.1. DNA Damaging Strategies of Leinamycin

With our experiments presented in Chapter 1, Chapter 2 and this Chapter, we can propose a map of the strategic reactions of leinamycin in facilitating the DNA-damaging Chemistry in host cells, while protecting the producing organism at the same time (Scheme 18). Accordingly, when leinamycin is produced by *Streptomyces,* the natural product might be sequestered in a thiol or chloride adduct to protect it from unproductive hydrolysis and to save the cell from suicide. In host cells, similar chemistries work in concert to save the DNA-damaging potential of the natural product, and to "carry" it to DNA for an effective DNA-damaging reaction.
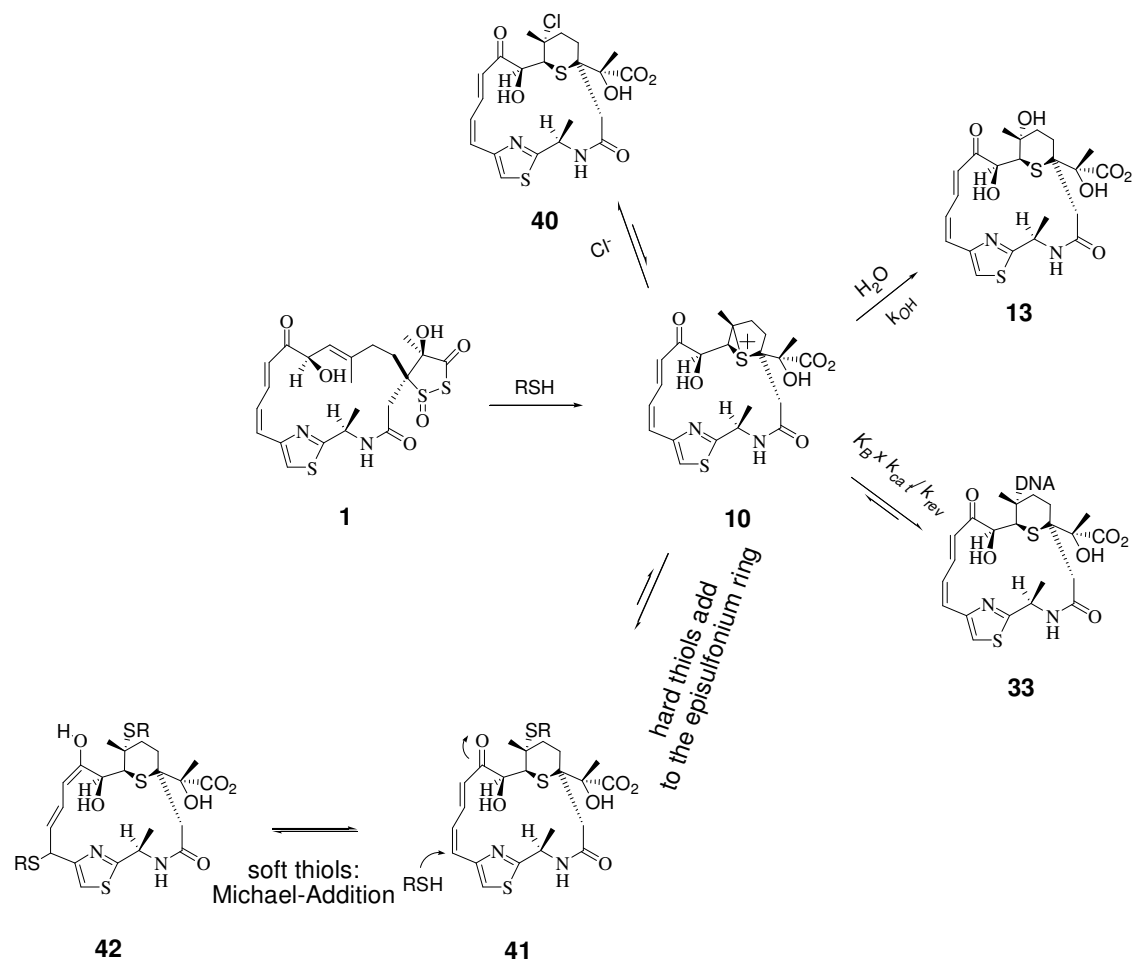
Scheme 18. The map of the strategic reactions of leinamycin (**1**) to protect the producing organism and to facilitate its DNA-damaging Chemistry in host cells.

_____

3.13.2. Reversal of Activated Leinamycin from DNA Makes DNA-Repair an Energy Wasting Process

Finally, it is interesting to imagine how reversal wastes the energy of the cell in its attempt to repair the DNA-adduct of leinamycin by nucleotide excision repair (NER). Accordingly, nucleotide excision repair excises a short piece of the adducted DNA, containing the DNA-adduct (Scheme 19).[31] The reversion of activated leinamycin takes place from this piece of single-stranded DNA-adduct. The activated leinamycin (**10**) alkylates DNA again. This cycling is simply a vain utilization of cellular energy.
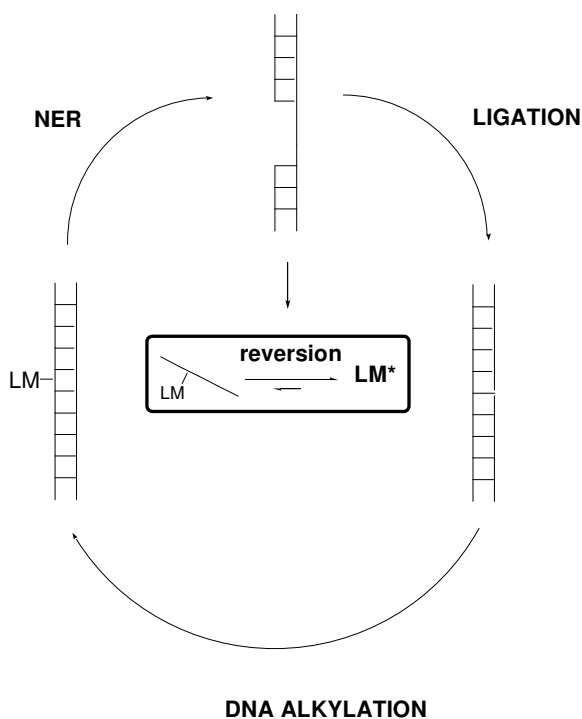
Scheme 19. Nucleotide excision repair of the leinamycin-DNA-adduct (**33**) shown as an "energy-wasting" process, only to elongate the cellular life-time of the activated leinamycin.

3.14. Experimental

3.14.1. Materials and Methods

Leinamycin (**1**) was a gift from researchers at Kyowa Hakko Kogyo Ltd. Additional reagents were purchased from the following suppliers and were of the highest purity available: MOPS buffer, sodium acetate and sodium phosphate buffers, trifluoroethanol, triethylamine, Aldrich Chemical Co. (Milwaukee, WI); HPLC grade solvents (water, acetonitrile, ethanol), Fisher (Pittsburgh, PA); herring sperm DNA, Roche Molecular Biochemicals (Indianapolis, IN); HPLC vials, National Scientific Corporation; analytical HPLC columns, Varian Inc. (Palo Alto, CA). HPLC: Varian Prostar Dynamax, vs. 5.1. LC-MS: ThermoFinnigan TSQ7000 triple-quadrupole with API2 source.

3.14.2. Preparation of The Leinamycin DNA-Adduct

In a 500 μL microcentrifuge tube 100 μL of 20 mM calf thymus DNA was added as well as 20 μL of 100 mM sodium phosphate buffer (pH 7.0), 20 μL of β-mercaptoethanol (in water) and 44 μL of HPLC water. The mixture was vortexed gently (5 s) and the DNA alkylation reaction was initiated with the addition of 16 μL leinamycin (5 mM in acetonitrile). The sample was incubated for 4 h at 4 °C. Under these conditions DNA alkylation proceeds with a minimum of 75% yield and the available alkylation sites are in excess. After the incubation samples were extracted using 200 μL butanol (twice) to purify the DNA adduct from small-molecular impurities and unbound **10** (activated leinamycin), the remaining aqueous phase was treated with 400 μL DNA precipitating solution (0.3 M sodium acetate in 70% ethanol), vortexed and kept on dry ice for 30 min. The frozen samples were centrifuged at 10,000 r.p.m. in a 4 °C for 30 min. The

supernatant was carefully discarded and the remaining DNA pellets were washed with 200 µL chilled 80% ethanol at 4 °C (twice). The pellets were dried under a stream of nitrogen gas, and kept at minus 20 °C before incubation for reversion studies.

3.14.3. Incubation of the leinamycin DNA-Adduct (33) at Varying Concentrations

To study the fate of the DNA adduct (depurination to the leinamycin guanine adduct **43** and reversion to **13**) we incubated **33** at six different concentrations (0.1 mM, 0.2 mM, 1 mM, 2 mM, 5 mM, 10 mM). The DNA adduct pellets were redissolved into water to make a 15 mM stock solution. The exact concentration was determined by U.V. absorbance measurements (A_{260nm} = 1 is 75 µM for base pairs or 50 µg/mL). The reactions were mixed in 500 µL microcentrifuge tubes to a final volume of 100 µL. In these samples the following components were mixed: DNA-adduct (0.7 µL, 1.4 µL, 6.7 µL, 13.3 µL, 33 µL, 66 µL), 10 µL sodium phosphate buffer (100 mM, pH 7.0), HPLC water (89.3 µL, 88.6 µL, 83.3 µL, 76.7 µL, 57 µL, 24 µL). Samples were vortexed gently and incubated at 37 °C for 48 h. Afterwards incubation samples were extracted with 100 µL butanol (three times) for their contents of **13** and **43**. The extracts were frozen on dry ice and dried in a speed-vac centrifuge. The dried samples can be stored at minus 20 °C before HPLC analysis.

_____

3.14.4. HPLC Analyses

HPLCs were run on a Varian-Prostar instrument with 210 solvent delivery system and Star Chromatography vs. 5.1.1. Column: RP-C18 (ODS), Supelco: 2.1 mm diameter x 250 mm, 5 μm. Applied flow rate: 0.2 mL/min, using A: 0.2 % TFA + 0.1 % TEA, B: acetonitrile in a gradient elution method (Table 9).

Time (min)	%B
Start	10
0-42	10-34
42-52	34-65
52-56	65
56-62	65-10
62-72	10

Table 9. The gradient HPLC-method used for the analysis of products in the work presented in chapter 3. Solvent system: A: 0.2% TFA + 0.1% TEA, B: acetonitrile. Column: ODS Supelco (RP-HPLC, C18) 2.1 x 250 x 5 μm. Flow rate: 0.2 mL/min.

3.14.5. Calculation of the Yields of 13 and 43 in the Complete Degradation of the DNA-Adduct via Depurination and Reversion.

The yields of reversion / depurination at the complete degradation of **33** (37 °C, 2 days) were calculated as is given in equations 12 and 13. P_{13} is the peak size for the hydrolysis product (**13**), P_{43} is the peak size for the depurination product (**43**).

$$\frac{P_{13}}{P_{13} + P_{43}} \qquad \qquad \textbf{Equation 49}$$

$$\frac{P_{43}}{P_{13} + P_{43}} \qquad \qquad \textbf{Equation 50}$$

3.14.6. Measurements of the Rate of Product (13, 43) Formation at 0.5 and 2 mM DNA-Adduct Concentrations for the Calculation of the Rate of Reversion: k_{rev}.

The synthesized DNA adduct pellet (synthesis described above) was removed from the minus 20 degree refrigerator and dissolved into water to make a stock solution (10 mM). The exact concentration was adjusted with the help of UV-absorbance measurement ($A_{260nm} = 1$ is 75 µM for base pairs or 50 µg/mL). The incubation mixtures for the 0.5 mM and the 2 mM reactions were composed as follows: 10 µL sodium phosphate (100 mM pH 7.0) and 5 µL or 20 µL DNA (10 mM in water) and 85 µL or 70 µL water (HPLC). Samples were gently vortexed for 5 s and placed into a 37 °C oven for incubation. At different times (1 h, 5 h, 12 h, 24 h, 44 h, 98 h) 10 µL was removed from the solution and diluted to 100 µL with 10 mM sodium phosphate buffer (pH 7.0). This diluted solution was extracted with 100 µL butanol (twice). The butanol phases were collected, frozen on dry ice and dried in a speed-vac instrument. The dried samples can be stored at minus 20 °C before HPLC analyses. At the time of HPLC analyses sample was redissolved into the HPLC injection mixture (90%A and 10% acetonitrile, where A is: 0.2% TFA). Samples were immediately injected into the HPLC as described above. The peak size for the sum of hydrolysis product and depurination product (P_{13} + P_{43}) were plotted vs. time (Figure 48). An exponential rising curve was fitted to these plots and the time factor of this curve was used as the rate constant for the given reaction. For the calculation of the rate of reversion (k_{rev}) in each case, the kinetic rate equation (Equation 45) devised in Section 3.5. was used.

3.14.7. Degradation of the Leinamycin-DNA-Adduct from ss-DNA.

In a 4 °C cold-room in a 500 μL eppendorf tube (microcentrifuge tube) was added 100 μL of a 20 mM 12-mer oligonucleotide (5'-TATAT$\underline{G}$CATATA-3', annealed earlier to duplex form) solution in water, 20 μL of sodium phosphate buffer (pH 7.0) and 20 μL β-mercaptoethanol (in water) and 44 μL of HPLC water. This mixture was vortexed gently, and the DNA alkylation reaction was initiated with the addition of 16 μL of leinamycin stock solution (5 mM in acetonitrile). The mixture was incubated at 4 °C for 4 h. After incubation, the samples were extracted with 200 μL butanol (twice). The remaining aqueous phase was treated with 400 μL DNA precipitating solution (0.3 M sodium acetate in 70% ethanol), vortexed gently and kept in dry ice for 30 min. The frozen samples were centrifuged at 10,000 r.p.m. in a 4°C for 30 min. The supernatant was carefully discarded and the remaining DNA pellets were washed with 200 μL chilled 80% ethanol at 4 °C (twice). The pellets were dried under a stream of nitrogen gas, and kept at minus 20 °C before incubation for reversion studies.

At the time of incubating the ss-DNA adduct for reversion studies, the dried 12-mer oligonucleotide-adduct was removed from the refrigerator and was dissolved using 10 mM sodium phosphate buffer. The final concentration was adjusted with the help of U.V. absorbance measurements (A_{260nm} = 1 is 75 μM for base pairs or 50 μg/mL). Incubation started in a 37°C-oven (12-mer melts to single-stranded) and at different times, aliquots of 10 μL were removed from the mixture, diluted to a final volume of 100 μL with water, and extracted with 100 μL of butanol (twice). The organic layer was collected, and dried

_____

in a speed-vac instrument. The dried samples can be stored at minus 20 °C. At the time of

HPLC analyses samples were analyzed as described before.

3.14.8. Synthesis of the N7-GUO Adducts of Chlorambucil (44) and CEES (47).

In a small vial (5 mL) 5.0 mg of guanosine (0.018 mmol) was dissolved in 1.5 mL TFE.

The solution was sonicated for 20 min to disperse guanosine. This resulted in the

formation of a blurred solution. To this solution 0.014 mmol chlorambucil was added

from a 500 mM stock solution in acetonitrile (29 μL). Stirring began and continued for

approximately 4 days. The disappearance of chlorambucil was followed by RP-HPLC.

After the completion of the reaction, the mixture was stored at minus 20 °C. The

synthesis of the N7-GUO-CEES adduct (**47**) was carried out similarly. After 4 days,

however, the mixture containing the CEES adduct was evaporated to dryness under high-

vacuum, to evaporate the unreacted CEES, as this species cannot be detected in HPLC.

The dried material was dissolved in TFE (1.5 mL) and stored at minus 20 °C. The

concentration of these solutions is 10 mM.

3.14.9. The fate of 44 and 47 in Aqueous Buffers.

The incubation mixtures were made of 500 mM MOPS buffer (pH 7.4, 40 μL) and 320

μL of HPLC water and 40 μL of the N7-GUO-chlorambucil adduct (10 mM) or the N7-

GUO-CEES adduct (in TFE, 10 mM). Solutions were mixed well and incubated at 37 °C.

At selected times, 35 μL of the mixture was added to 105 μL of 50 mM ammonium-

acetate buffer (pH 6.5), and injected to the HPLC for analysis. Samples were studied for

the reappearance of intact guanosine for both the chlorambucil and CEES adducts, and
for the appearance of the hydrolysis product of chlorambucil.

3.14.10. HPLC Analyses used to Study the Reactions of Chlorambucil (34) and CEES (37).

HPLC samples were made as described above and 25 μL was injected onto an RP-HPLC,
C18, Varian 4.6 mm x 250 mm x 5 Å column. Gradient elution program was used with
the following eluents: A: 50 mM ammonium-acetate (pH 6.5) and B: 50 mM ammonium
acetate (pH 6.5) in 50% acetonitrile. The gradient used was: 0% B for 5 min, 0%-100% B
in the next 30 min, 100% B for the next 9 min, 100%-0% B in the next 2 min, 0% B for 2
min. Detection: 265 nm.

3.14.11. Hydrolysis of Leinamycin (1) in the Presence of Increasing Amounts of Sodium Chloride.

The preparation of the reaction mixture with 1 M sodium chloride is explained: in a 500-
μL microcentrifuge tube we placed 44 μL of water, 20 μL MOPS buffer (500 mM, pH
7.0), 20 μL of β-mercaptoethanol in water (4.8 mM), 16 μL of leinamycin in acetonitrile
(5 mM) and 100 μL sodium chloride (1 M in water). Mixture was vortexed well (5 s) and
reactions were incubated at room temperature. At selected times 20 μl of the samples
were injected to 220 μL of a stop mixture (0.2 % TFA at pH 2.0). This mixture was
vortexed quickly (5 s) and placed on dry ice. This sample was melted prior to HPLC
injection, and 25 μL was injected onto an RP-C18 (ODS) HPLC column, Supelco: 2.1

mm diameter x 250 mm, 5 μm. Applied flow rate: 0.2 mL/min, using A: 0.2 % TFA + 0.1 % TEA, B: acetonitrile in a gradient elution method (Chapter 1, Experimental).

3.14.12. Hydrolysis of Leinamycin in the Presence of Increasing Concentrations of β-mercaptoethanol, Glutathione and Thiophenol.

The preparation of the reaction mixture containing 5 equivalents of added thiol is explained here. Into a microcentrifuge tube (500 μL) we added 69 μL HPLC water and 20 μL MOPS buffer (500 mM, pH 7.0) followed by 50 μL of thiol (8 mM in acetonitrile:water 30:70 v/v%) and 45 μL acetonitrile and finally 16 μL of leinamycin (5 mM in acetonitrile). Mixture was vortexed well (5s) and incubated at room temperature. Please, note that the reaction mixtures consist of 30% acetonitrile. At selected times 20 μl of the samples were injected to 220 μL of a stop mixture (0.2 % TFA at pH 2.0). This mixture was vortexed quickly (5 s) and placed on dry ice. This sample was melted prior to HPLC injection, and 25 μL was injected onto an RP-C18 (ODS) HPLC column, Supelco: 2.1 mm diameter x 250 mm, 5 μm. Applied flow rate: 0.2 mL/min, using A: 0.2 % TFA + 0.1 % TEA, B: acetonitrile in a gradient elution method (Chapter 1, Experimental).

_____

References

1.   Warpehoski, M. A.; Harper, D. E.; Mitchell, M. A.; Monroe, T. J., Reversibility of the covalent reaction of CC-1065 and analogs with DNA. *Biochemistry* **1992,** 31, 2502-2508.

2.   Boger, D. L.; Garbaccio, R. M., Catalysis of the CC-1065 and duocarmycin DNA alkylation reaction: DNA binding induced conformational change in the agent results in activation. *Bioorg. Med. Chem.* **1997,** 5, 263-276.

3.   Boger, D. L.; Yun, W., Reversibility of the duocarmycin A and SA DNA alkylation reaction. *J. Am. Chem. Soc.* **1993,** 115, 9872-9873.

4.   Asai, A.; Nagamura, S.; Saito, H.; Takahashi, I.; Nakano, H., The reversible DNA-alkylating activity of duocarmycin and its analogues. *Nucleic Acids Res.* **1994,** 22, 88-93.

5.   Zewail-Foote, M.; Hurley, L. H., Differential Rates of Reversibility of Ecteinascidin 743-DNA Covalent Adducts from Different Sequences Lead to Migration to Favored Bonding Sites. . *J. Am. Chem. Soc.* **2001,** 123, 6485-6495.

6.   Veldhuyzen, W. F.; Shallop, A. J.; Jones, R. A.; Rokita, S. E., Thermodynamic versus Kinetic Products of DNA Alkylation as Modeled by Reaction of Deoxyadenosine. *J. Am. Chem. Soc.* **2001,** 123, 11126-11132.

7.   Nooner, T.; Dutta, S.; Gates, K. S., Chemical Properties of the Leinamycin-Guanine Adduct in DNA. *Chem. Res. Toxicol.* **2004,** 17, 942-949.

8.   Gates, K. S.; Nooner, T.; Dutta, S., Biologically Relevant Chemical Reactions of N7-Alkylguanine Residues in DNA. *Chem. Res. Toxicol.* **2004,** 17, 840.

9.   Ouyang, A.; Skibo, E. B., Design of a Cyclopropyl Quinone Methide Reductive Alkylating Agent. *J. Org. Chem.* **1998,** 63, 1893-1900.

10.   Dedon, P. C.; Plastaras, J. P.; Rouzer, C. A.; Marnett, L. J., Indirect mutagenesis by oxidative DNA damage: formation of the pyrimidopurinone adduct of deoxyguanosine by base propenal. *Proc. Natl. Acad. Sci. Unit. States Am.* **1998,** 95, 11113-11116.

11.   Plastaras, J. P.; Riggins, J. N.; Otteneder, M.; Marnett, L. J., Reactivity and Mutagenicity of Endogenous DNA Oxopropenylating Agents: Base Propenals, Malondialdehyde, and Ne-Oxopropenyllysine. *Chem. Res. Toxicol.* **2000,** 13, 1235-1242.

12.   Upadhyaya, P.; Sturla, S. J.; Tretyakova, N.; Ziegel, R.; Villalta, P. W.; Wang, M.; Hecht, S. S., Identification of Adducts Produced by the Reaction of 4-(Acetoxymethylnitrosamino)-1-(3-pyridyl)-1-butanol with Deoxyguanosine and DNA. *Chem. Res. Toxicol.* **2003,** 16, 180-190.

13.   Wang, M.; Cheng, G.; Sturla, S. J.; Shi, Y.; McIntee, E. J.; Villalta, P. W.; Upadhyaya, P.; Hecht, S. S., Identification of Adducts Formed by Pyridyloxobutylation of Deoxyguanosine and DNA by 4-(Acetoxymethylnitrosamino)-1-(3-pyridyl)-1-butanone, a Chemically Activated Form of Tobacco Specific Carcinogens. *Chem. Res. Toxicol.* **2003,** 16, 616-626.

14.   Kampf, G.; Kapinos, L. E.; Griesser, R.; Lippert, B.; Sigel, H., Comparison of the acid-base properties of purine derivatives in aqueous solution. Determination of intrinsic

_____

proton affinities of various basic sites. *Journal of the Chemical Society, Perkin Transactions 2* **2002**, 1320-1327.

15.   Katritzky, A. R.; Brycki, B. E., The mechanisms of nucleophilic substitution in aliphatic compounds. *Chem. Soc. Rev.* **1990,** 19, 83-105.

16.   Marnett, L. J.; Tuttle, M. A., Comparison of the mutagenicities of malonaldehyde and the side products formed during its chemical synthesis. *Canc. Res.* **1980,** 40, 276-82.

17.   West, J. D.; Marnett, L. J., Endogenous Reactive Intermediates as Modulators of Cell Signaling and Cell Death. *Chem. Res. Toxicol.* **2006,** 19, 173-194.

18.   Thrall, B. D.; Mann, D. B.; Smerdon, M. J.; Springer, D. L., DNA polymerase, RNA polymerase and exonuclease activities on a DNA sequence modified by benzo[a]pyrene diolepoxide. *Carcinogenesis* **1992,** 13, 1529-34.

19.   Schaaper, R. M.; Loeb, L. A., Depurination causes mutations in SOS-induced cells. *Proc. Natl. Acad. Sci. Unit. States Am.* **1981,** 78, 1773-7.

20.   Mello, J. A.; Lippard, S. J.; Essigmann, J. M., DNA adducts of cis-diamminedichloroplatinum(II) and its trans isomer inhibit RNA polymerase II differentially in vivo. *Biochemistry* **1995,** 34, 14783-91.

21.   Hemminki, K., DNA adducts, mutations and cancer. *Carcinogenesis* **1993,** 14, 2007-12.

22.   Zewail-Foote, M.; Li, V.-S.; Kohn, H.; Bearss, D.; Guzman, M.; Hurley, L. H., The inefficiency of incisions of ecteinascidin 743-DNA adducts by the UvrABC nuclease and the unique structural feature of the DNA adducts can be used to explain the repair-dependent toxicities of this antitumor agent. *Chemistry & Biology* **2001,** 8, 1033-1049.

_____

23.   Gates, K. S., Mechanisms of DNA Damage by Leinamycin. *Chem. Res. Toxicol.* **2000,** 13, 953-956.

24.   Zang, H.; Gates, K. S., Sequence Specificity of DNA Alkylation by the Antitumor Natural Product Leinamycin. *Chem. Res. Toxicol.* **2003,** 16, 1539-1546.

25.   Pongracz, K.; Bodell, W. J., Synthesis of N2-(4-Hydroxyphenyl)-2'-deoxyguanosine 3'-Phosphate: Comparison by 32P-Postlabeling with the DNA Adduct Formed in HL-60 Cells Treated with Hydroquinone. *Chem. Res. Toxicol.* **1996,** 9, 593-8.

26.   Minchinton, A. I., Measurements of glutathione and other thiols in cells and tissues: a simplified procedure based on the HPLC separation of monobromobimane derivatives of thiols. *International journal of radiation oncology, biology, physics* **1984,** 10, 1503-6.

27.   Dalmark, M., Chloride transport in human red cells. *The Journal of physiology* **1975,** 250, 39-64.

28.   Silverman, R. B., *The Organic Chemistry of Drug Design and Drug Action.* 2004; p 617 pp.

29.   *J. Chem. Soc. Perkin 2* **1995**, 1503.

30.   Sudhakar, S.; Tew, K. D.; Schein, P. S.; Woolley, P. V.; Smulson, M. E., Nitrosourea interaction with chromatin and effect on poly(adenosine diphosphate ribose)polymerase activity. *Canc. Res.* **1979,** 39, 1411-17.

31.   Dronkert, M. L. G.; Kanaar, R., Repair of DNA interstrand cross-links. *Mutation Research* **2001,** 486, 217-247.
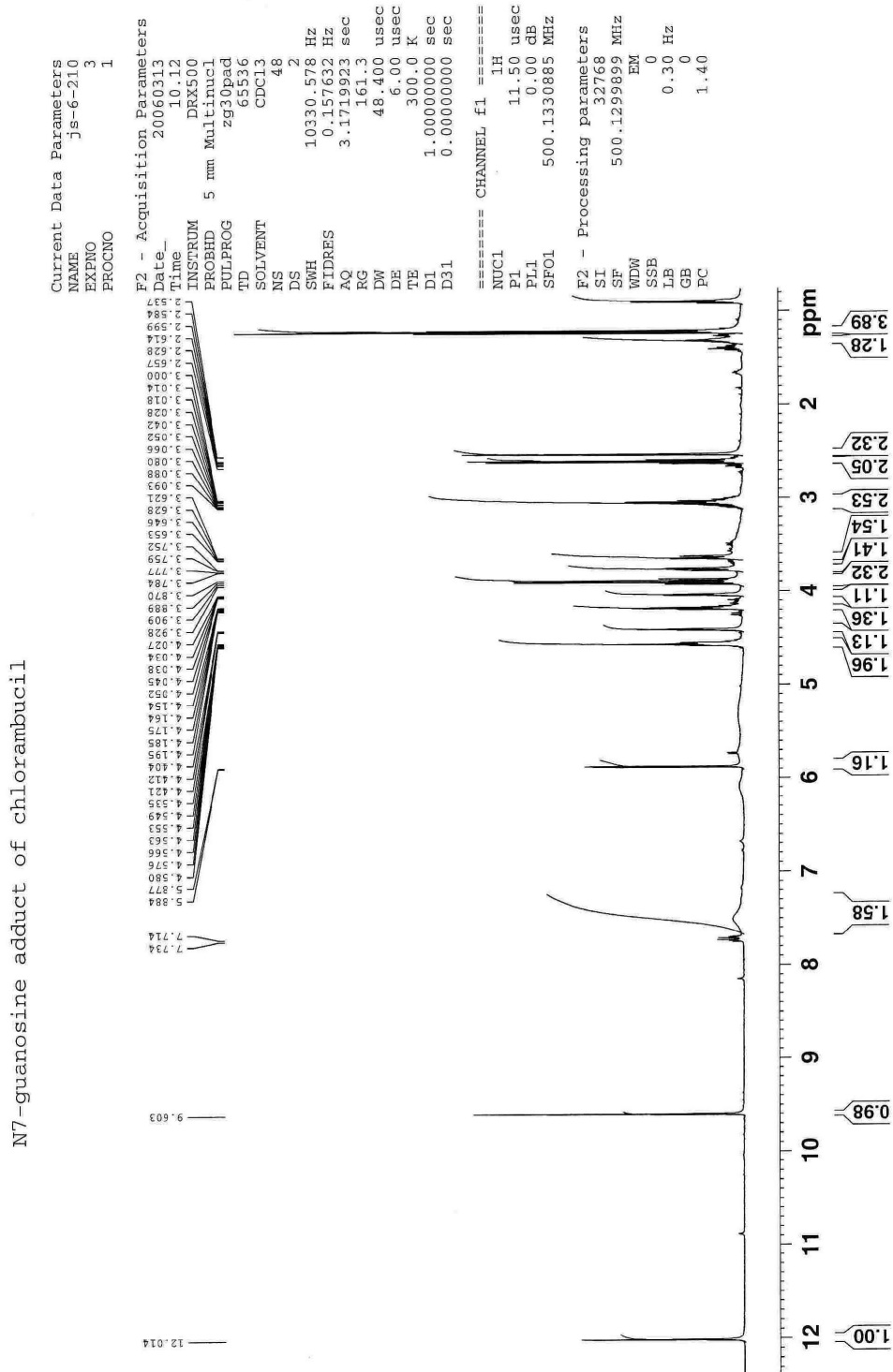
Figure 72. NMR of the N7-guanosine adduct of chlroambucil.

_____
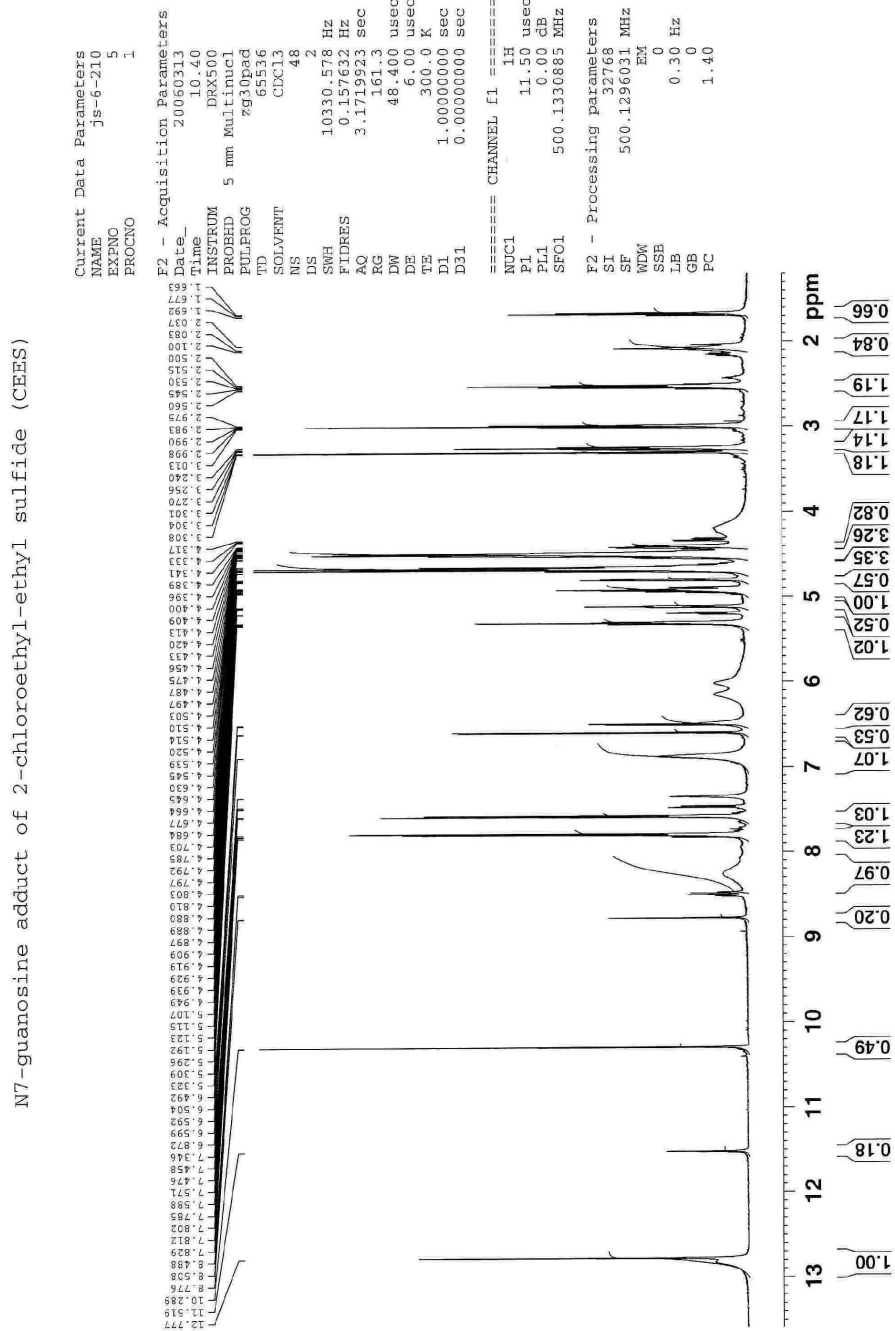
Figure 73. NMR of the N7-guanosine adduct of CEES.

Chapter 4. DNA Alkylation and DNA-Binding by Analogs of the Left-Half of Azinomycin: A Minimal DNA-Intercalating Structure

4.1.   The Chemistry and Biology of Azinomycins and the Left-Half of Azinomycin

Carzinophilin (Azinomycin B, **49,** Figure 74) was first reported in 1954 when it was found in the screening of soil anaerobes for antitumor activity. Azinomycin B was isolated from the fermentation broth of *Streptomyces sachachiroi*. [1] In addition, a structural analog (Azinomycin A, **50,** Figure 74) and Azinomycin B were independently isolated from *Streptmyces grizeofuscus.* [2] They show similar antitumor activities. [3,4] Azinomycin B was shown to increase the life-span of rodents with leukemia (P388) and provided up to a four times increase in the life expectancy in rodents with Ehrlich carcinoma and Yoshida carcinoma. [4] These compounds may decompose physiologically to the truncated analogs, the "left-halves" (Figure 75), which have been shown to retain most of the biological activity of the original natural product. [5] Studies on the left-half analogs showed that the epoxide functionality is essential for the biological activity of these molecules [4,6,7]

_____

Structural analyses of Azinomycin B later revealed that it is identical to Carzinophilin (**49**). [5] The total synthesis of these molecules [7-12] and their truncated analogs[6,10,13-16] have been carried out by a variety of routes.

carzinophilin, azinomycin B (**49**)   azinomycin A (**50**)
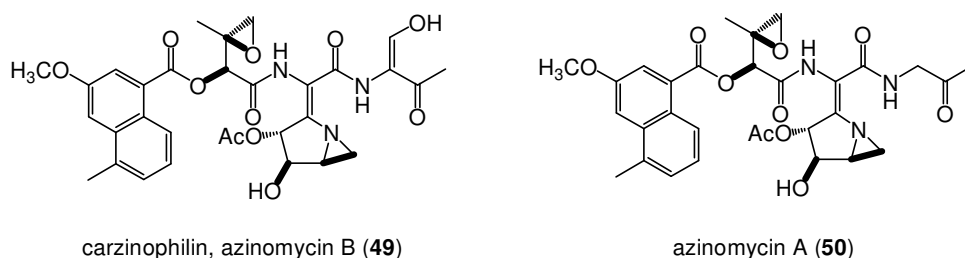
Figure 74. Carzinophilin (Azinomycin B) and Azinomycin A.

The Azinomycins were shown to associate with the major groove of duplex DNA sequence specifically (5'GNT3' and 5'GNC3' sequences).[17] These natural products are bifunctional DNA alkylating agents. They form interstrand crosslinks at the N-7 position of purine bases. In the crosslinking reaction, these molecules sequentially alkylate the N7 nitrogen of adenine in a ring opening of the aziridine moiety followed by the N7 nitrogen of guanine with the epoxide functionality (Scheme 20).
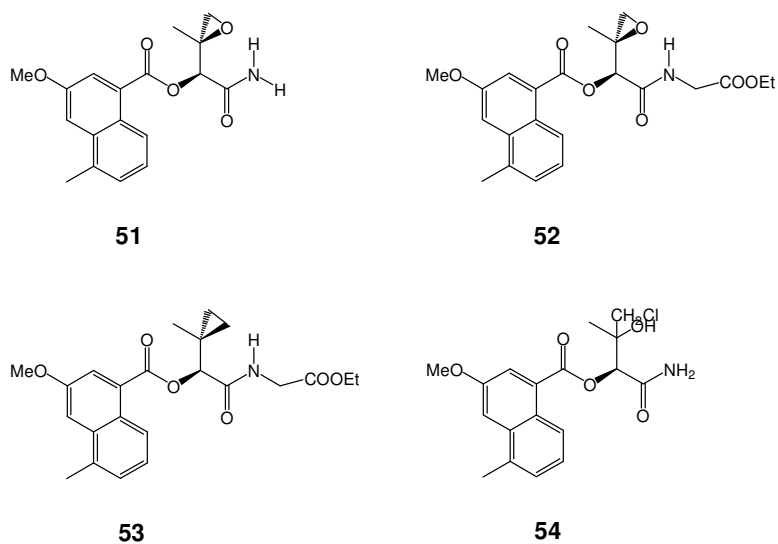
Figure 75. The analogs of the Left-Half of Azinomycin
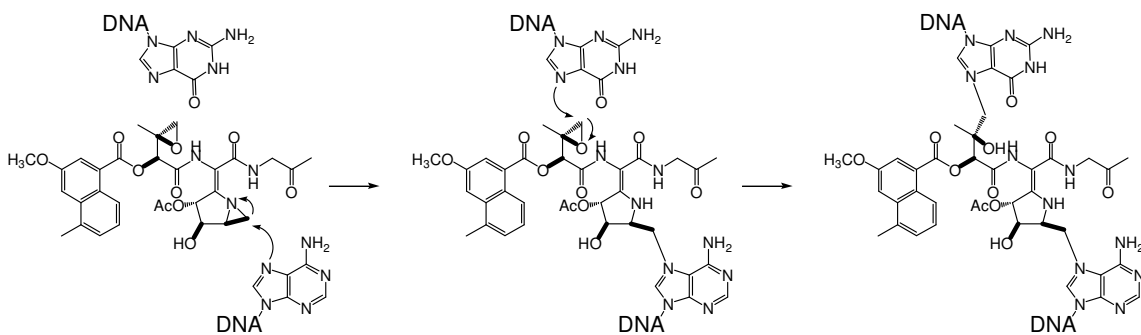
Scheme 20. DNA Alkylation and Crosslinking by the Azinomycins.

Our research group showed that the neutral naphthoate unit of **49** and **50** intercalates DNA. [18] This is noteworthy, because such functionalities only show DNA intercalation if they are in a *bis*-intercalating system or have a positive-charge that helps

their DNA-binding. [19-22] The contribution of intercalation by the aromatic rings to the

biological efficiency of these compounds was also demonstrated in cytotoxicity assays

with analogs of azinomycins devoid of this functional group. [6]

The left-half of azinomycin binds to DNA noncovalently [18] and retains DNA-

alkylating abilities (Figure 75). Our group showed that this DNA-alkylation is sequence

specific. [23] The DNA-binding mode of **51** and its analog **52** (Figure 78 and Figure 79) has

been a topic of debates, thus our goal was to carefully characterize mechanisms of non-

covalent DNA binding and DNA-alkylation by the left-half of azinomycin. [18,24,25]

4.2.   Goals of this Work

1. We wanted to confirm the structure of the azinomycin-epoxide guanine-adduct

using characteristic reactions and LC-MS methods (Section 4.3.).

2. We carried out model building experiments to determine whether intercalation of

the Azinomycin-guanine adduct is structurally reasonable.

3. We set out to examine whether the naphthoate ring of the azinomycin DNA-

adduct is intercalated, using a variety of biophysical and spectroscopic methods. We also

addressed the question of whether neutral naphthoates intercalate DNA without covalent

association.

4.3.   Identification of the DNA Alkylation Product by LC-MS

We alkylated CT DNA (1 mM) with **51** (250 μM) in MOPS buffer (50 mM, pH 7.0). We isolated the guanine adduct of **51** by quantitative depurination of the DNA-adduct. The guanine adduct was dissolved in HPLC water, and the mixture was injected into a Thermo-Finnigan TSQ7000 triple-quadrupole mass spectrometer with the API2 source (ThermoFinnigan, San Jose, CA). Similar identifications of N7-purine adducts have been reported earlier. [26,27] The Total Ion Current and the spectra are shown in Figure 76. The guanine adduct of **51** (Figure 77) was identified at the *m/z* value of 480.3. The regiochemistry of **51** on guanine in DNA was identified as N7-guanine adduct, in its characteristic depurination reactions, which are followed using HPLC.
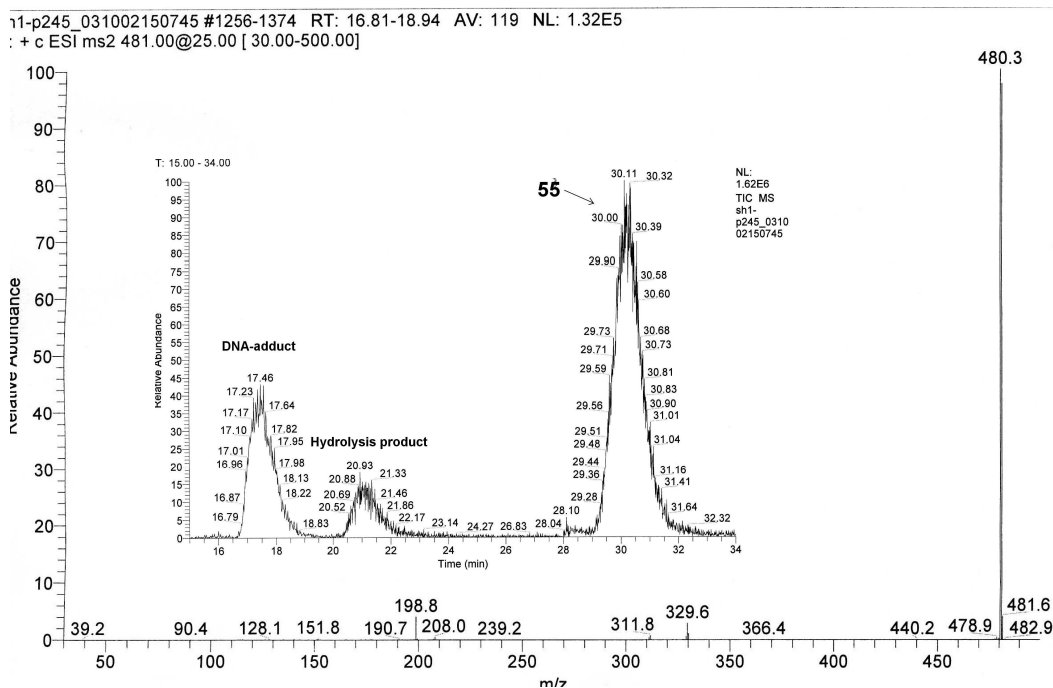
Figure 76. The TIC (a) and the LC-MS of the guanine adduct (b) of the left-half of Azinomycin (**51**). The guanine adduct of **51** is suggested by the m/z value at 480.3.
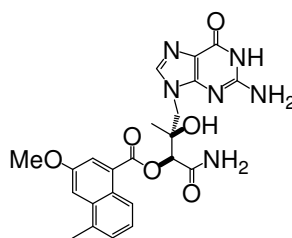
55

Figure 77. The guanine adduct of **51**.

4.4.   Initial Chemical Model of the Left-Half-Oligonucleotide Adduct

We constructed a molecular model of the DNA adduct of **51**. (Figure 78 and
Figure 79). This model revealed that intercalation of the aromatic naphthoate ring-system
onto the 3'-surface of the alkylated guanine can happen without disruption of the B-DNA
helix (Figure 78). On the other hand, the reorganization of the model to put the aromatic
rings in a stacking position over the 5'-surface of the alkylated DNA-base seemed to
cause steric clashes between the phosphate backbone of DNA and that of the 5-atom-
linker connecting the naphthoate to guanine (Figure 79). The distinction between these
two possibilities is not so well pronounced in the models, although overall they are in
close agreement with the sequence specificity observed by Dr. Hong Zang earlier in our
laboratory (Ph.D. thesis, University of Missouri-Columbia).[28]

_____
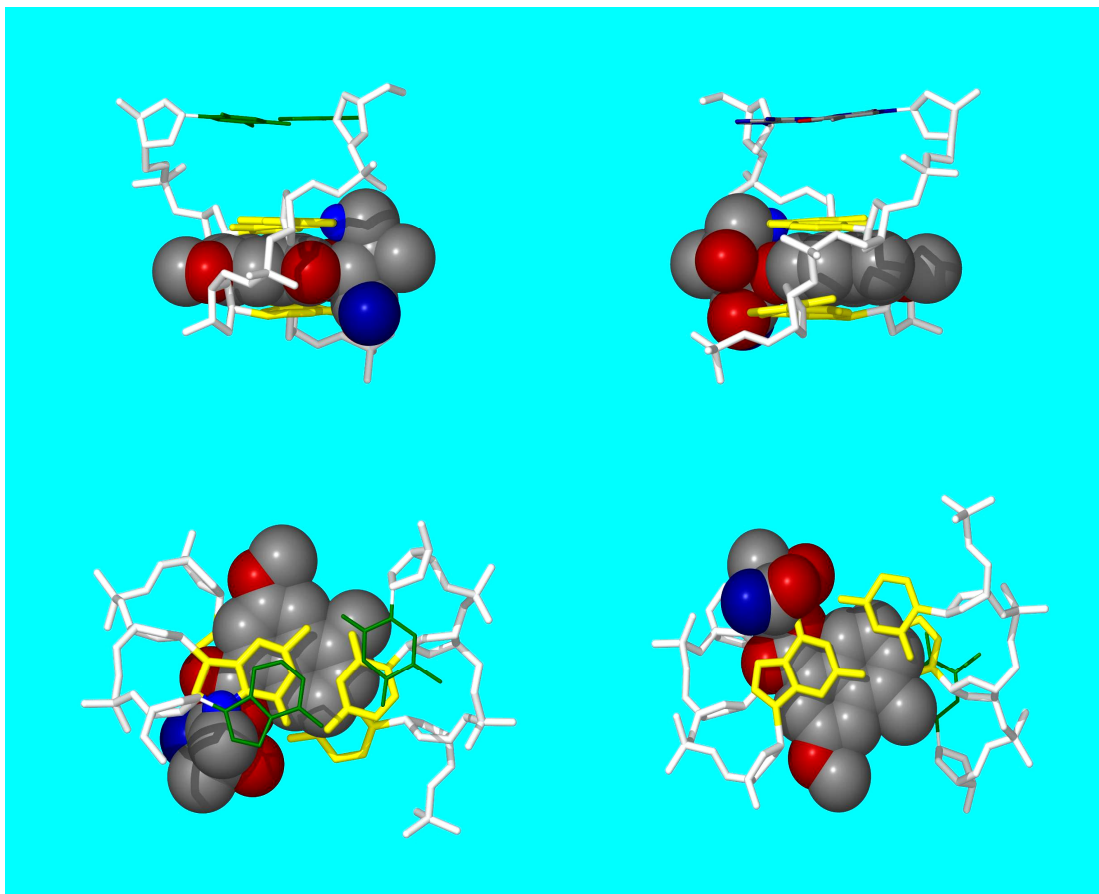
Figure 78. Chemical model showing **51** intercalated into a short oligonucleotide on the 3'-surface of the alkylated guanine residue. This model suggests efficient intercalation and a comfortable placement of the 5-atom-linker in the duplex without any obvious distortion of the B-DNA helix structure.

_____
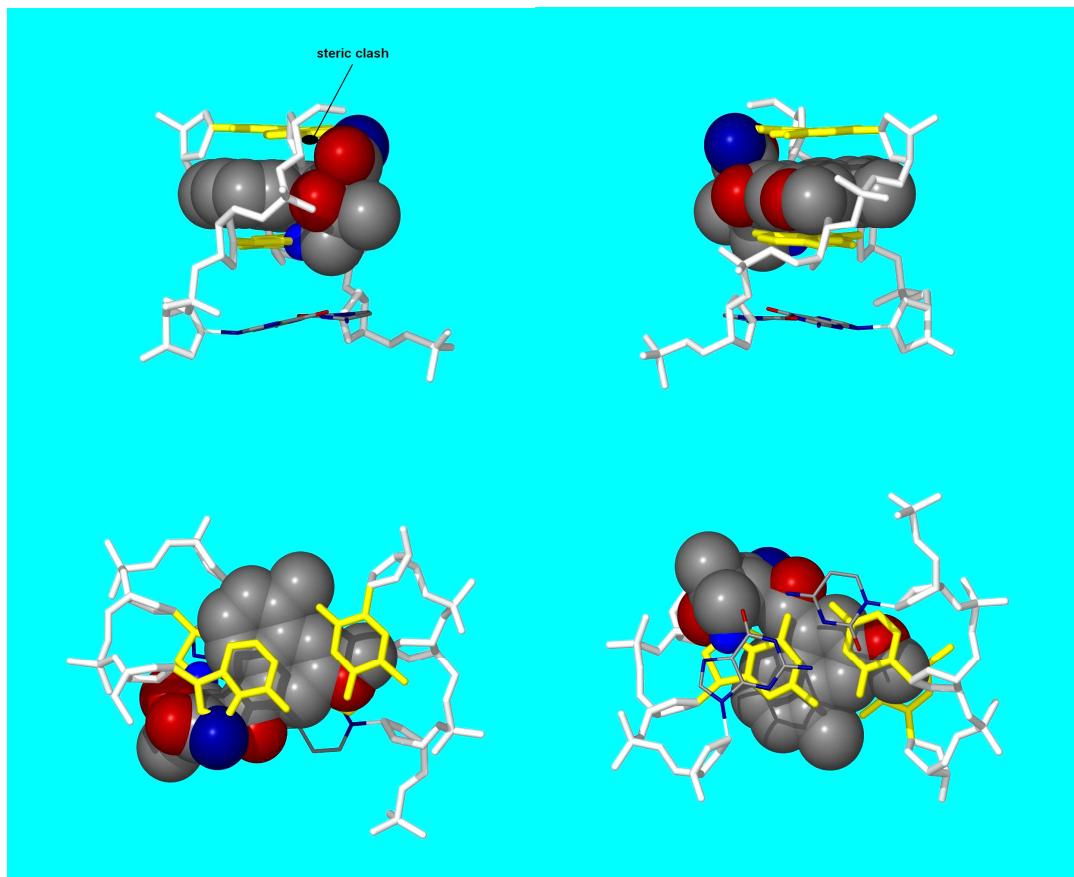
Figure 79. Chemical model showing **51** intercalated on the 5'-surface of the alkylated guanine residue. This model suggests an efficient intercalation but only with a simultaneous steric congestion of the 5-atom-linker with the backbone of DNA, which would distort the B-DNA helix.

4.5.   Kinetics of DNA Alkylation by 51 and its Rate Acceleration by Noncovalent Binding

We set out to characterize the noncovalent DNA-binding and DNA-alkylation by the left-half of azinomycin using kinetic tools, similar to our work with leinamycin (Chapter 1). As a part of this work we hoped to estimate the rate acceleration and equivalent molarity provided by noncovalent binding of the natural product's naphthoate residue.

4.5.1. DNA-alkylation by 51 Follows Michaelis-Menten Kinetics

Using a constant concentration of **51** (250 μM), we alkylated different concentrations of duplex DNA with a mixed sequence (600 μM, 2.4 equiv; 1200 μM, 4.8 equiv; 4000 μM, 16 equiv) in MOPS buffer (50 mM, pH 7.0) at room temperature. At different times the reaction mixture was extracted to remove unreacted **51** and heated to depurinate the DNA-adduct quantitatively. The depurination product (**52**) was isolated by extraction and studied by HPLC. The guanine adduct of **51** in this method shows up at 23 min, the hydrolysis product of **51** elutes at 27 min (Figure 80). Formation of the DNA adduct was followed by the gradual appearance of the guanine adduct peak of **51** and was plotted versus time (Figure 81).
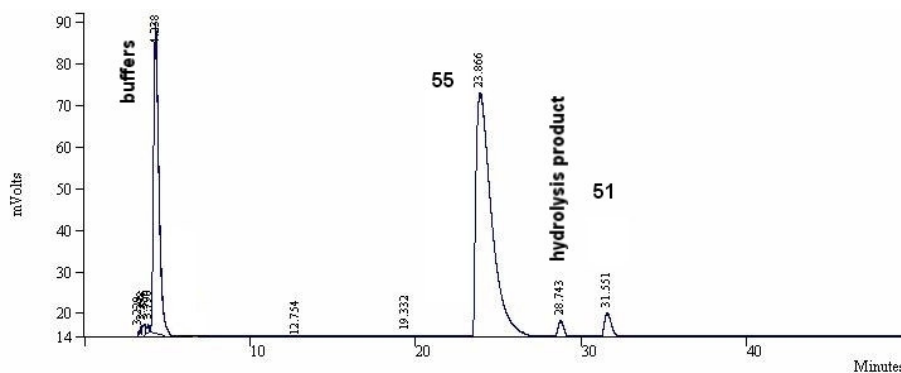
Figure 80. The products of DNA alkylation and hydrolysis of **51** separated by RP-HPLC. Buffers: 4 min, guanine adduct: 24 min; hydrolysis product: 28 min, **51**: 32 min.
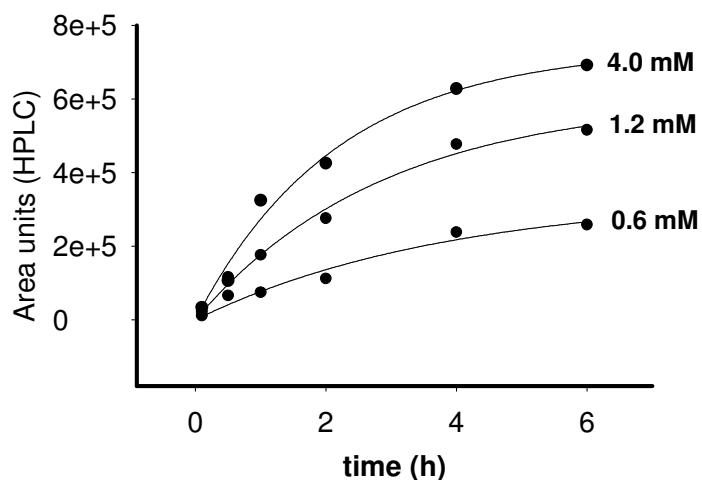
Figure 81. The appearance of the guanine adduct in the DNA alkylation reaction by **51** (250 μM) versus time and the applied DNA concentrations.

Since the only product of this reaction is the guanine adduct, a nonlinear regression was used to fit exponential curves to the data and the initial rates were calculated from the first derivatives at x $\rightarrow$ t_0 condition. [29] The initial rates and the half-lives of DNA alkylations are summarized in Table 10.

_____

[DNA] in (mM)	Initial rate of alk. by 51 in (s^{-1})	Half-life in (h)
0	0	n.a.
0.6	10.2 x 10^{-5}	1.9
1.2	13.9 x 10^{-5}	1.3
4.0	17.9 x 10^{-5}	1.1

Table 10. The initial rates and initial half-lives of DNA alkylation by **51** (250 μM). Applied concentrations of DNA (600 μM; 1200 μM; 4000 μM)

We realized that the rates of DNA alkylation follow a saturation curve when plotted against the concentration of DNA (Figure 82). This information suggested that we apply a pseudo-Michaelis-Menten model (Equation 51) to fit these rates of adduct formation vs. the applied DNA concentrations. The Michaelis-Menten plot and additional linearized forms of the initial rates versus DNA concentration data (Eadie-Hofstee, Hanes-Woolf, Lineweaver-Burk; Figure 83) were used to calculate the maximum rate of DNA alkylation (V_{MAX}), the Michaelis constant (K_M), the binding constant (K_B). These values are tabulated in Table 11.

$$[51] \; + \; [DNA] \; \underset{k_{-1}}{\overset{k_1}{\rightleftharpoons}} \; \underset{\text{noncovalent coomplex}}{[51]\bullet[DNA]} \; \overset{k_2}{\longrightarrow} \; \underset{\text{adduct}}{[51\text{-}DNA]} \qquad \textbf{Equation 51}$$
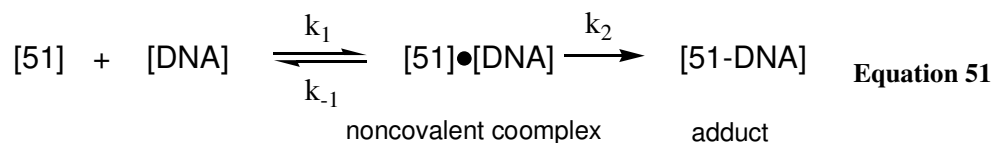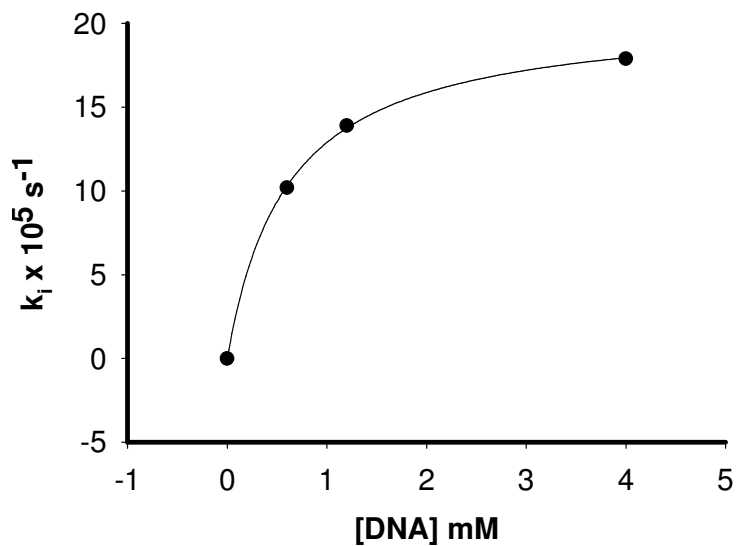
Figure 82. Michaelis-Menten plot of the initial rate constants of DNA alkylation by **51** vs. the applied DNA concentrations. The calculated Michaelis-parameters: The averaged values from the different graphical analysis: $K_M = 4.5 \times 10^{-4}$ M; $K_B = 2200$ M^{-1}; maximum rate of DNA alkylation: $k_2 = 18 \times 10^{-5}$ s^{-1} ($t_{1/2} = 1.1$ h)

_____
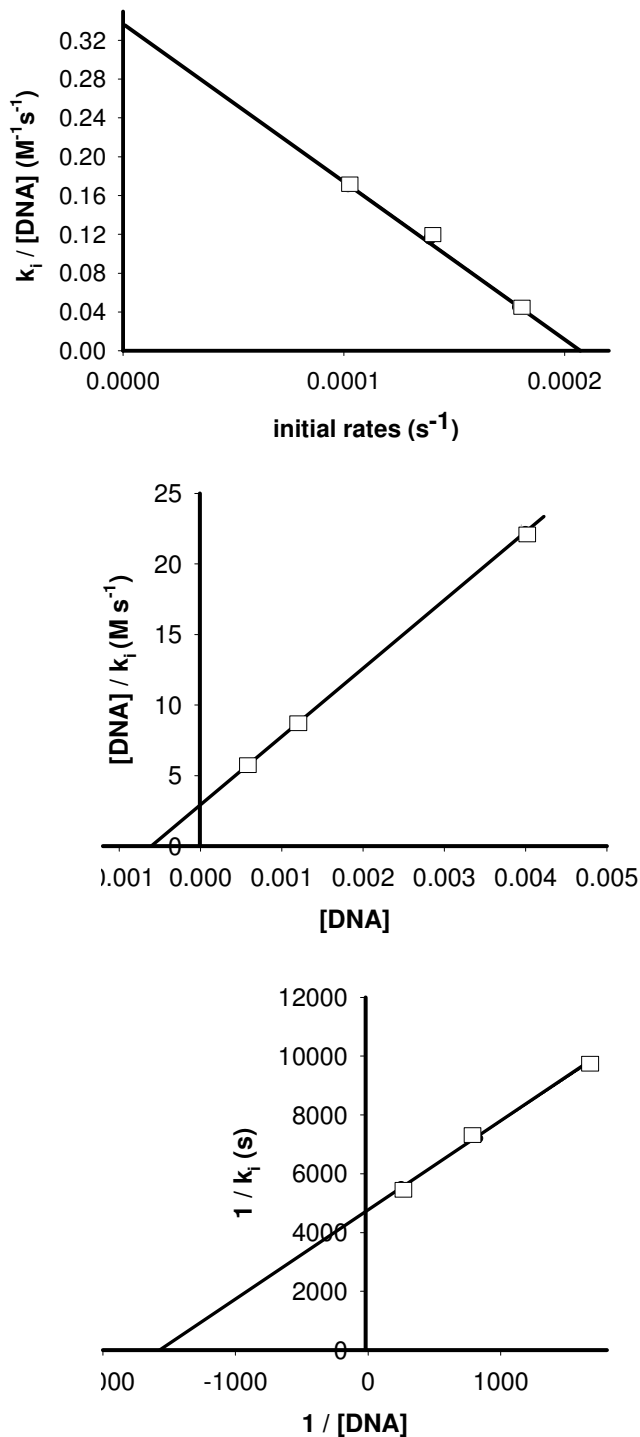
Figure 83. Linear representations of the initial rates of DNA alkylation by **51**, Eadie-Hoostee plot (*top*);
Hanes-Woolf plot (*middle*), Lineaweaver-Burk plot (*bottom*). The averaged values from the different
graphical analysis: $K_M = 5.89 \times 10^{-4}$ M M; $K_B = 1697$ M^{-1}; maximum rate of DNA alkylation: $k_2 = 14.34 \times 10^{-5}$ s^{-1}

_____

Method	V_{MAX} (s^{-1})	$t_{1/2}$ (h)	K_M (M)	K_B (M^{-1})
Michaelis plot	1.8 x 10^{-4}	1.1	4.5 x 10^{-4}	2 200
Eadie-Hofstee	2.0 x 10^{-4}	1.0	6.1 x 10^{-4}	1 600
Hanes-Woolf	2.0 x 10^{-4}	1.0	5.9 x 10^{-4}	1 680
Lineweaver-Burk	2.1 x 10^{-4}	1.0	6.2 x 10^{-4}	1 600

Table 11. Tabulated maximum rate (V_{MAX}) and half-life of DNA-alkylation by **51,** the Michaelis parameter (K_M) and the noncovalent binding constant (K_B).

DNA alkylation by **51** follows Michaelis-Menten kinetics (Equation 51). Effective DNA alkylation is facilitated by a pre-covalent association of the drug to the duplex-DNA molecule. Our measured binding constant is in good agreement with earlier measurements using biophysical methods.[28]

4.5.2. The rate of Hydrolysis of 51

We measured the rate of hydrolysis of **51** (250 µM) under conditions identical to our DNA alkylation reactions. HPLC analysis of the hydrolysis mixture was carried out and the appearance of the hydrolysis product together with the disappearance of **51** was followed (Figure 86). Linear regression analysis of these time-curves was used to calculate $k_{H2O,3}$ = 4.14.x 10^{-6} s^{-1}, ($t_{1/2}$ = 46.5 h).

_____
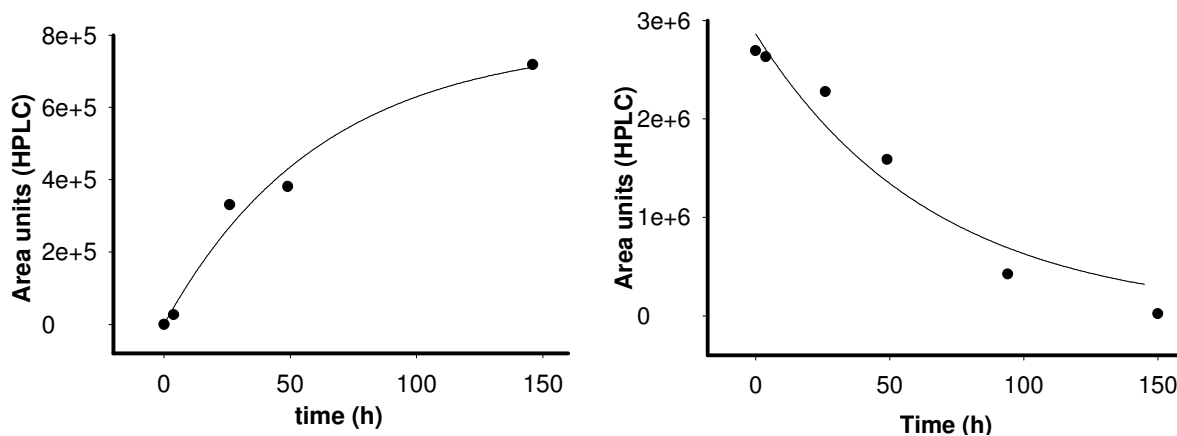
Figure 84. The appearance of the hydrolysis product of **51** (*left*) and the disappearance of **51** (*right*) in the hydrolysis reaction for the calculation of the rate of hydrolysis: $k_{H2O,3}$ = 4.14 x 10^{-6} s^{-1}, $t_{1/2}$ = 46.5 h.

The hydrolysis reaction of **51** is much slower ($t_{1/2}$ = *46.5 h*) than its DNA-alkylation (*1 h*). We can conclude that **51** is hydrolytically fairly stable. We compared these rates (Equation 52) and conclude that noncovalent DNA binding provides a *4.5 million* times faster rate of DNA-alkylation than hydrolysis under identical conditions.

$$\frac{\dfrac{k_{alk}}{K_M}}{\dfrac{k_{H2O}}{[55M]}} = \frac{\dfrac{s^{-1}}{M}}{\dfrac{s^{-1}}{M}} = \textbf{4.5 million times}$$ **Equation 52**

172

4.5.3. The Rate of Alkylation of 2'-Deoxyguanosine by 51

Finally, we wanted to study alkylation of 2'-deoxyguanosine by the left-half of Azinomycin, to understand if N7G alkylation is accelerated by noncovalent association. A comparison of the rates of 2'-deoxyguanosine and DNA alkylations under identical conditions will allow us to calculate the equivalent molarity and the rate acceleration provided by such weak binding events to DNA.

Accordingly, we measured the rate of degradation of **51** in 50%:50% TFE:buffer with a dielectric constant that mimics the dielectric environment of the major-groove of DNA, where N7 of guanine resides (Chapter 1).[30-32] The identification of the 2'-deoxyguanosine adduct of **51** was unachievable due to its short retention time, thereby, we followed the degradation of **51** in this reaction mixture. The only product formed in this reaction is the N7-2'dG adduct of **51**. Minimal amount of hydrolysis product (3% yield) was observed in these reactions. Due to the limited supply of **51** we measured the rate of 2'-deoxyguanosine alkylation at a single concentration (5 mM). We followed the appearance of the product by HPLC, calculated the first order rate of 2'-deoxyguanosine alkylation by non-linear regression of this data versus time, $k_{dG,3,\ 5mM} = 1.20 \times 10^{-6}$ s^{-1}, (t$_{1/2}$ = 160 h). We calculated the second order rate of alkylation with respect to the concentration of 2'-deoxyguanosine : $k_{dG,3,\ 5mM}$ /0.005 = $k_{sec,2'dG,3}$ = 2.4 x 10^{-4} s^{-1}M^{-1}.

4.5.4. Rate Acceleration and Effective Molarity Provided by Noncovalent Binding of 51 to Duplex DNA

To appreciate the rate acceleration provided by the noncovalent association of **51** to duplex-DNA, we compared the rate of N7-G alkylation in DNA to that in 2'-dG (Equation 53), and found that the duplex provides **1411 times** rate acceleration. The effective concentration of **51** on the surface of duplex-DNA was also calculated (Equation 54) to be **0.9 M.**

$$\frac{\dfrac{k_{alk}}{K_M}}{k_{dG}} = \frac{\dfrac{\{s^{-1}\}}{\{M\}}}{\{s^{-1}M^{-1}\}} = \quad \textbf{1411 times} \qquad \textbf{Equation 53}$$

$$\textbf{Equation 54}$$
$$\frac{k_{alk}}{k_{dG}} = \frac{\{s^{-1}\}}{\{s^{-1}M^{-1}\}} = \quad \textbf{0.9 M}$$

4.6. The Intercalation of the Left-Half of Azinomycin and its Significance

Studying the intercalation of the left-half of azinomycin (**51**) turned out to be interesting for two reasons. First, the minimum structural requirement for a small molecule to intercalate DNA has been suggested to be two annealed aromatic rings together with a functional group that is positively charged under physiological conditions. [33,34] We would like to see if this neutral system (**51**) intercalates as a result of covalent attachment to DNA. After the recognition of the cancer therapeutic advances of minimal DNA-intercalators, [35-37] such small molecules have been used in drug development. Interestingly, it was recognized early that classical intercalators with more than two aromatic rings could not penetrate cells appropriately. [37] The two-ring intercalators systems have been referred to as: *minimal intercalators.* [37]

A second motive to learn about intercalation by **51** and its analog **52** comes from debates about the intercalation of these analogs under different conditions, [24] which we will address in the conclusions Section.

_____

4.7. Plasmid DNA Unwinding by 51 and 52 and the Absence of Unwinding by 53 Supports DNA-Intercalation as a Result of DNA-alkylation

The phenomenon of plasmid DNA unwinding via DNA-intercalation has been discussed in detail in Chapter 2, Section 2.4.1, thereby we narrow our discussion to our results here. Since viscometric experiments showed that the DNA alkylating analogs of the left-half of azinomycin (**51, 52**) intercalate DNA upon alkylation, we alkylated Plasmid-DNA (PGL2BASIC, 35 µM/bp) by increasing equivalents of these molecules. After alkylation, electrophoretic separation and visualization of the topoisomers we observed that the epoxide analogs **51** and **52** unwound the plasmid DNA (Figure 85). Unwinding was not observed by the cyclopropene analog (**53**), which is unable to alkylate DNA (Figure 85).

Our data presented here suggests that the naphthoate ring of our analogs (**51, 52**) is capable of DNA-intercalation in the DNA-adduct. As evidenced by the absence of unwinding by **53** we can conclude that the neutral naphthalene ring does not intercalate DNA without covalent "linkage" to DNA bases. Control experiments were carried out to show that DNA alkylation by a small molecular epoxide glycidol does not result in plasmid unwinding (Figure 85).
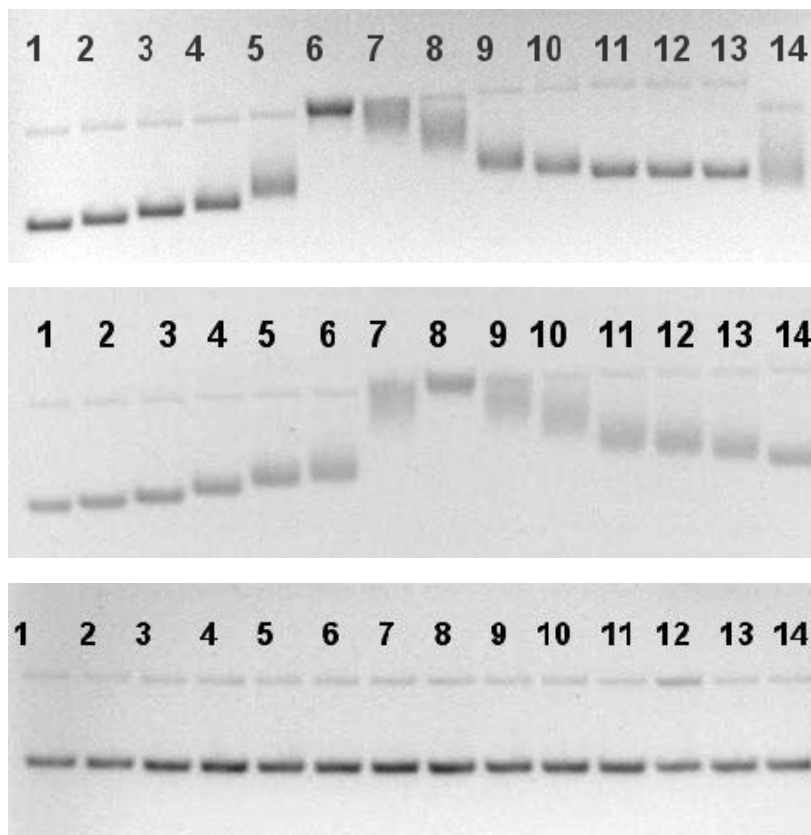
Figure 85. Plasmid-DNA unwinding (PGL2BASIC) by the epoxide analogs **51** (*top*), **52** (*middle*) and the cyclopropyl analog **53** (*bottom*). Conditions: MOPS (50 mM, pH 7.0), PGL2BASIC (70 μM/bp), Concentrations of drug in lanes: 1: DNA alone, 2: 20 μM 3: 40 μM, 4: 80 μM, 5: 100 μM, 6: 200 μM, 7: 300 μM, 8: 400 μM, 9: 500 μM, 10: 600 μM, 11: 700 μM, 12: 800 μM, 13: 900 μM, 14: 1 mM.

4.8. Viscosity Studies Demonstrate that 51 is Intercalated in the DNA-Adduct

We discussed the physical changes in the solution structure [38] and viscosity of DNA solutions [39,40] upon intercalation earlier (Chapter 2., Section 2.4.). We also talked about the biological consequences [41-43] that intercalation lends to a small organic molecule (Section 2.3.). We also outlined the classical structural requirements [33,34] for DNA-intercalation (Section 2.1. and 2.2.). This information will not be repeated here.

As we discussed in Chapter 2, increases in the viscosity of a DNA-solution in the presence of a small organic molecule can demonstrate its intercalation into DNA. [44] In our experiments calf thymus (CT) DNA (450 µM) was exposed to a DNA-alkylating epoxide analog (**51**) at different concentrations (15 µM, 30 µM, 45 µM) at room temperature and the viscosity of the reaction mixture was followed. The observed time dependent increases in the relative viscosity of the solution (Figure 86) suggested that the DNA-alkylation results in an intercalated structure. This idea was also supported by the observation that increasing equivalents of **51** in the alkylation reaction results in increasing absolute changes in the viscosity. In this experimental setup the viscometer responds linearly to increasing equivalents of a well known intercalator, ethidium bromide. This is observed at a range of DNA concentrations (Figure 87). This suggests that our experimental setup is capable of detecting intercalation.

_____
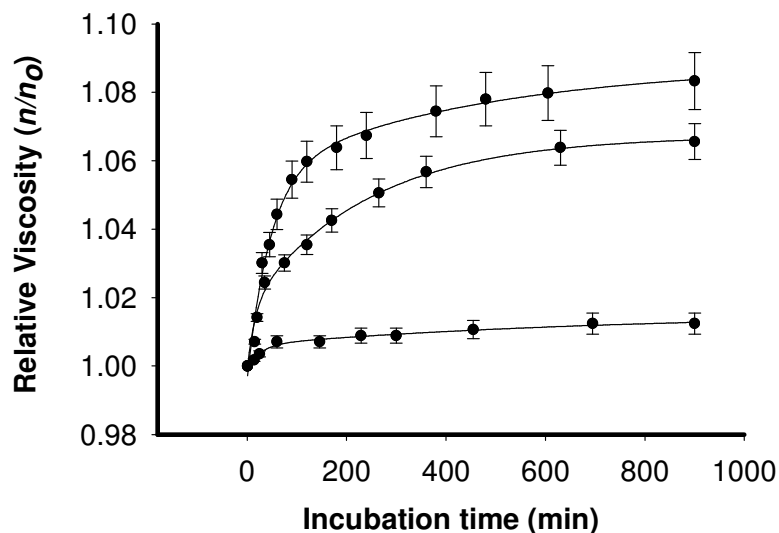
Figure 86. Changes in the relative viscosity of C.T. DNA solutions vs. time in the presence of **51**. The applied concentrations: [DNA]: 450 μM, 3: 15 μM, 30 μM, 45 μM. Buffer: MOPS (50 mM, pH 7.0).
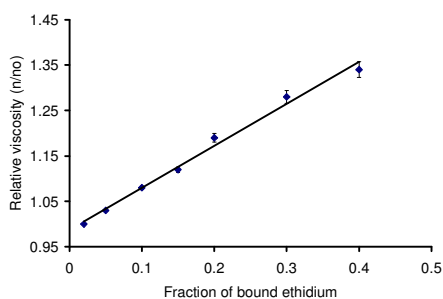
Figure 87. Changes in the relative viscosity of a CT DNA solution during the titration with the classical intercalator: ethidium bromide.

The observed exponential time dependence of the changes in the relative viscosity of our DNA solutions suggest that these changes are induced by chemical processes, reasonably the formation of the DNA-adduct of **51**. This experiment demonstrated that the DNA adduct of **51** is intercalated. We did not see any observable changes in the solution viscosity upon addition of **51** to the DNA-solution at zero time. This suggests that the naphthoate system is not intercalated before DNA-alkylation.

4.9. Fluorescence Contact Energy Transfer Experiments Demonstrate the Stacking of the Naphthoate Ring of 3 into DNA

We have discussed the changes in the spectral properties of DNA complexes upon intercalation earlier (Chapter 2. Section 2.4.2.). The fluorescence properties of duplex DNA and a free DNA-intercalator markedly differ from that of their intercalated complexes.[44,45] Intercalation brings the intercalators into such proximity to the DNA base that photon excitation of the otherwise non-fluorescent DNA will result in fluorescence at the emission wavelength of the intercalators (Figure 88). This phenomenon is termed: *Fluorescence Contact Energy Transfer.*[44-46] The excitation energy (200-300 nm) taken up by DNA will be transferred directly to excite the intercalator, which will then fluoresce at its characteristic wavelength. This type of energy transfer can only happen when the proximity of the organic molecule is as small as the distance between stacking molecules. Consequently, this method is capable of differentiating intercalation from other DNA-binding modes.[46] It is important to realize that by themselves the intercalators do not fluoresce when excited at this wavelength range (200-300 nm).

_____
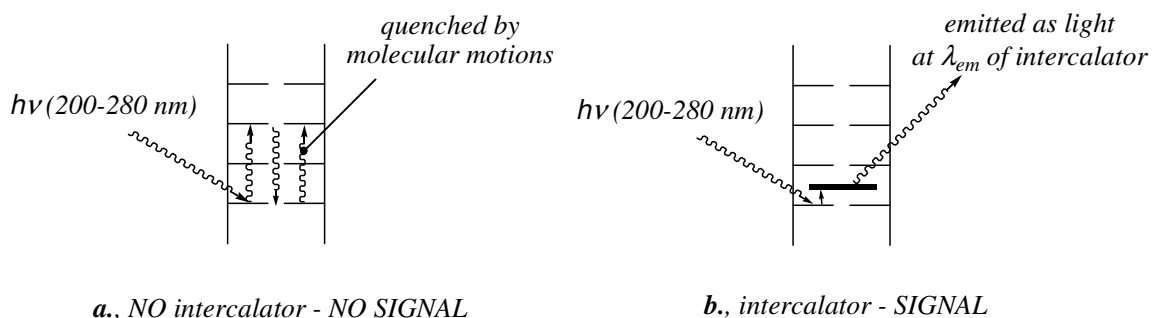
Figure 88. The theory of the FCET experiment. UV excitation of DNA will not result in fluorescence (**a**), since molecular motions will quench the excitation energy. Intercalators pick up some of the excitation energy and emit it as their own resonance energy (**b**) yielding fluorescence.

In an FCET experiment the samples are excited in the wavelength range (200-300 nm) and the fluorescence signal is collected at the emission wavelength of the suspected intercalators. The FCET spectrum is calculated by Equation 55, and plotted versus the excitation wavelength.[44] A positive FCET spectrum (evidence for intercalation) looks like the UV-spectrum of DNA, and the value of the calculated FCET should be largen than one (x > 1).

$$\frac{Q(\lambda)}{Q(310)} = (\frac{I(\lambda)E_{310}}{I_{310}E(\lambda)})_b (\frac{I(\lambda)E_{310}}{I_{310}E(\lambda)})_f$$

Equation 55

In the equation above, *Q(λ)/Q(310)* is the FCET function, *I* is fluorescence intensity, *b* – data for the bound ligand, *f* – data for the free ligand.

First, we recorded the emission fluorescence spectrum of our analogs (**51**, **52**) and found that there is a strong emission centered at 435 nm when the analogs were excited at 260 nm (the UV-absorption peak of DNA), data not shown. We used 435 nm as our

detection wavelength. The excitation fluorescence of **51** and **52** were recorded during

DNA-alkylation at zero time and after 11 h (Figure 89). An increase in fluorescence was

observed in the excitation spectrum as the DNA-alkylation reaction progressed. This was

a sign of energy transfer from the DNA to the alkylating agents (**51**, **52**).
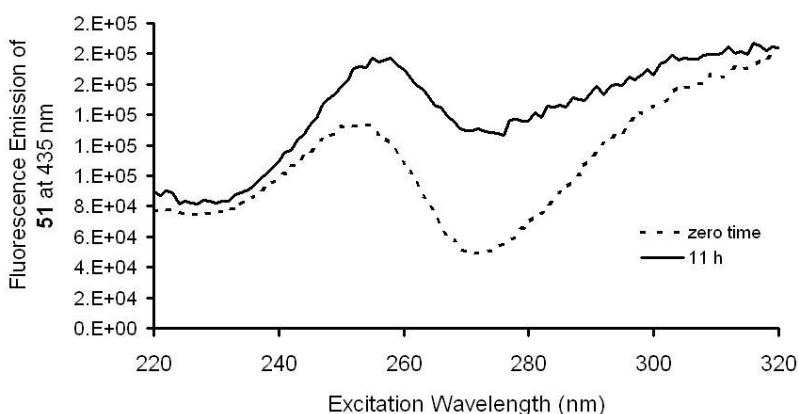
Figure 89. The fluorescence excitation spectrum of **51** before and after DNA-alkylation. Conditions:
[DNA]: 400 μM, [**51**]: 8 μM. Incubation at 37 °C.

Reading the fluorescence of the DNA-alkylating solution at different times and

calculating the FCET values over the range of excitation wavelengths resulted in the

FCET spectra (**51**: Figure 90, **53**: Figure 91). The appearance of the FCET signal strongly

supports the intercalation of the naphthoate ring as DNA-alkylation proceeds. The

cyclopropyl analog (**53**) did not yield an FCET signal under the same conditions. The

absence of the FCET signal for **53** tells us that intercalation happens as a consequence of

DNA alkylation.

_____
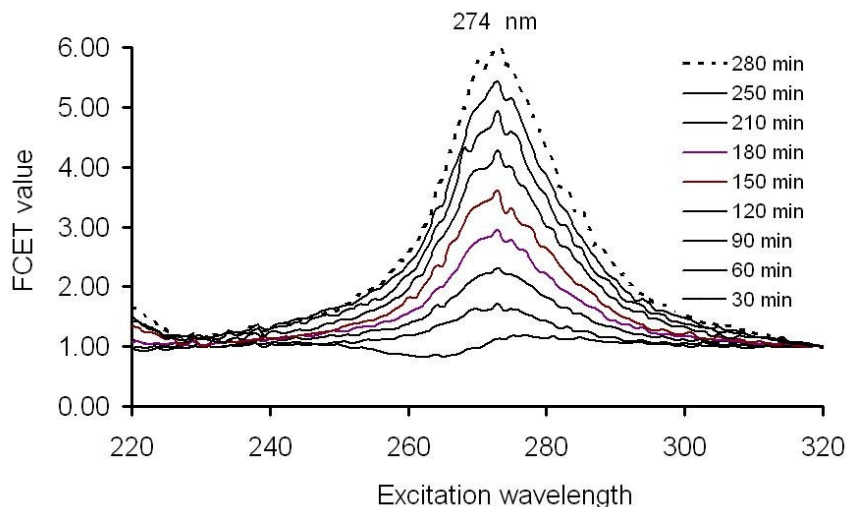
Figure 90. The FCET spectra calculated from fluorescence spectra recorded as DNA alkylation progressed in the presence of **51**. CT DNA (500 μM) was alkylated with **51** (100 μM) at 37 °C in 50 mM sodium phosphate buffer (pH 7.0). At selected times, solution was diluted 100 times into HPLC water and fluorescence readings were taken.
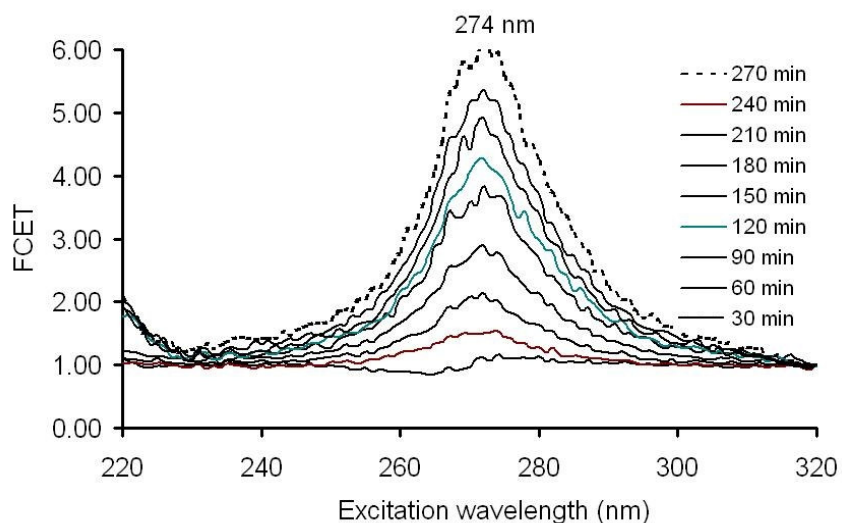
Figure 91. The FCET spectra calculated from fluorescence spectra recorded as DNA alkylation progressed in the presence of **52**. CT DNA (500 μM) was alkylated with **52** (100 μM) at 37 °C in 50 mM sodium phosphate buffer (pH 7.0). At selected times, solution was diluted 100 times into HPLC water and fluorescence readings were taken.

_____

Reading the FCET signal vs. time at a selected excitation wavelength (Figure 92)

shows exponential time-dependence, suggesting that the FCET signal is the result of a

chemical process. The calculated pseudo-first-order rates of DNA alkylation match the

magnitudes of the DNA-alkylation rates measured earlier (Section 4.5.), *1.2 x 10^{-4} s^{-1} < k*

< 8.6 x 10^{-4} s^{-1}.
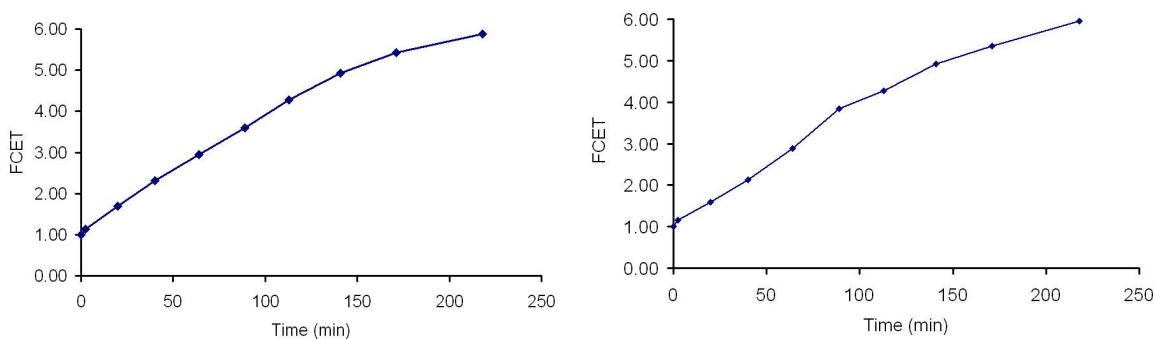
Figure 92. The appearance of the FCET signal at its corresponding maximum in the DNA-alkylation reaction by **51** and **52**. General conditions: [DNA]: 400 μM, [**51**]: 4 μM, incubation at 37 °C.

As expected, the FCET signal disappears after exposing the mixture to a heat

shock at 80 °C for half an hour, presumably due to the depurination process.

4.10. Chapter Conclusions

The DNA adduct of the left-half of azinomycin (**51**) was isolated and studied by LC-MS and identified as an N7-G adduct by its m/z value and its characteristic depurination reaction. A chemical model of the adduct was constructed, which revealed that intercalation of the aromatic naphthoate ring-system of **51** on the 3'-surface of the alkylated guanine is easily accomplished, whereas stacking over the 5'-surface of the alkylated DNA-base would probably result in steric clashes between the phosphate backbone of DNA and that of the 5-atom-linker attaching the naphthoate ring to the guanine base. This suggests that alkylation is more favored sterically when **51** can stack over the 3'-surface of the target guanine. This modeling showed agreement with the sequencing data collected by Dr. Hong Zang in our laboratory (Ph.D. Dissertation, University of Missouri-Columbia, 2001.).

The rate of DNA alkylation appears to follow Michaelis-Menten type saturation kinetics vs. increasing concentrations of DNA, which parallels with our earlier experiments suggesting that a noncovalent pre-equilibrium is required (Equation 51, Figure 82) before the alkylation step and this facilitates DNA alkylation (Section 4.5.1.). Graphical analysis of our data results in the following averaged kinetic and thermodynamic parameters for the DNA alkylation reactions: V_{max}: 2.1 x 10^{-4} s^{-1}, K_M = 6.2 x 10^{-4} M, K_B = 1600 M^{-1}. The rate of the hydrolysis reaction of **51** was also measured ($k_{H2O,3}$ = 4.14 x 10^{-6} s^{-1}, $t_{1/2}$ = 46.5 h).

To estimate the rate acceleration provided by the noncovalent binding of **51** to duplex DNA we measured the rate of alkylation of 2'-deoxyguanosine by **51** in a 50:50%

(v/v): $k_{dG,3,\ 5mM} = 1.20 \times 10^{-6}$ s^{-1}. We calculated the second order rate constant for the 2'-deoxyguanosine alkylation reaction for our condition: $k_{sec,2'dG,3} = 2.4 \times 10^{-4}$ s^{-1}M^{-1}. We calculated that the alkylation of N7G in DNA goes *1411 times* faster than that in 2'-deoxyguanosine. This corresponds to a *0.9 M* effective molarity on the surface of duplex-DNA. DNA-alkylation is *4.5 million times* faster than the hydrolysis of **51** under comparable conditions. In conclusion, noncovalent binding of **51** facilitates DNA alkylation, similar to other small molecular DNA-alkylating agents. [47,48]

We studied plasmid-DNA unwinding by the epoxide analogs (**51** and **52**) and the cyclopropyl analog (**53**). Plasmid DNA unwinding by the epoxide analogs was observed, but not with that of the cyclopropyl analog. This supports our model that the naphthoate ring is intercalated into DNA in the DNA-adduct, but not before alkylation is accomplished.

Next, we followed changes in the viscosity of CT DNA solution in the presence of our epoxide (**51**, **52**) and cyclopropyl (**53**) analogs. We observed time-dependent increases in the viscosity of DNA solution in the presence of the epoxide analogs. This demonstrated that a chemical process results in an intercalated DNA-adduct with these alkylating agents, and reinforced the idea that the DNA-adducts of **51** and **52** are intercalated. Such increases in viscosity were not observed in the presence of the cyclopropyl analog (**53**). This suggests that the neutral naphthoate ring is not intercalated unless the molecule is adducted to DNA.

Finally, we recorded the fluorescence of DNA solution in the presence of our analogs (**51-53**). A development of increasing fluorescence was observed in the presence

of our epoxides (**51**, **52**) as time progressed. In the presence of the cyclopropyl analog (**53**), we did not see any change in fluorescence. From the fluorescence signals, we calculated the Fluorescence Contact Energy Transfer from DNA to our chromophores (**51**, **52**), and gratifyingly, we found excellent FCET signals. The presence of the FCET signal demonstrated the formation of intercalated DNA adducts of **51** and **52** as a result of DNA-alkylation. The absence of the fluorescence enhancement and the absence of the FCET signal in the presence of the cyclopropyl analog showed us that the neutral naphthoate ring is not intercalated before DNA-alkylation. Overall, our experiments demonstrate that **51** and **52** are intercalated in the DNA-adduct.

It is interesting to correlate our data to the literature. It is reported that such small aromatic systems only intercalate DNA if they hold functional groups that are positively charged in solutions.[19-22] The positive charge facilitates their binding to DNA electrostatically. In our analog (**51**) there is no charge; however, covalent binding can concentrate the naphthoate ring close to the DNA-bases for intercalation. Interestingly, we do not see any change in the viscosity of DNA-solution in the presence of **53.** This analog contains the cyclopropyl ring, which does not act as an alkylating agent.

An earlier controversy between data from our laboratory[18] and the laboratory of Professor Robert Coleman requires discussion here.[24] We found that an analog of the left-half of Azinomycin (**54**) intercalated DNA. This analog does not alkylate DNA. The research group of Prof. Coleman found that such analogs do not intercalate DNA. This difference can be explained by our earlier belief that **54** was not able to alkylate DNA, and interpretation that intercalation simply takes places as the result of non-covalent

association between **54** and DNA. A careful control, however, needs to be carried out to test if **54** is capable covalent adduct formation. Based on the work presented in this Chapter, we suggest that **54** might be a DNA-alkylating agent. Our earlier examination of the intercalation of analog **54** did not test its DNA alkylating property. Based on its structural features, it might be possible that **54** forms a DNA-alkylating epoxide in solutions, with displacement of a chloride with the help of neighboring group participation of the hydroxyl functionality (Scheme 21). Eventually, both our group and the group of Dr. Colemann correctly concluded the available experimental data. In a fundamental view, intercalation on neutral naphthoate ring is only possible if the molecule is concentrated in the proximity of DNA. This can happen via electrostatic or covalent adduct formation.
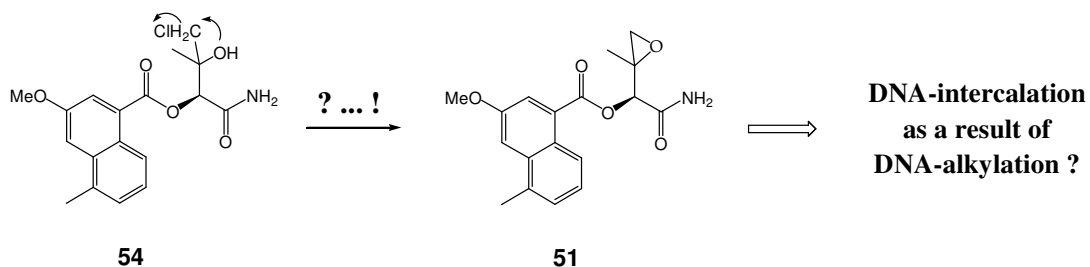
Scheme 21. Hypothesized regeneration of the DNA-alkylating epoxide in the hydroxyl-chloro analog (**54**).

Finally, it is interesting to know that a mimimum 30% of **51** is bound to DNA (K_B = 1500 M^{-1}) at an initial concentrations of 250 μM and 500 μM DNA. We should have seen increases in viscosity or FCET signal if **51** intercalated DNA before alkylation. The neutral naphthoate ring, consequently is not intercalated before DNA-alkylation.

4.11. Experimental

4.11.1. Materials and Methods

The analogs **51-54** were gifted to us by the research group of Professor Michael Shipman from the Department of Chemistry, Warwick University, London. Additional reagents were purchased from the following suppliers and were of the highest purity available: MOPS buffer, sodium acetate and sodium phosphate buffers, trifluoroethanol, triethylamine, Aldrich Chemical Co. (Milwaukee, WI); HPLC grade solvents (water, acetonitrile, ethanol), Fisher (Pittsburgh, PA); herring sperm DNA, Roche Molecular Biochemicals (Indianapolis, IN); HPLC vials, National Scientific Corporation; analytical HPLC columns, Varian Inc. (Palo Alto, CA). The plasmid PGL2BASIC was prepared and purified in our laboratory by expression in genetically engineered *E.Coli.* bacteria. [49] HPLC: Varian Prostar Dynamax, vs. 5.1. LC-MS: ThermoFinnigan TSQ7000 triple-quadrupole with API2 source.

4.11.2. Mass Spectrometric Analysis of the 51-DNA Adduct

The DNA adducts were synthesized as detailed below. The isolated guanine adduct was injected into LC-MS, and analized by a Thermo-Finnigan TSQ7000 triple-quadrupole mass spectrometer using electrospray ionization (ESI) in positive(+)ion mode, with an inlet capillary at 250 °C and an electrospray needle voltage at 4.5 kV. Nitrogen sheath gas was used at 80 psi. The LC-MS system is equipped with a Thermo-Finnigan LC system consisting of a P4000 quaternary LC pump and SCM1000 vacuum degasser, an AS3000 autosampler and a UV6000LP diode array detector.

4.11.3. Computer Model of 51 in ds-DNA 5'-A<u>G</u>G-3' Sequence

A protein database coordinate file of a short 10-mer oligonucleotide-bleomycin DNA adduct was downloaded from the protein database. The bleomycin molecule was erased from this structure and the oligonucleotide was truncated to the 5'-A<u>G</u>G-3' sequence. The middle guanine (underlined) was attached to a 3D chemical model of **51**. The naphthoate ring of **51** was positioned into a stacking position with either the 3'- or the 5'-surface of the alkylated guanine residue. The resulting structure was energy minimized by the MM2 package of ChemDraw 3D Ultra Software. The final coordinate file (*.pdb) was transferred to X-Seed [50] (software used for supramolecular crystallography). This software provides interactive tools of atom coloring and light/shadow effects. PovRay (Mathematical Modelling) [51,52] was used to render the image (*.jpg) of the molecules.

4.11.4. DNA Alkylation by 51

At 37 °C the following components were mixed: 50 μL of **51** (2.5 mM in acetonitrile), 50 μL of MOPS buffer (500 mM in water, pH 7.0), 6 – 40 μL of herring DNA (10 mM in water) and water (394 μL to 360 μL) in small 500 uL centrifuge-tubes. Samples were vortexed gently (10 s). At different times 50 μL-aliquots were removed from the reaction mixture and mixed with 150 μL water. This sample was extracted with butanol (200 μL) twice. The remaining aqueous phase was kept on a heat-block for depurination (85 °C, 1.5 h). The depurination times were optimized via additional experiments making sure of complete depurination without the degradation of the guanine-adduct of **51**. Samples

were cooled to room temperature and were further extracted for their guanine-adduct

content by butanol (200 μL) twice. The butanol samples were dried in a speed-vacuum

instrument and stored at -20°C before HPLC analyses. HPLC analyses were carried out

as described later.

4.11.5. HPLC Analyses of DNA-Adducts and Hydrolysis Samples

The dried samples from the DNA reactions were redissolved into an HPLC

injection mixture (150 μL of 60% A and 40% B, where A: 0.5% formic acid in water, B:

acetonitrile). 20 μL of the reaction samples was injected onto a C18 RP-HPLC 100 Å

column, 4.6 x 250 (Varian), and was eluted isocratically with 60% A and 40% B (A:

0.5% formic acid in water; B: acetonitrile) at a flow rate of 0.8 mL/min. The wavelength

of detection was 260 nm. The guanine adduct of **51** in this method elutes at 23 min,

followed by the hydrolysis product of **51** at 27 min (Figure 80).

4.11.6. Hydrolysis of 51

The following components were mixed together at 37 °C: 25 μL MOPS buffer

(500 mM in water pH 7.0), 25 μL **51** (2.5 mM in acetonitrile), 200 μL water (HPLC

grade). The mixture was vortexed gently, and at different times small aliquots (25 μL)

were removed and were immediately frozen on liquid nitrogen. This frozen sample was

stored at -20°C before HPLC analyses. HPLC analyses were carried out as described

above.

_____

4.11.7. Degradation of 51 in its Reaction with 2'-Deoxyguanosine

The following components were mixed and incubated at 37 °C: 100 μL of 2'-deoxyguanosine in TFE (10 mM), 20 μL of MOPS (500 mM, pH 7.0 in water), 20 μL of **51** (2.5 mM in acetonitrile). This mixture was mixed gently (10 s) and incubation begun. At different times, small aliquots of the sample (15 μL) were taken from the mixture and mixed with 85 μL water (HPLC grade), then frozen on liquid nitrogen, and dried in a speed-vacuum instrument. The dried samples were stored at minus 20°C. At the time of HPLC analysis, the dried samples were dissolved into 150 μL of HPLC injection mixture (60% A and 40% B, where A: 0.5 % formic acid in water, B: acetonitrile). HPLC analysis was performed as described above.

4.11.8. Plasmid DNA-Unwinding by 51, 52 and 53

Dilutions of the analogs in acetonitrile were carried out to 5 x of their final concentration (100 μM, 200 μM, 400 μM, 0.5 mM, 1 mM, 1.5 mM, 2 mM, 2.5 mM, 3 mM, 3.5 mM, 4 mM, 4.5 mM, 5 mM). The reaction mixtures were mixed at 4 °C accordingly: 2.5 μL of sodium phosphate buffer (500 mM, pH 6.5), 15.5 μL water (HPLC grade), 2 μL of PGL2BASIC (1 mg/mL stock solution), 5 μL of the acetonitrile stock solution of our analogs. Samples were vortexed gently (5 s), then incubated at 4 °C for 24 h. Then, samples were treated with 6 μL of glycerol loading buffer (7 μL) containing 0.25% bromophenol blue and 40% sucrose, and the mixtures were vortexed gently (5 s). Samples were loaded on a 2% (m/m%) agarose-gel and electrophoresed at 40 V for approximately 16 h in a 4°C cold-room.

_____

4.11.9. Plasmid DNA-unwinding by Glycidol

Dilutions of glycidol in acetonitrile were carried out to 5 x of its final concentration (10 μM, 20 μM, 40 μM, 0.05 mM, 0.1 mM, 0.15 mM, 0.2 mM, 0.25 mM, 0.3 mM, 0.35 mM, 0.4 mM, 0.45 mM, 0.5 mM). The reaction mixtures were mixed at room temperature accordingly: 2.5 μL of sodium phosphate buffer (500 mM, pH 6.5), 15.5 μL water (HPLC grade), 2 μL of PGL2BASIC (1 mg/mL stock solution), 5 μL of the acetonitrile stock solution of glycidol. Samples were vortexed gently (5 s), then incubated at 37 °C for 24 h. Then, samples were treated with 6 μL of glycerol loading buffer (7 μL) containing 0.25% bromophenol blue and 40% sucrose, and the mixtures were vortexed gently (5 s). Samples were loaded on a 2% (m/m%) agarose-gel and electrophoresed vs. 40 V for approximately 16 h in a 4 °C-cold-room. The outcome of alkylation by glycidol was checked in separate experiments, using base workup (DMEDA). These experiments were set up exactly the same way as the glycidol experiments above, however, after incubation samples were treated with 3 μL of DMEDA solution (1 M in HPLC water) and further incubated at 37 °C for 1 h. Then glycerol loading buffer (7 μL) was added to the samples and they were loaded to a 2% agarose gel for electrophoresis at 40 V for 16 h at 4 °C.

4.11.10. Viscometric Monitoring of DNA Alkylation by 51

For this experiment a custom made flow-viscometer was used (Ace Glass Co.) with a room temperature flow rate of 100 s for water and a sample volume of 1mL. The samples were prepared using 100 μL of DNA (4.5 mM in HPLC water), 100 μL NaPi buffer (100 mM, pH 7.0), 700 μL of HPLC-water. At this point the sample was mixed with bubbling (5-10 s). With the help of a Pasteur-pipette 100 μL of the 10 x stock solution **51** (150 μM or 300 μM or 450 μM) mixed into the viscometer and bubbled. Flow times were collected until their increase reached saturation. The flow time of the actual time-point: t and the flow time of the buffer solution t_0 was used to calculate the relative viscosity by the equation: *$(t-t_0)/t_0$*. Here t_0 is the flow time of the buffered DNA-solution without **51**. The calculated relative viscosities were plotted versus the reaction time (Figure 86) and fitted to a rising exponential using SigmaPlot 2001.

4.11.11. Viscometric Monitoring of DNA Titration by Ethidium Bromide (Control)

As a control we followed the changes in relative viscosity of C.T.DNA solutions (400-800 μM concentrations) as we titrated it with a classical intercalator ethidium bromide (Figure 85). A flow viscometer with a room temperature flow time of 100 s (for water) was used with 1 mL sample volume. The sample was made of 100 μL of C.T.DNA solution (10 times the final concentration), 100 μL of MOPS buffer (500 mM, pH 7.0), 700 μL of HPLC water. This solution was mixed by bubbling the flow-viscometer (10-15 s). The viscosity of this background solution was measured (t_0) as described above. After each reading, an aliquot of ethidium bromide solution (10 x the concentration of DNA

solution, containing C.T.DNA at the applied concentration to avoid the dilution) was mixed into the solution in the viscometer. Flow time was measured and relative viscosity was calculated. The relative viscosity was plotted versus the applied equivalents of ethidium bromide (Figure 85) to demonstrate that our experimental setup is applicable to detect DNA-intercalation and its "end-point".

4.11.12. Fluorescence Contact Energy Transfer (FCET) to follow DNA-alkylation by 51 and 52

For these fluorescence studies the following instrumental settings were applied: lamp power: 750 watts, optical slots 12 nm, multiplier voltage: 950 V, chopper: 51 Hz, automatic shutter control and 0.1 s integration time. 1 mL DNA-alkylation sample was made accordingly: 20 μL of acetonitrile solution of **51** or **52** (500 μM) was mixed with 100 μL sodium phosphate buffer (500 mM, pH 6.5) and 100 μL of C.T. DNA solution (5 mM in HPLC water) and finally 780 μL of HPLC water was added. The mixture was vortexed gently over a period of 5-10 s, then placed into a 4 °C refrigerator. At different times 10 μL-aliquots were taken from this sample and diluted into 990 μL of fluorescence solution (10 mM sodium phosphate, pH 6.5). A fluorescence excitation spectrum was recorded in the excitation range of 220-300 nm and at an emission wavelength of 435 nm. The fluorescence excitation spectrum was analized by means of Equation 55 (Section 4.9.), and FCET plots were calculated (Figure 89). The appearance of the FCET signal was also plotted vs. time at an excitation wavelength of 275 nm (Figure 92).

References

1.   Hata, T.; Koga, F.; Sano, Y.; Kanamori, K.; Matsumae, A.; Sugawara, R.; Hoshi, T.; Shima, T.; Ito, S.; Tomizawa, S., Carzinophilin, a new tumor inhibitory substance produced by streptomyces. I. *J. Antibiot.* **1954,** 7, 107-12.

2.   Nagaoka, K.; Matsumoto, M.; Ono, J.; Yokoi, K.; Ishizeki, S.; Nakashima, T., Azinomycins A and B, new antitumor antibiotics. I. Producing organism, fermentation, isolation, and characterization. *J. Antibiot.* **1986,** 39, 1527-32.

3.   Yokoi, K.; Nagaoka, K.; Nakashima, T., Azinomycins A and B, new antitumor antibiotics. II. Chemical structures. *Chem. Pharmaceut. Bull.* **1986,** 34, 4554-61.

4.   Ishizeki, S.; Ohtsuka, M.; Irinoda, K.; Kukita, K.; Nagaoka, K.; Nakashima, T., Azinomycins A and B, new antitumor antibiotics. III. Antitumor activity. *J. Antibiot.* **1987,** 40, 60-5.

5.   Salvati, M. E.; Moran, E. J.; Armstrong, R. W., Simplified method for the isolation of thermally labile drug-DNA adducts: characterization of chlorambucil and carzinophilin/azinomycin B alkylation products. *Tetrahedron Lett.* **1992,** 33, 3711-14.

6.   Hodgkinson, T. J.; Kelland, L. R.; Shipman, M.; Suzenet, F., Chemical synthesis and cytotoxicity of some azinomycin analogs devoid of the 1-azabicyclo[3.1.0]hexane subunit. *Bioorg. Med. Chem. Lett.* **2000,** 10, 239-241.

7.   Hashimoto, M.; Matsumoto, M.; Yamada, K.; Terashima, S., Synthesis, chemical property, and cytotoxicity of the carzinophilin congeners carrying a 2-(1-acylamino-1-

alkoxycarbonyl)methylidene-1-azabicyclo[3.1.0]hexane system. *Tetrahedron Lett.* **1994,** 35, 2207-10.

8.   Shibuya, M.; Terauchi, H., Synthetic studies toward azinomycins A and B. Synthesis and absolute stereochemistry of the minor component isolated from an azinomycin-producing strain. *Tetrahedron Lett.* **1987,** 28, 2619-22.

9.   Ando, K.; Yamada, T.; Shibuya, M., Synthetic approach toward azinomycins. *Heterocycles* **1989,** 29, 2209-18.

10.   Coleman, R. S.; Carpenter, A. J., The development of strategies for construction of the aziridine core of the antitumor agents azinomycins A and B. *Tetrahedron* **1997,** 53, 16313-16326.

11.   Hodgkinson, T. J.; Shipman, M., Chemical synthesis and mode of action of the azinomycins. *Tetrahedron* **2001,** 57, 4467-4488.

12.   Coleman, R. S.; Li, J.; Navarro, A., Total synthesis of azinomycin A. *Angew Chem* **2001,** 40, 1736-1739.

13.   Moran, E. J.; Armstrong, R. W., Highly convergent approach to the synthesis of the epoxy-amide fragment of the azinomycins. *Tetrahedron Lett.* **1991,** 32, 3807-10.

14.   Casely-Hayford Maxwell, A.; Pors, K.; James Colin, H.; Patterson Laurence, H.; Hartley John, A.; Searcey, M., Design and synthesis of a DNA-crosslinking azinomycin analogue. *Org. Biomol. Chem.* **2005,** 3, 3585-9.

15.   Konda, Y.; Machida, T.; Sasaki, T.; Takeda, K.; Takayanagi, H.; Harigaya, Y., Convenient synthesis of the epoxy fragment of azinomycin B. *Chem. Pharmaceut. Bull.* **1994,** 42, 285-8.

16.   Bryant, H. J.; Dardonville, C. Y.; Hodgkinson, T. J.; Shipman, M.; Slawin, A. M.

Z., Asymmetric synthesis of the epoxide portion of the azinomycins. *Synlett* **1996**, 973-

974.

17.   Armstrong, R. W.; Salvati, M. E.; Nguyen, M., Novel interstrand cross-links

induced by the antitumor antibiotic carzinophilin/azinomycin B. *J. Am. Chem. Soc.* **1992,**

114, 3144-5.

18.   Zang, H.; Gates, K. S., DNA Binding and Alkylation by the "Left Half" of

Azinomycin B. *Biochemistry* **2000,** 39, 14968-14975.

19.   Gabbay, E. J.; DePaolis, A., Topograpgy of Nucleic Acid Helices in Solutions.

Steric Requirements for Intercalation. *J. Am. Chem. Soc.* **1971,** 92, 562-564.

20.   Davidson, M. W.; Griggs, B. G.; Boykin, D. W.; Wilson, W. D., Molecular

Structural Effects Involved in the Interaction of Quinolinemet hanolamines with DNA.

Implications for Antimalarial Action. *J. Med. Chem.* **1977,** 20, 1117-1122.

21.   Povrik, L. F.; Dattagupta, N.; Warf, B. C.; Goldberg, I. H., Neocarzinostatin

Chromophore Binds to Deoxyribonucleic Acid by Intercalation. *Biochemistry* **1981,** 20,

4007-4014.

22.   Yu, L.; Golik, J.; Harrison, R.; Dedon, P., The Deoxyfucose-Anthranilate of

Esperamicin A1 Confers Intercalative DNA Binding and Causes a Switch in the

Chemistry of Bistranded DNA Lesions. *J. Am. Chem. Soc.* **1994,** 116, 9733-9738.

23.   Zhang, H., Dissertation, University of Missouri-Columbia. **2001**.

24.   Coleman, R. S.; Perez, R. J.; Burk, C. H.; Navarro, A., Studies on the Mechanism

of Action of Azinomycin B: Definition of Regioselectivity and Sequence Selectivity of

DNA Cross-Link Formation and Clarification of the Role of the Naphthoate. *J. Am. Chem. Soc.* **2002,** 124, 13008-13017.

25.   Casely-Hayford Maxwell, A.; Pors, K.; Patterson Laurence, H.; Gerner, C.; Neidle, S.; Searcey, M., Truncated azinomycin analogues intercalate into DNA. *Bioorg. Med. Chem. Lett.* **2005,** 15, 653-6.

26.   Balcome, S.; Park, S.; Dorr, D. R. Q.; Hafner, L.; Phillips, L.; Tretyakova, N., Adenine-Containing DNA-DNA Cross-Links of Antitumor Nitrogen Mustards. *Chem. Res. Toxicol.* **2004,** 17, 950-962.

27.   Liao, P.-C.; Li, C.-M.; Hung, C.-W.; Chen, S.-H., Quantitative detection of N7-(2-hydroxyethyl)guanine   adducts   in   DNA   using   high-performance   liquid chromatography/electrospray ionization tandem mass spectrometry. *J. Mass. Spectrom.* **2001,** 36, 336-343.

28.   Zang, H., Dissertation, University of Missouri-Columbia. **2001**.

29.   Atkins, P. W., *Physical Chemistry, 6th Edition*. 1998; p 1014 pp.

30.   Sierra, P. S.; Tejuca, C. C.; Garcia-Blanco, F.; Oliva, C. D.; Sierra, J. C.; Gorostidi, G. E., Properties of 2,2,2-trifluoroethanol/water mixtures: acidity, basicity, and dipolarity. *Helvetica Chimica Acta* **2005,** 88, 312-324.

31.   Jadhav, V. R.; Barawkar, D. A.; Ganesh, K. N., Polarity Sensing by Fluorescent Oligonucleotides: First Demonstration of Sequence-Dependent Microenvironmental Changes in the DNA Major Groove. *Journal of Physical Chemistry B* **1999,** 103, 7383-7385.

_____

32.   Chitra, R.; Smith, P. E., A comparison of the properties of 2,2,2-trifluoroethanol

and 2,2,2-trifluoroethanol/water mixtures using different force fields. *Journal of

Chemical Physics* **2001,** 115, 5521-5530.

33.   Atwell, G. J.; Bos, C. D.; Baguley, B. C.; Denny, W. A., Potential antitumor

agents. 56. Minimal DNA-intercalating ligands as antitumor drugs: phenylquinoline-8-

carboxamides. *J. Med. Chem.* **1988,** 31, 1048-52.

34.   Sartorius, J.; Schneider, H.-J., Intercalation mechanisms with ds-DNA: binding

modes and energy contributions with benzene, naphthalene, quinoline and indole

derivatives including some antimalarials. *Journal of the Chemical Society, Perkin

Transactions 2: Physical Organic Chemistry* **1997**, 2319-2328.

35.   Boehner, R.; Hagen, U., Action of intercalating agents on the activity of DNA

polymerase I. *Biochim. Biophys. Acta Nucleic. Acids. Protein. Synth.* **1977,** 479, 300-10.

36.   Sarris, A. H.; Niles, E. G.; Canellakis, E. S., The mechanism of inhibition of

bacteriophage T7 RNA synthesis by acridines, diacridines and actinomycin D. *Biochim.

Biophys. Acta Nucleic. Acids. Protein. Synth.* **1977,** 474, 268-78.

37.   Denny, W. A., *Acridine-4-carboxamides and the concept of minimal DNA

intercalators.* 2003; Vol. 2, p 482-502.

38.   Cairns, J., Application of autoradiography to the study of DNA [deoxyribonucleic

acid] viruses. *Cold Spring Harbor Symposia on Quantitative Biology* **1962,** 27, 311-18.

39.   Lerman, L. S., Structural considerations in the interaction of deoxyribonucleic

acid and acridines. *J. Mol. Biol.* **1961,** 3, 18-30.

40.   Waring, M. J., Variation of the supercoils in closed circular DNA by binding of antibiotics and drugs. Evidence for molecular models involving intercalation. *J. Mol. Biol.* **1970,** 54, 247-79.

41.   Gale, E. F.; Cundliffe, E.; Waring, M. J.; Reynolds, P. E.; Richmond, M. H., *The Molecular Basis of Antibiotic Action*. 1972; p 474 pp.

42.   Neidle, S., The molecular basis for the action of some DNA-binding drugs. *Progr. Med. Chem.* **1979,** 16, 151-221.

43.   Schwartz, H. S., Biochemical action and selectivity of intercalating drugs. *Advances in Cancer Chemotherapy* **1979,** 1, 1-60.

44.   Suh, D.; Chaires, J. B., Criteria for the mode of binding of DNA binding agents. *Bioorg. Med. Chem.* **1995,** 3, 723-728.

45.   Le-Pecq, J. B.; Paoletti, C., A fluorescent complex between ethidium bromide and nucleic acids. *J. Mol. Biol.* **1967,** 27, 87-106.

46.   Suh, D.; Oh, Y.-K.; Chaires, J. B., Determining the binding mode of DNA sequence specific compounds. *Process Biochem.* **2002,** 37, 521-525.

47.   Johnson, W. W.; Guengerich, F. P., Reaction of aflatoxin B1 exo-8,9-epoxide with DNA: kinetic analysis of covalent binding and DNA-induced hydrolysis. *Proc. Natl. Acad. Sci. Unit. States Am.* **1997,** 94, 6121-6125.

48.   Warpehoski, M. A.; Harper, D. E., Enzyme-like Rate Acceleration in the DNA Minor Groove. Cyclopropylpyrroloindoles as Mechanism-Based Inactivators of DNA. *J. Am. Chem. Soc.* **1995,** 117, 2951-2952.

_____

49.   Sambrook, J. F.; Russell, D. W.; Editors, *Molecular cloning: A laboratory manual, third edition*. 2000; p 2300 pp (approx).

50.   Barbour, L. J., X-seed - a software tool for supramolecular crystallography. *J. Supramol. Chem.* **2003,** 1, 189-191.

51.   Schamberger, J.; Herz, T., Molecular modeling for PCs. *Nachrichten aus Chemie, Technik und Laboratorium* **1997,** 45, 520-523.

52.   Whitwood, A., Molecules in a virtual world. *Chemistry Review (Deddington, United Kingdom)* **2004,** 13, 8-9.

Chapter 5. A Collaborative Study Toward Engineered Biosynthesis of Leinamycin Analogues

5.1.   Introduction to the Biosynthesis and Combinatorial Biosynthesis of Natural Poducts in the Example of Leinamycin [1,2]

Microorganisms make a wide variety of Natural Products with a broad range of pharmacological activities. [3] Novel bioactive natural products can turn out to be directly interesting to Medicine or Industry, or may, as well, promote research to understand the action behind the novel chemical structure. The natural products are constructed with the help of enzymes in microorganisms. The enzymes responsible for building or tailoring the natural product, regulatory proteins and many proteins of unknown function, are coded by genes (Scheme 22), which are either in clusters or isolated sporadically in the genome of the synthesizing organism. [2] These enzymes are either multifunctional or are in the form of enzyme clusters (*modules*) that carry out a few modifications before releasing the intermediate or the final product. A recombination of the order of genes or attempts to feed the biosynthetic enzymes with substrate analogs might be useful in the preparation of natural product analogs. [4]

In our simplified representation of the leinamycin biosynthetic machinery (Scheme 22) for our current discussion, it is important to recognize the presence of a cyclizing/condensing/oxidizing module (module-2) that forms the thiazole ring of leinamycin. This module eventually produces a PCP (peptidyl carrier protein) conjugate

of our target (**56**, Scheme 22, boxed). This protein conjugate is a substrate for further

elongation of the carbon skeleton in the macrocycle of leinamycin (from module-3).

Chain elongation, dehydration and methyl transfer steps follow in this biosyntesis.

Finally a "thioesterase" (TE) accomplishes the macrocyclization of the 18-member

lactam ring and a separate enzyme cluster (Post NRPS-PKS, nonribosomal-

polyketidesynthase) attaches the dithiolenone-S-oxide ring in a spiro-fashion to the

macrocycle.
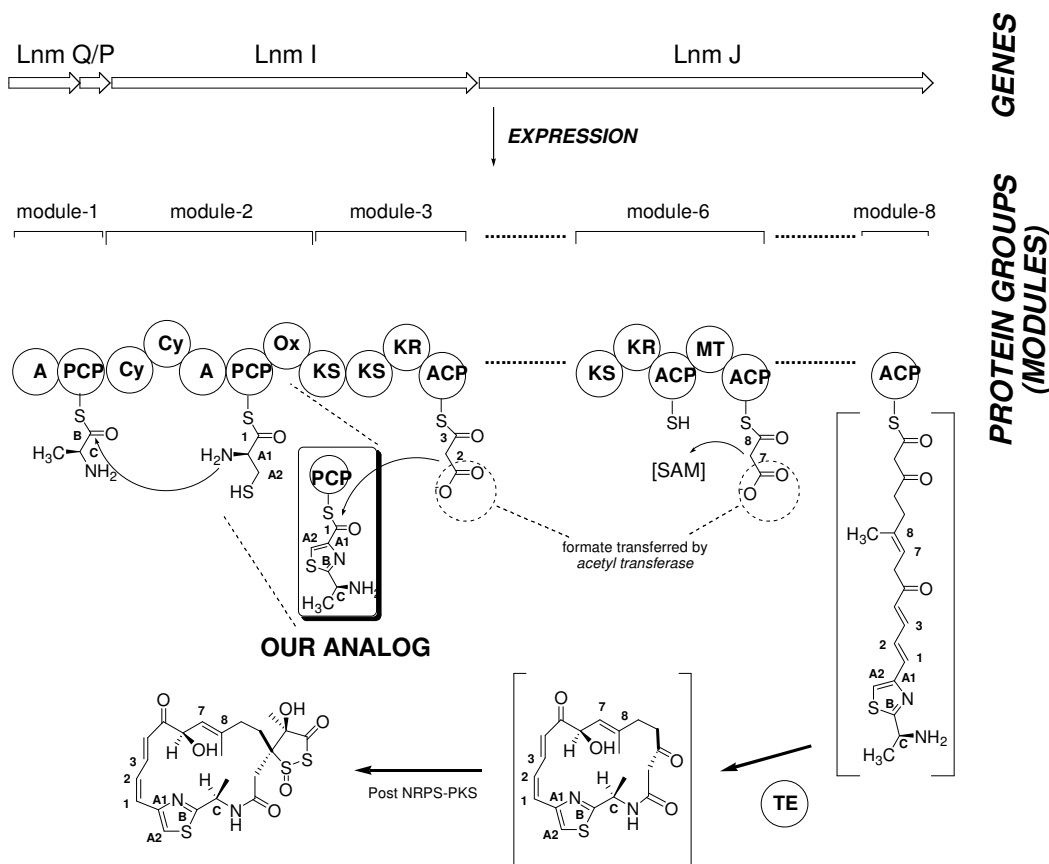
Scheme 22. Simplified hypothetical scheme for the biosynthesis of leinamycin (re-constructed with alterations from figure 1 in Yi-Qiang Cheng, Gong-Li Tang, and en Shen, PNAS, 100 (6), 2003. p.3149.). Abbreviations: **A**: adenilase, **PCP**: peptidyl carrier protein, **Cy**: cyclization, **Ox**: oxidase, **KS**: ketide synthase, **KR**: ketoreductase, **AC**: acyl carrier protein, **TE**: thioesterase, **SAM**: S-adenosyl-methionine

_____

5.2. Design of Precursors for the Biosynthesis of Leinamycin

In a broad view, preparation of natural product analogs via combinatorial biosynthesis may offer useful tools to prepare biologically active and medicinally useful agents. [4] Such attempts have been approached by either reconstructing the gene-clusters of natural product producing species or by replacing substrates of enzymes in a biosynthetic machinery with analogs recognizable as substrates by these enzymes. Here we hypothesize that in place of the PCP-conjugate of our target (**56** in module 2) other S-Nac species (**57, 59, 61, 63** Figure 93) might be applicable for the biosynthetic generation of leinamycin analogs.

To understand the role of the functional groups in leinamycin (**1**), their replacement with rationally designed functional groups can be useful. Drug development has also proven that the modification of natural products can yield agents which are biologically more potent than the original compound.[5] The synthesis of analogs can be achieved by means of total-synthesis or biosynthesis.

To prove that synthetic pre-cursors can be utilized by the biosynthetic machinery, we synthesized the natural substrate **56** of the enzyme system (module-3,Scheme 22). The research group of prof. Ben Shen (University of Wisconsin, Madison) has developed leinamycin producing strains with mutations which would allow the uptake of our synthetic substrate. In such mutants the biosynthesis of PCP-conjugate of **56** would be turned off.

We hypothesize that analogs of **56** might turn out to be useful for the biosynthesis of leinamycin analogs if they are accepted by the biosynthetic machinery (Figure 93). To

reveal the role of the aromatic thiazole ring in the activity of leinamycin its replacement with an aliphatic chain is suggested. For this, an aliphatic-S-NAc precursor (**57**) may be employed.[6] Additionally, extension of the aromatic surface area in place of the thiazole ring using rationally designed quinoline (**59, 61**)[7-9] or indole (**63**)[10-12] analogs would be taken into consideration.
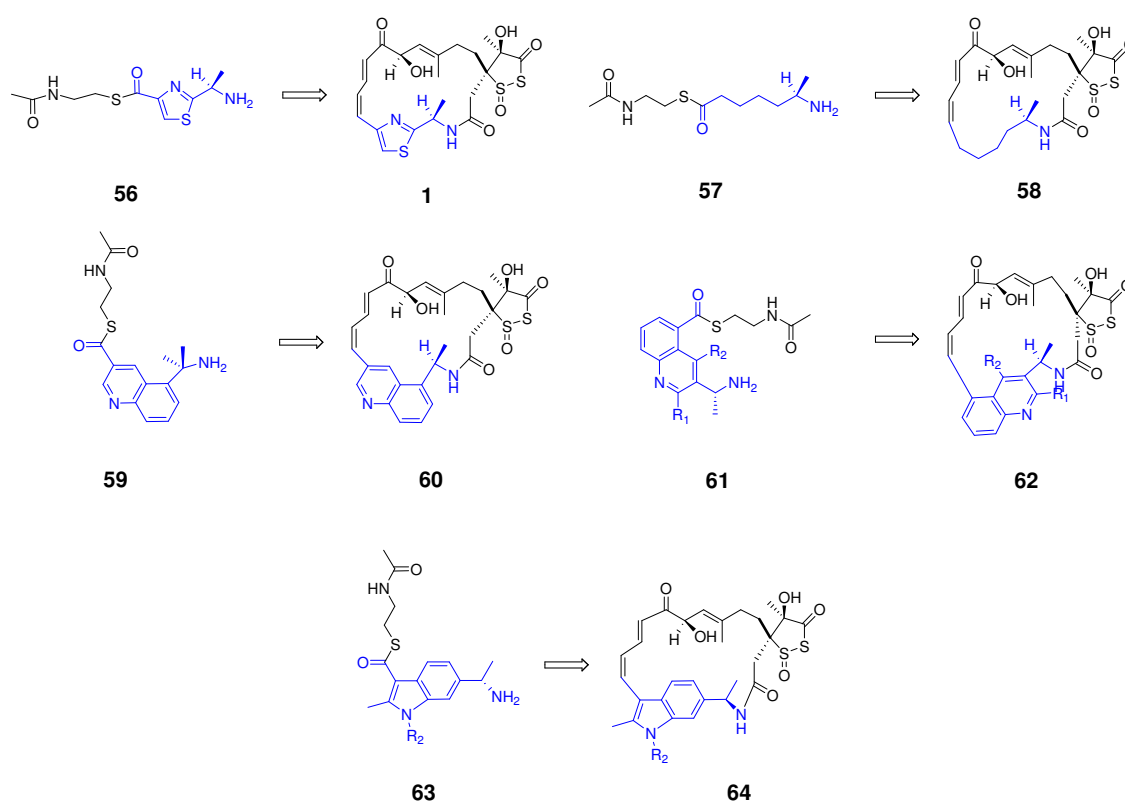
Figure 93. Design of S-Nac analogs as potential precursors for the biosynthesis of alternative leinamycin structures.

5.3. Synthesis of 2-*R*(1-Amino-ethyl)-thiazole-4-carbothioic acid S-(2-acetylamino-ethyl) ester

5.3.1. Retrosynthetic Analysis

The synthetic building blocks of our target molecule (**56**) are shown in Figure 94. Our laboratory has explored the synthesis of amino-thiazole carboxylic acid (**a**) analogs, [13] thereby it was sensible to build on the structure of **a**. The Thiol compound: N-acetyl cysteamide (**b**) is a commercially available molecule, and esterification of carboxylic acids under mild conditions has been reported exclusively with a variety of different reagents. [14-18] In addition, it is important to realize, amide formation between an aliphatic amine and acetic acid to provide building block **c** would have been a difficult and low yield process due to the potential simultaneous trans-esterification of the thioester. In conclusion, we planned to make the amino-thiazole carboxylic-acid and thioesterify it using S-acetyl cysteamide (Scheme 23, section 5.3.2.).
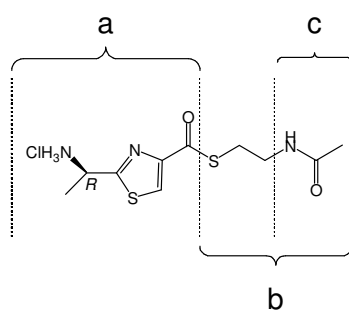
Figure 94. The building blocks of our target molecule (**56**). (**a**): amino-thiazole carboxylic acid, (**b**): N-acetyl cysteamide, (**c**): acetamide

_____
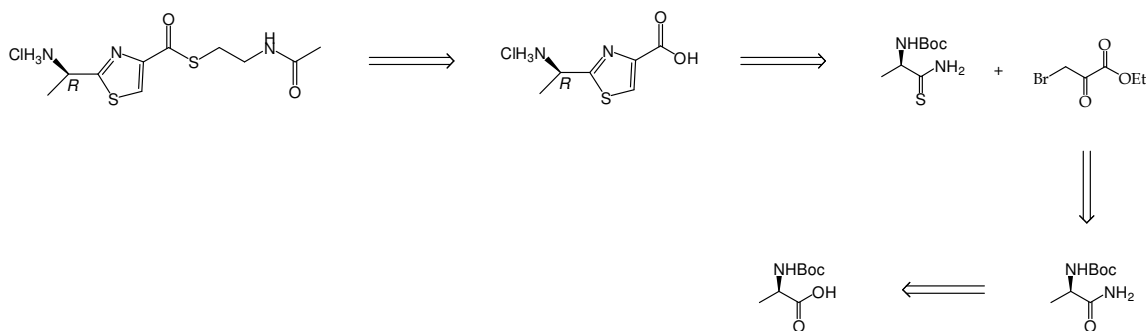
Scheme 23. Simplified retro-synthetic analysis of our synthesis.

5.3.2. Synthesis of biosynthetic precursor (56) and its metabolite (72)

In our synthesis (Scheme 24, below) we used steps from the work of Pattenden[19] and Fukuyama[20] for the construction of the leinamycin macrocycle. Our synthesis started from (*R*)-N-Boc alanine (**65**). The starting material was converted to an amide **66** (isobutyl chloroformate, *N*-methylmorpholine, then conc. NH₄OH) and then to a thioamide **67** (Lawesson's reagent, CH₂Cl₂, RT, 24 h). [21,22] This thioamide **67** was subjected to the modified Hantsch cyclization[23] using ethyl bromopyruvate to form the thiazole ring **68** (K₂CO₃; ethyl bromopyruvate, then TFAA and pyridine). At this point, earlier reports of applying low temperatures for the composition of the thiazole ring did not result in product formation. The resulting ester **68** was exposed to basic hydrolysis (Na, methanol), which after acidic workup results in an acid **69**.
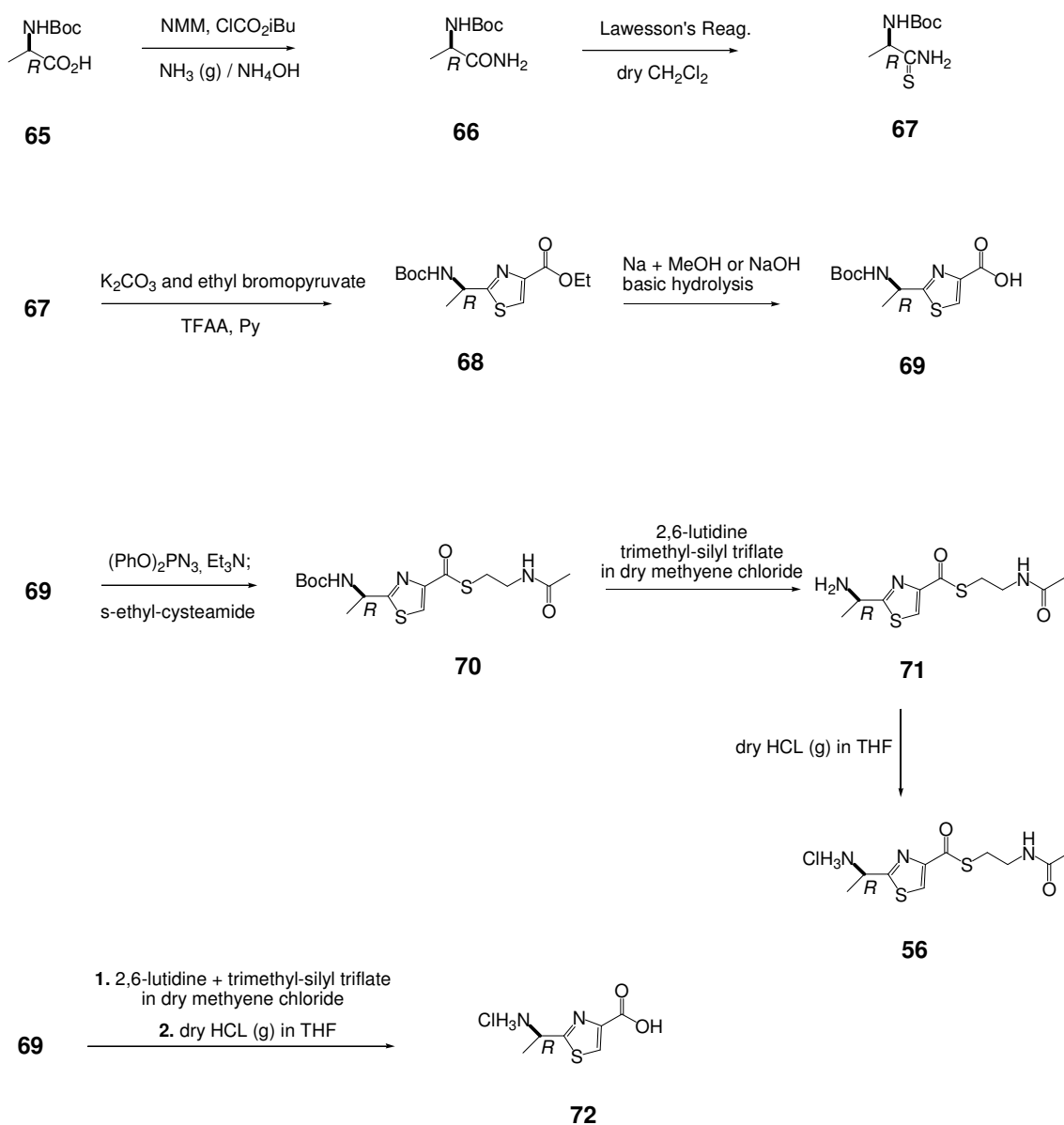
Scheme 24. The synthesis of our target molecule (precursor for the biosynthesis of leinamycin): *2-R(1-Amino-ethyl)-thiazole-4-carbothioic acid S-(2-acetylamino-ethyl) ester,* (**56***) and its in vitro degradation product (**72**)

This acid was (**69**) converted to the thioester of S-acetyl-cysteamide **70** (diphenyl phosphorylazide, triethyl-amine). Additionally, the thioesterification had been attempted with the use of isobutyl-chloroformate hydroxyl-activating agent, which resulted in impurities that co-eluted with the product and were not removable with recrystallization either.

For the deprotection of the exocyclic amine-nitrogen atom, we attempted a few different methods. Of these, in situ decarboxylation using mild oxygen silylating agent (trimethyl-silyl triflate) in the presence of a weak base (2,6-lutidine, pK_a of acid form: 5.0) proved to be useful. This reaction resulted in our amine-thiazole-cysteamide analog **71**. For purification of **71** we bubbled dry hydrogen-chloride gas into a THF solution of **71** and after trituration in diethyl-ether we obtained a highly pure HCl-form of our target (**56**).

Under in vitro/in vivo conditions **56** was noticed to degrade via hydrolysis of the labile thioester bond. To follow this process by HPLC, Prof. Ben Shen's group required an authentic standard of the degradation product (**72**), the exocyclic carboxylic-acid derivative. This molecule (**72**) was synthesized from **69** via deprotection of the exocyclic amine and precipitation of **72** in dry THF by HCl gas. The average yield of these synthetic steps were 70% and the overall yield of the 7-step-synthesis is 20%.

5.4. Results of Biosynthesis using our precursor (56)

The work outlined in this section have been carried out by the research group of Dr. Ben Shen, (Currently, Department of Chemistry, University of Wisconsin, Madison, WI 53705.). Dr. Ben Shen *et al.* developed reliable fermentation of leinamycin and its isolation and HPLC-detection from wild-type and mutant *S. atroolivaceus strains*. The

mutant strain has a dysfunctional protein up-stream from the adenilase (A) in module-2, with inhibited biosynthesis of the thiazol ring in leinamycin. Once **56** is transferred to the peptidyl carrier protein (PCP, module-2), hypothetically, it will be incorporated into the biosynthesized leinamycin molecule. **56** is the natural substrate for proteins in module-2 and module-3.

Our thiazole-SNAc analog (**56**) was fermented with LnmQ mutant which misses the ability to synthesize the thiazole ring. The detection of leinamycin from this ferment proved unsuccessful, presumably because of the low yield in the uptake of the analog by the cells, and apparently due to its hydrolysis in the broth. On the other hand in the presence of an LnmQ/LnmE mutant, the generation of a leinamycin analog (TG-25) in the cells was observed, which only can form if our thiazole-S-NAc analog is incorporated into the biosynthetic machinery. The detection of TG-25 is possible because it is more stable than leinamycin.

In conclusion the incorporation of our analog **56** was successful in the LnmQ/LnmE double mutant, which proves the principle of using synthetic substrates by the biosynthetic system. Further efforts are necessary to optimize fermentation times and broth conditions, as the degradation of **56** in the broth is probably responsible for the low yields of leinamycin in the presence of the LnmQ mutant.

5.5. Experimental

5.5.1. Materials and methods

Reagents were purchased from the following suppliers and were of the highest purity available: technical grade solvents (ethyl acetate, hexane, ether) and HPLC grade solvents (acetonitrile), Fisher; ethanol, McCormick Distilling company. All other reagents were purchased from Aldrich Chemical Company, except Lawesson's reagent, ethyl bromopyruvate (Lancaster). Water was distilled, deionized and glass redistilled. Thin layer chromatography was performed on silica gel plates (0.25) with F_{254} fluoropore (Aldrich) and visualization of compounds was achieved with UV light at 254 nm. Column chromatography was performed using 200-300 mesh silica gel (Merck) with technical grade solvents that were distilled prior to use. High resolution mass spectrometry was performed at the University of Missouri-Columbia Department of Chemistry Mass Spectrometry Center. Nuclear magnetic resonance spectra were recorded on Bruker 200 MHz or 250 MHz spectrometers. HPLC was performed on the Varian HPLC system equipped with single wavelength UV absorbance detector. pH measurements were performed with pH meter (Orion, model 420A). Dry CH_2Cl_2 was distilled from CH_2. THF was distilled from sodium benzophenone ketyl. Actonitrile and dichloromethane were distilled from CaH_2, and toluene was distilled from $LiAlH_4$. HPLC: Varian Prostar Dynamax, vs. 5.1. LC-MS: ThermoFinnigan TSQ7000 triple-quadrupole with API2 source.

5.5.2. Synthesis of our target molecule and its analogs

(1-Carbamoyl-ethyl)-carbamic acid tert-butyl ester, 66
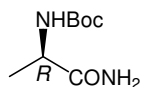
The synthesis of our target molecule (**56**) started from the commercially available R-N-Boc alanine (**65**). To 26 g of **65** (70 mmol, 1 equiv) in THF (90 mL) at 0 °C was added N-methylmorpholine (16 mls) (146 mmol, 2 equiv) and isobutyl-chloroformate (13 mls, 100 mmol, 1.4 equiv, dropwise). The reaction was stirred for 10 min, when concentrated ammonium-hydroxide solution (18.5 mL) was added to the system. The mixture was further stirred for 10-15 min. This solution was filtered at room temperature through a pad of Celite 545. The Celite pad was further washed by 50 mL of diethyl ether. The filtrate was concentrated under reduced pressure to approximately 15 mL volume. This concentrate was transferred into a 500 mL extraction funnel and brine (30 mL) was added to the filtrate followed by diethyl ether (100 mL). The organic layer was washed with saturated citric acid solution (pH 3.0) until the aqueous layer became weakly acidic (~ pH 4.0). System was further washed with brine (20 mL) and dried over K_2CO_3. The ether was evaporated on rotavap. The remaining powder was powdered and dried over high vacuo. This product (**66**) (23 g, 93%) was used without further purification. R_f (ethyl acetate:hexane 1:1 v/v%) = 0.2. ^{1}H-NMR: (500 MHz, $CDCl_3$): δ 6.1 (1H), 5.3 (1H), 4.9 (1H), 4.3 (1H), 1.45 (9H), 1.38 (d, J = 7 Hz, 3H).

_____

(1-Thiocarbamoyl-ethyl)-carbamic acid tert-butyl ester, 67
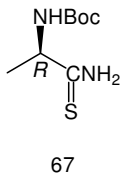
20.1 g of the amide **66** (106 mmol) was dissolved in THF (330 mL). In a separate flask, Lawesson's reagent (48 g, 120 mmol, 1.2 equiv) was dissolved in dry THF (500 mls). The solution of **66** was transferred to the solution of the Lawesson's reagent in 5 min. The reaction was stirred for 20-28 h at room temperature. The solution was filtered through a pad of Celite 545 and SiO_2 (2:1), and the pad was further washed with methylene-chloride (~ 500 mL). The organic layer was washed further with $NaHCO_3$ (3 x 250 mL). The sodium carbonate layer was re-extracted once with methylene-chloride (250 mL). This process resulted in a white solid **67** (18 g, 88% yield). R_f (ethyl acetate:hexane 1:1 v/v%) = 0.25. ^{1}H-NMR (250 MHz, CDCl$_3$): δ 7.9 (1H), 7.6 (1H), 5.4 (1H), 4.5 (1H), 1.47 (d, J = 7 Hz, 3H), 1.44 (s, 9H); ^{13}C-NMR (62.5 MHz, CDCl$_3$): δ 210.5, 155.6, 80.5, 28.3, 21.6.

2-(1-tert-Butoxycarbonylamino-ethyl)-thiazole-4-carboxylic acid ethyl ester, 68
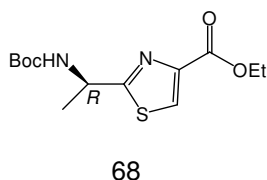
A heterogenous mixture of the thioamide **67** (4 g, 19.5 mmol) and powdered KHCO$_3$ (15.35 g, 8 equiv, 156 mmol) in DME (100 mL) was stirred vigorously in a 250 mL round bottom flask for 5-10 min at room temperature (*Note:* earlier reports from our lab applied lower temperatures, which did not result in the desired reaction). To this mixture ethyl-bromopyruvate was added (11.4 g, 58.5 mmol, 3 equiv, 7.6 mls). After stirring the mixture for 2 min at room temperature, the flask was immersed into a coolant at 0 °C with further stirring. In a separate flask a solution of trifluoroacetic anhydride (16.12 g, 76.8 mmol, 4 equiv, 10.8 mL) and pyridine (12.13 g, 154 mmol, 8 equiv, 12.4 mls) was

dissolved in DME (30 mL) and precooled to 0 °C. This pyridine solution was transferred

to the solution of **67** (above), which results in a yellow solution. After the transfer was

accomplished, the flask was allowed to equilibrate to room temperature on air. In the

meantime the yellow solution became orange, red and brownish gradually. After

approximately 3 h the volatile components were removed on rotatory evaporator and the

residue was resuspended in chloroform (300 mL) and extracted with water (2 x 100 mL).

The organic layer was further extracted with cc. $CuSO_4$ (2 x 30 mL) to chelate pyridine.

The remaining organic solution was washed with brine (100 mL) and dried over Na_2SO_4,

and purified via flash chromatography after filtration. (6:1 – 4:1 hexane:ethylacetate).

This resulted in a white solid **68** (4.2 g, 75%). R_f (ethylacetate:hexane 2:1 v/v%) = 0.75.

^{1}H-NMR (250 MHz, $CDCl_3$): δ 8.07 (s, 1H), 5.3 (1H), 5.09 (m, 1H), 4.4 (q, J = 7.2 Hz,

2H), 1.61 (d, J = 7 Hz, 3H), 1.43 (s, 9H), 1.38 (t, J = 7.2 Hz, 3H); ^{13}C-NMR (62.5 MHz,

$CDCl_3$): δ 174.8, 161.3, 154.8, 147.1, 127.0, 80.2, 61.3, 48.9, 28.2, 21.7.

2-(1-tert-Butoxycarbonylamino-ethyl)-thiazole-4-carboxylic acid, 69

69
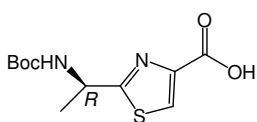
4.3 g of **68** (14.4 mmol) was dissolved in 100%-ethanol (65 mL).

The solution was cooled to 0°C. 400 mg sodium was added to

this mixture in small pieces (17.3 mmol, 1.3 equiv). After the

sodium dissolved, water (285 μL, 285 mg, 15.8 mmol, 1.2 equiv) was injected into the

flask. This solution was allowed to warm up to room temperature, and the starting

material gradually disappeared during the course of the following 6-12 h. After the

disappearance of the starting material the ethanol was evaporated on the rotavap and

water (400 μL) and cc. citric acid (80 mL, pH 3.0) were added. This system was extracted

with methylene chloride (3 x 600 mL). The organic phase was dried over Na_2SO_4 and evaporated under decreased pressure. This reaction yields in a yellowish foam **69** (4 g, 95%). Rf (ethyl acetate): 0-0.15 streaking. ^{1}H-NMR (250 MHz): δ 11.0 (bs, 1.3 H), 8.2 (s, 1H), 5.5 (bs, 0.5 H), 5.1 (bs, 1H), 1.63 (d, *J* = 7.5 Hz, 3H), 1.4 (s, 9H). ^{13}C-NMR (62.5 Hz, CDCl3): δ 176.8, 164.4, 146.3, 128.5, 81.5, 80.3, 48.8, 28.2, 20.9.

2-(1-tert-Butoxycarbonylamino-ethyl)-thiazole-4-carbothioic acid S-(2-acetylamino-ethyl) ester, 70

70
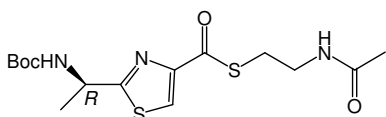
3.1 g of **69** (11.41 mmol, 1 equiv) was dissolved in DMF (60 mL) and treated with diphenyl-phosphorylazide (3.8 mL, 17.12 mmol, 1.5 equiv) and ethylamine (3.3 mL, 2 equiv, 22.82 mmol) at 0 °C. This reaction mixture was stirred at 0 °C for 2-3 h. In the meantime the reaction mixture gradually grew darker. Then, 2N-acetylcysteamide (2.6 mL, 22.9 mmol, 2 equiv) was added, and the mixture was allowed to reach room temperature on air. The mixture was further stirred for 2-3 h at room temperature. After this, water (100 mL) and ethyl acetate (400 mL) was added. The aqueous layer was further extracted with ethyl acetate (2 x 400 mL). The organic layer was dried with Na_2SO_4 and the solvent was removed by rotavap. The compound was purified by flash chromatography (gradient elution, 5:1 – 3:1 ethylacetate:hexane v/v%). (*Note:* this synthetic step was attempted with the use of isobutyl-chloroformate hydroxyl-activating agent. In that process impurities co-eluted with the product, and they could not be removed with recrystallization either.). This step results in a white powder **70** (2.6 g, 60% yield). Rf (ethylacetate:hexane, 2:1 v/v%): 0.3. ^{1}H-NMR (300 Mhz, CDCl3): δ 8.0

(s, 1H), 5.9 (bs, 1H), 5.1 (bs, 2H), 3.5 (t, J = 6 Hz, 2H), 3.2 (t, J = 6 Hz, 2H), 2.0 (s, 3H),

1.7 (d, J = 6 Hz, 3H), 1.5 (s, 9H). ^{13}C-NMR (62.5 Mhz, CDCl$_3$): δ 186.2, 170.1, 152.1,

123.3, 116.0, 106.0, 82.0, 48.8, 39.5, 28.3, 23.1, 21.3.

2-(1-Amino-ethyl)-thiazole-4-carbothioic acid S-(2-acetylamino-ethyl) ester, 71
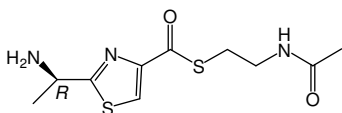
This reaction was run under inert athmosphere and the reagent and product are highly hygroscopic. 2.1 g of **70** (5.43 mmol) was dissolved in dry methylene chloride (120 mL). 5.8 g of lutidine-2,6 (6.4 mL, 55 mmol, 10 equiv) and trimethyl silyl triflate (6.05 g, 5 mL, 27.2 mmol, 5 equiv) and the reaction was stirred for the next approximately 6 h. Methylene chloride (50 mL) was added and solution was washed with NaHCO$_3$ (2 x 60 mL, pH 11.0). The organic layer was further washed with brine (60 mL). Crude was purified by flash column-chromatography (gradient elution: ethylacetate 100% to ethyl acetate:methanol 5:1 v/v%). This process results in a lime yellow powder **71** (1.2 g, 55% yield). Rf (ethylacetate:methanol, 5:1 v/v%): 0.25.

(*Note:* The removal of the Boc-group was attempted with the present method in the presence of TEA, a base that would be easier to remove from the crude. TEA at pH 9.0 does not give efficient cleavage. Lutidine works at pH 5.0. Attempts to deprotect the amino group in the presence of SiCl$_4$ and phenol failed.) ^{1}H-NMR (500 MHz, CDCl$_3$): δ 8.3 (1H), 7.3 (1H), 4.8 (q, J = 7.5 Hz, 1H), 3.3 (d, J = 7.5 Hz, 2H), 3.0 (d, J = 7.5 Hz, 2H), 1.8 (s, 3H), 1.6 (d, J = 7.5 Hz, 3H). ^{13}C-NMR (125 MHz, CDCl$_3$): δ 188.7, 175.1, 168.7, 152.2, 129.2, 127.4, 48.8, 39.2, 28.8, 22.6, 19.8.

2-(1-Amino-ethyl)-thiazole-4-carbothioic acid S-(2-acetylamino-ethyl) ester hydrochloride, 56
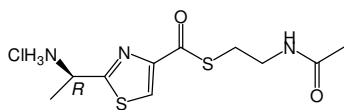
71 was dissolved in minimal amounts of THF at room temperature, and dry HCl gas was bubbled into the solution for the time course over 5-1 min. This hydrogen chloride gas was generated by dropping cc. H_2SO_4 over NaCl in a closed round bottom flask. The white precipitate was centrifuged in a benchtop centrifuge to compactness. The supernatant THF was removed, and the collected crystals washed with ether followed by ethyl-acetate and by hexane. In between each washing crystals were centrifuged to compactness. This treatment resulted in a quantitative transformation of **71** to **56** (lemon yellow powder , water soluble, 99% yield)**.** Water was removed by lyophilization. Lyophilized samples are highly hygroscopic, they need to be stored in sealed vials in the presence of drierite. ^{1}H-NMR (300 MHz, CDCl$_3$): δ: 8.4 (1H), 7.3 (1H), 4.9 (q, J = 6.5 Hz, 1H), 3.4 (t, *J* = 6.5 Hz, 2H), 3.2 (t, *J* = 6.5 Hz, 2H), 1.9 (s, 3H), 1.7 (d, *J* = 6.5 Hz, 3 H). ^{13}C-NMR (72.5 Mhz, CDCl$_3$): δ: 186.6, 173.6, 169.0, 153.4, 129.3, 126.7, 40.1, 29.0, 22.4, 20.9.

2-(1-Amino-ethyl)-thiazole-4-carboxylic acid-hydrochloride, 72
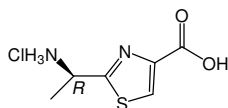
800 mgs of **69** (2.95 mmol) was dissolved in a mixture of 1 mL of cc. HCl + 3 mL of dioxane (4M to HCl). The solution was stirred for 6 h under nitrogen at room temperature. The solution was then removed by rotavap and toluene (30 mL) was added to the system and removed on the rotavap. Alternatively samples can be lyophilized to dryness. Solid was triturated from ether. This process resulted in a qualitative transformation (**72**, off white powder, 99% yield, water soluble). ^{1}H-NMR (500 Mhz, DMSO): δ 13.2 (bs, 1H), 8.8 (bs, 3H), 8.5 (s, 1H), 4.85 (q, *J* = 7.5 Hz, 1 H), 1.60 (d, J = 7.5 Hz, 3H). ^{13}C-NMR (125 Mhz, DMSO): δ 168.8, 163.8, 148.6, 130.7, 20.22.

_____

References

1.   Cheng, Y.-Q.; Tang, G.-L.; Shen, B., Type I polyketide synthase requiring a discrete acyltransferase for polyketide biosynthesis. *Proc. Natl. Acad. Sci. Unit. States. Am.* **2003,** 100, 3149-3154.

2.   Tang, G.-L.; Cheng, Y.-Q.; Shen, B., Leinamycin biosynthesis revealing unprecedented architectural complexity for a hybrid polyketide synthase and nonribosomal peptide synthetase. *Chem. Biol.* **2004,** 11, 33-45.

3.   Woodruff, H. B., Natural products from microorganisms. *Science* **1980,** 208, 1225-9.

4.   Walsh, C. T., Combinatorial biosynthesis of antibiotics: Challenges and opportunities. *ChemBioChem* **2002,** 3, 124-134.

5.   Thies, P. W., The modification of natural substances in modern drug synthesis. *New Nat. Prod. Plant Drugs Pharmacol., Biol. Ther. Act., Proc. Int. Congr., 1st* **1977**, 266-83.

6.   Maerki, H. P.; Crameri, Y.; Eigenmann, R.; Krasso, A.; Ramuz, H.; Bernauer, K.; Goodman, M.; Melmon, K. L., Optically pure isoproterenol analogs with side chains containing an amide bond. Synthesis and biological properties. *Helv. Chim. Acta.* **1988,** 71, 320-36.

7.   Pal, B.; Jaisankar, P.; Giri, V. S., Versatile reagent for reduction of azides to amines. *Synthetic Comm.* **2004,** 34, 1317-1323.

8.   Cho, C. S.; Kim, T. K.; Kim, T.-J.; Shim, S. C.; Yoon, N. S., Ruthenium-catalyzed synthesis of quinolines via reductive heteroannulation of nitroarenes with 3-amino-1-propanols. *J. Heterocycl. Chem.* **2002,** 39, 291-294.

9.   Reddy, G. V. S.; Rao, G. V.; Subramanyam, R. V. K.; Iyengar, D. S., A new novel and practical one pot methodology for conversion of alcohols to amines. *Synthetic Comm.* **2000,** 30, 2233-2237.

10.   Mukhanova, T. I.; Panisheva, E. K.; Lyubchanskaya, V. M.; Alekseeva, L. M.; Sheinker, Y. N.; Granik, V. G., b-(2-Benzofuranyl)enamines and (2-indolyl)enamines in the Nenitzescu reaction. *Tetrahedron* **1997,** 53, 177-184.

11.   Ketcha, D. M.; Wilson, L. J.; Portlock, D. E., The solid-phase Nenitzescu indole synthesis. *Tetrahedron Lett.* **2000,** 41, 6253-6257.

12.   Coscia, A. T.; Dickerman, S. C., Synthesis of pyrido[4,3-b]quinoline (2,10-diazaanthracene) and related compounds. *J. Am. Chem. Soc.* **1959,** 81, 3098-3100.

13.   Breydo, L.; Zang, H.; Gates, K. S., Synthesis and noncovalent DNA-binding properties of thiazole derivatives related to leinamycin. *Tetrahedron Lett.* **2004,** 45, 5711-5716.

14.   Wang, S. S.; Tam, J. P.; Wang, B. S. H.; Merrifield, R. B., Enhancement of peptide coupling reactions by 4-dimethylaminopyridine. *Int. J. Pept. Protein. Res.* **1981,** 18, 459-67.

15.   Kahns, A. H.; Buur, A.; Bundgaard, H., Prodrugs of peptides. 18. Synthesis and evaluation of various esters of desmopressin (dDAVP). *Pharmaceut. Res.* **1993,** 10, 68-74.

16.   Hays, S. J.; Novak, P. M.; Ortwine, D. F.; Bigge, C. F.; Colbry, N. L.; Johnson, G.; Lescosky, L. J.; Malone, T. C.; Michael, A.; et al., Synthesis and pharmacological evaluation of hexahydrofluorenamines as noncompetitive antagonists at the N-methyl-D-aspartate receptor. *J. Med. Chem.* **1993,** 36, 654-70.

17.   Mylari, B. L.; Beyer, T. A.; Siegel, T. W., A highly specific aldose reductase inhibitor, ethyl 1-benzyl-3-hydroxy-2(5H)-oxopyrrole-4-carboxylate and its congeners. *J. Med. Chem.* **1991,** 34, 1011-18.

18.   Lilo, B.; Moreau, M.; Bouchu, D., Synthesis and configurational assignment of bicyclic preactivated analogs of cyclophosphamide. *Tetrahedron Lett.* **1990,** 31, 887-90.

19.   Pattenden, G.; Thom, S. M., Polyene macrolactam construction using a Stille vinyl-vinyl coupling protocol: an approach to the antitumor antibiotic substance leinamycin. *Synlett* **1993,** 3, 215-216.

20.   Kanda, Y.; Fukuyama, T., Total synthesis of (+)-leinamycin. *J. Am. Chem. Soc.* **1993,** 115, 8451-2.

21.   Pedersen, B. S.; Scheibye, S.; Nilsson, N. H.; Lawesson, S. O., Studies on organophosphorus compounds. XX. Syntheses of thioketones. *Bull. Soc. Chim. Belg.* **1978,** 87, 223-228.

22.   Pedersen, B. S.; Scheibye, S.; Clausen, K.; Lawesson, S. O., Studies on organophosphorus compounds. XXII. The dimer of p-methoxyphenylthionophosphine sulfide as thiation reagent. A new route to O-substituted thioesters and dithioesters. *Bull. Soc. Chim. Belg.* **1978,** 87, 293-297.

23.   Bredenkamp, M. W.; Holzapfel, C. W.; Van Zyl, W. J., The chiral synthesis of thiazole amino acid enantiomers. *Synthetic Comm.* **1990,** 20, 2235-2249.
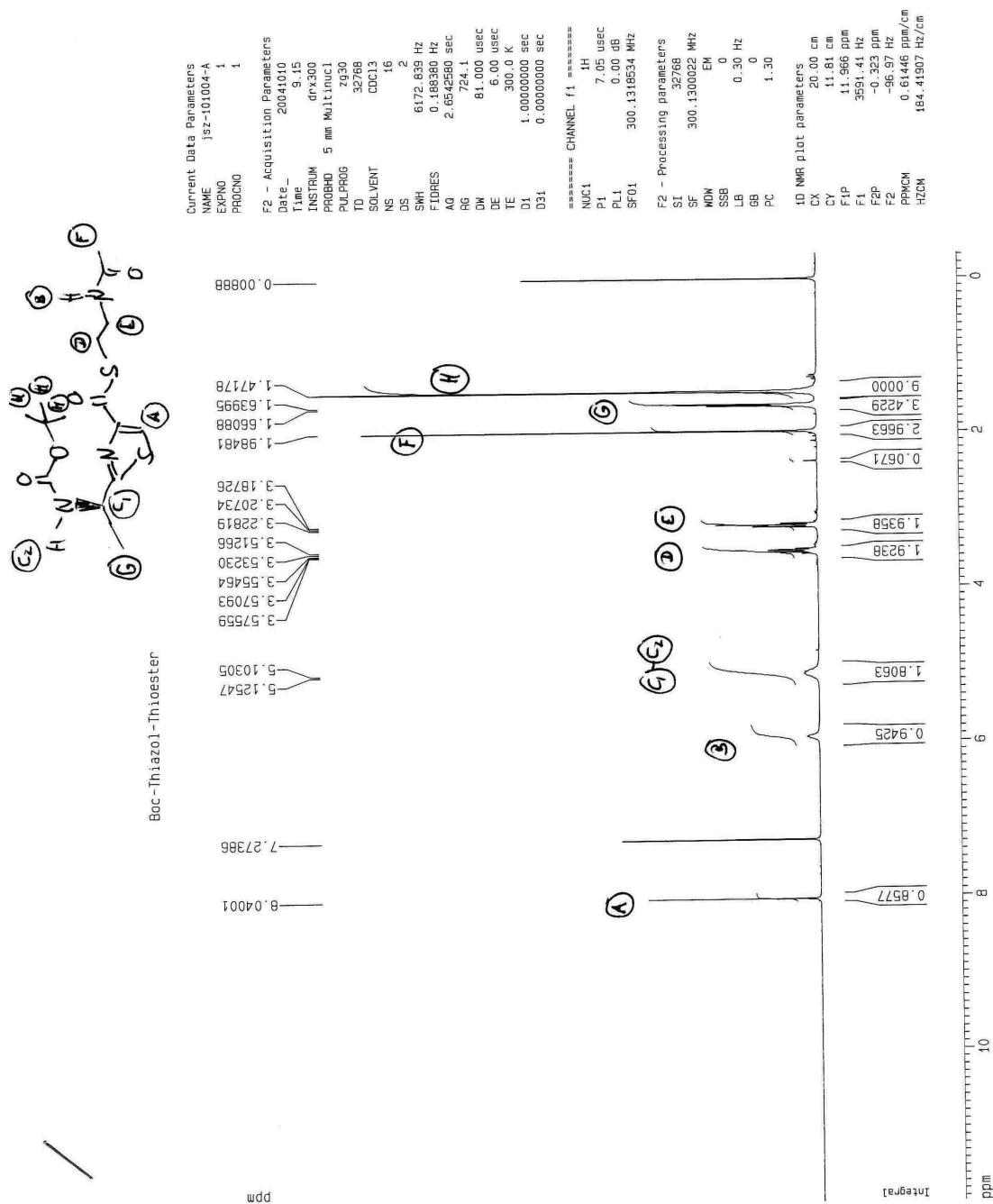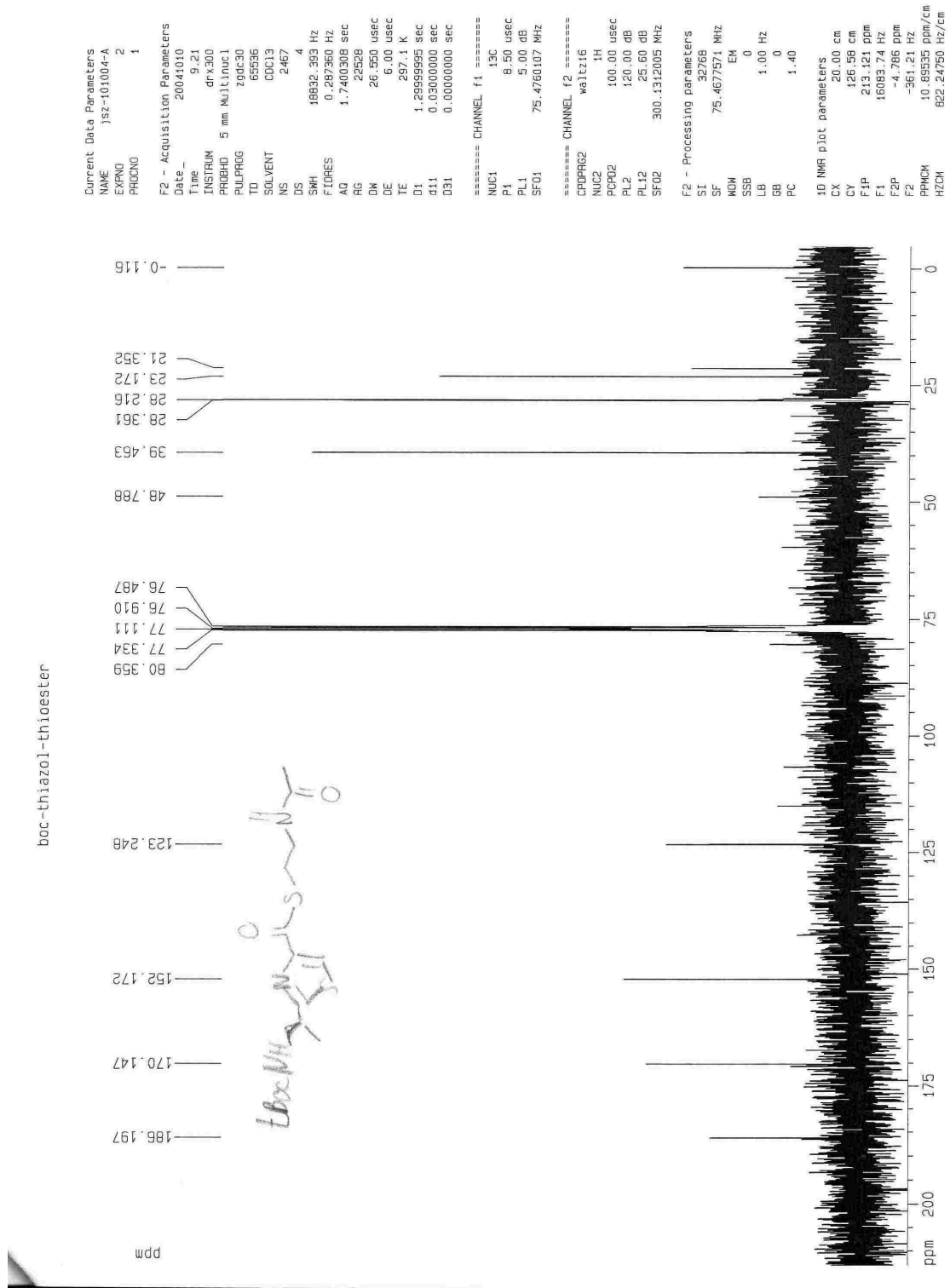
Boc-Thiazol-Thioester

boc-thiazol-thioester

13C dept135: CH and CH3 up, CH2 down
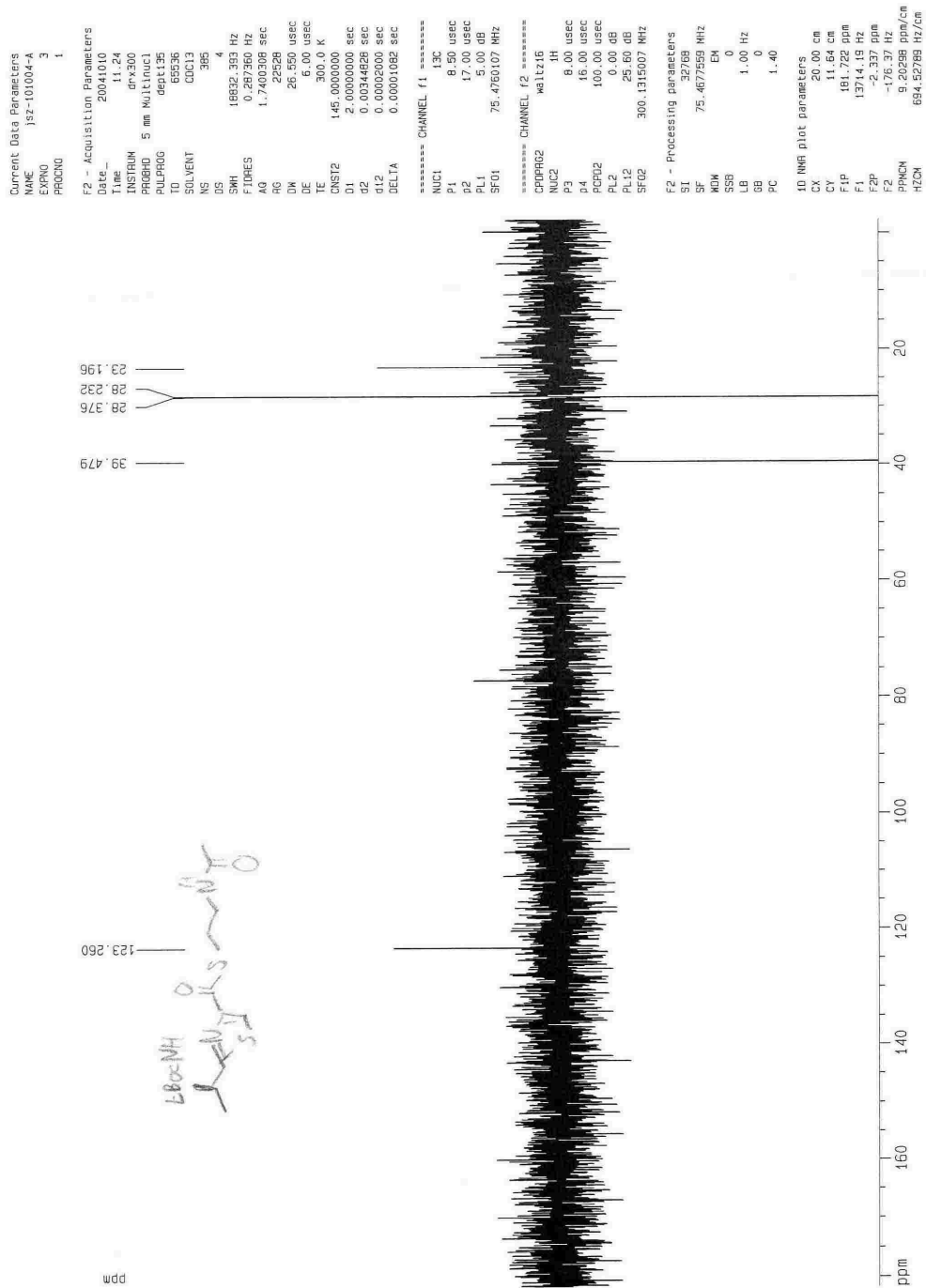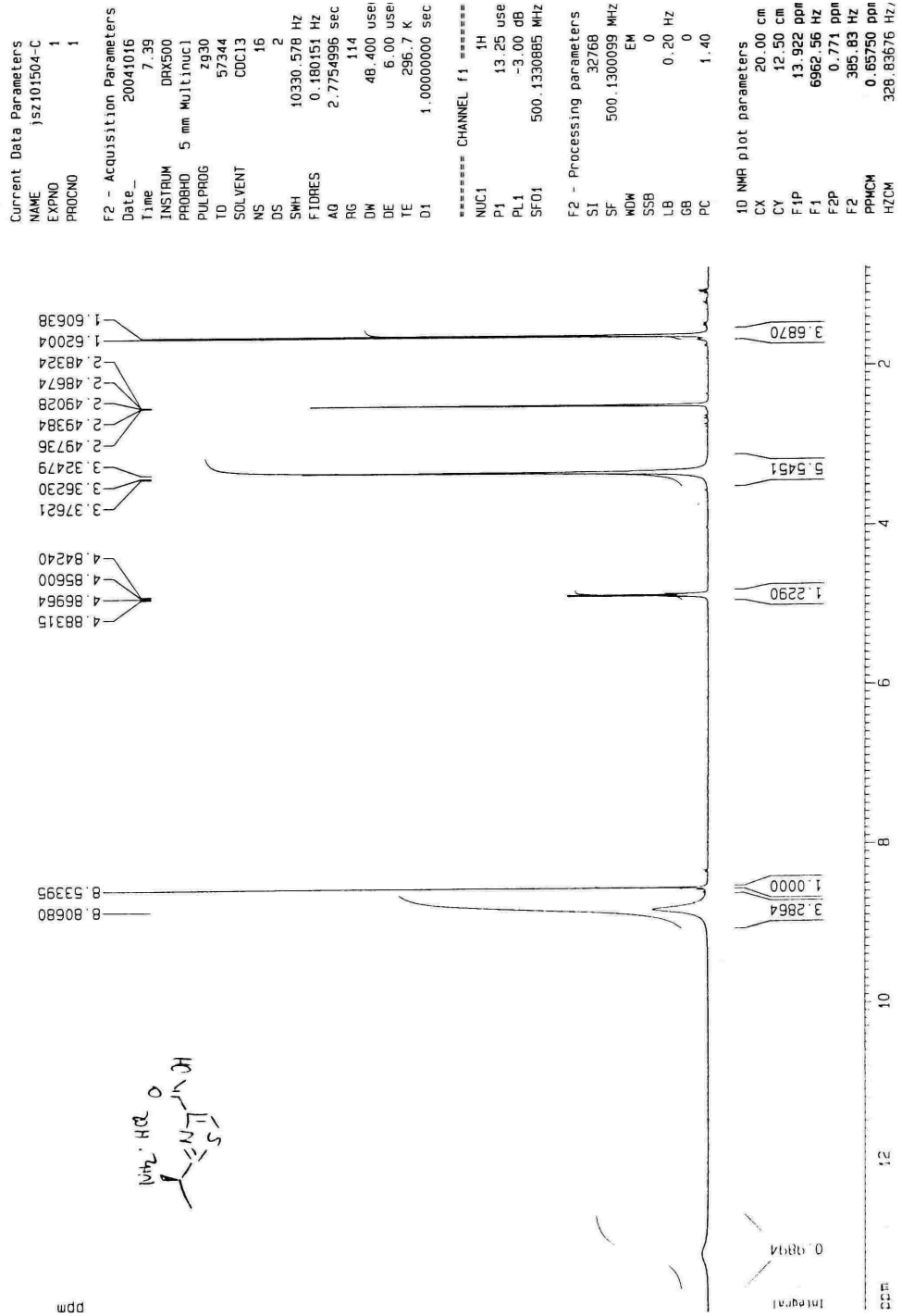
Amino-Acid HCl
Methanol-d4

Current Data Parameters
NAME   js2101504-B
EXPNO   2
PROCNO   1

F2 - Acquisition Parameters
Date_   20041015
Time   20.20
INSTRUM   DRX500
PROBHD   5 mm Multinucl
PULPROG   zgdc30
TD   65536
SOLVENT   CDC13
NS   13758
DS   4
SWH   39681.812 Hz
FIDRES   0.605496 Hz
AQ   0.8258188 sec
RG   16384
DW   12.600 usec
DE   6.00 usec
TE   298.0 K
D1   2.00000000 sec
d11   0.03000000 sec

======== CHANNEL f1 ========
NUC1   13C
P1   8.10 usec
PL1   3.00 dB
SFO1   125.7713108 MHz

======== CHANNEL f2 ========
CPDPRG2   waltz16
NUC2   1H
PCPD2   88.00 usec
PL2   0.00 dB
PL12   21.00 dB
SFO2   500.1320005 MHz

F2 - Processing parameters
SI   32768
SF   125.7576151 MHz
WDW   EM
SSB   0
LB   1.00 Hz
GB   0
PC   1.40

1D NMR plot parameters
CX   20.00 cm
CY   595.71 cm
F1P   251.083 ppm
F1   31575.59 Hz
F2P   11.980 ppm
F2   1506.63 Hz
PPMCM   11.95513 ppm/cm
HZCM   1503.44849 Hz/cm
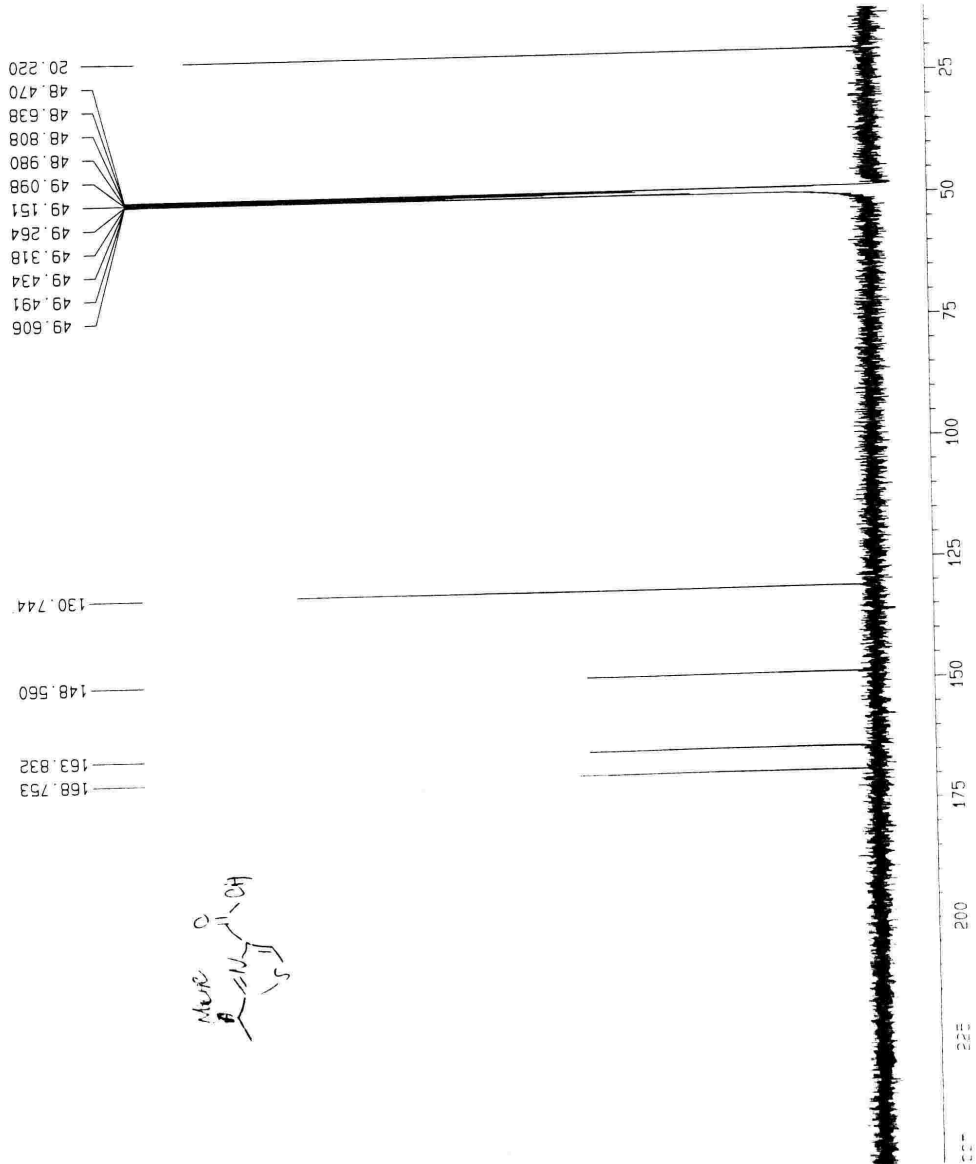
20.220
48.470
48.638
48.808
48.980
49.098
49.151
49.264
49.318
49.434
49.491
49.606

130.744

148.560

163.832
168.753

DEPT135-CH AND CH3 UP
Amino-Acid HCl
DMSO
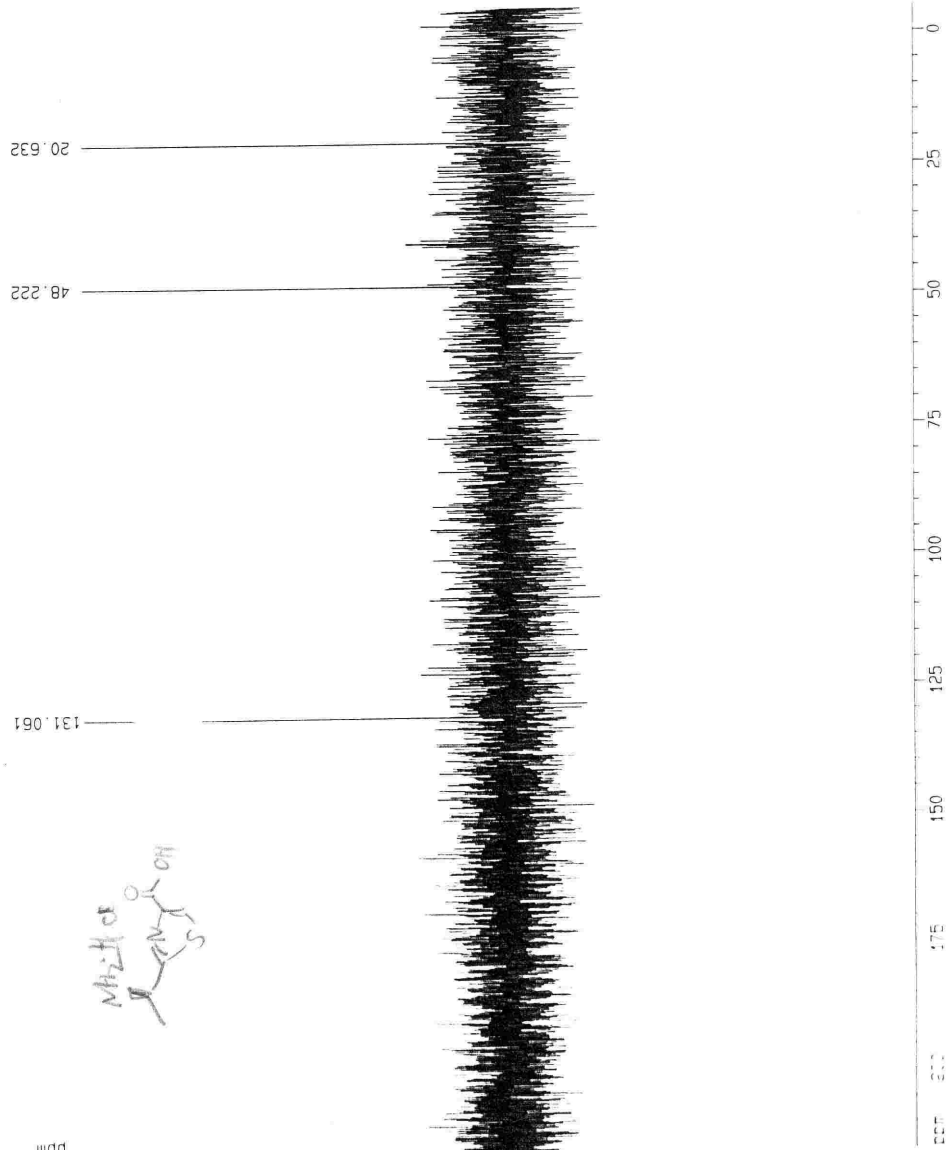
Current Data Parameters
NAME   lsz101504-C
EXPNO   3
PROCNO   1

F2 - Acquisition Parameters
Date_   20041016
Time   8.28
INSTRUM   DRX500
PROBHD   5 mm Multinucl
PULPROG   dept135
TD   65536
SOLVENT   CDCl3
NS   259
DS   4
SWH   39682.539 Hz
FIDRES   0.605507 Hz
AQ   0.8258036 sec
RG   16384
DW   12.600 usec
DE   6.00 usec
TE   300.0 K
CNST2   145.0000000
D1   2.00000000 sec
d2   0.00344828 sec
d12   0.00002000 sec
DELTA   0.00001031 sec

======== CHANNEL f1 ========
NUC1   13C
P1   8.10 usec
p2   16.20 usec
PL1   3.00 dB
SFO1   125.7713108 MHz

======== CHANNEL f2 ========
CPDPRG2   waltz16
NUC2   1H
P3   10.40 usec
p4   20.80 usec
PCPD2   88.00 usec
PL2   0.00 dB
PL12   21.00 dB
SFO2   500.1320005 MHz

F2 - Processing parameters
SI   32768
SF   125.7577390 MHz
WDW   EM
SSB   0
LB   1.00 Hz
GB   0
PC   1.40

1D NMR plot parameters
CX   20.00 cm
CY   10.98 cm
F1P   215.000 ppm
F1   27037.92 Hz
F2P   -5.000 ppm
F2   -628.79 Hz
PPMCM   11.00000 ppm/cm
HZCM   1383.33508 Hz/cm

20.632

48.222

131.061

Amino-thiazol-SNAC
After Liophilisation
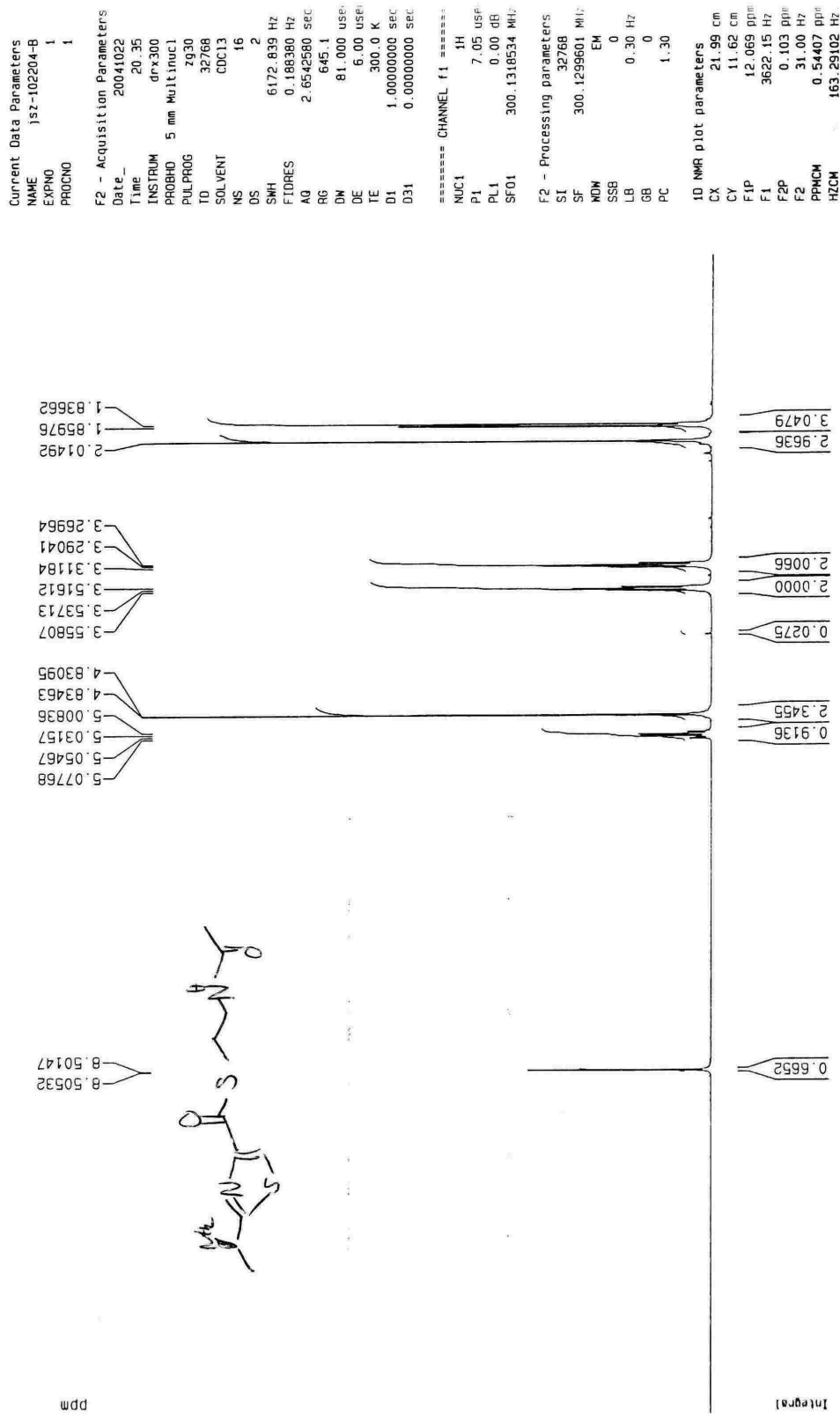
Current Data Parameters
NAME   jsz-102004-A
EXPNO   1
PROCNO   1

F2 - Acquisition Parameters
Date_   20041021
Time   19.24
INSTRUM   drx300
PROBHD   5 mm Multinucl
PULPROG   zg30
TD   32768
SOLVENT   CDCl3
NS   16
DS   2
SWH   6172.839 Hz
FIDRES   0.188380 Hz
AQ   2.6542580 sec
RG   512
DW   81.000 usec
DE   6.00 usec
TE   300.0 K
D1   1.00000000 sec
D31   0.00000000 sec

======== CHANNEL f1 ========
NUC1   1H
P1   7.05 usec
PL1   0.00 dB
SF01   300.1318534 MHz

F2 - Processing parameters
SI   32768
SF   300.1300078 MHz
WDW   EM
SSB   0
LB   0.30 Hz
GB   0
PC   1.30

1D NMR plot parameters
CX   20.00 cm
CY   12.50 cm
F1P   12.111 ppm
F1   3634.90 Hz
F2P   0.989 ppm
F2   296.87 Hz
PPMCM   0.55610 ppm/cm
HZCM   166.90149 Hz/cm

Peak labels (left axis):
1.74460
1.76756
1.93576
3.15252
3.17513
3.19748
3.28944
3.29492
3.30041
3.30579
3.31124
3.33923
3.40532
3.42768
3.45014
4.85620
4.92031
4.94327
7.31990
8.44011

Integral labels:
2.9688
3.0000
1.9491
0.5689
2.0151
1.0833
0.7084
0.8348

ppm

Integral
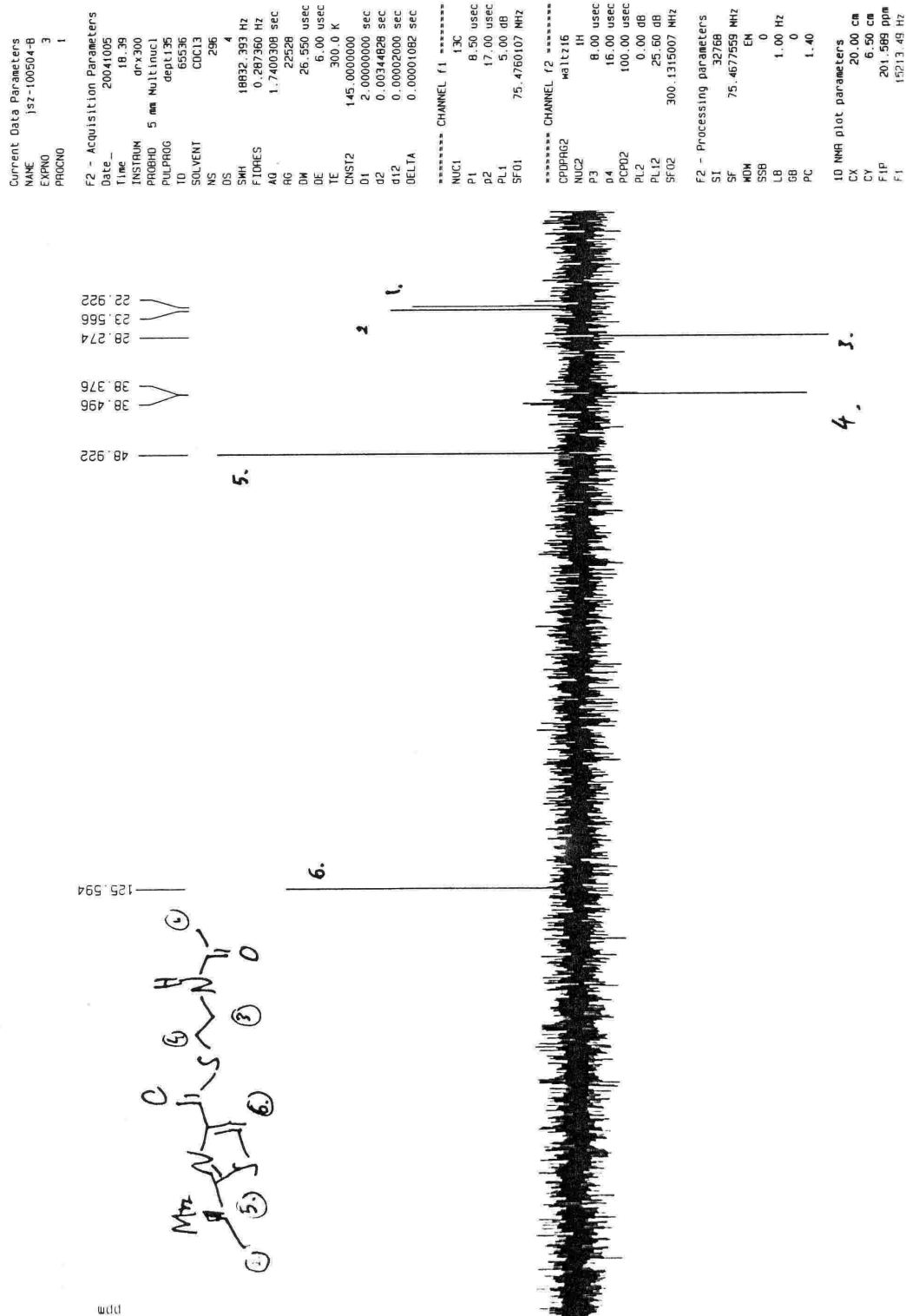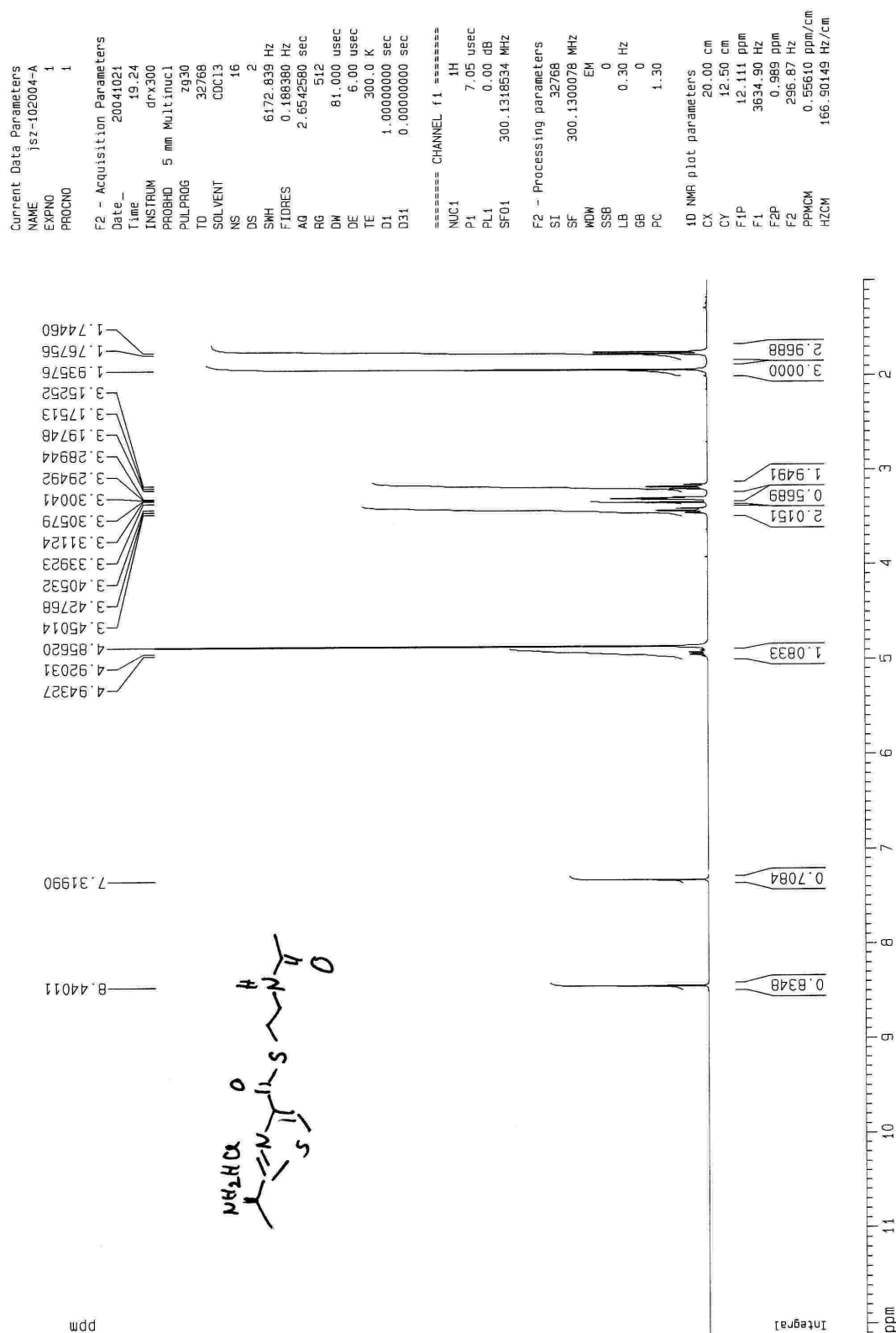
Chapter 6. Noncovalent DNA Binding and Oxidative DNA Damage by the Endogenous Mutagen: Fecapentaene-12

6.1. Discovery of Fecapentaenes and Introduction to their Biological Activity

Fecapentaenes (Figure 95) are a class of mutagenic polyunsaturated lipids that are produced endogenously in the human gastrointestinal tract. These compounds were discovered in etheral extracts of human feces in the late 1970's. [1-3] Since the amount of fecal mutagens were found to correlate with increased risks of colon cancer, [4] investigations began to find the responsible components. A wide variety of compounds were found to lend mutagenicity to human feces[3] like the heterocyclic aromatic amines, polycyclic aromatic hydrocarbons, N-nitroso compounds, fecal-steroids and the fecapentaenes. In works of Bruce and Kingston, direct acting mutagenic activity was soon correlated to acid and light sensitive compounds with a polyunsaturated hydrocarbon chain attached to a glycerol moiety, the fecapentaenes (**73, 74**).[5,6] Of these, the most abundant species is that of fecapentaene-12 (**73**). It is interesting to note that these molecules can be found only in samples from people on a non-vegetarian diet, but not in that of people on vegetarian eating.[4]

73   **74**
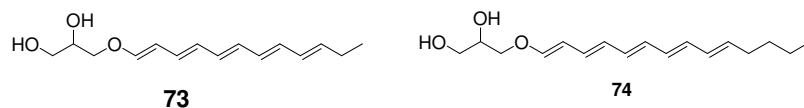
Figure 95. The structure of fecapentaenes, fecapentaene-12 (**73**) and fecapentaene-14 (**74**).

The biological activity of these compounds shows a wide scope of deleterious reactions both *in vivo* and *in vitro*. [7] Fecapentaenes are mutagenic in *S. typhimurium* strain TA 98 (a frameshift sensitive mutant) and TA 100 (a base pair substitution sensitive mutant) at micromolar concentrations.[8] Human fibroblasts grown *in vitro* exposed to 1-20 μM fecapentaene-12 for 1-3 h produced DNA single-strand breaks and DNA-DNA crosslinks. In human lymphocytes, a dose-response relationship between FP-12 exposure and DNA damage was established. [9] Finally, comparing the genotoxic potential of fecapentaenes and that of other direct acting mutagens (*N*-methyl-*N*-nitrosourea and formaldehyde) showed an average of 900-fold higher mutagenic activity of the fecapentaenes.[10]

Since DNA is a known biological target of these compounds, the nature of the DNA-damage processes underlying their potent mutagenic properties are of interest. The chemical mechanisms by which this occurs have been the subject of debates. [3,7,11-15] It has been shown that a decrease in the number of double-bonds results in diminished mutagenicity, which implies the importance of the conjugated π-bond system in the generation of mutagenic responses [16] either via DNA-alkylation or oxidative DNA damage (Figure 97).

Fecapentaenes were suspected to damage DNA via the alkylation of DNA bases directly by the electrophilic parent compound[17] or its aldehyde degradation products.[18] Once **73** was noticed to induce 2'-deoxy-7,8-dihydro-8-oxoguanosine (8-oxodG, Figure 96) in calf thymus and rat liver DNA, the involvement of reactive oxygen species was suspected behind its DNA-damaging potentials.

The generation of superoxide radical ($O_2^{\cdot-}$) by micromolar concentrations of fecapentaene-12 was shown to necessitate the actions of enzymatic peroxidation systems and the generation of singlet-oxygen was also suggested in the same report. [14] However, experiments to provide direct molecular analysis of the mechanism of DNA-damage and the direct generation of ROS without the involvement of cellular enzymes have not been performed yet.
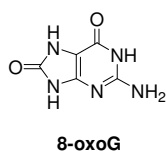
8-oxoG

Figure 96. 2'-deoxy-7,8-dihydro-8-oxoguanosine (8-oxodG) as an indicator of ROS in the DNA damaging reactions of fecapentaenes

Figure 97. Review of potential DNA damage mechanisms by fecapentaene-12.
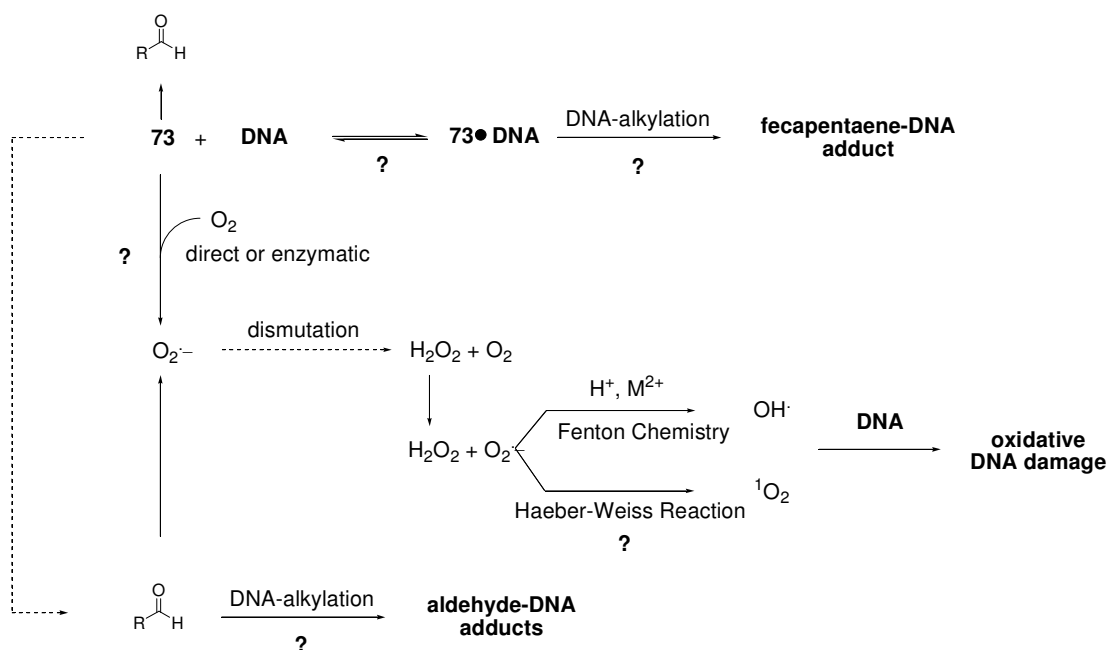
6.2. Rationale in Studying These Molecules

Difficulties in handling the fecapentaenes due to their intrinsic lability have been reported, [18-20] but a qualitative understanding of their stability under well-defined conditions has not been attained. We measured the stability of fecapentaene-12 under various conditions to develop storage conditions and conditions for our biochemical assays.

The role of reactive oxygen species (ROS) were clear in the DNA damaging potential of these molecules[14] however, nobody questioned the necessity of peroxidase enzymes in the DNA-damaging reactions of FP-12.[14] In addition, the role of singlet-oxygen or superoxide radicals in the direct oxidative DNA damage has not been elaborated. We carried out plasmid DNA based assays to study the mechanism of direct oxidative DNA damage by synthetic fecapentaene-12.

We also investigated the ability of **73** to associate with duplex DNA noncovalently. This is important because it is known that the DNA-damaging potential of agents that generate reactive oxygen species can be enhanced by noncovalent association with duplex DNA.[21] The grooves of the double helix are hydrophobic, [22-25] and there are indications that long-chain hydrocarbons can associate the duplex DNA noncovalently.

Aware of the electrophilic properties of **73** and of reports suggesting its degradation to aldehydes under physiological conditions, [13,18] we attempted to find covalent DNA adducts formed under a variety of conditions (Section 6.10.).

The identification of the degradation products of fecapentaene-12 is in progress during the completion of this thesis.

6.3. Overview of the Synthesis of Fecapentaene-12 (73)

We prepared compound **73** via the eight step synthetic route (Scheme 25 and Scheme 26) devised by Nicolaou and coworkers, [26,27] with one minor modification. We employed the tert-butyl dimethylsilyl groups to protect the alcohol moieties rather than the tert-butyl diphenylsilyl groups used previously. This approach decreased the reaction time required for the final deprotection step, thus minimizing degradation of the unstable product (Scheme 27).
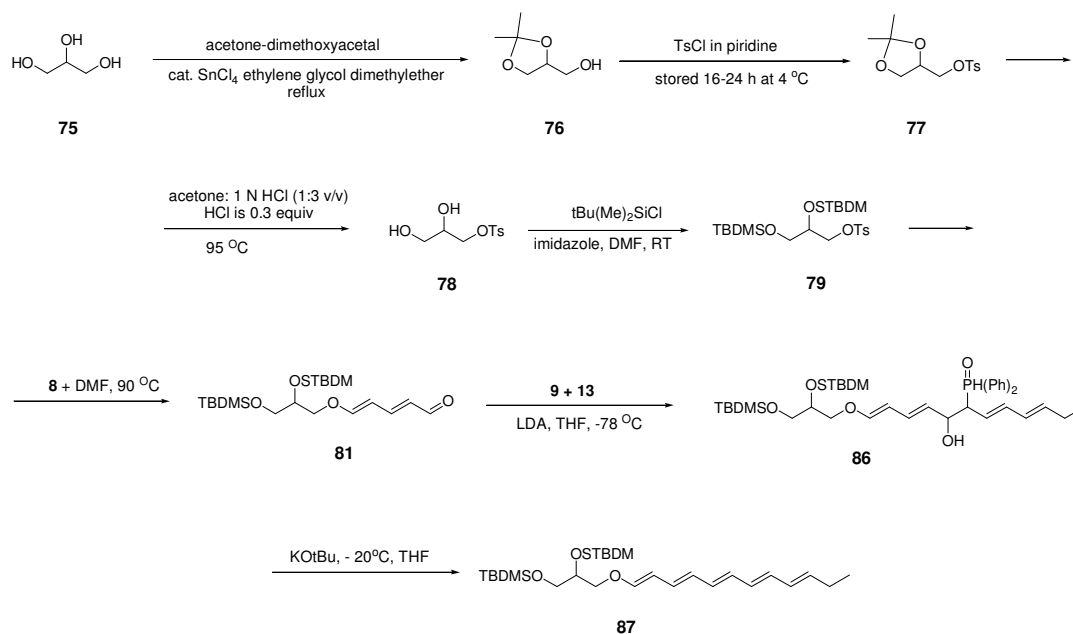
Scheme 25. The total synthesis of fecapentaene-12(**73**) as designed by Nicolaou et al.

We started our synthesis from the commercially available glycerol (**75**) and protected two of its adjacent hydroxyl groups selectively to form **76** (acetone-dimethoxyacetal). This allowed us to activate the terminal OH-group selectively (tosyl-chloride, pyridine), which gave us 1,2-O-acetonide-3-(R/S)-tosyl-glycerol (**77**). The acetal compound was hydrolyzed (acetone, HCl, reflux) to yield (S/R)-3-tosyloxi-

propanediol (**78**), and the free hydroxyl groups were again protected with *tert*-butyl

dimethylsilyl chloride to get 1,2-O-(t-butyl-dimethylsilyl)-3-O-tosyl-(S/R)-glycerol (**79**).

The terminal tosyl function of this molecule was substituted by potassium-glutaconate

(**80**) that had been prepared in a separate effort from the commercially available sulfur-

trioxide piridinium complex (Scheme 26). This substitution (in DMF, 90 °C) results in an

aldehyde **81**. The hydrocarbon chain of this aldehyde (**81**) was extended in a Horner-

Wittig reaction, using hepta-(*2E,4E*)-dienyl diphenyl-phosphineoxide (**85**). The

phosphineoxide compound **85** had been prepared in a four step route from the

commercially available heptadienal (Scheme 26).

Synthesis of **80**
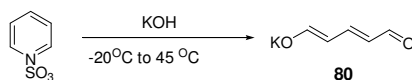
Synthesis of **85**
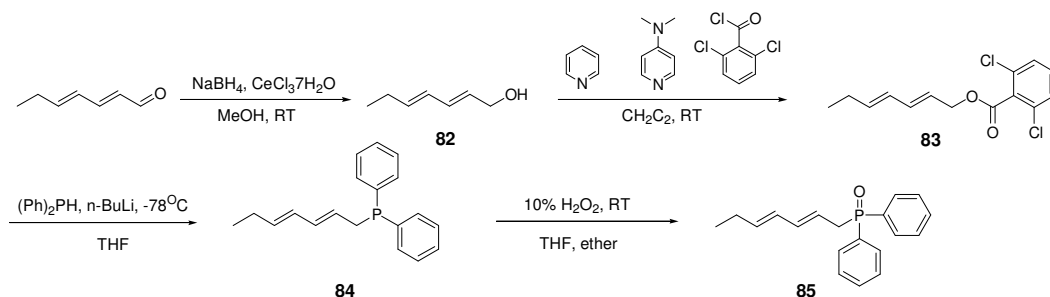
Scheme 26. Synthesis of intermediate synthons **80** and **85**.

The result of the extended chain product was an adduct (**86**) with isolated butadiene

systems. The Horner-Wittig reaction was accomplished via an elimination reaction from

86 (KOtBu, -20 °C, THF) yielding the protected fecapentaene-12 (**87**). The deprotection

was carried out by TBAF, which yields the target compound fecapentaene-12 (**73,** Scheme 27).
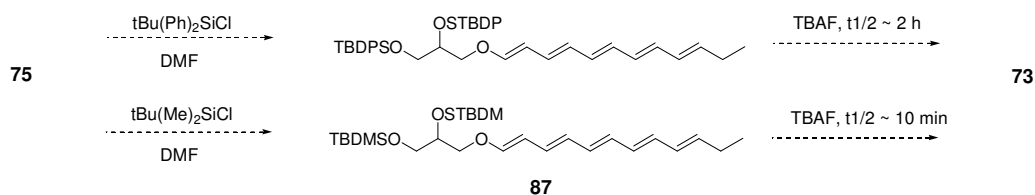
Scheme 27. Our modification in the synthesis of fecapentaene-12 (**73**). We applied tert-butyl dimethylsilyl protection instead of the tert-butyl diphenylsilyl protecting group to decrease deprotection time.

6.4. Quantitative Stability of Fecapentaene-12 in Organic and Aqueous media

The rapid degradation of pure fecapentaene-12 was reported [27] after its first synthesis and was observed in early carcinogenicity studies, too. [19] Confusingly, **73** showed variable decomposition rates in replicate experiments and it was generally accepted that biological assays are hampered due to the compound's apparent instability. [20] The stability of fecapentaene-12 has not been measured yet under well-defined conditions. The purity of our material in our assays and its fate during our experiments are equally important, since we wanted to identify the exact molecular species (*all-trans*-fecapentaene-12, fecapentaene-12 isomers, and degradation products) responsible for the observed DNA damaging Chemistry.

First, we wanted to develop storage conditions for repeated use. Storage at -70 °C in DMSO solutions, in sealed and dark vials, had been suggested in the literature. [19] However, due to the slow evaporation of DMSO, which makes it difficult to concentrate samples, we did not find this solvent an optimal solution. Aware of the reported aerobic

lability of **73** and its ability to generate radicals that can further catalyze the degradation

of the parent compound, we thought, that a radical scavenger medium: ethanol would be

a better choice. We stored our samples at different temperatures (1-2 mM) in ethanol. The

concentration of our FP-12 stock solutions were determined by U.V. absorbance

measurements (Figure 98.; $\varepsilon_{355nm} \sim 100\ 000\ M^{-1}cm^{-1}$). [19] We followed the degradation of

our stock solution by HPLC (Figure 99). The identity of fecapentaene in our

chromatograms had been established by diode array HPLC method (Figure 102). We

plotted the percentage of intact fecapentaene-12 vs. time (Figure 100). We observed that

the lower the temperature and the more dilute the solution of FP-12, the longer its life-

time.
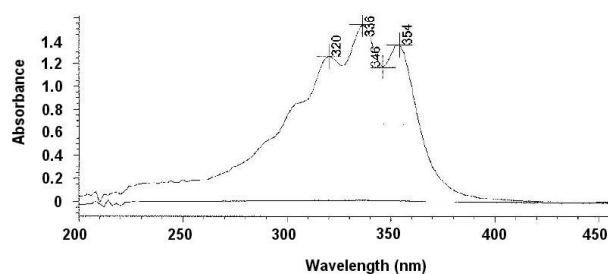
Figure 98. UV scan of freshly synthesized fecapentaene-12 in 100% ethanol ($\varepsilon_{355nm} \sim 100\ 000\ M^{-1}cm^{-1}$)
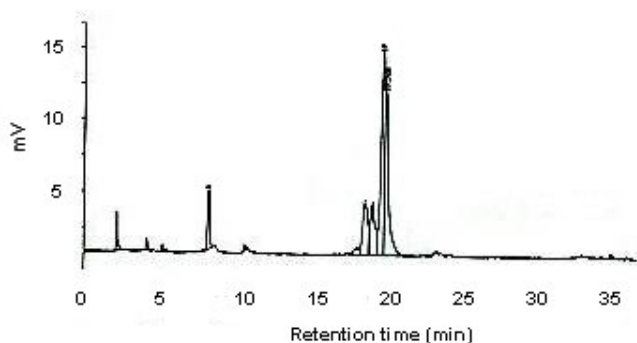
Figure 99. The HPLC of fecapentaene-12 (**73**). Peaks: 8 min: suggested polyconjugated hydrolytic degradation product, 18-20 min small peaks: *cis-trans* fecapentaene-12, 21 min: fecapentaene-12. Diode array HPLC was used in the identification of the 21 min peak as of **73**.

_____
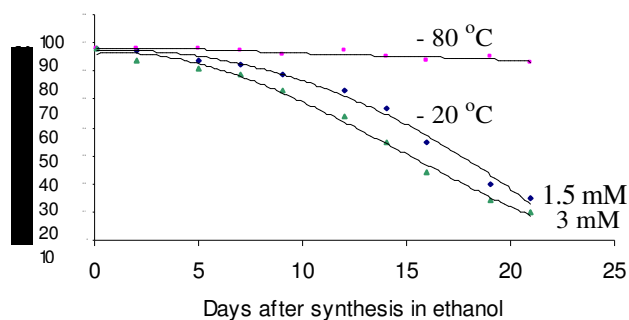
Figure 100. The degradation of fecapentaene-12 stock in absolute ethanol under refrigeration at different temperatures and concentrations

Next, we studied the stability of **73** under physiological conditions. In our DNA-damage studies with small organic molecular analogs of natural products [28] we mostly have used acetonitrile co-solvents and sodium phosphate buffer. We measured the half-life of **73** at different concentrations at 37 °C in the presence of 50 mM sodium phosphate buffer and 10% acetonitrile (v/v). The degradation of fecapentaene-12 (**73**) is first-order in **73** (Figure 101). This kinetic data and later spectral analysis suggested that the primary degradation is the hydrolysis of **73**.
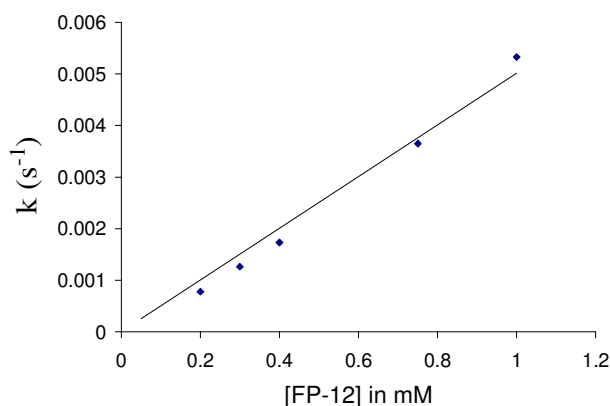
Figure 101. The rates of degradation of **73** vs. its concentration. Conditions: 50 mM sodium phosphate buffer, pH 7.0, 10 % acetonitrile (v/v), 37 °C incubation. Concentrations of fecapentaene-12: 0.2 M, 0.3 M, 0.4 M, 0.75 M, 1 M.

_____

6.5. Semi-Qualitative Analysis of the Degradation of 73 Under Inert, Dark, Ambient Conditions and Exposed to Sunlight Using Diode-Array HPLC.

To confirm the identity of the 21 min peak found in our earlier HPLC-s and to understand of the fate of **73** under physiological conditions we followed the degradation of fecapentaene-12 by diode-array HPLC. The 21 minute peak was positively identified as of **73** (Figure 102).

Upon exposure to aqueous buffer under inert conditions we observed that **73** (21 min) deconjugates to a compound with a possibly smaller molecular weight (8 min)[29] (Figure 103, *left panel*) with an intact conjugation system. Based on information about the hydrolysis of enolether compounds, [18] we suspect that **73** hydrolyzes with the disruption of the C-O-bond similar to the hydrolysis shown in Scheme 28.

Additional buffered samples of **73** were exposed to ambient air and their diode array HPLC (Figure 103, *right panel*) showed the appearance of a compound with longer retention time (31 min) and the disruption of the polyconjugated π-system. With information about the potential products in lipid peroxidation reactions [30] we suggest that under such conditions **73** polymerizes possibly via radical intermediates (Scheme 29).

Scheme 28. Suggested degradation pathway of fecapentaene-12 in aqueous buffer under inert conditions.

Scheme 29. Suggested degradation processes of **73** in aqueous buffers exposed to air.
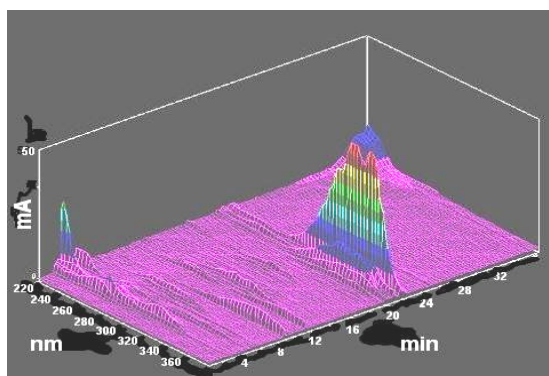
Figure 102. Diode array HPLC of **73** (21 min).
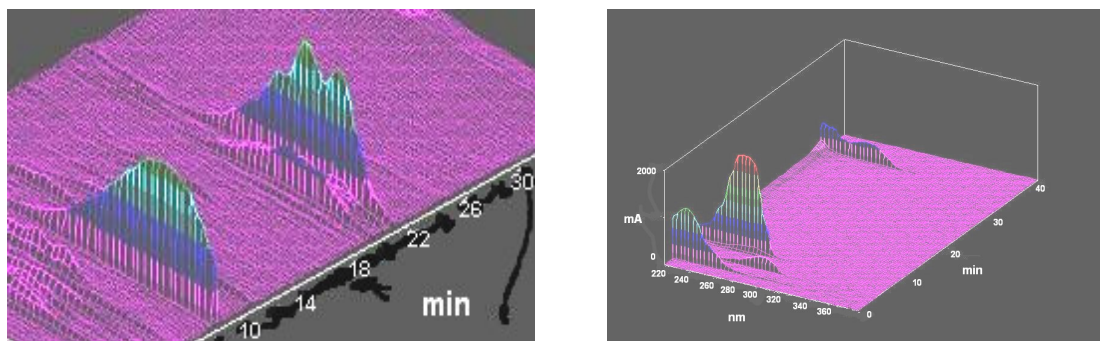
Figure 103. Diode array HPLC of a sample of fecapentaene-12 exposed to aqueous buffer under nitrogen (*left panel*) and ambient air (*right panel*).

245

Finally, we exposed a freshly made sample of **73** (200 μM) in sodium phosphate

buffer to sunlight for 5 min. Diode array HPLC of the resulting mixture showed that **73**

(21 min) and the hydrolytic aldehyde degradation peak (**89,** 8 min) appeared to turn into

multiple peaks of close retention times (Figure 104) suggesting the *cis-trans*

isomerization of their hydrocarbon chain. Prolonged exposure to neon-light did not result

in such isomerizations, which suggests that the high-energy UV-component of sunlight is

important in generating these isomers.
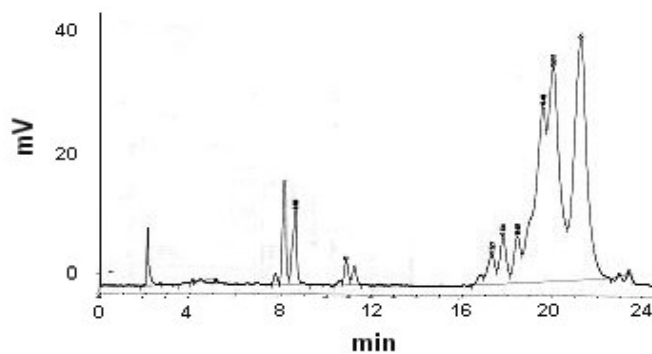
Figure 104. HPLC of freshly made fecapentaene-12 solution in 50 mM sodium phosphate buffer (pH 7.0), exposed to sunlight for 5 min under nitrogen.

6.6. The Mechanism of Oxidative DNA-Damage Caused by Fecapentaene-12 and Authentic Superoxide-Radical Generators: Vitamin A and Hydroquinone

We employed a plasmid-based assay to characterize the DNA-cleaving properties of **73**. In this assay, a single-strand DNA-cleavage converts supercoiled double-stranded plasmid (form I) into the open circular form (II). [31] The two forms of plasmid DNA are then separated using agarose gel electrophoresis and visualized by staining with ethidium bromide. We find that incubation of **73** with plasmid DNA leads to the production of direct single-strand breaks, and the amount of DNA cleavage increases with concentration of **73** and is more enhanced under aerobic compared to unaerobic conditions. Furthermore, when we used deionized (Chelexed) water and buffer an evident decrease in the cleavage efficiency was observed. (Figure 105).
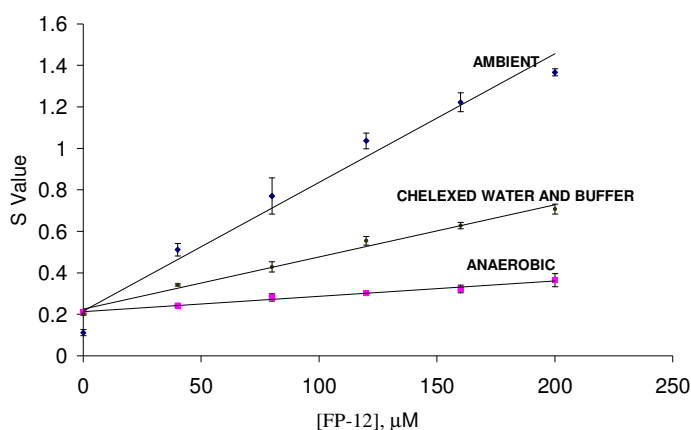
Figure 105. Plasmid DNA cleavage by increasing concentrations of freshly synthesized fecapentaene-12 under aerobic and anaerobic conditions, and using chelexed water and buffer under ambient conditions. Conditions: PGL2BASIC plasmid DNA (35 mM), sodium phosphate buffer (50 mM), acetonitrile (10% v/v). The concentrations of **73** were: 0 μM, 40 μM, 80 μM, 120 μM, 160 μM, 200 μM. Errors were calculated using 67% confidence (n=2). S value = - ln (%uncut / 100).

We then carried out a series of experiments designed to examine whether DNA strand cleavage by **73** occurs via the cascade of reactions involving reduced oxygen species shown in Equation 56, Equation 57, Equation 58 and Equation 59. We find that DNA cleavage by **73** can be inhibited by addition of typical radical scavengers methanol, ethanol and mannitol, by the hydrogen peroxide-destroying enzyme catalase, and by the chelator of adventitious trace metals, desferal, which is known to suppress the metal-dependent Fenton reaction (Equation 58, where M^{n+} is a transition metal such as Fe^{2+}). [30]Addition of the enzyme superoxide dismutase (SOD) also inhibits DNA strand cleavage, presumably by preventing superoxide-dependent reduction of the trace metals (Equation 59)[30] that are required for the Fenton reaction (Equation 58). The effect of these additives are summarized in Figure 106 and Table 12. The effect of SOD will be further discussed for authentic superoxide radical ($O_2^{\bullet-}$) generators in Section 6.6.

$$73 \ + \ O_2 \longrightarrow \ O_2^{\bullet-} + \ 73^{\bullet+} \qquad \text{Equation 56}$$

$$O_2^{\bullet-} + \ HO_2^{\bullet} \longrightarrow \ H_2O_2 \ + \ O_2 \qquad \text{Equation 57}$$

$$H_2O_2 \ + \ M^{n+} \longrightarrow \ HO^{\bullet} \ +\ ^{\ominus}OH \ + \ M^{(n+1)+} \qquad \text{Equation 58}$$

$$O_2^{\bullet-} + \ M^{(n+1)+} \longrightarrow \ O_2 \ + \ Mn^+ \qquad \text{Equation 59}$$
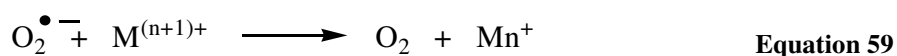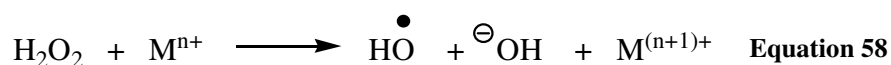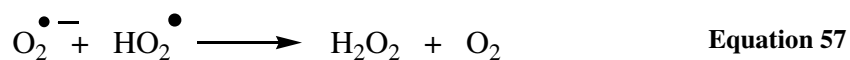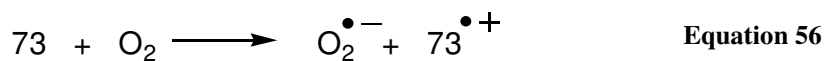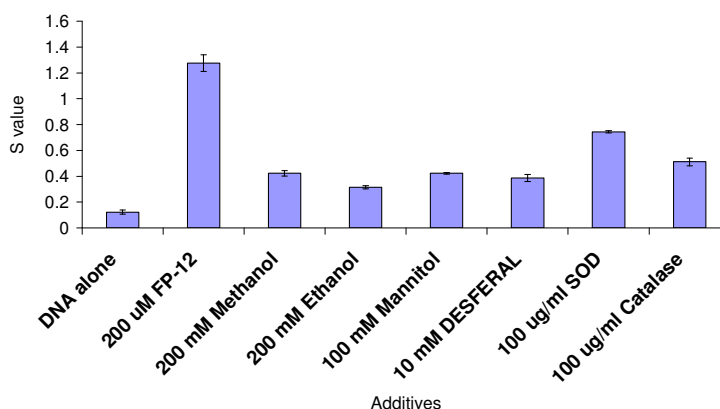
Figure 106. Plasmid DNA cleavage by fecapentaene-12 (200 μM) in the presence of various additives. Conditions: sodium phosphate buffer (50 mM, pH 7.0), acetonitrile (10%, v/v). The additives used were: methanol (200 mM), ethanol (200 mM), mannitol (100 mM), DESFERAL (10 mM), SOD (100 μg/mL), catalase (100 μg/ml). Errors were calculated using 67% confidence (n=2). S value = - ln (%uncut / 100).

We compared DNA damage by **73** to that by other authentic superoxide-radical generators vitamin A[32] (Figure 107) and hydroquinone[33] (Figure 107). Previous works have shown these agents to produce superoxide radical under physiologically relevant conditions, and accordingly we observed that they caused oxidative DNA damage via a mechanism similar to that of fecapentaene-12, but with lower efficiency (Figure 109, Figure 111).

Vitamin A
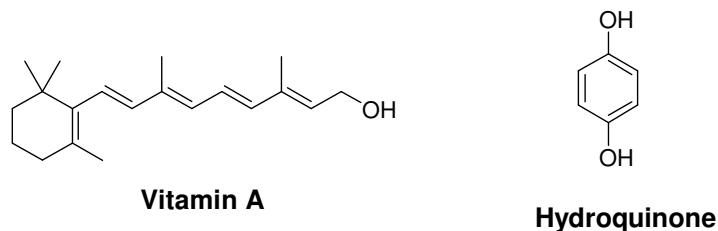
Hydroquinone

Figure 107. The structure of vitamin A and hydroquinone, known superoxide radical generators, used as positive controls in our experiments.
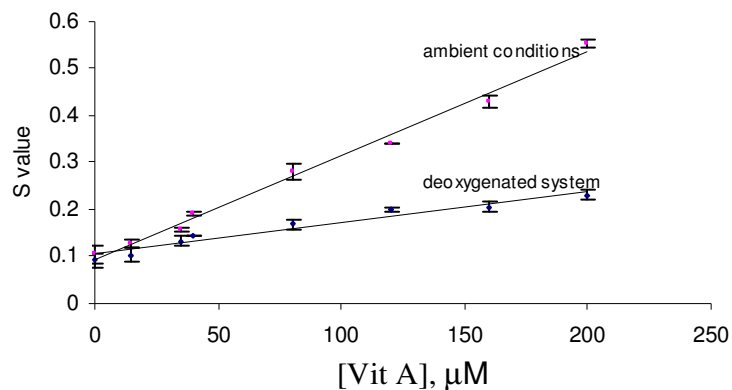
Figure 108. Plasmid DNA cleavage by increasing concentrations of vitamin A under aerobic and anaerobic conditions. Conditions: PGL2BASIC plasmid DNA (35 mM), sodium phosphate buffer (50 mM), acetonitrile (10% v/v). The concentrations of vitamin A were: 0 μM, 40 μM, 80 μM, 120 μM, 160 μM, 200 μM. Errors were calculated using 67% confidence (n=2). S value = - ln (%uncut / 100).
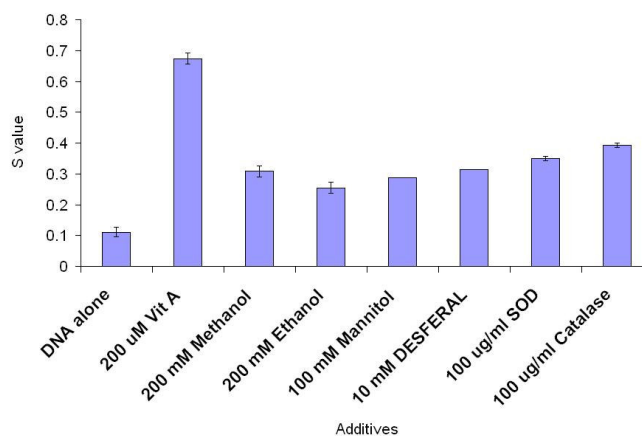
Figure 109. DNA cleavage by vitamin A (300 μM) in the presence of various additives. Conditions: sodium phosphate buffer (50 mM, pH 7.0), acetonitrile (10%, v/v). The additives used were: methanol (200 mM), ethanol (200 mM), mannitol (100 mM), DESFERAL (10 mM), SOD (100 μg/mL), catalase (100 μg/ml). Errors were calculated using 67% confidence (n=2). S value = - ln (%uncut / 100).
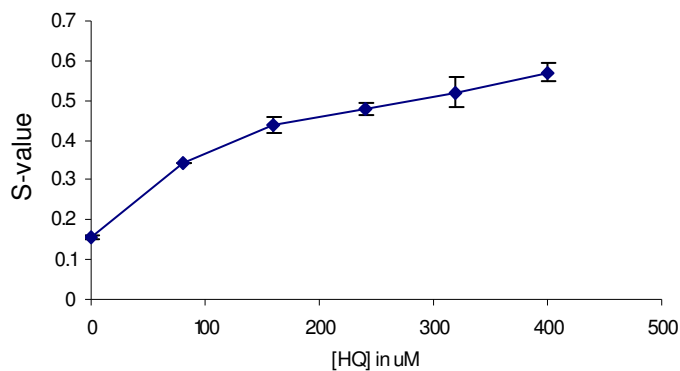
Figure 110. Plasmid DNA cleavage by increasing concentrations of hydroquinone under aerobic and anaerobic conditions. Conditions: PGL2BASIC plasmid DNA (35 mM), sodium phosphate buffer (50 mM), acetonitrile (10% v/v). The concentrations of hydroquinone were: 0 μM, 80 μM, 160 μM, 240 μM, 320 μM, 400 μM. Errors were calculated using 67% confidence (n=2). S value = - ln (%uncut / 100).
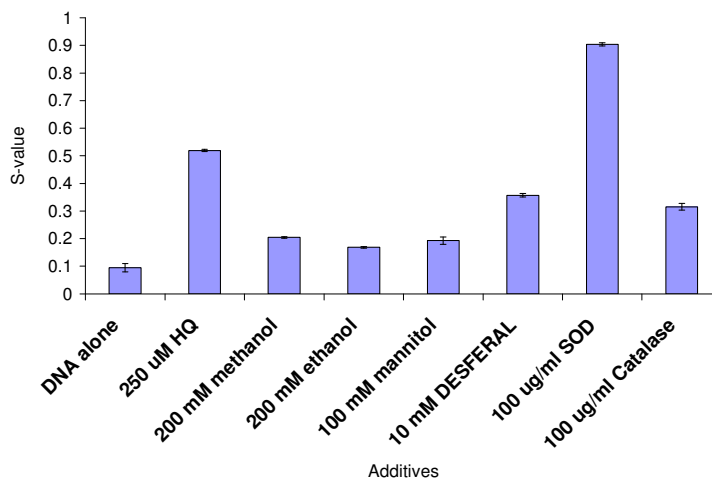
Figure 111. Plasmid DNA cleavage by hydroquinone (**HQ**: 250 μM) in the presence of various additives. Conditions: sodium phosphate buffer (50 mM, pH 7.0), acetonitrile (10%, v/v). The additives used were: methanol (200 mM), ethanol (200 mM), mannitol (100 mM), DESFERAL (10 mM), SOD (100 μg/mL), catalase (100 μg/ml). Errors were calculated using 67% confidence (n=2). S value = - ln (%uncut / 100).

6.7. Discussion of the Differences in the Effect of SOD on the Plasmid-DNA Cleavage by 73, Vitamin A and Hydroquinone

Vitamin A and hydroquinone are known superoxide radical generators. However, they respond differently in their DNA cleavage SOD (Figure 112). Vitamin A is inhibited by SOD, which we can understand in view of the fact that superoxide is removed by SOD, and superoxide is necessary to recycle the trace metals that have been oxidized in the production of hydroxyl radicals (Equation 58). Inhibition by SOD is observed in the context of *in vitro* systems where alternative metal-reducing agents such as ascorbate or thiols are not present.[30]

On the other hand SOD induces strand cleavage in the presence of hydroquinone, which we explain by the fact that HQ is known to generate superoxide radical in an equilibrium fashion (Scheme 30).[30] This equilibrium explains why our calibration curve was not linear (Figure 110). Addition of SOD will pull this equilibrium to the production of superoxide radical, and an immediate dismutation of this radical agent to hydrogen peroxide. An increased concentration of H_2O_2 will help the formation of hydroxyl radical (Equation 58), which is eventually the DNA damaging ROS. In addition, SOD generates H_2O_2 which further yields the DNA-damaging hydroxyl radical.
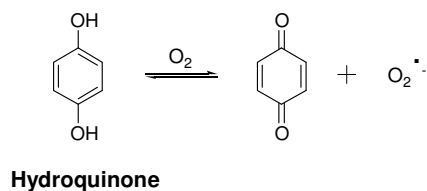
Hydroquinone

Scheme 30. Superoxide radical generation by hydroquinone is an equilibrium process.
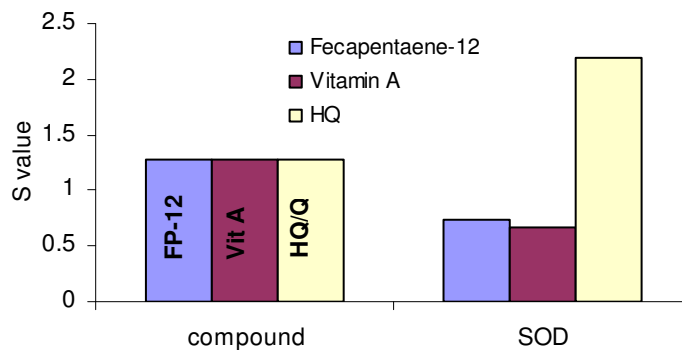
Figure 112. The response of different superoxide-radical generators to the presence of SOD in their DNA cleavage assay. (Cleavages were isoscaled). S value = - ln (%uncut / 100).

6.8. DNA Damage by Partially Degraded Fecapentaene-12

A number of reports have detailed that degraded fecapentaene-12 has vastly decreased ability to cause DNA strand breaks (Figure 113). As we described in sections 6.4 and 6.5 **73** indeed is labile. Here we further demonstrate that exposure of fecapentaene-12 for 5 h to buffered solutions in the resence of acetonitrile co-solvent (Figure 113, curve B) or ethanol co-solvent (Figure 113, curve C), essentially no DNA-cleaving activity remains. Earlier work has shown that the mutagenic activity of the fecapentaenes diminishes upon preincubation. [19]
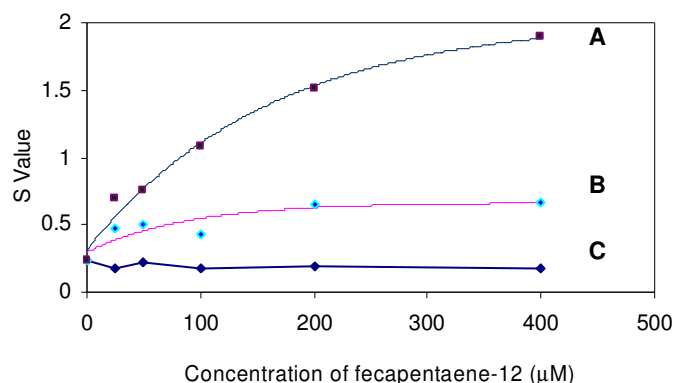
Figure 113. DNA cleavage by fecapentaene-12 (**A**)that of FP-12 pre-incubated in acetonitrile-buffer for 5 h (**B**) and that of FP-12 pre-incubated in ethanol-buffer for 5 h (**C**). Errors were calculated using 67% confidence (n=2). S value = - ln (%uncut / 100).

6.9. Noncovalent Binding by Fecapentaene-12

We investigated the ability of **73** to associate noncovalently to duplex DNA. Noncovalent binding is known to enhance the DNA damaging potential of natural products in general and that of agents that generate reactive oxygen species. [21] The grooves of the double helix are hydrophobic[22-25] and there are some intriguing indications that long-chain hydrocarbons can associate noncovalently with duplex DNA. [34-36] To date however, this mode of DNA binding has not been well characterized.

6.9.1. Ethidium Bromide Displacement by 73

To explore whether **73** associates noncovaletnly with DNA, first, we used the well-known ethidium-displacement assay. [37,38] This technique employs fluorescence spectroscopy to quantitatively monitor the ability of a putative DNA-binding agent to displace intercalated ethidium from the DNA double helix. A wide variety of DNA-

binding molecules including intercalators, groove binders and polycations are able to displace ethidium in this type of assay. [37-42]

We find that titration of the ethidium-DNA complex with micromolar concentrations of **73** causes displacement of the ethidium fluorophore from the duplex (Figure 114).
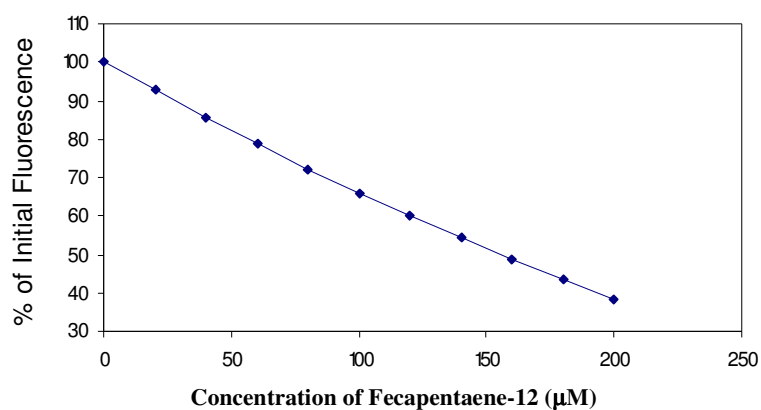
Figure 114. The remaining fluorescence of intercalated ethidium bromide vs. the concentrations of **73**.

Calculations [37,38] based upon the concentration of **73** required to displace 50% of the DNA-bound ethidium yield an association constant of $6.5 \pm 1.1 \times 10^4$ M^{-1} for the noncovalent association of **73** with duplex DNA. These calculations assume that **73** and ethidium bromide compete for the same binding sites on DNA and most likely overestimate the binding constant. Nonetheless, this measurement offers a useful estimate regarding the affinity of **73** for the double helix.

6.9.2. Effect of Added Duplex DNA on the UV-vis Spectrum of 73

We further confirmed the noncovalent interaction of **73** with duplex DNA using a UV-vis spectroscopic assay. The UV-vis spectra of organic ligands are often perturbed upon association with DNA. [38,43,44] We find that titration of **73** with duplex DNA yields a concentration-dependent change in the UV-vis spectrum of **73** (Figure 115., *left panel*). Specifically, addition of DNA to **73** causes a 40% decrease in the absorbance, without any significant change in the absorbance maxima. This type of hypochromism without a concurrent red shift or blue shift in the spectrum has been reported for other agents that associate with the duplex via a groove-binding mode. [45] A control experiment indicates that the changes observed in the UV-vis spectrum of **73** during the titration are not due to decomposition of the compound (Figure 115., *right panel*). While decomposition yields qualitatively similar changes in the spectrum of **73**, the control reaction shows that incubation of **73** with 10 mM bp DNA (in water) for 25 min yields relatively small (10%) changes in the UV-vis spectrum. The observed changes in the UV-vis spectrum of **73** also cannot be ascribed to a salt effect resulting from the addition of DNA-phosphate residues, as we find that addition of analogous amounts of sodium phosphate buffer does not cause a marked change in the spectrum. Perturbation of the UV-vis spectrum of **73** upon addition of DNA has been observed previously, [46] although the exact experimental conditions were not described.

_____
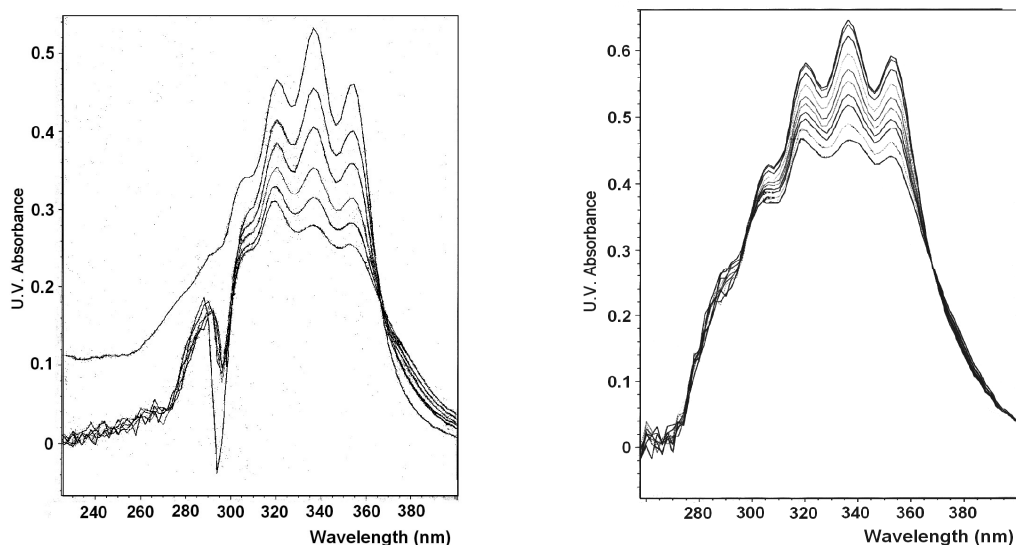
Figure 115. Changes in the UV-vis spectra of **73** with increasing concentration of duplex DNA. Aliquots of herring sperm (**A**, *left panel*) and UV-vis absorption of **73** (40 μM) in 50 mM sodium phosphate buffer (pH 7.0) and 25 % acetonitrile vs time (**B**, *right panel*). DNA were added to a solution of **73** (40 μM) in 50 mM sodium phosphate buffer (pH 7.0, containing 25% acetonitrile). The concentration of **73** was maintained at 40 μM for each measurement. The absorbance of **73** decreases with increasing DNA concentration. The DNA concentrations (in bp) for each curve (from top to bottom) were: 0, 1 mM, 2 mM, 4 mM, 6 mM, 8 mM. *Right panel:* Recordings were done at the following times: 0 min, 2 min, 5 min, 10 min, 20 min, 25 min, 30 min, 35 min, 40 min, 45 min.

6.9.3. Determining the Binding Constant and the Binding-Site Size by the McGhee-von Hippel Analysis[47]

To determine the size of space one fecapentaene-12 molecule can occupy in DNA, and to refine its binding constant, we followed the procedure described by McGhee and von Hippel earlier. [47] Accordingly, with a few iterations for different binding site sizes (Equation 60) we determined that fecapentaene-12 spans a range of 6 to 10 bp in DNA with a modest binding constant (K_B = 1029 ± 190 M^{-1} and n = 8 ± 2, Figure 116).

$$\frac{r}{C_f} = K(1-nr)[(1-nr)/(1-(n-1)r)]^{n-1} \qquad \textbf{Equation 60}$$

257
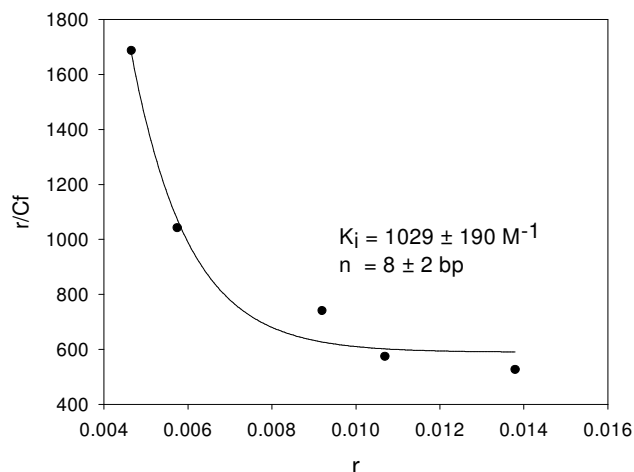
Figure 116. McGhee von Hippel analysis of the DNA binding by fecapentaene-12.

6.10.   Searching for DNA-adducts of 73 by Nuclease Digestion

We have tried to study DNA alkylation in a few different ways. Base mediated workup of our plasmid assays (using DMEDA) did not prove the presence of base labile DNA-adducts. Incubation of DNA in the presence of **73** and sodium cyanoborohydride to stabilize suspected adducts of the aldehyde degradation products, similar to the work of Lawrence J. Marnett,[48] and subsequent HPLC analysis of the reaction mixtures did not provide us with evidence for labile DNA adducts either.

Finally, we investigated the likelihood for the presence of non-labile DNA adducts, applying rapid acidic nuclease digestion as has been shown by Peter F. Guengerich *et al.* [49] Analysis of digests by HPLC (Figure 117) disclosed extra peaks in the presence of **73** but a more elaborate investigation of the origins of these peaks is still

required in the future. A revision of this work is strongly suggested along with the identification of degradation products of **73** after its incubation under physiological conditions, possibly using GC-MS and LC-MS methods.
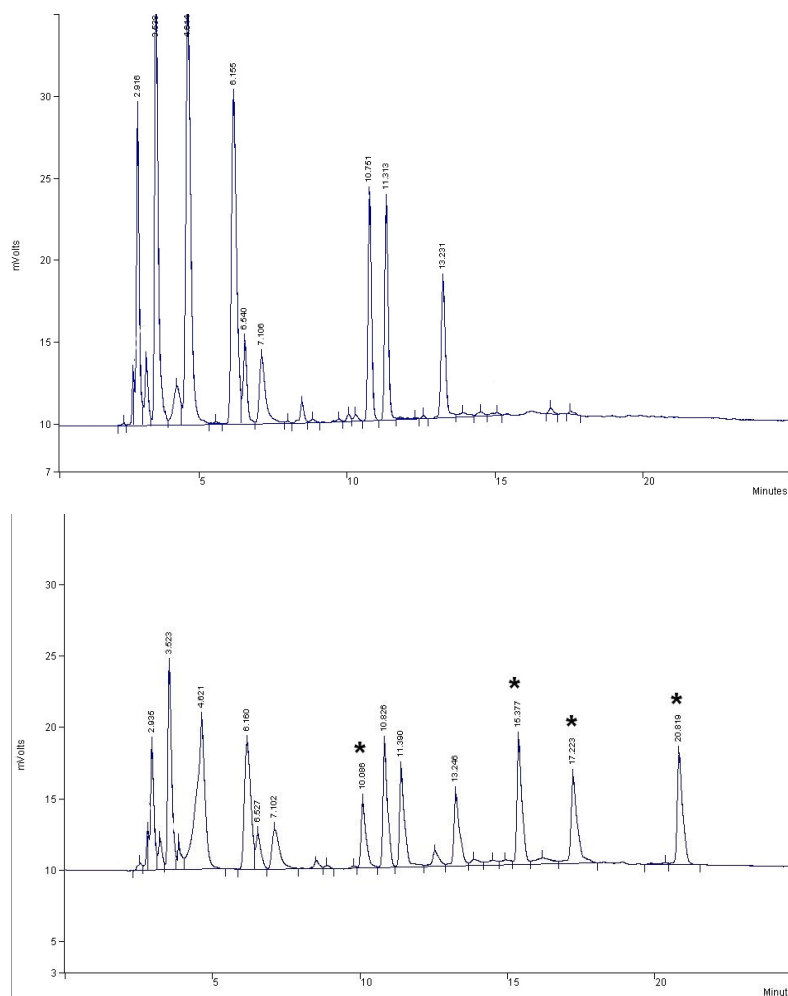
Figure 117. HPLC analysis of the digestion mixture of DNA + **73** after digestion with PDE + DNAse II + AcP-ase. The experiment revealed new peaks (10 min, 15 min, 17 min, 21 min, labelled) in the presence of **73** the origin of these is under investigation.

6.11.   Chapter Conclusions

We synthesized fecapentaene-12 and managed to find optimal conditions for its extended storage in absolute ethanol solution at minus 80 °C at a stock concentration of 1.5 mM. Higher concentrations and temperatures resulted in faster degradation of the molecule. To estimate the purity of our stocks we used RP-HPLC and we found the average purity of fecapentaene-12 used in our DNA reactions above 85%. Impurities were mostly constituted of light induced *cis-trans*-isomerization products of the parent compound. From the concentration dependence of its stability (Figure 101), we assume that degradation of **73** in buffers is the result of self-catalytic processes. After exposure of **73** to aqueous buffers under anaerobic and aerobic conditions and analyzing the samples by diode array HPLC, we suspected hydrolytic and oxidative processes as key players in the degradation of our molecule (Scheme 28 and Scheme 29). We also showed this by diode-array-HPLC analyses of the degradation mixture. Furthermore, quick exposure of freshly made buffer solutions of **73** to sunlight under inert conditions showed very rapid *cis/trans* isomerization of the hydrocarbon tail (Figure 99), which did not happen when samples were similarly exposed to neon-light.

Our synthetic fecapentaene-12 is a potent DNA damaging agent, more effective under aerobic than deoxygenated conditions. With the knowledge that oxidative chemistry can lend mutagenecity to a compound,[50-52] we wanted to identify the ROS responsible for the DNA damage by FP-12. We identified the ROS in the direct generation of superoxide-radical (O2•-), H_2O_2 and OH•, and they clearly can contribute to the potent mutagenicity of the fecapentaenes.[52] Interestingly, authentic superoxide-

radical generators respond differently to the addition of SOD in their plasmid DNA cleavage assays (Figure 112). The findings presented in Figure 112 are consistent with a mechanism where **73** causes DNA strand cleavage via the well-known [30] cascade of reactions shown in Equation 56 to Equation 59, in which hydroxyl radical is produced as the ultimate DNA-cleaving agent. Hydroxyl radical is a well-known DNA-damaging agent. [50,51,53,54] Additionally, it is reported that fatty acids generate superoxide radical upon their breakdown. [3] The initial steps in this overall process likely involve oxidation of the polyene framework in **73** to yield superoxide radical ($O_2^{\bullet-}$) and the resonance stabilized polyene radical cation. [18,55] Subsequent reactions involved in the aerobic degradation of **73** are poorly defined and undoubtedly complex. [55,56] While much recent work has focused on peroxidase dependent [57] production of superoxide by **73**, [3,14,15] our results demonstrate the potential of this compound to *directly* generate DNA-damaging reactive oxygen species via interaction with molecular oxygen.

Others have suggested [14,15] that the fecapentaenes may produce the DNA damaging species singlet oxygen and hydroxyl radical by means of the Haber-Weiss reaction (Equation 61). However, this seems unlikely in light of studies from several groups showing that this general pathway essentially does not occur under physiological conditions. [58-61] In fact, the evidence supporting the generation of singlet oxygen by the fecapentaenes is not overwhelming. For example, inhibition of DNA damage by sodium azide has been taken as a sign of singlet oxygen involvement. [15] However, while sodium azide does, indeed, quench singlet oxygen [62-64] it also effectively scavenges hydroxyl radical, with a rate constant of 1.2×10^{10} $M^{-1}s^{-1}$. [65] Furthermore, reactions of fecapentaene with DNA have been carried out in D_2O, which increases the lifetime of

singlet oxygen, but only minimal increases in damage yields were observed. [14] In cases where singlet oxygen is clearly involved, large increases in the yields of DNA damage typically are observed when the reaction is preformed in D_2O. [66] Rather than invoking singlet oxygen, it seems likely that much of the published data regarding oxidative DNA damage by the fecapentaenes (both enzyme dependent and spontaneous) can be rationalized in terms of the chemical reactions shown in Equation 56Equation 57 and Equation 58.

$$H_2O_2 \; + \; O_2^{\bullet \, -} \longrightarrow \; HO^{\bullet} \; + \; O_2 \; + \; HO^{-}$$

singlet oxygen

Equation 61
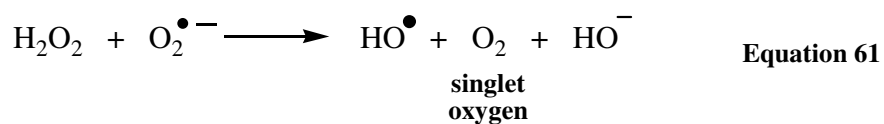
We have shown that the degradation products of fecapentaene-12 are less effective DNA damaging agents (Figure 113).

Studying fecapentaene-12-DNA complexes by two different spectroscopic methods revealed that **73** shows noncovalent association to duplex DNA with a modest binding constant ($2 \times 10^3 \, M^{-1} < K_B < 6.4 \times 10^4 \, M^{-1}$). Thus, the fecapentaenes provide an interesting new example highlighting the potential for long chain hydrocarbons to associate noncovalently with double-helical DNA. With the help of McGhee and von Hippel analysis, we refined our binding constants, and calculated that fecapentaene-12 might occupy a 6 to 8 base-pair size space on DNA.

Several of our attempts to find DNA adducts formed by fecapentaene-12, using stabilization of labile adducts and searching for base-labile and nonlabile adducts, failed to provide clues about DNA adducts. However, revision of adduct detection and that of the identification of degradation products of **73** is strongly suggested.

Our achievements clarified the mechanism of oxidative DNA damage directly by the endogenous fatty-acid metabolite: fecapentaene-12 without the involvement of any enzymes.

6.12. Experimental
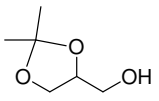
6.12.1. Materials and Methods

Materials were obtained from the following suppliers and were of the highest purity available: tetrabutylammonium fluoride, potassium carbonate, sodium phosphate, bromophenol blue, sucrose, EDTA, HEPES buffer, desferal, glycerol, *tert*-butyl dimethylsilyl chloride, tosyl chloride, imidazole, pyridine, *N, N'*-dimethyl amino pyridine, pyridine sulfur-trioxide complex, lithium di-isopropyl amide, *n-butyl* lithium, diphenyl phosphine, hepta-(2E, 4E)-dienal, Aldrich Chemical Co. (Milwaukee, WI); HPLC grade solvents (water, acetonitrile, ethanol, methanol, diethyl ether, tetrahydrofuran), 30% H_2O_2, Fisher (Pittsburgh, PA); ethidium bromide, herring perm DNA, Roche Molecular Biochemicals (Indianapolis, IN); agarose, Seakem; catalase, calf thymus DNA, SOD, DNA-digestion enzymes (nuclease, phosphatase), Sigma Chemical Co. (St. Louis, MO). The plasmid pGL2BASIC was prepared using standard methods.[67]
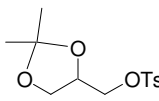
Instrumentation: balances: Denver Instrument M-220 D and Denver Instrument TR-4102; pipetmans: Gilson; HPLCs: RAINN 10 SS pump, VARIAN ProStar 210 25 SS pumps with Star Chromatography vs. 5.51 software; WATERS with Breeze Basic; pH meter: thermo-ORION 420; UV: Hewlett Packard HP8452A Diode Array w/89090A cuvette temperature controller; NMRs; Bruker; Agarose electrophoresis power supply: EC 154; Gel-imaging system: Alfaimager; Fluorimeter: Interational Technologies; Benchtop centrifuge: CLOVER LABS (6 x 2 mL); Medium-size centrifuge: Eppendorf 5415C; SpeedVac Instrument: SAVANT Speed Vac. SC 110; Vortex: Fischer VORTEX Genie 2. LC-MS: ThermoFinnigan TSQ7000 triple-quadrupole with API2 source.

6.12.2. Synthesis of Fecapentaene-12 (73)

1,2-O-acetonide-3-hydroxyglycerol (76)[68]

To a solution of glycerol (**75**, 12.8 g, 140 mmol) in ethylene glycol dimethyl ether (72 mL) acetone dimethoxyacetal was added (32.6 mL, 25.58 g, 168 mmol, 1.2 equiv) under stirring at room temperature. A catalytic amount of stannous chloride, $SnCl_4$, (30 mg, 0.7 mmol, 0.005 equiv) was added and the solution was refluxed for 1.5 h. The reaction mixture was cooled and treated with pyridine (25 μL). Solvents were removed via rotavap (100 Hgmm, 35-45 °C) and the concentrate was redissolved into ethyl acetate (80 mL). This solution was washed in a separatory funnel with an aqueous salt solution (5% NaOH in saturated NaCl, 3 x 25 mL). The organic layer was dried over Na_2SO_4 and concentrated on rotavap. This resulted in a crude mixture as a glacial transparent oil (**76**) (14 g, 98% yield). ^{1}H-NMR**:** (CDCl$_3$, 250 MHz) σ 1.3 (3H, s), 1.4 (3H, s), 3.2 (1H, m), 3.4 (1H, m), 3.5 (1H, m), 3.55 (1H, m), 3.75 (1H, m), 4.0 (1H, m), 4.3 (1H, m), ^{13}C-NMR: (CDCl3, 62.9 MHz) σ 24, 25, 27, 48, 58, 63, 66, 71, 75, 76, 100, 110.

1,2-O-acetonide-3-(R/S)-tosyl-glycerol (77)

Compound **76** (14g, 106 mmol) was added to pyridine (58 mL) and the solution was ice cooled. To the cooled solution, p-toluolsulfonic acid chloride (20.2 g, 98 mmmol, 1 equiv) was added in small portions over a period of 5 minutes. This results in a clear lemon-yellow solution. This was stored at 4°C overnight until ale-red needle crystals showed up in the reaction flask. Without filtration of the

mixture diethyl ether was added (60 mL), and the solution turned turbid. The organic layer was washed with HCl (1N in portions of 10 mL) until the washing liquid turned acidic. The organic layer was further washed with a saturated solution of NaHCO$_3$ (20 mL) and dried over Na$_2$SO$_4$, concentrated on rotavap. The resulting pink oil slowly solidifies into a pale yellow soap (**77**) (20 g, 75 % yield). ^{1}H-NMR**:** (CDCl$_3$, 250 MHz) σ 1.4 (3H, s), 1.5 (3H, s), 2.45 (3H, s), 3.7 (2H, dd), 4.0 (1H, d), 4.05 (1H, s), 4.2 (1H, p), 7.35 (2H, d), 7.85 (2H, d); ^{13}C-NMR: (CDCl3, 62.9 MHz) σ 21, 25, 26, 66, 70, 73, 110, 127, 130, 133, 145.

(S/R)-3-tosyloxi-propanediol (78)
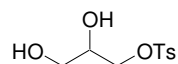
Compound **77** (7.1 g, 55 mmol) was dissolved in acetone (5.5 mL) and to this solution 1N HCl (16 mL) was added. The resulting mixture was heated on an oil bath for 30 min, then cooled and frozen on a dry ice-acetone cooling mixture. The frozen material was lyophilized at minus 43 °C temperature and 10^{-3} bar pressure overnight. This resulted in a yellow viscous oil (6.5 g, 98 % yield). Alternatively, the cooled reaction mixture can be extracted with ethylacetate (100 mL) washed with water (20 mL) twice and brine (20 mL), then dried over Na$_2$SO$_4$ and purified on a thin pad of silica (gel filtration). ^{1}H-NMR**:** (CDCl$_3$, 250 MHz) σ 2.4 (3H, s), 3.3 (2H), 3.5-3.7(3H, m), 3.9(1H, m), 4.1 (1H, dd), 7.35(2H, d), 7.85(2H, d).; ^{13}C-NMR: (CDCl3, 62.9 MHz) σ 21, 62, 69, 71, 128, 130, 133, 145.

_____

1,2-O-(t-butyl-dimethylsilyl)-3-O-tosyl-(S/R)-glycerol (79)
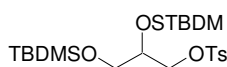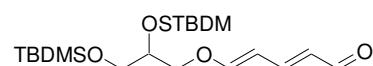
Compound **78** (14.4 g, 59 mmol) was dissolved in DMF (50 mL, predried on molecular sieves, or frehly purchased). Imidazole (25 g, 368 mmol, 6.3 equiv) was added to the system. Stirring began, and after all the components dissolved (clear yellow solution), dimethyl *tert*-butyl silylchloride (35 g, 128 mmol, 2.2 equiv) was added to the solution dropwise over a period of 5 minutes. After 1-2 h the reaction mixture turned turbid. After 8 h water (50 mL) and diethyl ether (1200 mL) were added. The organic layer was further washed with water (50 mL), brine (2 x 50 mL) and dried over K_2CO_3 and purified by flash column chromatography (10% diethyl ether in hexane), and **79** was isolated (23 g, 92% yield). Rf.: 0.3 (30% ether in hexane). ^{1}H-NMR: (CDCl$_3$, 250 MHz) δ 0.93 (9H, s), 0.98 (9H, s), 2.40 (3H, s), 3.55 (1H, t, J=4.7 MHz), 4.05 (2H, dd, J=5.2 Hz); 7.24 (4H, dd), 7.32 (6H, m), 7.39 (4H, t), 7.45 (4H, q), 7.54 (4H, q), 7.66 (2H, d); ^{13}C-NMR: (CDCl3, 62.9 MHz) δ 19 (m), 20 (m), 22 (m), 28 (str), 28 (str), 65 (m) 71 (m), 72 (m), 128 (m), 129 (m), 131 (m), 136 (str), 136.5 (str), 137 (str), 137.5 (str).

Potassium glutaconate (80)
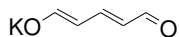
Potassium hydroxide (52 g) was dissolved in water (126 mL). This solution was cooled to minus 20 °C, and sulfur-trioxide pyridinium complex salt was dissolved in it (36 g, 225 mmol). The solution turned a lemon yellow color. A mechanical stirrer with a stirring rod was used for stirring of the mixture, and the temperature was maintained for one hour. After 1h the temperature was raised to room temperature over the course of four hours. During this time the color of the solution deepens to orange and
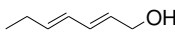
red, eventually. The mixture was heated quickly to 40 °C and stirred further at this temperature for 30 min. The mixture was finally cooled to 5 °C to facilitate the crystallization of the product. The crude material was filtered off and washed with acetone to remove water. The pad of brownish solid material was air dried for an hour on respirator vacuum. The remaining solid was further dried in high vacuum overnight at 60 °C, using a sand-bath. At this point checking the activity of **80** in our S_N2 displacement should be done. If compound does not show activity, then recrystallize it again from methanol (400 mL) at refluxing temperature; add charcoal (5-8 g) to remove impurities. After filtration, methanol was removed by rotavap at low temperature, and the resulting solid needs to be dried under vacuum overnight. This operation results in a redish-yellow to lemon yellow powder with matching NMR. (25 g, 70 % yield). ^{1}H-NMR**:** (CDCl$_3$, 250 MHz) δ 5.1 (2H, q, J$_1$ = 12 Hz, J$_2$ = 15 Hz), 7.0 (1H, t, J=15 Hz), 8.6 (2H, d, J = 12 Hz). ^{13}C-NMR: (CDCl3, 62.9 MHz) δ 105 (m), 160 (m), 185 (m).

5-[2,3-Bis-(tert-butyl-dimethyl-silanoxy)-propoxy]-penta-2,4-dienal (81)

 Compound **79** (1 g, 1.38 mmol) was dissolved in DMF (7 mls) or for better reults THF might be used. Potassium glutaconate (**80**, 0.85 g, 6.25 mmol, 4.5 equiv) was dissolved and the reaction mixture was kept under argon and stirred at 90 °C for 3-4 hrs. The appearance of the product should be followed by TLC (Rf.: 0.25 in 30% diethyl ether in hexane), as long exposures to this temperature also degrades the target aldehyde (**81**). The reaction mixture was cooled on ice and diethyl ether was added to it (150 mL), followed by water (20 mL). The organic layer was washed with water twice (20 mL), followed by brine (20 mL), then dried over potassium

carbonate. The solution was concentrated on rotavap and purified by quick flash column

chromatography (gradient, 10-20% diethyl ether in hexane) on a short column. Silica gel

was deactivated by TEA (3% w/w). After isolation the process results in a clear labile oil

(400 mg, 64 %)that needs to be refrigerated. Alternatively, an aseotropic drying and

storage over benzene at minus 20 °C is suggested. Rf.: 0.25 in 30% diethyl ether in

hexane. ^{1}H-NMR**:** (CDCl$_3$, 250 MHz) δ 1.02 (9H, s), 1.04 (9H, s), 3.60-3.72 (2H, m),

3.86-4.06 (3H, m), 5.63 (1H, t, J = 12 Hz), 5.99 (1H, dd, J$_1$ = 8 Hz, J$_2$ = 15 Hz), 6.78 (1H,

d, J = 12 Hz), 6.94 (1H, dd, J$_1$ = 12 Hz, J$_2$ = 15 Hz), 7.27-7.48 (12 H, m), 7.53-7.64 (8H,

m), 9.43 (1H, d, J = 8.1 Hz)**;** ^{13}C-NMR**:** (CDCl3, 62.9 MHz) δ 0 (m), 25 (m), 30 (str), 70

(m), 75 (m), 77 (m), 110 (m), 132 (m), 155 (m), 165 (m), 198 (m).

Hepta-(*2E, 4E*)-dienol (82)

 To avoid foaming out of the reaction flask, this procedure requires a

round bottom flask with a minimum 250 mL volume. Hepta-(*2E, 4E*)-dienal (2.55 g, 23.2

mmol) was dissolved in methanol (26 mL), and CeCl$_3$7H$_2$O (10.2 g, 27.3 mmol, 1.2

equiv) was added to the solution. In small portions NaBH$_4$ (1.2 g, 31.5 mmol, 5.5 equiv)

was added and heavy bubbling of hydrogen gas was observed. The progress of the

reaction was followed by TLC (30% diethyl ether in hexane, R$_f$ starrting material.: 0.6, R$_f$

product: 0.25). After 20 minutes methylene chloride (650 mL) was added to the reaction

mixture followed by water (16 mL). The organic layer was further washed with water (25

mL) and brine (25 mL). Product was dried over K$_2$CO$_3$, concentrated and purified on a

flash chromatographic column (30% ether in hexane), which yields a rancid fatty-acid

smelling viscous oil (2.3 g, 95% yield). ^{1}H-NMR**:** (CDCl$_3$, 250 MHz) δ 0.95 (3H, t, J =

_____

12 Hz), 2.1 (2H, q, J = 12 Hz), 4.1 (2H, t), 5.6-5.8 (2H, m, J = 15 Hz), 6-6.2 (1H, t, J =

15 Hz). ^{13}C-NMR: (CDCl3, 62.9 MHz) δ 13, 25, 63, 127, 129, 131, 137.

Hepta-(*2E, 4E*)-dienyl-1,6-dichlorobenzoate (*83*)
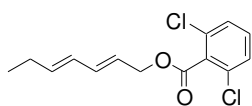
 Hepta-(*2E, 4E*)-dienol (**82**, 2 g, 18 mmol) was dissolved in methylene chloride (20 mL) under argon/nitrogen. Pyridine (10

mL, 123 mmol, 6.8 equiv) was added to the system. **Note:** the catalytic amounts of

pyridine suggested by the literature do not result in appreciable reaction. DMAP (285 mg,

2.3 mmol, 0.13 equiv) was added and 2,6-dichlorobenzoyl chloride (4.42 g, 21 mmol,

1.18 equiv). The reaction mixture was stirred at room temperature for 24-48 h. During

this time, the mixture turns darker. Diethyl ether (450 mL) and water (25 mL) were added

to the reaction. The organic layer was washed with portions of cupper sulfate solution

(1M, ~ 2 x 70 mL) until pyridine is removed from the solution (R.f.: 0.2 in 30% ether in

hexane). The organic layer was further washed with water (40 mL) and brine (40 mL),

then dried over MgSO$_4$, concentrated and purified by flash chromatography (R.f. 0.7,

30% diethyl ether in hexane). The product is a viscous oil (3g, 78 %). ^{1}H-NMR: (CDCl$_3$,

250 MHz) δ 1.0 (3H, t, J = 12 Hz), 2.1 (2H, p, J = 12 Hz), 4.9 (2H, d, J = 12 Hz), 5.7-5.9

(2H, m, J$_1$ = 12 Hz, J$_2$ = 15 Hz), 6.0 (1H, t, J = 15 Hz), 6.4 (1H, dd, J$_1$ = 12 Hz, J$_2$ = 15

Hz), 7.2-7.4 (3H, m, J = 8 Hz).

_____

Hepta-(*2E, 4E*)-dienyl-diphenylphosphine (84)
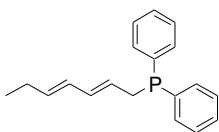
Hepta-(*2E, 4E*)-dienyl-1,6-dichloro benzoate (**83**, 3.52 g, 13.1 mmol) was dissolved in THF (30 mL) and cooled to minus 78 °C. In a separate flask in THF (30 mL), diphenyl phosphine (4.24 g, 23 mmol, 1.7 equiv) was dissolved and cooled to minus 78 °C. *nBu*-Li (1.85 M, 2.3 equiv) was injected and the solution turned red. After this step, the first solution of **83** was transferred to the solution of *nBu*-Li-diphenyl phosphine mixture, using a canula and applied nitrogen pressure on the source flask. The disappearance of the benzoate derivative and the appearance of the phosphine product was followed by TLC (10% diethyl ether in hexane). After 20-40 minutes, the reaction was quenched with a saturated solution of NH$_4$Cl (22 mL) and the material was used in the next step without purification.

Hepta-(*2E, 4E*)-dienyl-diphenylphosphineoxide (85)
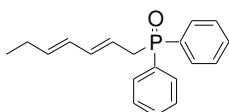
After quenching the reaction in the preparation of **84** with NH$_4$Cl, diethyl ether (600 mL) was added to the mixture, followed by water (55 mL). The organic layer was then washed with hydrogen peroxide (10-30% H$_2$O$_2$, 20 mL portions) until the appearance of the oxidized product **85** (R.f.: 0.28 in 2% methanol in ether). Then sodium sulfite (Na$_2$SO$_3$, 10% in water, 35 mL) was added to the system to degrade the excess hydrogen peroxide. The mixture was dried over MgSO$_4$, concentrated on the rotavap and purified via flash column chromatography (gradient elution, 1-2% methanol in ether). The product is a pale-yellow powder with an overall yield in the formation of **84** and **85** of ~ 2.5 g (70 % yield). ^{1}H-NMR**:** (CDCl$_3$, 250 MHz) δ 0.9 (3H,

d-tr, 7 Hz), 2.05 (2H, m), 3.15 (2H, dd, J₁=16Hz, J₂=8 Hz), 5.43-5.68 (2H, m), 5.84-6.14

(2H, m), 7.4-7.88 (10H, m).

1-[2,3-Bis-(tert-butyl-dimethyl-silanyloxy)-propoxy]-6-(diphenyl-phosphinoyl)

dodeca-1,3,7,9-tetraen-5-ol (86)
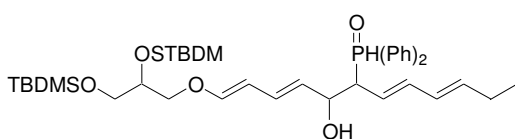
Our intermediate aldehyde product 5-[2,3-Bis-(tert-butyl-dimethyl-silanoxy)-propoxy]-penta-2,4-dienal (**81**, 70 mg, 0.11 mmol) was

dissolved in THF (1 mL) and cooled to minus 78 °C. In a separate flask hepta-(*2E, 4E*)-

dienyl phosphineoxide (30 mg, 0.12 mmol, 1.1 equiv) was dissolved in THF (1 mL) and

cooled at minus 78 °C. This later solution was treated with LDA (1.8 M, 135 μL, 0.24

mmol, 2 equiv), and the solution turned deep red. Two minutes later, the solution of our

aldehyde **81** was transferred via a canula applying nitrogen pressure on the source flask.

After 20-30 minutes, the reaction was quenched by adding brine (1.5 mL) to the solution

at minus 78 °C and adding ether (50 mL). The organic layer was further washed with

water (3 mL) and brine (3 mL) and dried over K₂CO₃. After concentration of the organic

phase we had a crude mixture containing the adduct **86**. This mixture was dried

azeotropically over benzene (3 x 6 mL), dried and used without further purification in the

next step.

Protected fecapentaene-12 (87)
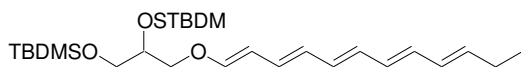
The azeotropically dried mixture of **86** was redissolved in THF (1 mL), cooled to minus 20 °C and treated with potassium tert-butoxide solution in THF (1 M, 0.165 mmol, 165 µL, 1.5 equiv). The appearance of product was observed by TLC (R.f.: 0.3 in 5% diethyl ether in hexane). After apprx. 20 minutes, the reaction was quenched with ice-water (1.5 mL) and ether (40 mL). The organic layer was washed with water (1.5 mL) and brine (3 mL) and dried over K_2CO_3 under a stream of nitrogen to protect against the flow of air. The solution was filtered off from the drying agent under nitrogen athmosphere, and solvents were removed with a purge of nitrogen. Flasks and glassware are suggested to be covered by aluminum foil, as later, sunlight was observed to cause isomerization of the double bonds. The crude mixture was purified quickly on silica column (gradient: hexane to 2% ether in hexane) and resulted in **87** (oil, fluoresce green on TLC under 320 nm light, 40 mg, 70% yield). ^{1}H-NMR**:** ($CDCl_3$, 250 MHz) δ 1.0 (9H, s), 1.02 (9H, s), 2.13 (2H, m), 3.63 (1H, d, J = 4.9 Hz), 3.74 (1H, dd, J_1 = 4.8 Hz, J_2 = 9.8 Hz), 3.87 (1H, dd, J_1 = 4.8 Hz, J_2 = 9.8 Hz), 3.96 (2H, dd, J_1=5 Hz, J_2 = 10 Hz), 5.0 (1H, d), 5.2 (1H, d), 5.41-5.54 (1H, m, olefinic), 5.82-5.66 (1H, m, olefininc), 5.98-6.28 (7H, m, olefinic), 6.39 (1H, d, J = 13 Hz).

Fecapentaene-12 (73)
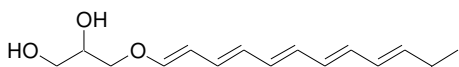
At this step, the absolute exclusion of sunlight and ambient air is important. Extractions, filtrations, solvent evaporation, purfication need to be done under inert conditions, and with deoxygenated solvents. Solvents were deoxygenated with fresh bubbling of a stream of nitrogen or argon for a minimum of 30 min. The protected fecapentaene-12 (**87**, 40 mg, 0.06 mmol) was dissolved in THF (1 mL) at room temperature. The solution was treated with a <u>fresh</u> TBAF solution (1 M in THF, 200 μL, 0.2 mmol, 1.7 equiv). The appearance of the product was followed by TLC (2% methanol in ether, R.f.: 0.35) and the reaction was strirred until the disappearance of the starting material. The product shows green fluorescence under long-wave lamp (320 nm). After approximately 10 minutes (2 h if the *tert*-butyl diphenylsilyl protecting group is used) the solution was quenched by the addition of degassed diethyl ether (60 mL). The organic layer was washed with water (1 mL) and brine (1 mL) and dried over K_2CO_3. The organic phase was filtered off from the drying agent, and the ether was removed by purging with nitrogen in a sealed round-bottom flask covered with aluminum foil. The mixture was purified for fecapentaene-12 quickly with deactivated silica gel column using degassed solvent (gradient: ether to 2% methanol in ether). Fraction collection and chromatography should be done under a stream of nitrogen/argon gas. Solvent was removed by nitrogen purging, and this resulted in lemon yellow crystals (3 mg, 30% yield). NMR, HPLC and UV matched the literature. Due to the incomplete removal of organic solvent and the fast degradation of the samples, the NMR showed identifiable impurities (20%). The purity of our fecapentaene-12 stock solution (2 mM in abs. ethanol, minus 80 °C) was assayed each time prior to DNA assays, using HPLC and UV.

^{1}H-NMR**:** (CDCl[3], 500 MHz) δ 0.95 (3H, m), 2.5 (2H, m), 3.68 (1H, m), 3.75 (2H, m), 3.85 (1H, m), 3.90 (1H, m), 3.92 (1H, m), 5.1 (1H, dd), 5.6 (1H, m), 5.7 (2H, m), 6.0-6.4 (4H, m), 6.5 (1H, dd), 6.6 (1H, d).

6.12.3. Quantitative Stability of Fecapentaene-12 in Organic and Aqueous Media

The freshly synthesized fecapentaene-12 had been redissolved into degassed absolute ethanol to a final 1.5 mM concentration. Higher concentrations result in more rapid decompositions. Samples were stored at minus 80 °C for a month without noticeable degradation (Figure 100). For the determination of the actual fecapentaene-12 concentrations UV absorbance was measured at 355 nm, and concentrations calculated using light extinction coefficient: $\varepsilon_{355nm} \sim 100\,000\ M^{-1}cm^{-1}$.[19]

6.12.4. HPLC Method for the Analysis of Fecapentaene-12

Reverse phase HPLC (C18 column: 4.2 mm x 25 cm) was used with gradient elution using acetonitrile and water eluent as shown in Table 12.

Time	% Acetonitrile	% Water
0-25 min	Gradient: 40 – 70	Gradient: 60 – 30
25-30 min	Gradient: 70 – 90	Gradient: 30 – 10
30-35 min	90	10
35-40 min	Gradient: 90 – 40	Gradient: 10 – 60

Table 12. The gradient elution method for the HPLC separation and analysis of products in our reactions with fecapentaene-12

6.12.5. Measuring the Percentage Remaining Fecapentaene-12 in Organic Solutions under Refrigeration

Aliquots of fecapentaene-12 stock solution in ethanol (20 μL) were diluted 5 times with HPLC eluent (30% acetonitrile – 70% water) and 25 μL of this mixture was injected onto RP-HPLC (4.2 mm, 25 cm C18 column). The size of the peak corresponding to *all-trans* fecapentaene-12 (20-21 min) was plotted against time (Figure 101).

6.12.6. Stability of 73 in Aqueous Buffers at Different Concentrations and Semi Qualitative Analysis of Degradation Pathways Under Inert Dark, Inert Sunlighted and Ambient Buffered Conditions Using Diode-Array HPLC

We used acetonitrile co-solvent at a final 10% volume. Fecapentaene-12 was removed from the freezer. Calculated amounts were injected into an amber HPLC vial and evaporated to dryness. This was re-dissolved with HPLC grade acetonitrile and water and sodium phosphate buffer to reach the selected final concentration of the drug and 50 mM sodium phosphate at pH 7.0[28] The concentrations of fecapentaene-12 were as follows: 200 μM, 400 μM, 500 μM, 750 μM, 1 mM. At different time intervals, 25 uL of these samples were injected onto HPLC for analyses. For the calculation of half-lives a pseudo-first order degradation was assumed. The disappearance of the FP-12 HPLC peak was fitted onto a decaying exponential function by SigmaPlot (Chapter 1), and half lives were calculated as $t_{1/2} = ln\ 2/k$. Half lives were plotted vs. the concentration of fecapentaene-12 (Figure 101). At the end of reactions compounds were injected onto a BECKMAN diode array HPLC and the UV of HPLC peaks were plotted in a 3D view in the wavelength range of 220 – 400 nm for analyses.

To study the effect of sunlight, freshly made buffered sample of fecapentaene-12 (200 μM) was exposed to sunlight for 5 min under nitrogen, and analyzed by HPLC as described above.

6.12.7. The Mechanism of Oxidative DNA-Damage Caused by Fecapentaene-12 and Authentic Superoxide-Radical Generators: Vitamin A and Hydroquinone

DNA Cleavage by 73 Under Aerobic and Anaerobic Conditions and Under Ambient Conditions in the Presence of Chelexed Water and Chelexed Buffer

Fecapentaene-12 (**73**) was used as a stock solution stored in absolute ethanol at minus 80 °C. The fecapentaene-12 solution was removed from the freezer, evaporated to dryness under a stream of nitrogen and dissolved into acetonitrile to a final concentration: 2 mM. In an 500-μL Eppendorf tube the following components and final concentrations were used: PGL2BASIC plasmid DNA was (35 μM / bp), sodium phosphate buffer (pH 7.0, 50 mM), acetonitrile (10%) and increasing concentrations of **1** in a final reaction volume 50 μL. The concentrations of **73** were as follows: 0 μM, 40 μM, 80 μM, 120 μM, 160 μM, 200 μM. The last component added was **73**. Samples were vortexed carefully for 5 sec, and placed into an incubator at 37 °C in dark for 15 h. Following incubation, glycerol loading buffer (7 μL) containing 0.25% bromophenol blue and 40% sucrose, and the mixture vortexed. The resulting mixtures were loaded onto a 0.9% agarose gel. The el was electrophoresed at 80 V for approximately 4 h and then stained in an aqueous ethidium bromide solution (0.2 μg/mL) for 6-8 h. The DNA gel was then visualized by

UV-transillumination and the data documented using an Alpha Innotech IS1000 digital imaging system, with Alphaimager software.

For the anaerobic assays, the stock solution of buffer (500 mM sodium phosphate, pH 7.0) and HPLC-water were degassed via three cycles of freeze-pump-thaw, sealed off under vacuum, brought into a glove box saturated with argon. All reactions were set up and kept for incubation on a heat block at 37 °C in the argon filled glove box. Addition of the loading buffer and gel loading were done under ambient conditions. For the reactions with chelexed water and buffer, HPLC-water and the buffer stock (500 mM NaPi, pH 7.0) were run through a column of Chelex100 (Sigma) in plastic column, to chelate multiply-charged transition metal trace elements. All experiments were run twice, and statistical error analysis was applied to calculate errors. DNA cleavage was converted to the mean number of cleavages on a plasmid molecule (S value = - ln (%cleavage/100) and these values were plotted vs. the concentration of fecapentaene-12 (Figure 105).

DNA Cleavage by Increasing Concentrations of Vitamin A Under Aerobic and Anaerobic Conditions

Vitamin A was used as a stock in acetonitrile (2 mM). In an 500-µL Eppendorf tube the following components and final concentrations were used: PGL2BASIC plasmid DNA was (35 µM / bp), sodium phosphate buffer (pH 7.0, 50 mM), acetonitrile (10%) and increasing concentrations of vitamin A in a final reaction volume 50 µL. The concentrations of vitamin A were as follows: 0 µM, 40 µM, 80 µM, 120 µM, 160 µM, 200 µM. The last component added was vitamin A. Samples were vortexed carefully for 5 sec, and placed into an incubator at 37 °C in dark for 15 h. For the anaerobic assays, the

stock solution of buffer (500 mM sodium phosphate, pH 7.0) and HPLC-water were degassed via three cycles of freeze-pump-thaw, sealed off under vacuo, brought into a glove box saturated with argon. All reactions were set up and kept for incubation on a heat block at 37 °C in the argon filled glove box. Addition of the loading buffer and gel loading happened under ambient conditions. Gel assay and analysis was carried out as described above. All experiments were run twice, and statistical error analysis was applied to calculate errors. Percentage cleavage was converted to the mean number of cleavage in a plasmid molecule (S value) and these values were plotted against the concentration of vitamin A (Figure 108).

DNA Cleavage by Increasing Concentrations of Hydroquinone Under Aerobic Conditions

Crystalline hydroquinone was used to make a stock in acetonitrile (4 mM). In an 500-µL Eppendorf tube the following components and final concentrations were used: PGL2BASIC plasmid DNA was (35 µM / bp), sodium phosphate buffer (pH 7.0, 50 mM), acetonitrile (10%) and increasing concentrations of hydroquinone in a final reaction volume 50 µL. The concentrations of hydroquinone were as follows: 0 µM, 80 µM, 160 µM, 240 µM, 3200 µM, 400 µM. The last component added was hydroquinone. Samples were vortexed carefully for 5 sec, and placed into an incubator at 37 °C in dark for 15 h. After incubation the electrophoresis and analysis of DNA was done as described above. All experiments were run twice, and statistical error analysis was applied to calculate errors. S values were plotted against the concentration of hydroquinone (Figure 110).

6.12.8. Mechanism of Oxidative DNA Cleavage by 73 in the Presence of Various Additives

In 500 µL Eppendorf tubes the following components and their final concentrations were used: sodium phosphate buffer (50 mM, pH 7.0), acetonitrile (10%, v/v), PGL2BASIC plasmid DNA (35 µM/bp) fecapentaene-12 (200 µM). The components were mixed to a final volume of 50 µL. One of the following additives were used in each reaction: methanol (200 mM), ethanol (200 mM), mannitol (100 mM), DESFERAL (10 mM), SOD (100 µg/ml), catalase (100 µg/ml). Reaction mixture was gently vortexed and incubated at 37 °C for 15h in dark. After incubation the reactions were treated with glycerol loading buffer (17 µL) containing 0.25% bromophenol blue and 40% sucrose, and the mixture vortexed gently. Samples were loaded onto 0.9% agarose gel and elecrophoresed, dyed and analyzed for the percentage DNA-cleavage as described earlier. The corresponding S values were calculated from two sets of experiments using statistical error-analysis to calculate confidence limits (67%) represented as error-bars and plotted in a bar-graph against the applied additives (Figure 106).

6.12.9. Mechanism of Oxidative DNA Cleavage by a Known Superoxide-Radical Generator: Vitamin A in the Presence of Various Additives

In 500 µL Eppendorf tubes the following components and their final concentrations were used: sodium phosphate buffer (50 mM, pH 7.0), acetonitrile (10%, v/v), PGL2BASIC plasmid DNA (35 µM/bp) vitamin A (300 µM). The components were mixed to a final volume of 50 µL. One of the following additives were used in each reaction: methanol (200 mM), ethanol (200 mM), mannitol (100 mM), DESFERAL (10 mM), SOD (100

μg/ml), catalase (100 μg/ml). Reaction mixture was gently vortexed and incubated at 37 °C for 15h in dark. After incubation the reactions were treated with glycerol loading buffer (17 μL) containing 0.25% bromophenol blue and 40% sucrose, and the mixture vortexed gently. Samples were loaded onto 0.9% agarose gel and elecrophoresed, dyed and analyzed for the percentage DNA-cleavage as described earlier. The corresponding S values were calculated from two sets of experiments using statistical error-analysis to calculate confidence limits (67%) represented as error-bars and plotted in a bar-graph against the applied additives (Figure 109).

6.12.10. Mechanism of Oxidative DNA Cleavage by a known Superoxide Radical Generator: Hydroquinone in the Presence of Various Additives

In 500 μL Eppendorf tubes the following components and their final concentrations were used: sodium phosphate buffer (50 mM, pH 7.0), acetonitrile (10%, v/v), PGL2BASIC plasmid DNA (35 μM/bp) hydroquinone (250 μM). The components were mixed to a final volume of 50 μL. One of the following additives were used in each reaction: methanol (200 mM), ethanol (200 mM), mannitol (100 mM), DESFERAL (10 mM), SOD (100 μg/ml), catalase (100 μg/ml). Reaction mixture was gently vortexed and incubated at 37 °C for 15h in dark. After incubation the reactions were treated with glycerol loading buffer (17 μL) containing 0.25% bromophenol blue and 40% sucrose, and the mixture vortexed gently. Samples were loaded onto 0.9% agarose gel and elecrophoresed, dyed and analyzed for the percentage DNA-cleavage as described earlier. The corresponding S values were calculated from two sets of experiments using statistical

error-analysis to calculate confidence limits (67%) represented as error-bars and plotted in a bar-graph against the applied additives (Figure 111).

6.12.11. DNA Damage by Partially Degraded Fecapentaene-12 (73)

Eppendor tubes containing various amounts of neat **1** were prepared as described above. Acetonitrile or ethanol (12.5 µL) and sodium phosphate buffer (5 µL of a 500 mM stock solution in water), followed by water (31.5 µL) were added and the mixture agitated on a vortex mixer for 20 s. Before the addition of plasmid DNA, the mixtures were pre-incubated for 5 h at 37 °C. Plasmid DNA (1 µL of a 1 mg/mL solution) was added with gentle vortex mixing and the cleavage reactions incubated in the dark for 5 h at 37 °C. Analysis of DNA damage was performed as described above.

6.12.12. Noncovalent DNA-Binding by 73

Displacement of Ethidium from Duplex DNA by 73.

A solution of calf thymus DNA-ethidium bromide complex was prepared (final concentrations: DNA, 4 µM; ethidium bromide, 2 µM; HEPES buffer, 10 mM, EDTA, 0.5 mM and sodium chloride, 8 mM, pH 7.0; acetonitrile, 30% v/v) and placed into a quartz fluorescence cuvette (400 µL). The sample was then analized using a Photon International Technology fluorimeter with the following settings: excitation wavelength at 545 nm, emission wavelength at 596 nm, optical slits at 8 nm, lamp power 75 W, detector amplification at 1000 V. Light was integrated for 0.1 s. The fluorimeter wa zeroed on a solution containing ethidium without DNA. Aliquots of a concentrated solution of **1** (2-5 µL of a 5 mM solution in ethanol) were added and changes in

fluorescence emission of DNA-bound ethidium monitored. As a control, the effect of the addition of pure ethanol on the fluorescence of the DNA-ethidium bromide complex was studied. The data was used to estimate the binding constant of **73** with duplex DNA using the general approach described by Baguley et al.[37] (figure 19). The calculations utilized the binding constant of 9.6 x 10^6 M^{-1} for association of ethidium bromide with calf thymus DNA as reported previously.[38]

Calculation of the Binding Constant of Fecapentaene-12 in the Ethidium Bromide Displacement Assay.

The binding constant of ethidium bromide to calf thymus DNA at pH 7.0 was obtained from the literature [69] (**K_e = 9.5 x 10^6 M^{-1}**). The concentration of fecapentaene-12 at 50% displacement of ethidium bromide was at 155 µM. As a general approach, the drug concentration which produces 50% inhibition of fluorescence is used for the calculation of the binding constant. This concentration is approximately inversely proportional to the binding constant. However, this approximation does not take account of different binding site sizes.[70]

Effect of Added Duplex DNA on the UV-vis Spectrum of 73

A solution of **73** in sodium phosphate buffer was placed in a UV-vis cuvette (final concentrations: **73**, 40 μM; sodium phosphate 50 mM, pH 7; acetonitrile, 25% by volume). To this mixture, aliquots of a solution containing herring sperm DNA (5 mM bp) and **73** (40 μM) in sodium phosphate buffer (50 mM, pH 7) and acetonitrile (25% by volume) were added and the resulting mixtures analyzed by UV-vis spectroscopy. The

aliquots of added DNA contained fecapentaene to ensure that changes in the spectrum were not due to dilution. The DNA titration experiment was complete within 25 min. A control experiment was carried out to show that the changes in the UV-vis spectrum are not due to chemical degradation of **73** or reaction of the compound with DNA over the course of the experiment. Specifically, the control showed that the degradation of **73** in the presence of DNA (10 mM bp) over the course of 25 min yields relatively small changes in the UV-vis spectrum compared to those seen in the DNA titration (Figure 115).

Determining the Binding Constant and the Binding-Site size by the McGhee-von Hippel Analysis[47]

Following our titration of **73** with herring DNA, we calculated the extinction coefficient of DNA-bound form of **73** by extrapolating A_{335nm} . We calculated the amount of **73** per unit of DNA (r) and the free drug concentration (C_f) at each titration point, and plotted these values as r/C_f vs. r Figure 116). The resulting plot was fitted non-linearly according to a polynom containing the binding site size (Equation 60), and the binding constant and the binding site size were calculated (K_B = 1029 ± 190 M^{-1}, n = 8 ± 2 bp.).

6.12.13. Searching for DNA-adducts of FP-12 by Nuclease Digestion

      73 (200 μM) was incubated in the presence of 2 mM herring sperm DNA in 50 mM TRIS-EDTA (pH 7.5) and acetonitrile (10%) for 20 h at 37°C in a final volume of 500 μL. After incubation, small molecules were extracted from the mixture using butanol (500 μL, twice). The remaining solution was treated with DNA precipitating solution

containing 0.3 M sodium acetate and 70% (v/v) ethanol (500 μL). This cocktail was mixed on a vortex mixer and kept on dry-ice for 30 minutes form complete freezing. The frozen samples were centrifuged at 10.000 r.p.m. for 30 min at 4 °C. The DNA pellets were collected, and further washed with 80% ethanol in water (200 μL, twice). The pellets then were redisolved into water (352 μL) and a digestion-buffer mixture (40 μL) containing sodium acetate (830 mM) and magnesium sulfate (83 mM). Then 0.2 U of PDE and 330 U of DNAse II was added to the system and it was incubated for 1 h at 37 °C. After incubation, 1.22 mg AcP was added and mixture incubated for additional 2 h at 37 °C. Enzymes were removed via centrifugation in an amicon filter (3 kD cutoff). Filtrate was analyzed by reversed phase HPLC using method reported by Guengerich et al.[49] (Figure 117).

_____

References

1.   Bruce, W. R.; Varghese, A. J.; Furrer, R.; Land, P. C., A mutagen in the feces of normal humans. *Cold Spring Harbor Conferences on Cell Proliferation* **1977,** 4, 1641-6.

2.   Kingston, D. G. I.; Van Tassell, R. L.; Wilkins, T. D., The fecapentaenes, potent mutagens from human feces. *Chem. Res. Toxicol.* **1990,** 3, 391-400.

3.   de Kok, T. M. C. M.; van Maanen, J. M. S., Evaluation of fecal mutagenicity and colorectal cancer risk. *Mutat. Res.* **2000,** 463, 53-101.

4.   Reddy, B. S.; Sharma, C.; Darby, L.; Laakso, K.; Wynder, E. L., Metabolic epidemiology of large bowel cancer. Fecal mutagens in high- and low-risk population for colon cancer. A preliminary report. *Mutat. Res.* **1980,** 72, 511-22.

5.   Bruce, W. R.; Varghese, A. J.; Land, P. C.; Krepinsky, J. J. F., Properties of a mutagen isolated from feces. *Banbury Report* **1981,** 7, 227-38.

6.   Kingston, D. G. I.; Wilkins, T. D.; Van Tassell, R. L.; Macfarlane, R. D.; McNeal, C. J., Structural studies on a mutagenic bacterial product from human feces. *Banbury Report* **1981,** 7, 215-26.

7.   Plummer, S. M.; Grafstrom, R. C.; Yang, L. L.; Curren, R. D.; Linnainmaa, K.; Harris, C. C., Fecapentaene-12 causes DNA damage and mutations in human cells. *Carcinogenesis* **1986,** 7, 1607-1609.

8.   Govindan, S. V.; Kingston, D. G. I.; Gunatilaka, A. A. L.; Van Tassell, R. L.; Wilkins, T. D.; De Wit, P. P.; Van der Steeg, M.; Van der Gen, A., Synthesis and biological activity of analogs of fecapentaene-12. *J. Nat. Prod.* **1987,** 50, 75-83.

9.   Schmid, E.; Bauchinger, M.; Braselmann, H.; Pfaendler, H. R.; Goeggelmann, W., Dose-response relationship for chromosome aberrations induced by fecapentaene-12 in human lymphocytes. *Mutat. Res.* **1987,** 191, 5-7.

10.   Weston, A.; Plummer, S. M.; Grafstrom, R. C.; Trump, B. F.; Harris, C. C., Genotoxicity of chemical and physical agents in cultured human tissues and cells. *Food and chemical toxicology : an international journal published for the British Industrial Biological Research Association* **1986,** 24, 675-9.

11.   Kingston, D. G. I.; Van Tassell, R. L.; Wilkins, T. D., The fecapentaenes, potent mutagens from human feces. *Chem. Res. Toxicol.* **1990,** 3, 391-400.

12.   Dypbukt, J. M.; Edman, C. C.; Sundqvist, K.; Kakefuda, T.; Plummer, S. M.; Harris, C. C.; Grafstroem, R. C., Reactivity of fecapentaene-12 toward thiols, DNA, and these constituents in human fibroblasts. *Canc. Res.* **1989,** 49, 6058-6063.

13.   Povey, A. C.; Wilson, V. L.; Zweier, J. L.; Kuppusamy, P.; O'Neill, I. K.; Harris, C. C., Detection by phosphorus-31-postlabelling of DNA adducts induced by free radicals and unsaturated aldehydes formed during the aerobic decomposition of fecapentaene-12. *Carcinogenesis* **1992,** 13, 395-401.

14.   de Kok, T. M. C. M.; Pachen, D. M. F. A.; van Maanen, J. M. S.; Lafleur, M. V. M.; Westmijze, E. J.; Hoor, F. t.; Kleinjans, J. C. S., Role of oxidative DNA damage in the mechanism of fecapentaene-12 genotoxicity. *Carcinogenesis* **1994,** 15, 2559-2565.

15.   De Kok, T. M. C. M.; Van Maanen, J. M. S.; Lankelma, J.; Ten Hoor, F.; Kleinjans, J. C. S., Electron spin resonance spectroscopy of oxygen radicals generated by synthetic fecapentaene-12 and reduction of fecapentaene mutagenicity to Salmonella typhimurium by hydroxyl radical scavenging. *Carcinogenesis* **1992,** 13, 1249-1255.

16.   Peters, J. H.; Riccio, E. S.; Stewart, K. R.; Reist, E. J., Mutagenic activities of fecapentaene derivatives in the Ames/Salmonella test system. *Canc. Lett.* **1988,** 39, 287-96.

17.   De Wit, P. P.; Van der Steeg, M.; Van der Gen, A., Remarkable electrophilic properties of the pentaenol ether system of fecapentaene-12. *Tetrahedron Lett.* **1986,** 27, 6263-6.

18.   Nieuwenhuis, S. A. M.; Vertegaal, L. B. J.; de Zoete, M. C.; van der Gen, A., Acid-catalyzed solvolysis of polyenol ethers. III. Effect of the alkoxy moiety. *Tetrahedron* **1994,** 50, 13207-13230.

19.   Streeter, A. J.; Donovan, P. J.; Anjo, T.; Ohannesian, L.; Sheffels, P. R.; Wu, P. P.; Keefer, L. K.; Andrews, A. W.; Bradford, W. W., III; al., e., Decomposition and quality control considerations in biological work with fecapentaene preparations. *Chem. Res. Toxicol.* **1989,** 2, 162-168.

20.   Shamsuddin, A. M.; Ullah, A.; Baten, A.; Hale, E., Stability of fecapentaene-12 and its carcinogenicity in F-344 rats. *Carcinogenesis* **1991,** 12, 601-607.

21.   Hertzberg, R. P.; Dervan, P. B., Cleavage of double helical DNA by methidium-propyl-EDTA-iron(II). *J. Am. Chem. Soc.* **1982,** 104, 313-315.

22.   Jadhav, V. R.; Barawkar, D. A.; Ganesh, K. N., Polarity Sensing by Fluorescent Oligonucleotides: First Demonstration of Sequence-Dependent Microenvironmental Changes in the DNA Major Groove. *J. Phys. Chem. B* **1999,** 103, 7383-7385.

23.   Jin, R.; Breslauer, K. J., Characterization of the minor groove environment in a drug-DNA complex: bisbenzimide bound to the poly[d(AT)]×poly[d(AT)duplex. *Proc. Natl. Acad. Sci. Unit. States. Am.* **1988,** 85, 8939-8942.

24.   Barawkar, D. A.; Ganesh, K. N., Fluorescent d(CGCGAATTCGCG): characterization of major groove polarity and study of minor groove interactions through a major groove semantophore conjugate. *Nucleic. Acids. Res.* **1995,** 123, 159-164.

25.   Young, M. A.; Jayaram, B.; Beveridge, D. L., Local Dielectric Environment of B-DNA in Solution: Results from a 14 ns Molecular Dynamics Trajectory. *J. Phys. Chem. B* **1998,** 102, 7666-7669.

26.   Nicolaou, K. C.; Zipkin, R.; Tanner, D., Total synthesis of the potent mutagen (S)-3-(dodeca-1,3,5,7,9-pentaenyloxy)propane-1,2-diol. *J. Chem. Soc. Chem. Comm.* **1984,** 6, 349-350.

27.   Zipkin, R. E. Ph.D., University of Pennsylvania, Pennsylvania, 1984.

28.   Chatterji, T.; Kizil, M.; Keerthi, K.; Chowdhury, G.; Pospisil, T.; Gates, K. S., Small Molecules That Mimic the Thiol-Triggered Alkylating Properties Seen in the Natural Product Leinamycin. *J. Am. Chem. Soc.* **2003,** 125, 4996-4997.

29.   Rissler, K., Improved separation of poly(ethylene glycol)s widely differing in molecular weight range by reversed-phase high performance liquid chromatography and evaporative light scattering detection. *Chromatographia* **1999,** 49, 615-620.

30.   Halliwell, B.; Gutteridge, J. M. C., Role of free radicals and catalytic metal ions in human disease: an overview. *Meth. Enzymol.* **1990,** 186, 1-85.

31.   Behroozi, S. J.; Kim, W.; Dannaldson, J., 1,2-Dithiolan-3-one 1-Oxides: A Class of Thiol-Activated DNA-Cleaving Agents That Are Structurally Related to the Natural Product Leinamycin. *Biochemistry* **1996,** 35, 1768-1774.

32.   Murata, M.; Kawanishi, S., Oxidative DNA damage by vitamin A and its derivative via superoxide generation. *J. Biol. Chem.* **2000,** 275, 2003-2008.

33.   Ikota, N.; Ueda, J.-i.; Gamage, R.; Shimazu, Y.; Hama-Inaba, H.; Takusakawa, M.; Ozawa, T.; Satoh, T., Histidine-containing peptides and hydroquinone derivatives as synthetic antioxidants. *Biodefence Mechanisms against Environmental Stress* **1998**, 3-12.

34.   Berry, D. E.; Chan, J. A.; MacKenzie, L.; Hecht, S. M., 9-Octadecynoic acid: a novel DNA binding agent. *Chem. Res. Toxicol.* **1991,** 4, 195-198.

35.   Barr, J. R.; Murty, V. S.; Yamaguchi, K.; Singh, S.; Smith, D. H.; Hecht, S. M., 5-Alkylresorcinols from Hakea amplexicaulis that cleave DNA. *Chem. Res. Toxicol.* **1988,** 1, 204-207.

36.   Scannell, R. T.; Barr, J. R.; Murty, V. S.; Reddy, K. S.; Hecht, S. M., DNA strand scission by naturally occurring 5-alkylresorcinols. *J. Am. Chem. Soc.* **1988,** 110, 3650-3651.

37.   Baguley, B. C.; Denny, W. A.; Atwell, G. J.; Cain, B. F., Potential antitumor agents. 34. Quantitative relationships between DNA binding and molecular structure for 9-anilinoacridines substituted in the anilino ring. *J. Med. Chem.* **1981,** 24, 170-177.

38.   Jenkins, T. C., *Optical absorbance and fluorescence techniques for measuring DNA-drug interactions.* . Fox, K. E., Ed.: New Jersey, 1997; p 195-218.

39.   Hsieh, H.-P.; Muller, J. G.; Burrows, C. J., Structural Effects in Novel Steroidal Polyamine-DNA Binding. *J. Am. Chem. Soc.* **1994,** 116, 12077-12078.

40.   Schneider, H. J.; Blatter, T., Interaction of acyclic and cyclic peralkylammonium compounds and DNA. *Angew. Chem. Int. Ed.* **1992,** 31, 1207-1208.

41.   Tse, W. C.; Boger, D. L., A fluorescent intercalator displacement assay for establishing DNA binding selectivity and affinity. *Accounts. Chem. Res.* **2004,** 37, 61-69.

42.   R, M. A.; H, E. D.; S, L. J.; E, P. D., Ethidium fluorescence assays. Part 1. Physicochemical studies. *Nucleic. Acids. Res.* **1979,** 1979, 3.

43.   Long, E. C.; Barton, J. K., On demonstrating DNA intercalation. *Accounts. Chem. Res.* **19909,** 23, 271-273.

44.   Suh, D.; Chaires, J. B., Criteria for the mode of binding of DNA binding agents. *Bioorg. Med. Chem.* **1995,** 3, 723-728.

45.   Wang, X.; Zhang, X.; Lin, J.; Chen, J.; Xu, Q.; Guo, Z., DNA-binding property and antitumor activity of bismuth(3+) complex with 1,4,7,10-tetrakis(2-pyridylmethyl)-1,4,7,10-tetraazacyclododecane. *Dalton Trans.* **2003,** 12, 2379-2380.

46.   Kassaee, M. Z.; Bekhradnia, A. R., The kinetics of interactions between fecapentaene-12 and DNA. *J. Biosci. Bioeng.* **2003,** 95, 526-529.

47.   McGhee, J. D.; Von Hippel, P. H., Theoretical aspects of DNA-protein interactions.   Cooperative and noncooperative binding of large ligands to a one-dimensional homogeneous lattice. *J. Mol. Biol.* **1974,** 86, 469-489.

48.   Chaudhary, A. K.; Reddy, G. R.; Blair, I. A.; Marnett, L. J., Characterization of an N6-oxopropenyl-2'-deoxyadenosine adduct in malondialdehyde-modified DNA using liquid chromatography/electrospray ionization tandem mass spectrometry. *Carcinogenesis* **1996,** 17, 1167-1170.

49.   Marsch, G. A.; Mundkowski, R. G.; Morris, B. J.; Manier, M. L.; Hartman, M. K.; Guengerich, F. P., Characterization of Nucleoside and DNA Adducts Formed by S-(1-Acetoxymethyl)glutathione   and   Implications   for   Dihalomethane-Glutathione Conjugates. *Chem. Res. Toxicol.* **2001,** 14, 600-608.

50.   Evans, M. D.; Dizdaroglu, M.; Cooke, M. S., Oxidative DNA damage and disease: induction, repair and significance. *Mutat. Res.* **2004,** 567, 1-61.

51.   Marnett, L. J., Oxyradicals and DNA damage. *Carcinogenesis* **2000,** 21, 361-370.

52.   Wallace, S. S., Biological consequences of free radical-damaged DNA bases. *Adv. Free. Radic. Biol. Med.* **2002,** 33, 1-14.

53.   Pogozelski, W. K.; McNeese, T. J.; Tullius, T. D., What Species Is Responsible for Strand Scission in the Reaction of [FeIIEDTA]2- and H2O2 with DNA? *J. Am. Chem. Soc.* **1995,** 117, 6428-6433.

54.   Breen, A. P.; Murphy, J. A., Reactions of oxyl radicals with DNA. *Adv. Free. Radic. Biol. Med.* **1995,** 18, 1033-1077.

55.   Zuilhof, H.; Vertegaal, L. B. J.; van der Gen, A.; Lodder, G., Quantum chemical analysis of the mechanism of the solvolysis of polyenol ethers. PM3 calculations on fecapentaene-12 and related compounds. *J. Org. Chem.* **1993,** 58, 2804-2809.

56.   Porter, N. A., Mechanisms for the autoxidation of polyunsaturated lipids. *Accounts. Chem. Res.* **1986,** 19, 262-268.

57.   Chamulitrat, W.; Hughes, M. F.; Eling, T. E.; Mason, R. P., Superoxide and peroxyl radical generation from the reduction of polyunsaturated fatty acid hydroperoxides by soybean lipoxygenase. *Arch. Biochem. Biophys.* **1991,** 290, 153-159.

58.   J, M. G.; A, F. J., Stopped flow spectrophotometric observation of superoxide dismutation in aqueous solution. *FEBS Lett.* **1976,** 67, 294-298.

59.   Halliwell, B., An attempt to demonstrate a reaction between superoxide and hydrogen peroxide. *FEBS Lett.* **1976,** 72, 8-10.

60.   Liochev, S. I.; Fridovich, I., The Haber-Weiss cycle - 70 years later: an alternative view. Comments. *Redox Report* **2002,** 7, 55-57.

61.   MacManus-Spencer; A., L.; McNeill, K., Quantification of Singlet Oxygen Production in the Reaction of Superoxide with Hydrogen Peroxide Using a Selective Chemiluminescent Probe. *J. Am. Chem. Soc.* **2005,** 127, 8954-8955.

62.   Kochevar, I. E.; Dunn, D. A., Photosensitized reactions of DNA: cleavage and addition. *Photochemistry* **1990,** 1, 273-315.

63.   Li, M. Y.; Cline, C. S.; Koker, E. B.; Carmichael, H. H.; Chignell, C. F.; Bilski, P., Quenching of singlet molecular oxygen (1O2) by azide anion in solvent mixtures. *Photochem. Photobiol.* **2001,** 74, 760-764.

64.   Catalan, J.; Diaz, C.; Barrio, L., Analysis of mixed solvent effects on the properties of singlet oxygen (1Dg). *Chem. Phys.* **2004,** 300, 33-39.

65.   Buxton, G. V.; Greenstock, C. L. H., W. Phillip; Ross, A. B., Critical review of rate constants for reactions of hydrated electrons, hydrogen atoms and hydroxyl radicals (×OH/×O-) in aqueous solution. *J. Phys. Chem. Ref. Data.* **1988,** 17, 513-886.

66.   Blazek, E. R.; Peak, J. G.; Peak, M. J., Singlet oxygen induces frank strand breaks as well as alkali- and piperidine-labile sites in supercoiled plasmid DNA. *Photochem. Photobiol.* **1989,** 49, 607-613.

67.   Sambrook, J.; Fritisch, E. F.; Maniatis, T., *Molecular Cloning: A Lab Manual*. Cold Spring Harbor Press, Cold Spring Harbor, NY.: 1989.

68.   Baldwin, J. J.; Raab, A. W.; Mensler, K.; Arison, B. H.; McClure, D. E., Synthesis of (R)- and (S)-epichlorohydrin. *J. Org. Chem.* **1978,** 43, 4876-8.

69.   Fox, K. R., *Drug-DNA Interaction Protocols*. Humana Press: Totowa, New Jersey, 1997; p 213.

70.   Morgan, A. R.; Lee, J. S.; Pulleyblank, D. E.; Murray, N. L.; Evans, D. H., Ethidium fluorescence assays. Part 1. Physicochemical studies. *Nucleic. Acids. Res.* **1979,** 7, 547-69.

Dissertation Conclusions

We have studied the reactions of small molecules with DNA. Since DNA is the central molecule in cells[1,2] that determines its proper function, this type of Chemistry is relevant to the understanding of the Biology of both anticancer drugs and mutagens.[3] Within this field, we have looked to study molecules that damage DNA by unusual chemical mechanisms. Finding new chemical reactions to modify biomolecules covalently under physiological conditions is fundamentally relevant to medicinal chemistry, toxicology and biotechnology. The novel chemistries will invite the development of new experimental methods and analytical tools, too.[4-12]

Finally, it is important to appreciate our position as research scientists. Not too many people have access to the fascinating natural products given by nature, and to the tools of exploration of their functions. In addition, the ability to wisely utilize the information media in the forms of presentations, publications and conferences will help our minds and hands unite for this exceptional adventure.

References

1.   Manuelidis, L.; Chen, T. L., A unified model of eukaryotic chromosomes. *Cytometry* **1990,** 11, 8-25.

2.   Alberts, B.; Alexander, J.; Lewis, J.; Raff, M.; Roberts, K.; Walter, P., *Molecular Biology of the Cell, 4th Edition*. 2004; p 2000 pp.

3.   Silverman, R. B., *The Organic Chemistry of Drug Design and Drug Action*. 2004; p 617 pp.

4.   DeRisi, J.; Penland, L.; Brown, P. O.; Bittnber, M. L.; Meltzer, P. S.; Ray, M.; Chen, Y.; Su, Y. A.; Trent, J. M., Use of a cDNA microarrays to analyze gene expression patterns in human cancer. *Nat. Genet.* **1996,** 14, 457-460.

5.   Anon, Focus on bio informatics. *Nature (London, United Kingdom)* **2001,** 413, 9-19.

6.   Miki, R.; Kadota, K.; Bono, H.; Mizuno, Y.; Tomaru, Y.; Carninci, P.; Itoh, M.; Shibata, K.; Kawai, J.; Konno, H.; Watanabe, S.; Sato, K.; Tokusumi, Y.; Kikuchi, N.; Ishii, Y.; Hamaguchi, Y.; Nishizuka, I.; Goto, H.; Nitanda, H.; Satomi, S.; Yoshiki, A.; Kusakabe, M.; DeRisi, J. L.; Eisen, M. B.; Iyer, V. R.; Brown, P. O.; Muramatsu, M.; Shimada, H.; Okazaki, Y.; Hayashizaki, Y., Delineating developmental and metabolic pathways in vivo by expression profiling using the RIKEN set of 18,816 full-length enriched mouse cDNA arrays. *Proc. Natl. Acad. Sci. Unit. States Am.* **2001,** 98, 2199-2204.

7.   Zhao, Y.; Zhou, C., Drug characteristics prediction. *IEEE Computational Systems Bioinformatics Conference, Workshops & Poster Abstracts, Stanford, CA, United States, Aug. 8-11, 2005* **2005**, 395-397.

8.   Lin, C.-Y.; Su, Y.-N.; Lee, C.-N.; Hung, C.-C.; Cheng, W.-F.; Lin, W.-L.; Chen, C.-A.; Hsieh, S.-T., A rapid and reliable detection system for the analysis of PMP22 gene dosage by MP/DHPLC assay. *J. Hum. Genet.* **2006,** 51, 227-235.

9.   Lo, C.-J.; Leake, M. C.; Berry, R. M., Fluorescence measurement of intracellular sodium concentration in single Escherichia coli cells. *Biophys. J.* **2006,** 90, 357-365.

10.   Novak, P.; Tepes, P.; Fistric, I.; Bratos, I.; Gabelica, V., The application of LC-NMR and LC-MS for the separation and rapid structure elucidation of an unknown impurity in 5-aminosalicylic acid. *J. Pharmaceut. Biomed. Anal.* **2006,** 40, 1268-1272.

11.   Rodriguez-Nogales, J. M.; Garcia, M. C.; Marina, M. L., High-performance liquid chromatography and capillary electrophoresis for the analysis of maize proteins. *J. Separ. Sci.* **2006,** 29, 197-210.

12.   Rossi, M.; Campa, C.; Gamini, A.; Coslovi, A.; Donati, I.; Vetere, A.; Paoletti, S., Separation of O- and C-allyl glycoside anomeric mixtures by capillary electrophoresis and high-performance liquid chromatography. *J. Chrom.* **2006,** 1110, 125-132.

VITA

Joseph (Jozsef) Szekely was born to Jozsef and Margit Szekely on March 16, 1973 in Hatvan, Hungary. He received a high school Diploma as a High Precision Serial Production Tool Designer in Godollo, Hungary with honors in 1990. He graduated from the University of Debrecen, Hungary with a Master of Sciences degree from the Antibiotic Research Group of the Department of Chemistry in 1999. He joined the Ph.D. program in Chemistry at the University of Missouri-Columbia in the fall of 2000 working under the direction of Professor Kent Gates. He graduated in the spring of 2006 and currently is serving as a postdoctoral fellow in the Department of Biochemistry, School of Medicine at Vanderbilt University in the research groups of Professor Lawrence J. Marnett and Professor Carmelo Rizzo.